

Submitted to Maynooth University for the degree of Doctor of Philosophy



**Stephen Gargan, B. Sc.**

**May 2024**

**Supervisor**

Professor Kay Ohlendieck  
Department of Biology  
Maynooth University  
Co. Kildare

**Co-Supervisor**

Doctor Paul Dowling  
Department of Biology  
Maynooth University  
Co. Kildare

**Head of Department**

Professor Paul Moynagh  
Department of Biology  
Maynooth University  
Co. Kildare

## TABLE OF CONTENTS

Table of contents	ii	
List of figures	iii	
List of tables	vi	
Publications	vii	
Acknowledgements	ix	
Declaration	x	
Abbreviations	xi	
Abstract	xiv	
<b>Chapter 1</b>	<b>INTRODUCTION</b>	<b>1</b>
1.1	Skeletal muscle	2
1.1.1	Muscle biology	2
1.1.2	Muscle development and regeneration	3
1.1.3	Muscle structure	3
1.1.4	Muscle contraction	4
1.2	Duchenne muscular dystrophy	6
1.2.1	Dystrophin protein	8
1.2.2	Dystrophin-glycoprotein complex	8
1.2.3	Dystrophin isoforms	11
1.3	Treatments for dystrophinopathy	11
1.3.1	Corticosteroids	11
1.3.2	Anabolic steroids	12
1.3.3	Insulin growth factor IGF-1	13
1.3.4	Anti-fibrotic treatments	14
1.3.5	Genetic engineering	15
1.4	Muscle stimulation and dystrophinopathy	16
1.5	Animal models of dystrophinopathy	17
1.5.1	Murine <i>mdx-4cv</i>	17
1.5.2	GRMD Golden retriever dog	18
1.5.3	<i>Caenorhabditis elegans</i>	18
1.5.4	Zebrafish	18
1.5.5	Dmd <sup>mdx</sup> rat	19

1.6	Proteomics	19
1.6.1	Mass spectrometry	19
1.7	Aims and outlines	21
<b>Chapter 2</b>	Sample preparation for proteomics and mass spectrometry from clinical tissue	22
<b>Chapter 3</b>	Sample preparation and protein determination for 2D-DIGE proteomics	53
<b>Chapter 4</b>	Proteomic identification of markers of membrane repair, regeneration and fibrosis in the aged and dystrophic diaphragm	68
<b>Chapter 5</b>	Mass spectrometric profiling of extraocular muscle and proteomic adaptations in the <i>mdx-4cv</i> model of Duchenne muscular dystrophy	105
<b>Chapter 6</b>	Identification of marker proteins of muscular dystrophy in the urine proteome from the <i>mdx-4cv</i> model of dystrophinopathy	137
<b>Chapter 7</b>	General discussion	167
7.1	Analysis of altered proteome in aged dystrophic diaphragm	170
7.1.1	Extracellular matrix proteins	170
7.1.2	Excitation contraction coupling proteins	173
7.1.3	Membrane repair and calcium sensing	176
7.2	Extraocular muscle proteome analysis	178
7.2.1	Sarcomeric proteins found in extraocular muscle	180
7.2.2	Extraocular muscle proteomic changes in dystrophinopathy	183
7.3	Analysing the urine proteome in dystrophinopathy	185
<b>Chapter 8</b>	Conclusion	189
<b>Chapter 9</b>	Bibliography	190

## List of figures

### Chapter 1

Figure 1.1	Arrangement of the proteins involved in excitation–contraction	5
Figure 1.2	Histological and immunofluorescence microscopical analysis of dystrophic <i>mdx-4cv</i> skeletal muscle	7
Figure 1.3	Main functions of the dystrophin node	9
Figure 1.4	structure of dystrophin and the diverse interactions	10

	of the dystrophin–glycoprotein complex	
Figure 1.5	Comparative immunoblot analysis of the dystrophic <i>mdx-4cv</i> mouse diaphragm muscle	20
<b>Chapter 2</b>		
Figure 2.1	Preparation of muscle biopsy specimens for proteomic analysis	32
Figure 2.2	Workflow of the mass spectrometry-based proteomic analysis of clinical tissue samples	34
<b>Chapter 3</b>		
Figure 3.1	Preparation of samples for the comparative proteomic analysis using fluorescence difference gel electrophoresis	55
Figure 3.2	Summarizing scheme of tissue preparation for analysis by fluorescence two-dimensional difference gel electrophoresis	56
Figure 3.3	Overview of a standardized dye-metal based colorimetric assay for the determination of protein	57
Figure 3.4	Determination of protein concentration in unknown samples to be used for two-dimensional difference gel electrophoresis	58
<b>Chapter 4</b>		
Figure 4.1	Bioinformatic analysis of changed protein classes in 3-month old <i>mdx-4cv</i> diaphragm muscle	75
Figure 4.2	Bioinformatic analysis of changed protein classes in 15-month old <i>mdx-4cv</i> diaphragm muscle	75
Figure 4.3	Proteomic analysis of the expression of the dystrophin glycoprotein complex in 3-month versus 15-month old <i>mdx-4cv</i> diaphragm muscle	76
Figure 4.4	Proteomic analysis of the expression of established proteomic markers of X-linked muscular dystrophy in 3-month versus 15-month old <i>mdx-4cv</i> diaphragm muscle	77
Figure 4.5	Proteomic identification of changes in the expression levels of key proteins involved in excitation-contraction coupling, calcium homeostasis and triad integrity in 3-month versus 15-month old <i>mdx-4cv</i> diaphragm muscle.	79
Figure 4.6	Proteomic identification of changes in the expression levels of key proteins involved in membrane repair and calcium sensing in 3-month versus 15-month old <i>mdx-4cv</i>	80

	diaphragm muscle	
Figure 4.7	Proteomic identification of changes in the expression levels of collagens and related extracellular matrix proteins in 3-month versus 15-month old <i>mdx-4cv</i> diaphragm muscle	82
Figure 4.8	Immunoblot analysis of Collagen VI, Periostin and Annexin 2 in <i>mdx-4cv</i> diaphragm	83
Figure 4.9	Overview of pathobiochemical and adaptive changes in the aged and dystrophin-deficient <i>mdx-4cv</i> diaphragm muscle	85
<b>CHAPTER 5</b>		
Figure 5.1	Overview of the proteomic profiling approach to characterize extraocular muscle, as well as determine changes in the <i>mdx-4cv</i> mouse model of Duchenne muscular dystrophy	101
Figure 5.2	Comparative display of mass spectrometrically identified proteins of the sarcomere in extraocular muscle versus diaphragm from wild type mice	106
Figure 5.3	Immunoblot analysis of extraocular muscle versus diaphragm muscle from wild type mice	108
Figure 5.4	Bioinformatic analysis of the comparative proteomic profiling of extraocular muscle from wild type versus the <i>mdx-4cv</i> model of X-linked muscular dystrophy	112
Figure 5.5	Histological and immunofluorescence microscopical characterization, as well as immunoblot analysis, of extraocular muscle from the <i>mdx-4cv</i> mouse	114
<b>Chapter 6</b>		
Figure 6.1	Immunofluorescence microscopical characterization of the dystrophic diaphragm from the <i>mdx-4cv</i> mouse	129
Figure 6.2	Distribution of protein classes within the mouse urine proteome as determined by mass spectrometry-based proteomics and bioinformatic PANTHER analysis	132
Figure 6.3	Heat map of the urinomic analysis of changed proteins in wild type versus the <i>mdx-4cv</i> mouse model of dystrophinopathy	134
Figure 6.4	Proteomic fingerprint and immunoblot analysis of titin in urine from wild type versus dystrophic mice	137

Figure 6.5	Bioinformatic STRING analysis of potential protein-protein interactions of increased versus decreased proteins in urine from the <i>mdx-4cv</i> mouse	140
------------	---	-----

## List of tables

### Chapter 2

Key resources table	26
---------------------	----

### Chapter 5

Proteomic identification of sarcomere-associated proteins and related isoforms in mouse extraocular muscle	113
Comparative proteomic analysis of the <i>mdx-4cv</i> extraocular muscle cone	121

### Chapter 6

Mass spectrometric identification of abundant proteins in mouse urine	141
Proteomic identification of increased proteins in urine from the <i>mdx-4cv</i> mouse model of Duchenne muscular dystrophy	145

### Chapter 7

Summary and major findings of publications	166
--	-----



## PUBLICATIONS

Gargan S, Dowling P, Ohlendieck K. Sample preparation for proteomics and mass spectrometry from clinical tissue. In: *Proteomics Mass Spectrometry Methods, Sample Preparation, Protein Digestion, and Research Protocols*, 1st Edition - February 16, 2024, Editor: Paula Meleady, Paperback ISBN: 9780323903950 (In press)

Dowling P, Gargan S, Zweyer M, Swandulla D, Ohlendieck K. Extracellular Matrix Proteomics: The *mdx-4cv* Mouse Diaphragm as a Surrogate for Studying Myofibrosis in Dystrophinopathy. *Biomolecules*. 2023;13(7):1108. Published 2023 Jul 12. doi:10.3390/biom13071108

Dowling P, Gargan S, Swandulla D, Ohlendieck K. Fiber-Type Shifting in Sarcopenia of Old Age: Proteomic Profiling of the Contractile Apparatus of Skeletal Muscles. *Int J Mol Sci*. 2023;24(3):2415. Published 2023 Jan 26. doi:10.3390/ijms24032415

Gargan S, Ohlendieck K. Sample Preparation and Protein Determination for 2D-DIGE Proteomics. *Methods Mol Biol*. 2023;2596:325-337. doi:10.1007/978-1-0716-2831-7\_22

Dowling P, Gargan S, Swandulla D, Ohlendieck K. Identification of Subproteomic Markers for Skeletal Muscle Profiling. *Methods Mol Biol*. 2023;2596:291-302. doi:10.1007/978-1-0716-2831-7\_20

Gargan S, Dowling P, Zweyer M, et al. Proteomic Identification of Markers of Membrane Repair, Regeneration and Fibrosis in the Aged and Dystrophic Diaphragm. *Life (Basel)*. 2022;12(11):1679. Published 2022 Oct 22. doi:10.3390/life12111679

Dowling P, Gargan S, Swandulla D, Ohlendieck K. Proteomic profiling of impaired excitation-contraction coupling and abnormal calcium handling in muscular dystrophy. *Proteomics*. 2022;22(23-24):e2200003. doi:10.1002/pmic.202200003

Dowling P, Gargan S, Zweyer M, Sabir H, Swandulla D, Ohlendieck K. Proteomic profiling of carbonic anhydrase CA3 in skeletal muscle. *Expert Rev Proteomics*. 2021;18(12):1073-1086. doi:10.1080/14789450.2021.2017776

Zweyer M, Sabir H, Dowling P, et al. Histopathology of Duchenne muscular dystrophy in correlation with changes in proteomic biomarkers. *Histol Histopathol*. 2022;37(2):101-116. doi:10.14670/HH-18-403

Gargan S, Dowling P, Zweyer M, et al. Mass Spectrometric Profiling of Extraocular Muscle and Proteomic Adaptations in the *mdx-4cv* Model of Duchenne Muscular Dystrophy. *Life (Basel)*. 2021;11(7):595. Published 2021 Jun 22. doi:10.3390/life11070595

Dowling P, Gargan S, Zweyer M, et al. Proteomic profiling of the interface between the stomach wall and the pancreas in dystrophinopathy. *Eur J Transl Myol.* 2021;31(1):9627. Published 2021 Mar 26. doi:10.4081/ejtm.2021.9627

Dowling P, Gargan S, Murphy S, et al. The Dystrophin Node as Integrator of Cytoskeletal Organization, Lateral Force Transmission, Fiber Stability and Cellular Signaling in Skeletal Muscle. *Proteomes.* 2021;9(1):9. Published 2021 Feb 2. doi:10.3390/proteomes9010009

Dowling P, Gargan S, Zweyer M, et al. Protocol for the Bottom-Up Proteomic Analysis of Mouse Spleen. *STAR Protoc.* 2020;1(3):100196. Published 2020 Dec 3. doi:10.1016/j.xpro.2020.100196

Dowling P, Gargan S, Zweyer M, et al. Proteome-wide Changes in the *mdx-4cv* Spleen due to Pathophysiological Cross Talk with Dystrophin-Deficient Skeletal Muscle. *iScience.* 2020;23(9):101500. Published 2020 Aug 26. doi:10.1016/j.isci.2020.101500

Gargan S, Dowling P, Zweyer M, Swandulla D, Ohlendieck K. Identification of marker proteins of muscular dystrophy in the urine proteome from the *mdx-4cv* model of dystrophinopathy. *Mol Omics.* 2020;16(3):268-278. doi:10.1039/c9mo00182d

Dowling P, Gargan S, Zweyer M, Swandulla D, Ohlendieck K. Proteomic profiling of fatty acid binding proteins in muscular dystrophy. *Expert Rev Proteomics.* 2020;17(2):137-148. doi:10.1080/14789450.2020.1732214

## **ACKNOWLEDGMENTS**

My sincerest gratitude to my supervisor and co-supervisor.

Professor Kay Ohlendieck, thank you for the guidance and patience you have shown to me over my time as your student. You have been an enormous help and inspiration to me.

Dr. Paul Dowling, thank you for taking the time to train me in our lab procedures, and for answering my many related questions over the 4 years.

To Professor Dieter Swandulla and Margit Zweyer at the Institute of Physiology at Bonn University, Germany. Thank you for many successful collaborations.

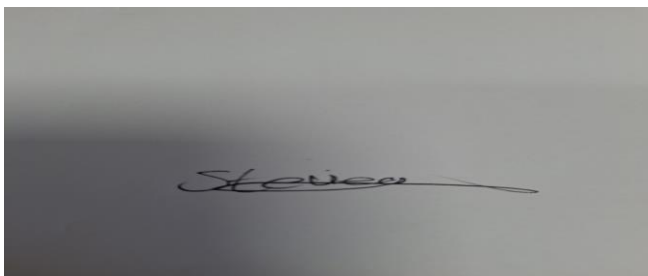
Thank you to all of the biology staff and PhD students in Maynooth, who have helped me in many ways. Special thanks to my lab mate Katie Dunphy.

To my mother Siobhan, without your eternal love and support I do not know where I would be. I am grateful for everything you have done for me.

To my father Damien, nobody was as invested or as interested in my academics as you were. It is of deep regret that you will not get to see me graduate. You are missed.

## DECLARATION

This thesis has not been submitted in whole or part to this or any other university for any degree and is the original work of the author except where stated.

A rectangular area containing a handwritten signature in black ink. The signature appears to be "Stephen Gargan".

Signed \_\_\_\_\_

Stephen Gargan, B.Sc

Date \_\_\_\_\_ 12/02/2024 \_\_\_\_\_

## Abbreviations

1D	One-dimensional
2D	Two-dimensional
2D-DIGE	Two-dimensional difference in-gel electrophoresis
2D-GE	Two-dimensional gel electrophoresis
4E-BP1	Eukaryotic translation initiation factor 4E-binding protein 1
ACh	Acetylcholine
AChR	Acetylcholine receptor
ACTC1	Alpha-Actinin 1
ALK5	Activin receptor-like kinase 5
ANGPTL2	Angiopoietin Like Protein 2
ANOVA	Analysis of variance
BIN1	Bridging Integrator 1
BM	Basement Membrane
BMD	Becker muscular dystrophy
CASQ1	Calsequestrin1
CASTOR1	Cytosolic Arginine Sensor For MTORC1 Subunit 1
CAV	Caveolin
DGC	Dystrophin-glycoprotein Complex
DHPR	Dihydropyridine receptor
DMD	Duchenne Muscular Dystrophy
DNA	Deoxyribonucleic acid
E-C	Excitation-Contraction
ECM	Extracellular matrix
eEF2	Eukaryotic elongation factor 2
eIF4E	Eukaryotic translation initiation factor 4E
EMILIN	Elastin microfibril interfacier
eNOS	Endothelial nitric oxide synthase
EOM	Extraocular muscle
FAK	Focal adhesion kinase

GAPDH	Glyceraldehyde 3-phosphate dehydrogenase
GATOR	GTPase activating proteins toward Rags
GC	Glucocorticoid
GLUT4	Glucose transporter type 4
GR	Glucocorticoid receptor
GRMD	Golden retriever muscular dystrophy
HSP70	Heat shock protein 70
HSP90	Heat shock protein 90
IGF-1	Insulin like growth factor-1
IGF-1R	Insulin like growth factor-1 receptor
JP	Junctophilin
kDa	Kilo Daltons
LC-MS	Liquid chromatography mass spectrometry
mAb	Monoclonal antibody
MALDI-TOF	Matrix-assisted laser desorption/ionization
MD	Muscular dystrophy
<i>mdx</i>	X-linked muscular dystrophy mouse model
<i>mdx-4cv</i>	X-linked muscular dystrophy mouse model-4cv
MRF-5	myogenic regulatory factor 5
mTOR	Mamallian target of rapamyocin
Myf5	Myogenic factor 5
MYH	Myosin Heavy chain
MYL	Myosin light chain
MyoD	myogenic differentiation
m/z	Mass/charge ratio
nAChR	Nicotinic acetylcholine receptor
NCAM	Neuronal cell adhesion molecule
NF-KB	Nuclear factor kappaB
nNOS $\mu$	Neuronal nitric oxide synthase
PANTHER	Protein analysis through evolutionary relationships
PBS	Phosphate buffered saline
PI3K	Phosphoinositide 3-kinases
PITX2	Paired-like homeodomain transcription factor 2
PSA	Polysialic Acid

RyR1	Ryanodine receptor 1
S6K1	Ribosomal protein S6 kinase beta-1
SARMs	Selective androgen receptor modulators
SDS	Sodium dodecyl sulphate
SDS-PAGE	Sodium dodecyl sulphate polyacrylamide gel Electrophoresis
SERCA	Sarco(endo)plasmic Reticulum Calcium ATPase
SLR	Spectrin-like repeats
SLRP	Small leucine-rich proteoglycans
SR	Sarcoplasmic Reticulum
STRING	Search Tool for the Retrieval of Interacting Genes/Proteins
TGF	Transforming growth factor
CTGF	Connective tissue Growth Factor
TGFβi	Transforming growth factor beta-induced
T-tubules	Transverse tubules
TnC	Troponin C
UBL40	ubiquitin fusion ribosomal protein L40
UDG	Uracil-DNA glycosylase
VCAM	Vascular cell adhesion molecule
<i>wt</i>	Wild type
μg	Microgram
μl	Microlitre
μm	Micrometre

## **Abstract**

Duchenne muscular dystrophy is a progressive neuromuscular disorder of early childhood. Genetic abnormalities in the *DMD* gene result in a lack of the crucial cytolinker protein named dystrophin. In skeletal muscles, the full-length dystrophin isoform Dp427-M is expressed in the membrane cytoskeleton. Without this membrane stabilising protein, cellular damage occurs, resulting in muscle weakness, severe myonecrosis, chronic inflammation and reactive myofibrosis. Mass spectrometry allows for accurate identification of proteins present in a tissue or biofluid sample. The proteome of a dystrophin-deficient muscle can be compared to that of a healthy control. If a protein shows significant changes in its abundance in dystrophinopathy, then it may be considered a novel biomarker candidate for this disease. This thesis has focused on the description of mass spectrometry-based proteomics with special reference to dystrophic skeletal muscle and biofluids from an established murine animal model. The proteomic profiling was mostly concerned with the chemically induced *mdx-4cv* mutant mouse model of Duchenne muscular dystrophy. Studies have included (i) the detailed description of sample preparation for proteomics and mass spectrometry for bottom-up proteomics, (ii) sample preparation and protein determination for top-down proteomics, (iii) the proteomic identification of markers of membrane repair, regeneration and fibrosis in the aged and dystrophic *mdx-4cv* mouse diaphragm, (iv) the mass spectrometric profiling of extraocular muscle and proteomic adaptations in the *mdx-4cv* mouse, and (v) the identification of biofluid marker proteins of muscular dystrophy in the urine proteome from the *mdx-4cv* mouse. The newly identified proteomic biomarker candidates can now be evaluated for their suitability as indicators of disease initiation and progression. Future studies could potentially establish new protein markers for improved diagnostic and prognostic methods, as well as therapeutic monitoring.



## **Chapter 1**

### **1. Introduction**

## 1.1 MUSCLE BIOLOGY

Muscle is the most abundant tissue in the body, making up approximately 50% of biomass in the human body. It can be categorised into four distinct groups, skeletal muscle, cardiac muscle, smooth muscle and myoepithelial cells. Both skeletal and cardiac muscle are known as striated muscle, for their streaky appearance. The contractile unit of the muscle cell, the sarcomere, is responsible for these striations. It is responsible for the generation of force and rapid movements that are characteristic of this type of muscle. Skeletal muscle fibres are long cylindrical structures that are multi-nucleated. A specific alpha-motor neuron and all its innervated myofibres form a functional motor unit that participates physiologically in an all-or-none response (Mukund and Subramaniam., 2020). In contrast to the below mentioned muscle types, skeletal muscle is voluntary, and controlled by the somatic nervous system. Cardiac muscle contractions pump blood through the body. In order to effectively perform this restless process, cardiomyocytes must be highly resistant to fatigue. This is facilitated by a high concentration of mitochondria (Nguyen et al., 2019). Cardiac muscle is not under voluntary control of the nervous system, and this is a feature that it shares with smooth muscle and myoepithelial cells. Smooth muscle is generally found in the walls of circulatory, respiratory and digestive systems (Donadon and Santoro., 2021). Contraction of smooth muscle is controlled by hormones, nerves, and chemical signals (Webb., 2003). Myoepithelial muscle cells form the basal layer of sweat glands, mammary glands, lacrimal glands and salivary glands. They can contract to expel secretions from these glands (Balachander et al., 2015). In addition to Myocytes, there exists a variety of cell types within muscle tissue. Since it is virtually impossible to separate myocytes from those cells during proteomic analysis preparation, it is worth discussing them. Satellite cells are muscle resident stem cells. These cells proliferate and differentiate to form myofibres and repair muscle. A portion of sc's return to a resting state to replenish the pool (Dowling et al., 2024). Non myogenic cells may also contribute to muscle regeneration, particularly FAP's are considered to be regulators of stem cell function and skeletal muscle regeneration. These mesenchymal stromal cells can differentiate into either fibroblasts or adipocytes. While FAP differentiation can cause fibrosis and muscle degeneration, it also appears that they may support muscle repair by organising the crosstalk between muscle and immune cells (Chen et al., 2022). One example of immune cells that interact with myocytes are macrophages. These white blood cells are heavily involved in the inflammatory response to muscle injury. Macrophages may secrete anti-inflammatory factors to promote muscle tissue repair.

## **1.2 Skeletal muscle development and regeneration**

In early embryogenesis, three germ layers are formed as the precursors to all bodily tissues that will develop. These are the ectoderm, mesoderm, and endoderm. The mesoderm gives rise to muscle cells and connective tissue (Arnold and Robertson., 2009). Smooth muscle in the pupil and sphincter, and myoepithelial cells in the sweat and mammary glands are exceptions to this, as they are ectodermic in origin. The transcription factors PAX-3 and PAX-7 control migration of myoblasts, the muscle precursor cells. When these myoblasts have migrated to their desired location, the process of differentiation begins. MyoD and Myf5 are two additional myogenic regulatory factors, both considered to be indicators that muscle specification is beginning (Pownall et al., 2002). Myogenin and MRF-5 are two additional regulatory factors activated later, to initiate differentiation of myoblasts into myocytes. The mono-nucleated myocytes eventually fuse to form multinucleated, mature, contracting muscle fibres (Mukund and Subramaniam., 2020). A subset of precursor cells do not differentiate, instead, they remain in a quiescent state, located between the basal lamina of the extracellular matrix, ECM, and the sarcolemma membrane (Lepper and Fan., 2010). This group of cells are termed the satellite cells. When skeletal muscle is injured, satellite cells awaken from their resting state, proliferate and differentiate into mature fibres to replace the injured ones (Yin et al., 2013). In a case of chronic muscle damage, such as Duchenne muscular dystrophy, the satellite cells are unable to keep up with the constant need for muscle repair. A lack of proper asymmetric satellite cell divisions and impaired differentiation is most likely the underlying mechanism of impaired repair mechanisms in X-linked muscular dystrophy (Chang et al., 2016). The balance between self-renewal of muscle stem cells and differentiation appears to be abnormal in dystrophin-deficient muscles. Satellite cell activation fails to efficiently recover dystrophic muscles due to impaired asymmetric cell divisions. The lack of dystrophin expression seems to affect key regulators of satellite cell polarity causing a reduced differentiation of myogenic precursors, which are essential for myofibre regeneration.

### **1.1.3 Skeletal muscle structure**

Skeletal muscle is composed of bundles of myofibres. Each myofiber contains thousands of myofibrils, which run parallel to each other on the long axis of the myocyte. Each myofibril has a diameter of between one and two micrometres, and contains sarcomeres, capable of producing contractile force. Sarcomeres have thick myosin-containing filaments and thin actin-containing filaments. Thin filaments are made up of two strands of actin, which twist together to form an alpha helix, bound to this helix are the regulatory proteins tropomyosin and troponin.

Tropomyosin lies in the grooves of the actin helix. Each tropomyosin molecule has an associated troponin complex, containing troponin-C, the binding site for calcium ions, troponin-I that inhibits actin-myosin binding, and troponin-T that binds strongly to tropomyosin (Squire and Morris., 1998). Thick filaments are composed of myosin, an enzymatic molecular motor protein formed from the polymerisation of two heavy chains and four light chains.

#### **1.1.4 Skeletal muscle contraction**

Skeletal muscle can be considered as the mechanical device of the central nervous system, an intermediary between the brain and the world, that converts as a biochemical transducer potential energy into movement (Mukund and Subramaniam., 2020). Electrical signals sent from the motor cortex coordinate contraction and relaxation of these muscles. These signals are carried by the mesh of nerves extending out from the brain. Motor neurons make contact with muscles at specialised regions, the neuromuscular junctions. Voltage-gated channels open in response, and flux of calcium ions causes a local conformational change, releasing acetylcholine. The neurotransmitter acetylcholine crosses the cleft-like gap between muscle and nerve. Upon binding to its receptor, the nicotinic acetylcholine receptor, on the muscle plasma membrane, sodium and potassium ion channels open. As potassium ions exit the cell and are replaced by the positively charged sodium ions, a charge builds up. This charge produces the propagation of an action potential (Raghavan et al., 2019). The term excitation-contraction coupling, ECC, refers to the conversion of this action potential into muscle contraction. Figure 1 shows an overview of the complex arrangement of the proteins involved in excitation–contraction coupling. This potential energy travels across the oppositely charged sarcolemma and enters into socket-like indents known as transverse tubules, the T-tubules.

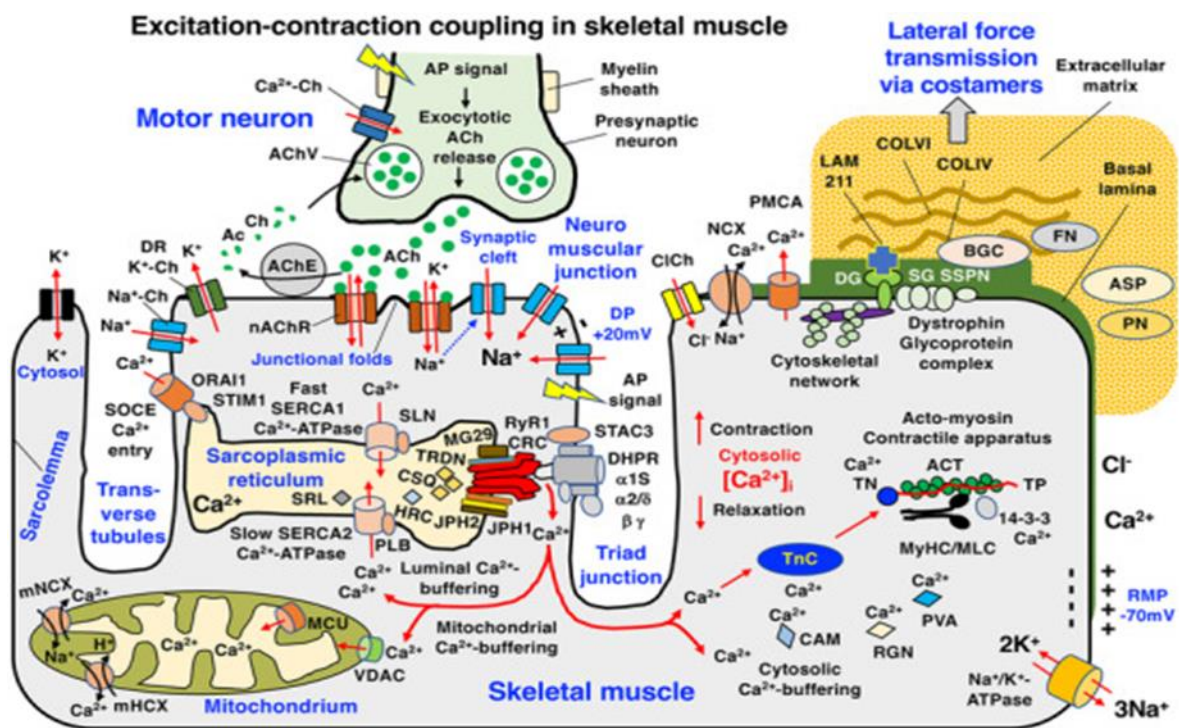


**Figure 1.** Diagrammatic overview of the complex arrangement of the proteins involved in excitation–contraction coupling and  $\text{Ca}^{2+}$ -homeostasis in skeletal muscles. ACh, acetylcholine; AChE, acetylcholinesterase; AChV, acetylcholine vesicle; ACT, actin; AP, action potential; ASP, asporin; BGC, biglycan; CaCh, calcium channel; CAM, calmodulin; ClCh, chloride channel; COL, collagen; CSQ, calsequestrin; DG, dystroglycan; DHPR, dihydropyridine receptor; DP, depolarisation; DR, delayed rectifier; FN, fibronectin; HRC, histidine-rich calcium binding protein; JPH, junctophilin; KCh, potassium channel; LAM, laminin; MCU, mitochondrial calcium uniporter; MG29, mitsugumin-29; MLC, myosin light chain; mHcX, mitochondrial hydrogen-calcium exchanger; mNCX, mitochondrial sodium-calcium exchanger; MyHC, myosin heavy chain; NaCh, sodium channel; nAChR, nicotinic acetylcholine receptor; NCX, sodium-calcium exchanger; ORAI1, calcium release-activated calcium modulator 1; PLB, phospholamban; PMCA, plasmalemma calcium ATPase; PN, periostin; PVA, parvalbumin; RGN, regucalcin; RMP, resting membrane potential; RyR1-CRC, ryanodine receptor calcium release channel; SERCA; sarcoplasmic reticulum calcium ATPase; SG, sarcoglycan; SLN, sarcolipin; SOCE, store-operated calcium entry; SRL, sarcolumenin; SSPN, sarcospan; STAC3, SH3 and cysteine-rich domain 3 protein; STIM1,

stromal interaction molecule 1; TN, troponin; TP, tropomyosin; TRDN, triadin; VDAC, voltage-dependent anion channel. Image taken from Dowling et al., 2020

The dihydropyridine, DHPR, receptor complex is located in these T-tubules, subunit  $\alpha$ -1 of this protein senses the voltage from the action potential, and changes conformation. This in turn alters the shape of the associated ryanodine receptor, RyR1, on the sarcoplasmic reticulum, SR. The SR is a specialised organelle responsible for storing calcium ions. The conformational change to RyR1 causes a flux of  $\text{Ca}^{2+}$ -ions from the SR to the cytoplasm of the cell (Bolaños and Calderón., 2022). As  $\text{Ca}^{2+}$  floods into the cytoplasm, it binds with the specialised calcium binding module of troponin-C, termed the EF-hand domain. This is a highly efficient mechanism for grabbing calcium ions, and the sequence of this domain is conserved across many calcium binding proteins (Grabarek., 2011). Troponin-C with calcium attached can no longer mediate the binding of tropomyosin to actin. This frees up binding sites for myosin to attach to (Kuo and Ehrlich., 2015). Myosin heads will crawl along the actin filament, hydrolysing ATP and generating muscle contraction as they move. This process is known as cross bridge cycling (Huxley., 1957). Muscle is attached to bones through sheaths of connective tissue, called tendons. The contraction patterns of skeletal muscle allows for rhythmic movements of the skeletal system, to mediate locomotion of the body (Maurel et al., 2017).

## **1.2 Duchenne muscular dystrophy**

Duchenne muscular dystrophy, DMD, is a debilitating genetic muscle wasting disease, brought about by primary abnormalities to the *DMD* gene (Guiraud et al., 2015). DMD is an X-linked recessive disorder, affecting approximately 1 in 5,000 live male births globally (Mah et al., 2016). In Ireland, the prevalence of DMD in the adult population is approximately 3 in 100,000, while the prevalence of Becker's muscular dystrophy, BMD, a milder form of this disease, is 2.2 in 100,000 (Lefter et al., 2017). It is estimated that about two-thirds of DMD mutations are passed on from mothers to their sons. As females are usually unaffected, these mothers would likely not have known that they carried the mutations. the remaining cases result from spontaneous mutations (Lee et al., 2014).

DMD is induced by out of frame reading mutations to the X-linked *DMD* gene. This is one of the largest human genes, comprising 0.1% of the total human genome. it spans around 2.4 million bases and comprises 79 exons (Koenig et al., 1988). Genetic defects to this gene result in the almost complete loss of the membrane cytoskeletal protein dystrophin, Dp427-M. These mutations can be duplications, point mutations, or small rearrangements.

Symptoms of this disease typically start at 3-5 years of age, and often include difficulty with motor skills and frequent falls. The calf muscles may be large and feel rubbery or firm due to pseudo-hypertrophy, this is the replacement of functioning muscle fibres with fibro-fatty tissue (Cros et al., 1989). Diagnosis is usually confirmed by a blood test confirming raised levels of the serum creatine kinase (Adam et al., 1993). Under examination, dystrophic fibres display abnormal diameters, central nucleation, cellular degeneration, and inflammation. These phenotypic alterations are clear from multiple perspectives. The *mdx-4cv* mice have less muscle mass than their wild type counterparts. Upon examination of histological stains, as seen in figure 2, central nucleation and abnormal fibres are visible. When the muscles of these two phenotypes are compared, we see the proteomic evidence of muscle wasting and fibrosis. Chapter 4 delves into the effects that ageing plays in this disease. Boys with duchennes are often wheelchair bound by their early 20's, and have a much decreased life expectancy compared to the general population. Our study details the alterations that occur when severe muscular dystrophy is compounded by ageing. Figure 2 shows the histological and immunofluorescence microscopical characterisation of these dystrophic fibres.

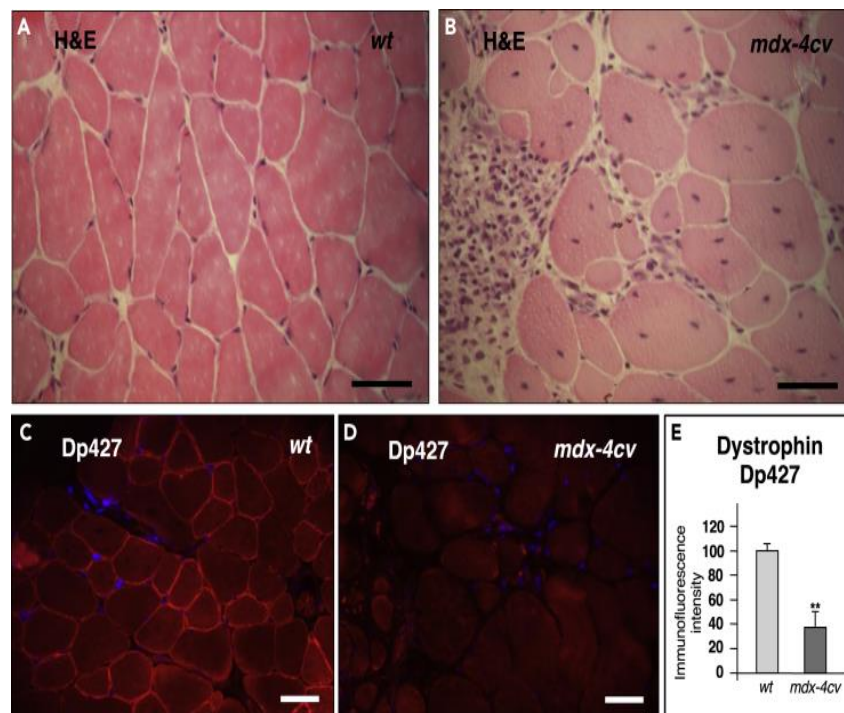


**Figure 2.** Histological and immunofluorescence microscopical characterization of skeletal muscle from the *mdx-4cv* mouse model of Duchenne muscular dystrophy. Shown are transverse cryosections of wild-type (wt) (A and C) and *mdx-4cv* *gastrocnemius* muscle stained with

hematoxylin and eosin (H&E) (A and B) and labelled with antibodies to the full-length Dp427 isoform of dystrophin (C and D). In (E) the analysis of immunofluorescence intensities is shown Dystrophic muscle fibers show abnormal fiber diameters, central nucleation, cellular degeneration, and inflammation, as well as the almost complete loss of dystrophin. Scale bar, 50  $\mu\text{m}$ . \*Image taken from Dowling et al., 2020

### **1.2.1 Dystrophin protein**

Full-length dystrophin is a 427 kDa membrane cytoskeletal protein. It provides structural stability to the sarcolemma as part of a multi-protein complex. The structure of Dp427-M highly resembles that of a similar protein, utrophin. In DMD and animal models, utrophin is up regulated to compensate for lack of dystrophin. Dp427-M consists of 4 distinct functional domains. The N-terminal actin binding domain that contains two  $\alpha$ -helical rich calponin homology motifs. The calponin domains of dystrophin and utrophin share high sequence similarity but differ in their structural stability and actin-binding affinity (Bandi et al., 2015). Nearly one-half of DMD-causing missense mutations are located in this actin-binding region of dystrophin (Henderson et al., 2010). A large central rod domain follows, containing twenty-four spectrin-like repeats, SLR, interspaced by 4 proline-rich hinge regions. Utrophin contains one less SLR, resulting in a 395 kDa protein transcript (Culligan and Ohlendieck., 2002). The presence of these SLR places dystrophin into the spectrin family of proteins (Broderick and Winder., 2005). Actinin, a protein responsible for attaching actin filaments to the sarcomeric Z-line, is thought to be the ancestor of this group of proteins (Murphy and Young., 2015). The rod domain also mediates dystrophin interaction with microtubules, a crucial component of the cytoskeletal structure (Belanto et al., 2014). Between the rod and the C-terminal of this protein is a cysteine-rich domain that binds the transmembrane beta-dystroglycan complex, as well as ankyrin, a protein that helps localise dystrophin to the sarcolemma (Ayalon et al., 2008). the two EF-hands, and a zinc finger are located in this region, both involved in calcium binding. The carboxy-terminal contains two coils with high similarity to SLR. These coils provide binding sites for the signalling proteins dystrobrevin and syntrophins (Sadoulet-Puccio et al., 1997).

### **1.2.2 Dystrophin-glycoprotein complex**

Dp427-M forms the core of a sarcolemma located complex of proteins known as the dystrophin–glycoprotein complex, DGC. The major role of this molecular assemble is to provide a stabilizing linkage between the intracellular actin cytoskeleton and laminin-211 in

the basal lamina of the extracellular matrix (Ervasti and Sonnemann., 2008). The DGC also serves a scaffold for various enzymes to anchor to and signal from (Constantin., 2014). This supramolecular complex helps mediate the transmission of force laterally from the sarcomere to the connective tissue surrounding the muscle (Peter et al., 2011). Figure 3 illustrates the functions of this complex.

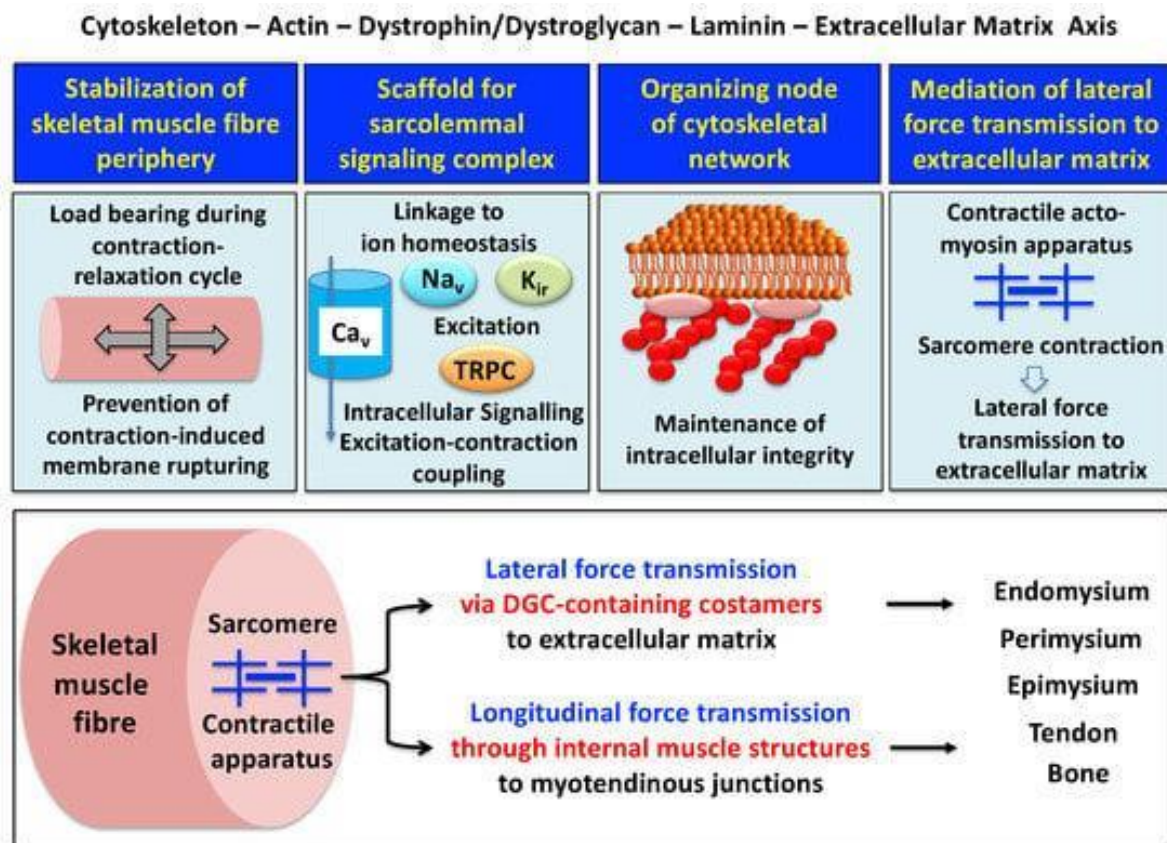


Figure 3 Outline of the main functions of the dystrophin node and its associated protein complex as integrators of fiber stability, cellular signaling. Cytoskeletal organization and lateral force transmission. The upper panels summarize the main functions of the trans-sarcolemmal axis formed by the intracellular actin cytoskeleton, the dystrophin–dystroglycan complex, the basal lamina component laminin and the extracellular matrix. The lower panel illustrates the physiological concept of force transmission in skeletal muscles, which can be divided into a laterally and a longitudinally acting system. In conjunction with other costameric proteins, the dystrophin–glycoprotein complex (DGC) is majorly involved in lateral force transmission to the extracellular matrix. Taken from Dowling et al 2021.

In addition to Dp427-M, many diverse proteins converge to form the DGC. These are: (i) the cytosolic components alpha/beta-dystrobrevin and alpha/beta-syntrophin, which interact with

the cysteine-rich domain of dystrophin (Bhat et al., 2019), (ii) integral glycoproteins, including the alpha/beta/gamma/delta-sarcoglycan subcomplex, (iii) the highly hydrophobic protein sarcospan, (iv) the main carboxy-terminal dystrophin-binding partner beta-dystroglycan (Tarakci and Berger., 2016), (v) Laminin-211 and its extracellular receptor alpha-dystroglycan, which is a proteolytic cleavage product of the pre-dystroglycan molecule (Barresi and Campbell, 2006), and (vi) the intracellular actin cytoskeleton that links to an amino-terminal and a rod domain site of full-length dystropin (Rybakova and Ervasti., 1997).

Figure 4 shows how these proteins organise molecularly.

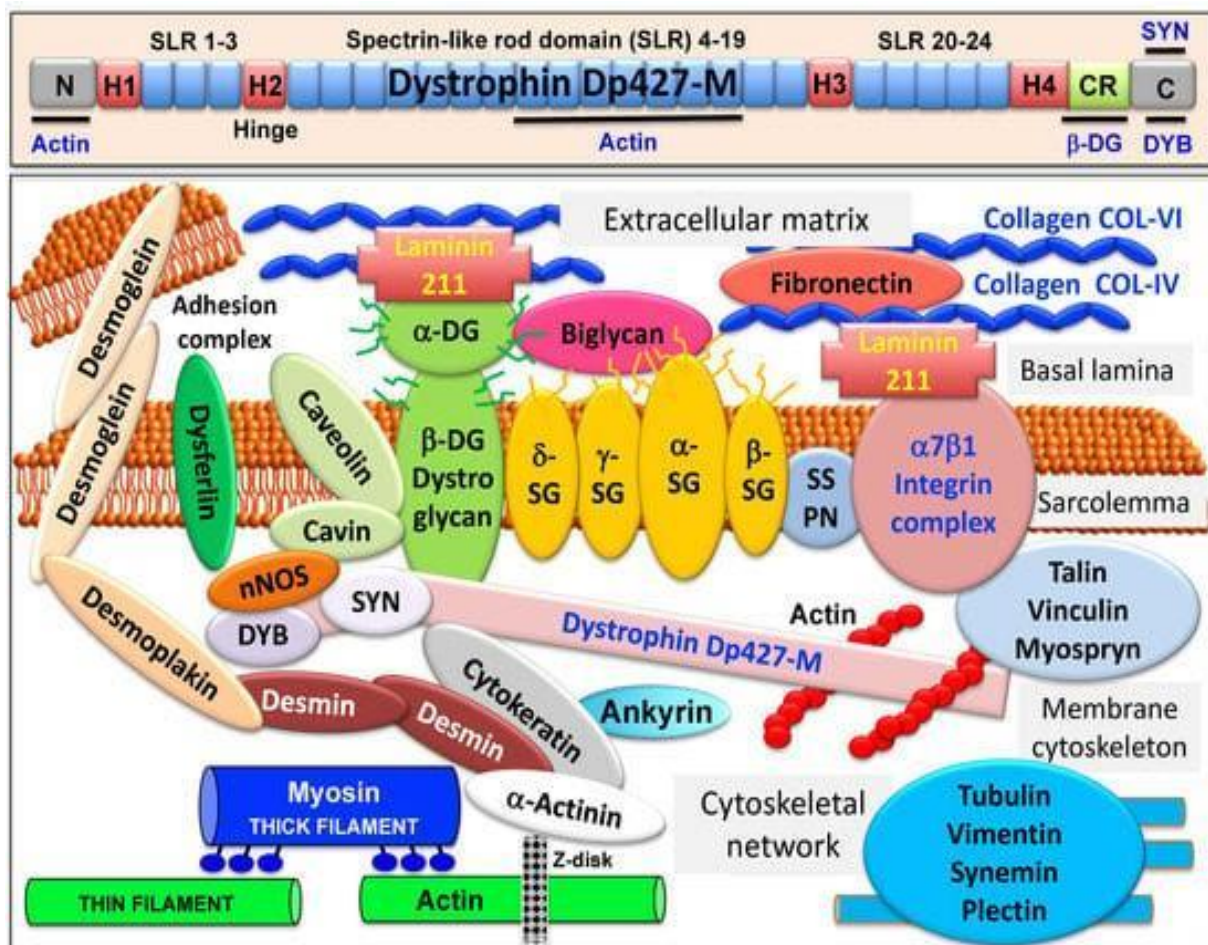


Figure 4 Overview of the domain structure of dystrophin and the diverse interactions of the dystrophin–glycoprotein complex in skeletal muscle tissues. The upper panel shows a diagrammatic presentation of the main molecular domains of dystrophin isoform Dp427-M, including actin-binding sites at the N-terminus and central rod domain, proline-rich hinge regions (H1 to H4), spectrin-like rod (SLR) domains 1–3, 4–19 and 20–24, a cysteine-rich domain with binding sites for integral beta-dystroglycan (DG), the cysteine-rich domain (CR) and the C-terminus with binding sites for dystrobrevin (DYB) and syntrophin (SYN). The

lower panel shows a model of the spatial configuration of the dystrophin complexome in skeletal muscle fibers. Shown is the dystrophin core complex consisting of the dystrophin isoform Dp427-M, dystroglycans (DG), sarcoglycans (SG), sarcospan (SSPN), syntrophins (SYN) and dystrobrevins (DYB), as well as the wider dystrophin-associated network that forms associations with the extracellular matrix, the sarcolemma, the cytoskeleton and the sarcomere. Taken from Dowling et al, 2021.

Deficiency of dystrophin results in a destabilised DGC, and subsequently leads to micro-rupturing of the unstable sarcolemma. This micro-rupturing appears to play a major role in triggering degeneration of muscle fibres, and is associated with impaired calcium homeostasis, sterile inflammation, and reactive myofibrosis.

### **1.2.3 Dystrophin isoforms**

In addition to the Dp427-M isoform expressed in skeletal and cardiac muscle, There also exist full length isoforms in the brain cortex, Dp427-B, and in the Purkinje neurons, Dp427-P (Upadhyay et al., 2020). In addition, four shorter isoforms that arise through transcription from different promoters in the *DMD* gene also exist. These are Dp260-R found in the retina, Dp140-B/K expressed in the brain and kidney, Dp116-S in Schwann cells, and Dp71-B/U in brain and nonmuscle tissues (Tennyson et al., 1995). Disruption to the brain located isoforms is likely involved in the cognitive impairment and low IQ often associated with DMD (Anderson et al., 2002). DMD is also associated with a high incidence of a host of neurological disorders, including epilepsy, autism, ADHD, and dyslexia (Hendriksen et al., 2018).

## **1.3 Treatments for Duchenne muscular dystrophy**

### **1.3.1 Corticosteroids**

Glucocorticoid therapy is currently the leading standard for treating DMD. Prednisone & deflazacourt are the most commonly prescribed treatments for DMD (Patterson *et al.*, 2023). Corticosteroids are a group of catabolic anti-inflammatory steroid hormones released by the adrenal cortex. Glucocorticoids, GC, are the most well studied member of this group. Most of the cortisol released by the adrenal cortex is inactive through its binding to corticosteroid-binding globulins in the blood, and much of the remainder is bound to albumin (Ramamoorthy et al., 2016). Furthermore, free cortisol is liable to conversion to cortisone by 11 $\beta$ -hydroxysteroid dehydrogenase. Various synthetic GC have been developed based on the

structure of cortisol and hydrocortisone, the endogenous GC's (Buchwald and Bodor., 2004). Most of these synthetic hormones are not bound to globulins, and are not converted to cortisone, in addition they bind with high affinity to the glucocorticoid receptor, GR. Upon forming a complex with their receptor, both molecules translocate inside the nucleus, Where it binds with DNA sequences and mediates transcription of anti-inflammatory proteins (Kinyamu and Archer., 2004). In addition to this, GR interacts with pro-inflammatory transcription factors, such as NF-KappaB. The cross-talk between these proteins is likely important in maintaining homeostasis for an organism during an immune response (McKay and Cidlowski., 1999). These actions take about 30-60 minutes to initiate, far more rapid effects are also possible through non-translational interactions with membrane associated receptors. An example of this is the activation of eNOS through the pi3k/akt pathway (Hafezi-Moghadam et al., 2002).

The synthetic glucocorticoids prednisone and deflazacort are the current standard of treatment for DMD sufferers. Many randomized control trials using these drugs have shown a significant improvement in strength and function (Bonifati et al., 2000, Mendell et al., 1989). The precise mechanism in which GC improve strength in MD has not been fully elucidated, but there is evidence that they can protect the sarcolemma from dystrophic related injuries. A single dose of GC is enough to stimulate production of annexin A1 and A6, proteins crucial for plasma membrane repair (Quattrocelli et al., 2017). This increased sarcolemmal repair may improve E-C coupling, and reduce cytosolic calcium levels (Metzinger et al., 1995). A study of mice cardiomyocytes found that Dexamethasone promotes the development of T-tubules and reduces the distance between L-type voltage channels and ryanodine receptors (Seidel et al., 2019). Dexamethasone also up-regulates utrophin, an orthologue of dystrophin, in DMD myotube cultures (Pasquini et al., 1995), while prednisone can protect muscle proteins from proteolysis (Rifai et al., 1995).

Despite the many benefits of using GC's as a treatment for DMD, it is not without ill consequences. The prolonged usage of GC's is associated with many adverse effects including, but not limited to, weight gain, osteoporosis, and behavioural changes (Matthews et al., 2016). Various dosing methods have been tested in attempts to maintain the benefits while avoiding the negatives, such as 10 days on followed by 10 days off. This treatment method resulted in fewer vertebral fractures than the daily control cohort, at the cost of a decreased ambulation (Crabtree et al., 2018).

### **1.3.2 Anabolic steroids**

There have been a limited number of studies examining the effects of anabolic steroid use on DMD symptoms, mainly occurring in the 1960's. Administration of norethandrolone to dystrophic mice at a dosage of 5mg/kg thrice weekly slowed progression of the disease and prolonged the median life from 13 weeks to 33 weeks. This steroid did not restore any already lost muscle function (Dowben et al., 1959). Following these findings, a double blind clinical trial was undertaken, where 30 patients with muscular dystrophy were given 0.5 mg/kg body weight norethandrolone daily for five months. Initial results were a slight improvement in muscle function along with increased feeling of wellbeing. This trial did not progress long enough to determine if norethandrolone slowed the rate of progression and enhanced lifespan. However, it was noted that in some patients, cessation of the drug led to a rapid progression of disease (Dowben and Perlstein., 1961). A similar result of moderate improvement followed by rapid degeneration was seen in a study administering the steroid dianabol (Gamstorp et al., 1964). Patients who received the anabolic steroid oxandrolone over a 6 month period had stronger elbow flexion and knee extension than control patients. The main benefit of the drug from this study was the absence of adverse effects reported (Fenichel et al., 2001). Usage of selective androgen receptor modulators, SARMs, may provide some of the benefits of androgenic steroids while negating the unwanted side effects. This class of drugs is relatively new, but results are optimistic. *Mdx* mice treated with the SARM GLPG0492 showed a clear improvement in both strength, and fatigue resistance (Cozzoli et al., 2013).

### **1.3.3 Insulin-like growth factor IGF-1**

Growth factor therapies offer an alternative to steroid treatment. One such growth factor that has been identified as being potentially beneficial for dmd patients is insulin-like growth factor, IGF-1. IGF-1 stimulates both the proliferation and differentiation of skeletal muscles. It is thought that IGF-1 could preserve motor function while reducing unwanted GC side effects. Insulin-like growth factor-1, IGF-1, is a crucial growth factor involved in regulating protein synthesis, as well as degradation. Muscle specific expression of IGF-1 can counter negative aspects of dystrophin loss by increasing hypertrophy and strength, while reducing fibrosis and myonecrosis (Barton et al., 2002). When this protein is secreted from the liver, many molecules of it will bind to the associated plasmalemmal transmembranous receptor protein, signalling for muscle hypertrophy to begin, through the PI3k/akt/mTor pathway.

The extent of this signalling is significant, mice with IGF-1 or IGF-1R genes knocked off, were up to 45% smaller than controls (Accili et al., 1999). A disrupted myofibril structure is also observed, similar to that in muscular dystrophies (Powell-Braxton et al., 1993). A

transgenic over-expression of IGF-1 in *mdx* mice muscles can prevent the usual muscle loss associated with aging (Barton et al., 2002). This improves EC coupling in *mdx* muscle fibres, through an increased transcription of the DHPR isoforms (Schertzer et al., 2008).

A reduction in the amount of signals that radiate out from IGF-1, in a *Caenorhabditis elegans* model of muscular dystrophy, has been shown to protect muscle cells from the increased necrosis often associated with dystrophin deficient flesh (Oh and Kim., 2013). The *mdx* diaphragm was also found to have an increased contractile ability following 8 weeks of IGF-1 treatment (Gregorevic et al., 2002).

Reduced vertical growth is a feature of DMD, and this growth retardation can be compounded by glucocorticoid use (Schäcke et al., 2002). A six-month study administering recombinant human IGF-1, alongside glucocorticoids to boys with DMD resulted in increased growth but did not improve motor function (Rutter et al., 2020). Similar results were found in *mdx* mice administered with IGF-1 and growth hormone (Wood et al., 2022). IGF-1 also calls for hypertrophy by competing with myostatin, the myokine protein that has a direct inhibiting effect on muscle hypertrophy. Genetic reduction of myostatin results in reduced atrophy and collagen disposition in a model of Oculopharyngeal muscular dystrophy, OPMD, associated with muscle weakness around the upper eyelids and the pharynx (Harish et al., 2020, Harish et al., 2019). It is possible that a reduction of myostatin would have similar effects in other muscular dystrophies.

IGF-1 seems to work synergistically with other therapeutic approaches. Co-treatment with glucocorticoids promotes myogenic differentiation (Fang et al., 2020), and co-injecting viral vectors for micro-dystrophin along with IGF-1 had better results than either of these individually (Abmayr et al., 2005). Using a combination of therapies for DMD can often give better results (Cordova et al., 2018).

#### **1.3.4 Anti-fibrotic therapy**

In DMD, the chronic muscle fibre degeneration, and subsequent regeneration process, results in progressive substitution of skeletal muscle fibres with noncontractile fibrotic tissue. This results in decreased muscular motor function (Desguerre et al., 2009). The gradual accumulation of ECM proteins such as collagen, impairs muscle function, negatively affects muscle regeneration after injury and increases muscle susceptibility to re-injury (Mahdy, 2019).

One approach to reducing fibrosis is modulation of the effects of transforming growth factor- $\beta$ , TGF- $\beta$ , and Connective tissue growth factor, CTGF. These growth factors drive fibrosis.

The small proteoglycan, decorin, can interact with and inhibit both of these pro-fibrotic growth factors (Vial et al., 2011, Yamaguchi et al., 1990). Another method of regulating these pathways is the reduction of angiotensin-ii. The main function of this protein is to regulate blood pressure, but it also induces the expression of TGF and CTGF. Losartan is a drug that has been used to block the angiotensin-ii receptor and reduce fibrosis (Garg et al., 2014). In DMD, the prolonged activation of the innate immune response leads to chronic inflammation, and subsequently to more fibrosis (Tulangekar and Sztal., 2021). The antioxidant N-acetylcysteine has been implemented previously to combat this inflammation and reduce fibrosis (Burns et al., 2019). Various different drugs have been trialled at clinical and pre-clinical levels to determine their effectiveness as anti-fibrotic treatments (Muraine et al., 2023).

### **1.3.5 Genetic engineering**

Adenovirus-associated virus, AAV, are small viruses that infect humans. due to their general lack of pathogenicity and stable integrative ability, they are widely used for gene transfer. AAV-based therapies show promising results for treatment of various genetic disorders, including muscular dystrophy (Muraine *et al.*, 2022). Through the use of vectors based on the recombinant AAV, it is possible to implant healthy genes, dystrophin however, is too large to be correctly generated by the adeno-virus. To combat this, synthetic micro-dystrophin genes have been developed. Many of these truncated genes protect the sarcolemma from contraction-induced injury and increase force generation (Davies and Guiraud., 2019). Solid biosciences have developed a novel AAV gene transfer called SGT-003. This gene transfer contains an engineered microdystrophin, which has been designed to produce a functioning form of the dystrophin in skeletal and cardiac muscles. Exon skipping is another genetic therapy, that aims to read over the out of frame mutations, to produce functional dystrophin (Eser and Topaloğlu., 2022). There are currently exon skipping therapies undergoing clinical trials. One such therapy being developed by Sarepta Therapeutics aims to administer high doses of eteplirsen to skip exon 51 of the DMD gene. This randomised, double-blind study has been underway since 2020, and results look promising. Muscular exercise helps to mediate the restoration of dystrophin, following exon skipping therapy (Monceau et al., 2022).

### **1.4 Muscle stimulation and dystrophinopathy**

Resistance training leads to increased muscle size and strength, as well as muscle protein synthesis (Adams and Bamman., 2012). This increased level of MPS is due to the activation of the mammalian/mechanistic target of rapamycin, mTOR, pathway (Rennie et al., 1982). The

muscle weakness that affects boys with DMD is highly progressive and accompanied by sterile inflammation and reactive myofibrosis. Natural muscle aging, often referred to as sarcopenia of old age, is also characterized by muscle degeneration and fibrotic changes. Chapter 4 explores how the proteomes of these pathologies compare, and whether aging compounds the dystrophic phenotype. The only reliable treatment to sarcopenia is exercise (Butler-Browne et al., 2018). Unfortunately, this treatment does not work so well for DMD patients. Multiple studies demonstrate that dystrophic muscle incurs greater damage than healthy skeletal muscle when eccentrically contracted (Petrof et al., 1993, Moens et al., 1993). When muscles are eccentrically lengthened under load, the actomyosin bonds are forcibly detached (Flitney and Hirst., 1978). This cross-bridge disruption places a heavy load on the sarcomere. In the dystrophic muscle, where the plasma membrane is not secured, the damage occurred is too great for the body to adequately repair. Passive stretching of muscles may provide a safer method of exercising dystrophic muscles. Stretching the muscle also activates the mTor pathway, and does so to a greater degree in dystrophic muscle than in healthy (Dogra et al., 2006). Another way to stimulate the muscles while avoiding the stretch-shortening cycle, and the damage that it occurs, is through isometric contraction. A person performing a wall-sit, or trying to push or pull an immovable object, is isometrically contracting. Force is generated, but the muscle is not lengthened. In *mdx* mice, 4 weeks of performing isometric training increased hypertrophy and the number of satellite cells present. It also decreased fibrosis (Lindsay et al., 2019). DMD Boys who completed a 12 week isometric exercise programme, in which they trained 3 times a week, displayed significantly greater leg strengths and a greater ability to descend stairs (Lott et al., 2021). Performing resistance training with minimal weight seems to be another avenue to gaining muscle. The minimised loads result in less muscle damage. For DMD patients, submaximally exercising one quad, while using the other quad as a control muscle, results in greater torque in the exercised muscle during the protocol, and for a limited time afterwards (de Lateur and Giaconi., 1979). Water based aerobic exercise has also been suggested and trialled as an alternative way to exercise dystrophic muscle, while minimising the force placed on muscles (Suslov et al., 2023, Hind et al., 2017). Progressive respiratory muscle weakness leads to deterioration of pulmonary function. Pulmonary function tests can be used to determine the severity of the disease (Levine et al., 2023). This chronic respiratory weakness is a major contributing factor to mortality in DMD (Robertson and Roloff., 1994). Respiratory exercises have therefore been recommended as part of the exercise regime for sufferers of muscular dystrophies (Gozal and Thiriet., 1999). Respiratory endurance has been shown to be improved by 46% after 6 weeks of respiratory training (Topin et al., 2002).

Assisted cycling is one method in which boys with DMD can train their respiratory function, and this has also been shown to delay functional deterioration in the disease (Jansen et al., 2013). Studies have shown that yoga breathing exercises are capable of increasing pulmonary function in DMD patients (Dhargave et al., 2021, Rodrigues et al., 2014). Similarly, yoga exercises have also been linked to improved heart function in DMD patients (Pradnya et al., 2019).

## **1.5 Animal models of DMD**

### **1.5.1 *mdx* mice**

In 1984, it was discovered that some members of a C57BL/10 mice colony had 3+ fold the expected levels of serum pyruvate kinase. Upon closer inspection, these mice also had above average serum levels of creatine kinase, and displayed signs of progressive degenerative myopathy, similar to DMD. It was determined that these abnormalities were caused by a mutation on the X-chromosome, and so, this variant of mice was named *mdx* (Bulfield et al., 1984). Since this time, it has become the most popular animal model for studying DMD. Additional studies determined that these mice displayed muscle degeneration following three weeks of age, but that a full rapid regeneration occurred soon after. The authors declared that *mdx* was not an adequate model of DMD (Dangain and Vrbova., 1984). Five years following the discovery of the *mdx* mice, four additional alleles were induced through chemical mutagenesis with the known mutagen N-ethylnitrosourea (Chapman et al., 1989). One of these mutations, termed *4cv*, was caused by a nonsense mutation at base 7916 of exon 53 caused by a C to T transition (Im et al., 1996). Often with *mdx* models, dystrophin-positive muscle cells called revertants will occur, interfering with data. The *mdx-4cv* mice have approximately 10-fold fewer mutant revertant fibres than the *mdx* and *mdx-2cv* mutants (Danko et al., 1992). This lack of revertant fibres, combined with an increased severity of disease pathology, makes the *mdx-4cv* mouse the ideal model for studying dystrophic myofibrosis. While other models like the double knockout *mdx-utr* offer a more severe phenotype, it is difficult to determine if improvements are due to addressing the lack dystrophin, or that of utrophin. For this reason *mdx-4cv* remains the ideal model to study this disease. Many mice models of DMD have developed from the original *mdx* mice, A comprehensive list can be found in (Dowling et al., 2023).

### **1.5.2 GRMD**

Cases of dystrophic dogs have been described as early as 1951 (Innes et al., 1951). Over twenty different dog breeds have been confirmed to be dystrophin deficient, and of these the golden retriever GRMD model is the most widely studied. The dystrophin deficiency of this model comes from an mRNA reading mistake, and not from gene deletion. A point mutation at an intron 6 splice site leads to a truncated dystrophin transcript (Sharp et al., 1992). This mutation results in a more severe phenotype than that seen in mdx mice. Many preclinical trials of potential treatments for DMD have been tested in this model (Kornegay et al., 2012).

### **1.5.3 *Caenorhabditis elegans***

*Caenorhabditis elegans* have a short lifespan, and a transparent body, which makes tracking cell lines easy. This coupled with the complete sequencing of their genome, which contains many homologous genes to those found in humans, makes them a viable animal model for studying many diseases (Markaki and Tavernarakis., 2020). Many of these homologous proteins form an intracellular complex similar to the DGC. Mutations to either *dys-1* or *dyb-1*, will result in a similar phenotype to that of their equivalents dystrophin and dystrobrevin, respectively (Gieseler et al., 1999). In addition to *dys-1*, a gene orthologous to human DMD exists in *Caenorhabditis elegans*, named *hll-1*. Mutant knock offs of both of these genes result in a sufficient DMD model (Gieseler et al., 2000). *C. elegans* is largely considered to be one of the best models for studying drug discovery and screening.

### **1.5.4 Zebrafish**

Due to their high proliferation, rapid growth, and early stage transparency, the zebrafish has been extensively used to model disease. The *sapje* model of DMD are missing their version of dystrophin protein, and display a phenotype similar to DMD. Along with *C. elegans*, This model is ideally suited for drug screening to determine compounds capable of treating the dystrophic phenotype (Kawahara et al., 2011). This model has also been used to analyse the capabilities of exon skipping therapies. In particular, it was demonstrated that 20-30% of dystrophin transcript levels are required to rescue a severe dystrophic phenotype (Berger *et al.*, 2012).

### **1.5.5 *Dmd*<sup>mdx</sup> rat**

An advantage of using a rat model over mice is that rat behaviour has been better characterised. The larger size of a rat also makes them somewhat more convenient to study. One rat model with a lot of potential was developed by (larcher et al., 2014). These

genetically altered rats display severe necrosis, fibrosis, and adipose tissue infiltration. *Dmd*<sup>mdx</sup> show a significant reduction in muscle strength and a decrease in motor activity.

### **1.6.1 Proteomics**

The term proteomics was first coined in 1996 to describe the protein complement of a genome (Wilkins et al., 1996). Proteins are composed of chains of amino acids held together by peptide bonds. The 22 amino acids that make up protein play the role of the building blocks of life. All amino acids share an amino group and a carboxyl group and are linked via peptide bonds. The individual side chain of each amino acid alters their pH and hydrophobicity. Different reading orders of this 22 code sequence results in the expression of all known proteins (Bischoff and Schlüter., 2012). It is estimated that there are approximately 20,000 protein encoding genes in the human genome (Clamp et al., 2007). The number of distinct proteins, known as proteoforms is much higher however, due in part to alternative splicing, where exons from the same gene are joined in different combinations leading to different mRNA transcripts. This accounts for the complexity of the human proteome. In the case of the *DMD* gene, the same gene contains 8 different promoters that produce different tissue-specific isoforms of dystrophin. Two proteins encoded in the exact same manner from the same gene may still differ from each other if they receive any post-translational modification. This addition or removal of different groups leads to altered properties of proteins, and contributes to progression of many diseases, including DMD. For example, the addition of a nitric oxide group to the SR calcium release channel, results in greater calcium leakage from the SR (Bellinger et al., 2009).

### **1.6.2 Mass Spectrometry**

Protein mass spectrometry, MS, measures the mass-to-charge ratio ( $m/z$ ) of a charged peptide particle. In a matrix-assisted laser/desorption ionisation time-of-flight, MALDI-TOF, mass spectrometer, a pulsed laser can release ions from a biological sample. An electrical field applies equal charge to all ions, allowing them to travel as fast as their mass allows. The time of flight sensor measures how long ions take to reach it. This process is a more intricate reflection of how individual proteins will separate in gel-electrophoresis. Prior to MS analysis, the peptides present in the sample have been cleaved at arginine and lysine residues by the digestive enzyme trypsin. This leaves peptide residues of the protein they once formed. A peptide mass fingerprint is generated, showing a spectrum of peaks. This fingerprint can be compared with a fingerprint containing every protein sequence in a genome. This allows the

identification of which peaks represent which peptides. Through comparative MS-based studies, it is possible to identify how proteomes are altered as the body enters different states. An alternative and frequently used MS method, liquid chromatography tandem mass spectrometry, LC-MS/MS, is a powerful tool in proteomic studies. It is a technique combining the physical separation capabilities of liquid chromatography with the mass analysis capabilities of mass spectrometry (Henry & Meleady., 2023). If a protein is expressed differently in diseased state compared to a healthy control, then that protein may be identified as a suitable biomarker of said disease. A biomarker is defined as an objective indication of medical state observed from outside the patient, which can be measured accurately and reproducibly, and which can be evaluated as an indicator of normal biological processes, pathological processes and/or pharmacologic responses to therapy (Strimbu and Tavel., 2010). Classic biomarkers of DMD include lack of dystrophin, as well as raised serum creatine kinase levels. Following a proteomic analysis, gel electrophoresis may be used to separate the constituent proteins of a proteome based on their molecular weight. Subsequent antibody binding and staining allows for a visual confirmation of altered protein levels, as shown in Figure 5.

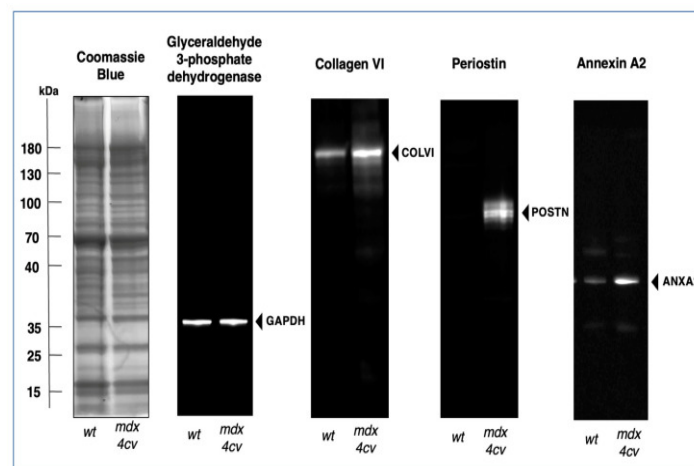


Figure 5 Comparative immunoblot analysis of the dystrophic mdx-4cv mouse diaphragm muscle. Shown is the immunoblotting of the glycolytic enzyme glyceraldehyde-3-phosphate dehydrogenase, used here as a house-keeping protein and loading control, alpha chain-containing collagen VI of the endomysium as an abundant marker of the extracellular matrix, the matricellular protein periostin, and the membrane repair protein annexin A2. Gel electrophoretic separation was carried out with total protein extracts from aged wild-type versus aged and dystrophic mdx-4cv diaphragm. Lanes 1 and 2 contain protein extracts from 15-month-old wt and age-matched mdx-4cv muscle, respectively. On the left is shown a

Coomassie Brilliant Blue-stained protein gel. The other images are identical immunoblots generated by electrophoretic transfer and then labelled with monoclonal antibodies to GAPDH, COL-VI, POSTN, and ANXA2. The position of immuno-labelled protein bands is indicated by arrowheads. Molecular weight standards are marked on the left. Image from Dowling et al., 2023

### **1.7 Aims and outline of this project**

The primary aim of this project was to carry out comparative proteomic profiling studies on tissues and biofluids taken from the *mdx-4cv* animal model of DMD. The absence of Dp427-M dysregulates many aspects of the muscle proteome. It is hoped that by examining these changes, it may be possible to better understand the molecular pathogenesis of dystrophinopathy and also identify novel biomarker candidates of X-linked muscular dystrophy. Chapters 2 and 3 describe the optimization of the methods used to perform the analyses in this thesis. Chapters 4 to 6 describe the findings from proteomic analyses of the young versus aged and severely dystrophic *mdx-4cv* diaphragm muscle, the mildly affected *mdx-4cv* extraocular muscles, and *mdx-4cv* urine, respectively. Chapter 7 is a general discussion of this project. Chapter 8 concludes this thesis.

## Chapter 2

### Sample preparation for proteomics and mass spectrometry from clinical tissue

Published as Chapter 4 in *Proteomics Mass Spectrometry Methods, Sample Preparation, Protein Digestion, and Research Protocols* (Elsevier, 2024)

Gargan S, Dowling P, Ohlendieck K. Sample preparation for proteomics and mass spectrometry from clinical tissue. In: *Proteomics Mass Spectrometry Methods, Sample Preparation, Protein Digestion, and Research Protocols*, 1st Edition - February 16, 2024, Editor: Paula Meleady, Paperback ISBN: 9780323903950 (In press)

**Abstract:** The mass spectrometric analysis of human tissue samples has evolved into a sub-discipline of clinical biochemistry and can be used to determine proteome-wide changes in pathological specimens. This protocol outlines sample preparation for proteomics and mass spectrometry from clinical tissue. The article describes in detail the various steps involved in sample preparation from muscle biopsy material for proteomic surveys, which includes the harvesting, storage and homogenization of tissue material. This is followed by a description of the determination of protein concentration and removal of potentially interfering chemicals, as well as the controlled digestion of proteins to produce representative peptide populations to be analyzed by mass spectrometry.

**Key words:** Biopsy; Clinical proteomics; Mass spectrometry; Neuromuscular disease; Skeletal muscle

#### BEFORE YOU BEGIN

The mass spectrometric analysis of human samples should be based on an optimized proteomic workflow for the unequivocal identification of proteins that are involved in pathogenic processes (Macklin et al., 2020) and should ideally also take into account important ethical principles and a critical assessment of bioanalytical limitations (Mann et al., 2021). Tissue

proteomics can be carried out with freshly biopsied specimens or can be based on stored material in the form of freshly quick-frozen samples, optimal cutting temperature-embedded cellular material or formalin-fixed and paraffin-embedded tissue (Dapic et al., 2019). This protocol describes the proteomic analysis of freshly dissected muscle biopsy material (Nix and Moore, 2020). Most muscle biopsies are taken from *quadriceps*, *deltoid* or *biceps* muscles (Joyce et al., 2012), because extensive histological and histochemical knowledge has been assembled on these types of human skeletal muscles, such as size and distribution of different contractile fiber types (Staron et al., 2000). A video link is available that describes in detail the percutaneous needle biopsy procedure to obtain a tissue sample from the *vastus lateralis* muscle (Shanley et al., 2014). The proteomic analysis of muscle biopsy specimens is crucial for studying the complex pathogenesis of neuromuscular disorders (Dowling et al., 2019) such as sarcopenia of old age (Staunton et al., 2012) or inherited muscular dystrophy (Capitanio et al., 2020). Proteomic analysis of quick-frozen human muscle samples has been shown to result in an excellent coverage of the skeletal muscle proteome (Deshmukh et al., 2021). Prior to the preparation of tissue samples and the extraction of proteins, solutions and buffers should be freshly prepared. In order to avoid the potential degradation of chemicals in biological buffers, solutions should ideally be used the same day. It is crucial to have all essential pieces of equipment needed for the proteomic analysis of biopsy specimens, as listed in below key resources table, in good working order.

### **Timing: 3-4 h**

Buffers and solutions are required for biopsy preparation, tissue homogenization, the determination of protein concentration, the controlled digestion of extracted proteins and the removal of potentially interfering chemicals, as well as the liquid chromatographic separation of digested peptide populations and their subsequent mass spectrometric analysis. It is crucial to prepare all solutions with ultrapure and LC-MS compatible water and analytical grade/suprapure reagents.

1. Biopsy buffer (phosphate-buffered saline, pH 7.4)
  - a) 0.137 M NaCl
  - b) 2.7 mM KCl
  - c) 10 mM Na<sub>2</sub>HPO<sub>4</sub>
  - d) 1.8 mM KH<sub>2</sub>PO<sub>4</sub>

Dissolve 8 g NaCl, 0.2 g KCl, 1.44 g Na<sub>2</sub>HPO<sub>4</sub> and 0.25 g of KH<sub>2</sub>PO<sub>4</sub> by stirring in dH<sub>2</sub>O and bring to 1 L with dH<sub>2</sub>O, and adjust pH to 7.4.

2. Tris buffer, pH 7.8

- a) 0.1 M Tris
- b) HCl (36%)

Dissolve 12.11 g of Tris base by stirring in dH<sub>2</sub>O and bring to 1 L with dH<sub>2</sub>O, and adjust pH to 7.8 with HCl.

3. Ammonium bicarbonate buffer

- a) 50 mM ammonium bicarbonate
- b) 0.1 M Tris buffer, pH 7.8

Dissolve 1.95 g of ammonium bicarbonate in Tris buffer, pH 7.8 and bring to 0.5 L with Tris buffer.

4. Sample homogenization buffer

- a) 4% (w/v) sodium dodecyl sulfate
- b) 0.1 M dithiothreitol
- c) 50 mM ammonium bicarbonate buffer, pH 7.8

Dissolve 4 g of sodium dodecyl sulfate and 1.54 g of dithiothreitol in 50 mM ammonium bicarbonate buffer and bring to 100 mL with 50 mM ammonium bicarbonate buffer, pH 7.8.

5. Urea buffer

- a) 8 M urea
- b) 0.1 M Tris buffer, pH 8.5

Dissolve 120.12 g of urea in 0.1 M Tris buffer and bring to 0.25 L with 0.1 M Tris buffer, pH 8.5.

6. Iodoacetamide solution

- a) 50 mM iodoacetamide
- b) 8 M urea buffer

Dissolve 46 mg of iodoacetamide in urea buffer and bring to 5 mL with urea buffer.

7. Protein digestion buffer

- a) Trypsin protease, MS-grade (50:1 protein:trypsin ratio)
- b) 50 mM ammonium bicarbonate buffer, pH 7.8

Dissolve 20 ng of MS-grade trypsin (per 1000 ng of protein) in ammonium bicarbonate buffer and bring to 5 mL with ammonium bicarbonate buffer.

8. MS sample buffer

- a) 2% (v/v) trifluoroacetic acid
- b) 20% (v/v) acetonitrile
- c) LC-MS grade water

Mix 1.0 mL trifluoroacetic acid with 10.0 mL acetonitrile and bring to 50 mL with dH<sub>2</sub>O.

9. MS activation buffer

- a) 50% (v/v) acetonitrile
- b) LC-MS grade water

Mix 10 mL acetonitrile with dH<sub>2</sub>O and bring to 20 mL with dH<sub>2</sub>O.

10. MS equilibrium/wash solution

- a) 0.5% (v/v) trifluoroacetic acid
- b) 5% (v/v) acetonitrile
- c) LC-MS grade water

Mix 0.25 mL trifluoroacetic acid with 2.5 mL acetonitrile and bring to 50 mL with dH<sub>2</sub>O.

11. MS elution buffer

- a) 80% (v/v) acetonitrile
- b) LC-MS grade water

Mix 4 mL of acetonitrile with dH<sub>2</sub>O and bring to 5 mL with dH<sub>2</sub>O.

12. MS resuspension buffer

- a) 2% (v/v) acetonitrile

b) 0.1% (v/v) trifluoroacetic acid

c) LC-MS grade water

Mix 0.1 mL acetonitrile with 5  $\mu$ L trifluoroacetic acid and bring to 5 mL with dH<sub>2</sub>O.

### 13. MS trapping buffer

a) 2% (v/v) acetonitrile

b) 0.1% (v/v) trifluoroacetic acid

c) LC-MS grade water

Mix 20 mL of acetonitrile with 1 mL trifluoroacetic acid and bring to 1 L with dH<sub>2</sub>O.

### 14. Solvent A for liquid chromatography

a) 0.1% (v/v) formic acid

b) LC-MS grade water

Mix 1 mL formic acid with dH<sub>2</sub>O and bring to 1 L with dH<sub>2</sub>O.

### 15. Solvent B for liquid chromatography

a) 80% (v/v) acetonitrile

b) 0.08% (v/v) formic acid

c) LC-MS water

Mix 800 mL acetonitrile with 80  $\mu$ L formic acid and bring to 1 L with dH<sub>2</sub>O.

## KEY RESOURCES TABLE

REAGENT or RESOURCE	SOURCE	IDENTIFIER
Biological samples		
Pathological human muscle biopsy / autopsy specimens	Clinical samples	n/a
Unaffected human control biopsy specimens	Control samples	n/a
Chemicals, Proteins		
Acetonitrile	Sigma	34851
Ammonium bicarbonate	Sigma	A6141

Bovine serum albumin	ThermoFisher Scientific	23208
Dithiothreitol	ThermoFisher Scientific	BP172-5
Formic acid	Sigma	5330020050
Hydrochloric acid	Merck	1.15186
Iodoacetamide	Acros Organics	122270050
Isopentane	Merck	PHR1661
LC-MS grade water	Sigma	39253
Liquid nitrogen	BOC Gases Ireland	n/a
Potassium chloride	Sigma	P9541
Potassium phosphate, monobasic	Sigma	P9791
Sodium chloride	Sigma	S3014
Sodium phosphate, dibasic	Sigma	S3264
Sodium dodecyl sulfate	Sigma	L3771
Trifluoroacetic acid	Sigma	T6508
Tris base	Sigma	T1503
Trypsin protease	ThermoFisher Scientific	90305
Urea	Sigma	U0631
Critical Commercial Assays		
Halt Protease Inhibitor Cocktail	ThermoFisher Scientific	78429
Ionic Detergent Compatibility Reagent for Pierce 660 nm Protein Assay Reagent	ThermoFisher Scientific	22663
Pierce 660 nm Protein Assay Reagent	ThermoFisher Scientific	1861426
Software and Algorithms		
Progenesis QI for Proteomics	Waters Chromatography Ireland Ltd.	n/a

Proteome Discoverer 2.2 using Sequest HT	ThermoFisher Scientific	OPTON-30945
Other		
Analytical weighing scale	Farnell	3290043
Benchtop centrifuge	Eppendorf	5427R
Filter unit Vivacon 500	Sartorius	VN0H22
Heated electrospray ionization (H-ESI) ion source	ThermoFisher Scientific	H-ESI probe
Incubator	Memmert	INB200
Liquid nitrogen-cooled mini mortar plus pestle	ThermoFisher Scientific	H37260-0100
Manual single channel pipettes (20 $\mu$ L, 100 $\mu$ L, 1000 $\mu$ L)	Mettler Toledo	17014391
Microplate reader	ThermoFisher Scientific	VL0000D0
Open Dewar flask for liquid nitrogen	BOC Gases Ireland	11880462
Orbitrap Fusion Tribrid mass spectrometer	ThermoFisher Scientific	IQLAAEGAAPFA DBMBCX
Pierce C18 spin columns	ThermoFisher Scientific	89870
Polypropylene micro pellet pestles for plastic tubes	Thomas Scientific	3411E25
Reverse-phased capillary high-pressure liquid chromatography system	ThermoFisher Scientific	UltiMate 3000 HPLC
Safe-lock plastic tubes for sample storage	Eppendorf	0030121597
Sonicator	Bandelin	UW2200
Thermomixer	Eppendorf	5382000031
Vacuum evaporator	Genevac	DNA-12060-C00
Vortex	Sigma	Z258423

## MATERIALS AND EQUIPMENT

- Sterile medical gauze for transportation of fresh muscle biopsy material
- Analytical weighing scale

- Phosphate-buffered saline for preparation of biopsy samples
- Liquid nitrogen storage facility
- Open Dewar flask and metal beaker for quick-freezing of biopsy material in liquid nitrogen-cooled isopentane
- Liquid nitrogen-cooled mini mortar plus pestle
- Sample homogenization buffer for resuspension of pulverized biopsy material
- Commercial protein assay system to determine protein concentration using bovine serum albumin or another suitable protein as standard
- Buffers for protein preparations (Tris buffer, ammonium bicarbonate buffer, urea buffer, iodoacetamide solution)
- Suitable filter units for filter-aided sample preparation, such as Vivacon 500 (10000 MWCO)
- Thermomixer
- Trypsin-containing protein digestion buffer
- Benchtop centrifuge
- Incubator
- Manual single channel pipettes
- Microplate reader
- Pierce C18 spin columns
- Polypropylene micro pellet pestles for plastic tubes
- Safe-lock plastic tubes for sample storage
- Sonicator
- Vacuum evaporator
- Vortex
- MS sample buffer
- MS activation buffer
- MS equilibrium/wash solution
- MS elution buffer
- MS resuspension buffer
- MS trapping buffer
- Solvent A for liquid chromatography
- Solvent B for liquid chromatography
- Reverse-phased capillary high-pressure liquid chromatography system
- Heated electrospray ionization (H-ESI) ion source

- Mass spectrometer (Orbitrap Fusion Tribrid MS apparatus)
- Software (Progenesis QI for Proteomics; Proteome Discoverer 2.2 using Sequest HT)

**Alternatives:** This protocol describes the proteomic identification of proteins extracted from skeletal muscle biopsy specimens using liquid chromatographic separation combined with analysis by an Orbitrap Fusion Tribrid mass spectrometer from ThermoFisher Scientific. Alternatively, a variety of other proteomic methods, mass spectrometers and proteomic analysis software packages can be employed for the systematic identification and characterization of proteins extracted from clinical tissue specimens (Macklin et al., 2020). The determination of protein concentration described here is carried out with the help of a Pierce 660 nm Protein Assay system. Alternatively, various other commercially available protein assays can be used to measure the amount of protein being present in fractions extracted from clinical tissue samples.

## STEP-BY-STEP METHOD DETAILS

### Preparation of biopsy specimens

#### **Timing: 1-2 h**

1. Skeletal muscle tissue samples received from diagnostic biopsies, operational remnants or autopsy material should initially not be immersed in any buffer or solution but kept in their original state for transportation (Joyce et al., 2012).
2. Properly label all sampling containers for the transportation or storage of individual tissue samples. The labelling system should be adopted to accommodate the analysis of individual samples or multiplexing approaches to study large sets of tissue specimens.
3. Strictly follow national regulations and ethical guidelines if anonymization of human tissue specimens is required (Mann et al., 2021).
4. Transport freshly dissected muscle samples in sterile medical gauze following extraction by open biopsy or a needle biopsy procedure (Barthelemy et al., 2020).
5. Carefully remove excess fat and connective tissue, if necessary, by physical means from the muscle specimen.
6. Determine the wet weight of the biopsy material with an analytical weighing scale.

7. Depending on whether the biopsied tissue specimens will be used for both histological/histochemical examinations and biochemical analyses or only for proteomic studies, the samples should be prepared differently, as outlined below.
8. The initial handling of fresh biopsy specimens and their preparation for proteomic analysis versus long-term storage for subsequent studies is outlined in **Figure 1**:
  - a) If tissue specimens are exclusively used for biochemical studies, the sample can be briefly washed with ice-cold biopsy buffer, such as phosphate-buffered saline at pH 7.4, to remove excess blood.
  - b) Importantly, if the biopsy material was dissected for both histological analyses and proteomic surveys, samples should not be immersed in any solution or buffer. In this case, tissue specimens should be immediately quick-frozen in liquid nitrogen-cooled isopentane.
9. For quick-freezing of muscle samples for proteomic analysis, carefully fill an open 2 L Dewar flask with liquid nitrogen and insert a small metal container with an isopentane solution.
10. The metal container should easily fit into the larger Dewar flask and be fixed in position by hanging from a metal rod over the opening of the open Dewar flask.
11. Fill the metal container approximately half-full with the isopentane solution and slowly suspend it into the liquid nitrogen-filled Dewar container.
12. During the initial cooling process of the isopentane solution, white aggregates will start to appear at the edges of the container, often referred to as ‘caking’. This is the optimum period for introduction of the biopsy material into the cooled isopentane solution.
13. Once the tissue sample is thoroughly frozen, it can be removed and transferred to a labelled and pre-cooled plastic safe-lock tube.

**Note:** Avoid the immersion of freshly dissected muscle biopsy material in solutions if it is planned to use the sample for both the microscopical assessment of transverse cryosections and mass spectrometry-based proteomic analysis. The presence of liquids may cause freezing artefacts in skeletal muscle specimens and should therefore be avoided during the initial preparation, transportation and storage for the subsequent diagnostic usage in the form of histological and histochemical staining procedures (Nix and Moore, 2020).

**Critical:** Excess blood, fat and connective tissue are routinely removed from skeletal muscle biopsies prior to diagnostic procedures. However, if muscle fiber populations are supposed to be studied by proteomics in their entire tissue environment to evaluate necrosis, fibrosis, inflammation, fat substitution or other pathological changes, it is critical to skip this preparative step and take the entire biopsy material as starting material for biochemical and mass spectrometric analysis.

**Pause Point:** If frozen biopsy samples do not have to be immediately processed for diagnostic procedures or mass spectrometric analysis, they can be transferred to a  $-80^{\circ}\text{C}$  freezer or a large liquid nitrogen containing Dewar container for long-term storage. Properly quick-frozen skeletal muscle specimens obtained by biopsy procedures or sampling during autopsy can be stored for many years without significant degradation of proteins (Deshmukh et al., 2021).

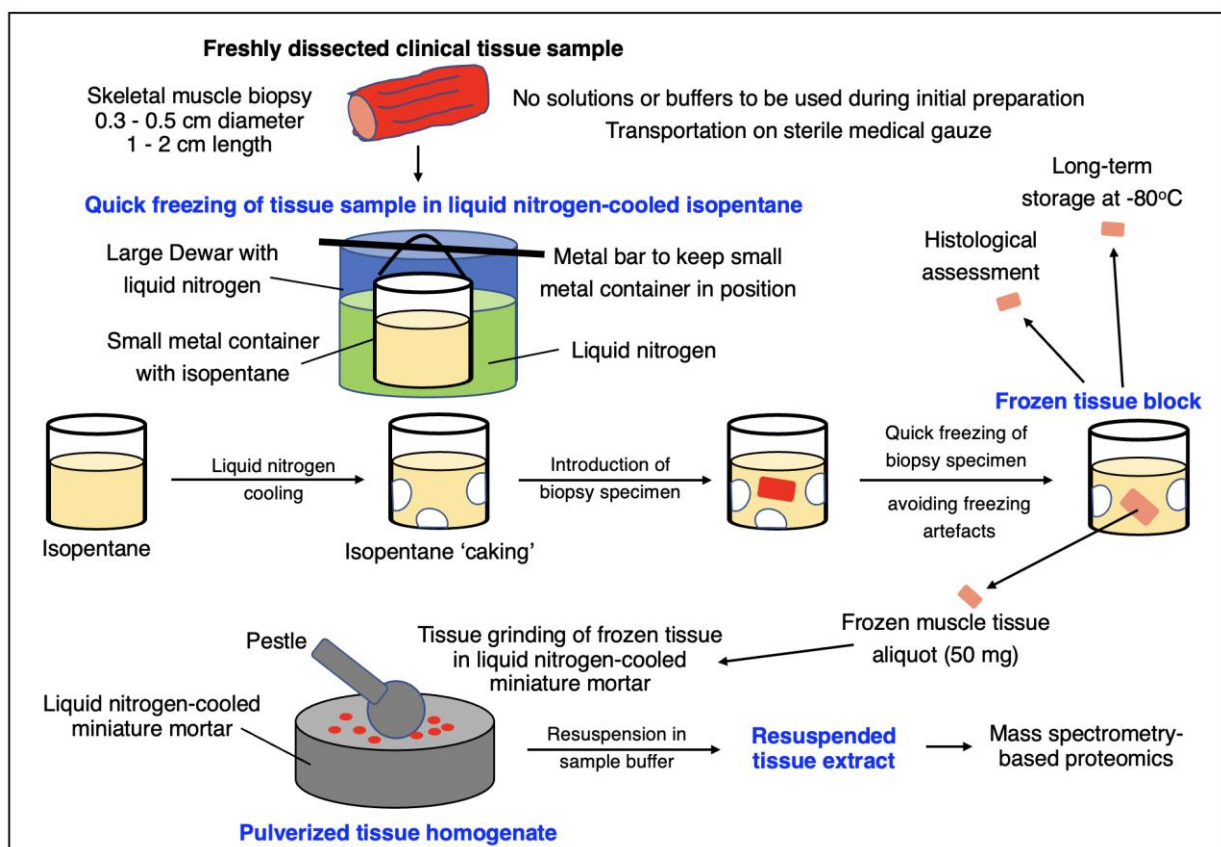


**Figure 1:** Initial handling and preparation of fresh muscle biopsy specimens for proteomic analysis

Homogenization of tissue material

**Timing:** 2-3 h

1. The overall analytical workflow of the mass spectrometry-based proteomic analysis of clinical tissue samples is summarized in **Figure 2**. For the proteomic analysis of small amounts of tissue material from needle biopsies (50 mg), pulverization of frozen tissue samples is often advantageous over the usage of mechanical tissue homogenizers (Dias et al., 2020) and usually gains a satisfactory yield of extracted proteins:
  - a) Prior to homogenization, the weight of the pulverized tissue sample should be determined with an analytical weighing scale.
  - b) Transfer the frozen biopsy material into a suitably sized mortar. If a conventional mortar is used, the device should be pre-cooled with liquid nitrogen.
  - c) For optimum grinding of tissue samples, ideally a commercially available liquid nitrogen-cooled miniature mortar should be employed.
  - d) Carefully grind the tissue material with the help of a cooled pestle until a fine powder is created. It is crucial to keep the system properly cooled with liquid nitrogen so that the tissue material does not thaw during the homogenization process.
  - e) Transfer the frozen tissue powder to a small and pre-cooled plastic tube. For small samples, 1.5 ml microcentrifuge tubes are suitable for the next homogenization step.
  - f) Add ice-cold sample homogenization buffer to the tissue powder in a 1.5 ml microcentrifuge tube.
  - g) For proteomic studies, the ratio of extracted skeletal muscle tissue to homogenization buffer should be 1:6 (mg/ $\mu$ L).
  - h) Carefully mix this solution and resuspend the protein pellet with a polypropylene micro pellet pestle.
2. Heat the suspended tissue extract for 5 min at 95°C.
3. If the suspension is excessively viscous, which can be the case with multi-nucleated contractile fibers following homogenization, large DNA molecules can be treated by sonication. Usually, 4 bursts of sonication lasting approximately 5 s sufficiently reduce the viscosity of muscle homogenates.
4. Centrifuge the suspended muscle biopsy material for 10 min at 20,000 x *g* in a benchtop centrifuge.

- Use the supernatant fraction for biochemical and proteomic analyses.

**Note:** If additional biochemical studies are planned, such as gel electrophoresis or immunoblot analysis, the homogenization buffer should be supplemented with a protease inhibitor cocktail to avoid the proteolytic degradation of sensitive skeletal muscle proteins.

**Critical:** During all preparative steps involved in the harvesting and preparation of potentially infectious clinical tissue samples, as well as handling of liquid nitrogen and potentially harmful chemicals such as sodium dodecyl sulfate and iodoacetamide, a double layer of protective gloves, safety goggles, face mask and a laboratory coat should be worn.

**Pause Point:** Following tissue grinding and resuspension, the cleared supernatant fraction containing biopsy extracts can be quick-frozen in liquid nitrogen and stored in a -80°C freezer until further processing.

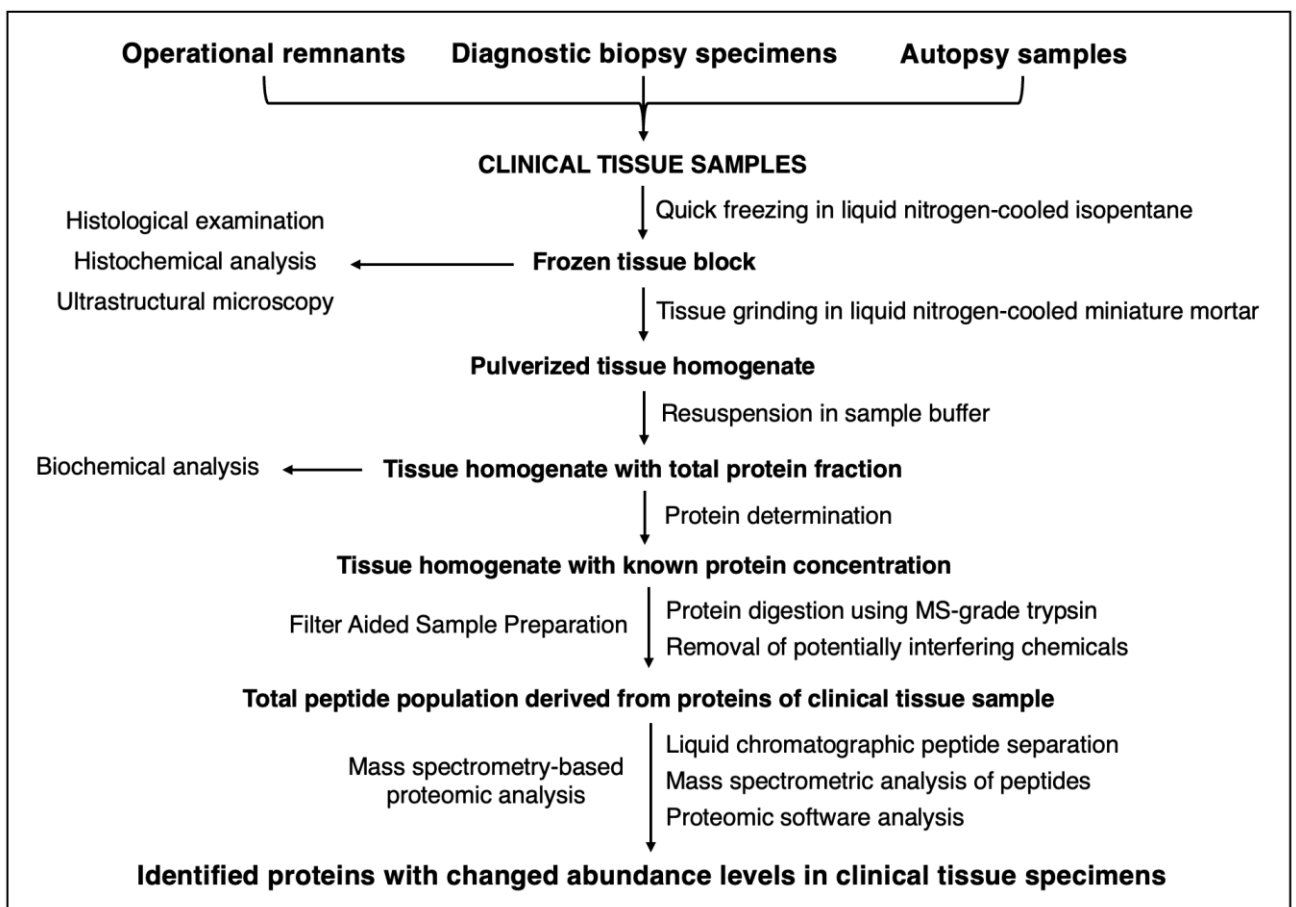


**Figure 2:** Workflow of the mass spectrometry-based proteomic analysis of clinical tissue samples.

## Determination of Protein Concentration

### Timing: 1-2 h

1. Prior to mass spectrometric analysis, the protein concentration of the supernatant fraction containing extracted biopsy material should be determined.
2. Use bovine serum albumin as a protein standard. A standard graph can be established with 25, 50, 125, 250, 500, 750, 1000, 1500 and 2000  $\mu\text{g}$  protein per mL.
6. Transfer 10  $\mu\text{L}$  of each bovine serum albumin protein standard to individual microplate wells in triplicate.
7. Transfer 10  $\mu\text{L}$  of the extracted biopsy samples with unknown protein concentration to individual wells on the same microplate in triplicate.
8. To zero the plate reader, a blank sample is also needed. Transfer 10  $\mu\text{L}$  of a blank sample, such as the homogenization buffer into individual wells on the same microplate in triplicate.
9. If a commercial assay system is used, such as the Pierce 660 nm Protein Assay system (Antharavally et al., 2009), add 150  $\mu\text{L}$  of the protein assay reagent that is supplemented with ionic detergent compatibility reagent to each well in the microplate.
10. The plate should be covered and then carefully mixed on a plate shaker at medium speed. Shaking at approximately 600 rpm for 1 min is usually sufficient for the mixing of the protein samples and the dye reagent.
11. Incubate the mixture of the protein suspension and the assay reagent for 5 min at 20°C.
12. Zero the plate reader by using the blank wells as baseline values.
13. To establish a standard graph with bovine serum albumin, measure the absorbance of the various standards ranging from 50 to 2000  $\mu\text{g}$  protein per mL at a wavelength of  $\lambda = 660$  nm.
14. Plot the average blank-corrected 660 nm measurement for each protein standard versus its concentration in  $\mu\text{g}/\text{mL}$  to prepare a standard curve.
15. Measure the absorbance of the biopsy samples with unknown protein concentration at a wavelength of  $\lambda = 660$  nm.
16. Compare the absorbance values of the biopsy samples with the standard curve to determine the protein concentration of each unknown sample.

**Note:** To avoid potential issues with linearity across a limited range of concentration magnitudes, a four-parameter curve fit should be used.

**Critical:** The sample homogenization buffer contains 1% (w/v) sodium dodecyl sulfate, which can interfere with protein concentration measurements. It is therefore critical to add ionic detergent compatibility reagent to the protein assay reagent.

### Digestion of Protein Sample

**Timing: 10-24 h**

1. Transfer the sample homogenate containing 25  $\mu\text{g}$  protein and 200  $\mu\text{L}$  of urea buffer to a centrifugal filter unit, such as the Sartorius Vivacon 500 unit.
2. Briefly vortex the suspension.
3. Centrifuge the filter unit for 15 min at 14,000  $\times g$ .
4. Add another 200  $\mu\text{L}$  of urea buffer to the filter unit.
5. Briefly vortex the suspension.
6. Centrifuge the filter unit for 15 min at 14,000  $\times g$ .
7. Discard the flow-through solution.
8. Add 100  $\mu\text{L}$  of iodoacetamide solution and cover the filter units in tinfoil.
9. Mix the solution for 1 min at 600 rpm in a thermomixer.
10. Incubate the solution without mixing for 20 min in the dark.
11. Centrifuge the filter unit for 15 min at 14,000  $\times g$ .
12. Add 100  $\mu\text{L}$  of urea buffer to the filter unit.
13. Briefly vortex the suspension.
14. Centrifuge the filter unit for 15 min at 14,000  $\times g$ .
15. Add another 100  $\mu\text{L}$  of urea buffer to the filter unit.
16. Briefly vortex the suspension.
17. Centrifuge the filter unit for 15 min at 14,000  $\times g$ .
18. Add 100  $\mu\text{L}$  of ammonium bicarbonate buffer.
19. Briefly vortex the suspension.
20. Centrifuge the filter unit for 15 min at 14,000  $\times g$ .
21. Add another 100  $\mu\text{L}$  of ammonium bicarbonate buffer.

22. Briefly vortex the suspension.
23. Centrifuge the filter unit for 15 min at 14,000 x *g*.
24. Transfer the centrifugal filter units to fresh collection tubes.
25. Add 40  $\mu\text{L}$  of digestion buffer containing trypsin (50:1 protein:protease ratio) and keep this solution on ice.
26. Mix the solution for a 1 min at 600 rpm in a thermomixer.
27. The filter units containing the protein sample and trypsin should then be positioned in a suitable wet chamber.
28. Incubation should be carried out for 4-18 h at 37°C in a sterile incubator.
29. Following the digestion step, the filter units should be placed in new collection tubes.
30. Centrifuge the filter unit for 10 min at 14,000 x *g*.
31. The filtrate contains the generated peptide fraction.
32. Add 40  $\mu\text{L}$  of ammonium bicarbonate buffer to the filter unit.
33. Centrifuge the filter unit for another 10 min at 14,000 x *g*.
34. The filtrate contains the combined peptide fraction.
35. Transfer 60  $\mu\text{L}$  of each sample to new plastic tubes.
36. Add 15  $\mu\text{L}$  of MS sample buffer, which contains 2% (v/v) trifluoroacetic acid and 20% (v/v) acetonitrile).
37. The final peptide sample solution should contain 0.5% trifluoroacetic acid in 5% acetonitrile.

**Note:** If incubation with trypsin does not result in a sufficient rate of proteolysis, other types of proteases or combinations of proteolytic enzymes can be used for the consecutive treatment of proteins (Murphy and Ohlendieck, 2018).

**Critical:** The digestion step should be carried out in a wet chamber environment, which can be conveniently constructed with a sterile pipette box containing dH<sub>2</sub>O and soaked tissue sheets. Sample tubes undergoing protein digestion can be held in a foam floater (Dowling et al., 2020).

**Pause Point:** Following digestion of protein samples, the generated peptide solutions can be quick-frozen in liquid nitrogen and stored in a -80°C freezer until further processing.

## Removal of Interfering Chemicals from Peptide Fraction

### Timing: 1-2 h

1. For the simultaneous processing of multiple clinical samples, porous C18 tubes are placed into their respective receiver tubes.
2. Rinse the walls of C18 spin tubes and wet the reverse-phase resin by the addition of 200  $\mu\text{L}$  of activation solution.
3. Centrifuge the C18 tubes for 1 min at 1,500  $\times g$ .
4. Discard flow-through solution.
5. Add another 200  $\mu\text{L}$  of activation solution.
6. Re-centrifuge the C18 tubes for 1 min at 1,500  $\times g$ .
7. Discard flow-through solution.
8. Add 200  $\mu\text{L}$  of equilibration/wash solution.
9. Centrifuge the C18 tubes for 1 min at 1,500  $\times g$ .
10. Discard flow-through solution.
11. Add another 200  $\mu\text{L}$  of equilibration/wash solution.
12. Re-centrifuge the C18 tubes for 1 min at 1,500  $\times g$ .
13. Discard flow-through solution.
14. Transfer the sample on top of the resin bed.
15. Place the C18 spin tubes containing the samples into receiver tubes.
16. Centrifuge the C18 tubes for 1 min at 1,500  $\times g$ .
17. Recover the flow-through fraction.
18. Pipette the flow-through fraction on top of the resin bed.
19. Re-place the C18 spin tubes into receiver tubes.
20. Re-centrifuge the C18 tubes for 1 min at 1,500  $\times g$ .
21. Transfer C18 spin tubes into new receiver tubes.
22. Add 200  $\mu\text{L}$  of equilibration/wash solution to C18 spin tubes.
23. Centrifuge the C18 tubes for 1 min at 1,500  $\times g$ .
24. Discard the flow-through solution.
25. Add another 200  $\mu\text{L}$  of equilibration/wash solution to C18 spin tubes.
26. Re-centrifuge the C18 tubes for 1 min at 1,500  $\times g$ .
27. Discard the flow-through solution.
28. Transfer the C18 spin tubes into new receiver tubes.

29. Add 20  $\mu\text{L}$  of elution buffer to top of the resin bed.
30. Centrifuge the C18 tubes for 1 min at 1,500  $\times g$ .
31. Add another 20  $\mu\text{L}$  of elution buffer to top of the resin bed using the same receiver tubes.
32. Re-centrifuge the C18 tubes for 1 min at 1,500  $\times g$ .
33. Dry the eluted and combined fraction in a vacuum evaporator.
34. Resuspend the sample in 50  $\mu\text{L}$  of resuspension buffer.

**Note:** Following resuspension, the final solution containing the digested and washed peptide fragments should contain 2% (v/v) acetonitrile and 0.1% (v/v) trifluoroacetic acid for transfer to the trapping column of a liquid chromatography system.

**Critical:** To avoid potential complications due to detergents with the subsequent mass spectrometric analysis, interfering chemicals are removed by washing and centrifugation of the resin-associated peptide fraction using commercially available spin columns prior to elution and separation by liquid chromatography (Antharavally, 2012). Importantly, to ensure complete binding of sample protein, the flow-through solution resulting from the initial incubation of washed C18 tubes is re-administered to the resin and incubated for a second time, as described above.

**Pause Point:** Resuspended peptide solutions can be quick-frozen in liquid nitrogen and then stored in liquid nitrogen or a  $-80^{\circ}\text{C}$  freezer for future analysis in a mass spectrometer.

Mass spectrometric LC-MS/MS analysis

**Timing: 12-72 h**

1. Use a suitable liquid chromatography system for optimum peptide separation, such as the ThermoFisher Scientific UltiMate 3000 UHPLC system.
2. Load a 2  $\mu\text{L}$  aliquot of peptides, generated by trypsin digestion and cleared of interfering chemicals, onto the trapping column, such as a PepMap100 (C18, 300  $\mu\text{m} \times 5 \text{ mm}$ ) column from ThermoFisher Scientific.
3. Run the trapping column at a flow rate of 25  $\mu\text{L}/\text{min}$  with trapping buffer for 3 min.

4. Following the application to the trapping column system, the sample is resolved by an analytical column, such as an Acclaim PepMap 100 (75  $\mu\text{m}$   $\times$  50 cm, 3  $\mu\text{m}$  bead diameter) column.
5. Elute peptides with a binary gradient as follows: LC Solvent A and LC Solvent B using 2-32% Solvent B for 75 min, 32-90% Solvent B for 5 min and holding at 90% for 5 min at a flow rate of 300 nL/min.
6. Select a data-dependent acquisition method for the identification of peptides using a voltage of 2.0 kV and a capillary temperature of 320°C.
7. Perform data-dependent acquisition with full scans in the 380-1500 m/z range using a mass analyzer, such as the ThermoFisher Scientific Orbitrap Fusion Tribrid.
8. Use a resolution of 120,000 (at m/z 200), a targeted automatic gain control (AGC) value of 4E+05 and a maximum injection time of 50 ms.
9. The top-speed acquisition algorithm determines the number of selected precursor ions for peptide fragmentation.
10. Isolation of selected precursor ions is performed in the quadrupole unit with an isolation width of 1.6 Da.
11. Peptides with a charge state ranging from 2+ to 7+ are analyzed and a dynamic exclusion is applied after 60 s.
12. Fragmentation of precursor ions is carried out with higher energy collision-induced dissociation using a normalized collision energy of 28%.
13. Generated MS/MS ions are measured in the linear ion trap using a targeted AGC value of 2E+04 and a maximum fill time of 35 ms.

**Note:** Prior to mass spectrometric analysis, an important step in the proteomic workflow is the separation of peptides by reverse-phased liquid chromatography (Sethi et al., 2015). A variety of high-performance liquid chromatography systems are commercially available. In this protocol, ultra high-performance liquid chromatography was carried out with the Thermo Scientific UltiMate 3000 UHPLC system. Alternatively, many other excellent chromatographical systems are available for proteomic applications. If liquid chromatography is carried out in a multi-user core facility, make sure that (i) columns are properly washed, (ii) there is no sign of column deterioration, (iii) the system is not contaminated by previous applications, (iv) buffers are freshly made and (v) the separation system is in good working order.

**Critical:** If peptide-centric approaches are employed for the unequivocal identification of individual proteoforms from clinical tissue specimens, it is crucial to use an optimized enzymatic or chemical protocol for controlled protein digestion. If the routine application of trypsin for proteolysis does not result in the satisfactory production of characteristic peptide populations, as evidenced by the pure mass spectrometric identification of proteins, then alternative digestion methods should be tested.

## Protein identification

### Timing: 2-3 h

1. Search the generated mass spectrometric files (.raw) against the *Homo sapiens* UniProtKB-SwissProt database with Proteome Discoverer 2.2 using Sequest HT and Percolator.
2. Locate the proteome data for 'human' by searching by name or by taxonomy ID, i.e. *Homo sapiens* at: <https://www.uniprot.org/proteomes/>.
3. Click on the Proteome ID link - UP000005640 for 'human' (78,120 proteins)
4. Select the most suitable database in UniProt, such as the reviewed (UniProtKB/Swissprot), the unreviewed (UniProtKB/TREMBL) or the combined (UniProtKB) option.
5. Click on the Download button and choose: 'All protein entries, FASTA (Canonical and isoform), compressed'.
6. Use suitable search parameters for protein identification, including settings for peptide mass tolerance, MS/MS mass tolerance, the number of missed peptide cleavages, carbamido-methylation of cysteines and methionine oxidation:
  - a) Set the peptide mass tolerance to 10 ppm.
  - b) Set MS/MS mass tolerance to 0.6 Da.
  - c) Allow up to two missed peptide cleavages.
  - d) Set carbamido-methylation of cysteine as a fixed modification.
  - e) Set methionine oxidation as a variable modification.
7. Consider only highly confident peptide identifications.

8. Aim for a false discovery rate of  $FDR \leq 0.01$ , identified using a SEQUEST HT workflow coupled with Percolator validation in Proteome Discoverer 2.2.

**Note:** A variety of commercially available software programs can be employed to analyze mass spectrometric files. Reviewed databases contain highly curated entries with a minimal level of redundancy and the ability to efficiently integrate with other databases for the identification of human proteoforms.

**Critical:** In order to carry out reliable protein identifications, it is important to define suitable search parameters in relation to peptide mass tolerance, MS/MS mass tolerance and the number of allowable missed peptide cleavages, as well as settings for the carbamido-methylation of cysteines and methionine oxidation.

Comparative profiling of protein abundance

**Timing: 12-48 h**

1. Import mass spectrometric raw files into a suitable software analysis program, such as Progenesis QI (Waters), for the comparative abundance profiling of proteins in normal controls versus the diseased state.
2. Run an automatic alignment to combine and compare the result from different LC-MS runs.
3. Carry out an automatic peak picking and matching across all data files.
4. Create an aggregate data set from the aligned runs, which contains all peak information from all sample files and allows the detection of a single map of peptides.
5. Apply this map to each individual sample, which then allows 100% matching of peaks with no missing values.
6. Normalize the peptide ion abundance measurements to allow the comparisons between the normal controls and the pathological specimens from clinical tissue specimens in order to identify peptides of pathobiological interest.
7. Base the determination of the peptide ions of interest on the significance measure of ANOVA with a  $p$ -value of 0.05.

8. Export MS/MS spectra from these peptides and carry out identifications by using the above-described process with Proteome Discoverer 2.2 software.
9. Re-import the result file into Progenesis QI, which then allows a detailed review of all peptide ions used to quantify and identify individual proteoforms.
10. Finally, base the determination of the human protein species of interest on the significance measure of ANOVA with a *p*-value of 0.05.

**Note:** A variety of commercially available software analysis programs can be utilized to carry out the comparative proteomic profiling of different protein fractions. In this protocol, Progenesis QI (Waters) software was used. User guides and tutorial data sets for Progenesis QI are available online: <http://www.nonlinear.com/progenesis/qi-for-proteomics/v4.0/user-guide/>). The proteomic comparison of extracts from clinical tissue preparations isolated from normal control specimens versus patient specimens can lead to the identification of large numbers of differentially expressed proteins in human disease (Capitanio et al., 2020).

**Critical:** Prior to finalizing the list of significant human proteoforms that exhibit a significantly changed abundance in a particular disorder, it is important to review crucial quality control metrics in relation to sample preparation, instrumentation and experimental parameters. The review of sample preparation metrics should address potential problems with the isolation and preparation of protein extracts for mass spectrometric analysis, such as issues with protein yield and/or a sub-optimal digestion efficiency for the production of characteristic peptide populations. The critical assessment of instrument metrics should examine the suitability and configuration of the liquid chromatography system and mass spectrometer for optimum bioanalytical performance. In addition, a review of experiment metrics should ideally investigate the scale of protein identification and review the mass spectrometric identification of statistical outliers in an individual sample set.

## EXPECTED OUTCOMES

The expected yield of total protein from clinical tissue samples to be used for proteomic studies depends on the amount and quality of starting material and the optimization of the protocol used for tissue harvesting, dissection, preparation and storage of tissue specimens prior to mass spectrometric analysis. In contrast to relatively large amounts of tissue that can be obtained from open biopsy procedures, operational remnants or autopsy samples, which might result in several grams of wet weight, only small amounts of human muscle specimens can be routinely obtained by the less invasive and most frequently used needle biopsy method (Meola et al., 2012). Diagnostic procedures and testing regimes during clinical trials use different types of

biopsy procedures, which depend heavily on the anticipated range of histological, ultrastructural and/or biochemical tests. Most procedures produce cylindrical muscle samples of 0.3 to 0.5 cm in diameter and 1 to 2 cm in length of approximately 0.1 to 0.5 mg wet weight (Barthelemy et al., 2020; Joyce et al., 2012). Crucial aims for the conduction of needle biopsy techniques include toleration of the procedure by both pediatric and adult patients, minimum interference with pharmacological substances such as anesthetics, technical reliability, patient safety and the harvesting of sufficient amounts of high-quality tissue for routine histological and histochemical analyses. For additional pathobiochemical investigations, such as enzyme testing, immunoblotting or mass spectrometry-based proteomic screening of clinical tissue samples, usually 50 mg muscle tissue can be made available from patient biopsy material (Joyce et al., 2012). The expected outcome of a mass spectrometric analysis depends heavily on the proteomic approach, such as targeted versus discovery studies or bottom-up versus top-down proteomics, and the sensitivity of the mass spectrometer used for protein identification (Uzozie and Aebersold, 2018; Kang et al., 2020; Dupree et al., 2020). The usage of an Orbitrap type mass spectrometer usually results in the identification of several thousand proteoforms. Proteomic studies with crude skeletal muscle biopsy material cover routinely proteins involved in excitation-contraction coupling, ion homeostasis, the contraction-relaxation cycle, the cellular stress response, metabolite transportation, energy metabolism, cellular signaling cascades, cytoskeletal networks and the various layers of the extracellular matrix (Capitanio et al., 2020).

## QUANTIFICATION AND STATISTICAL ANALYSIS

The usage of sufficient technical and biological repeats during biochemical assays and proteomic surveys, as well as suitable software analysis programs and proper search parameters for protein identification, are essential for the successful conduction of a proteomic survey of clinical tissue specimens. Following protein extraction, the determination of the protein concentration of the unknown protein suspension and the absorbance values of the bovine serum albumin protein standards should be carried out in triplicate. In order to prevent issues with linearity across a limited range of protein concentration magnitudes, use a four-parameter curve fit. For the analysis of protein species derived from human tissue specimens, search the generated mass spectrometric files against a suitable databank, such as the *Homo sapiens* UniProtKB–SwissProt database with Proteome Discoverer 2.2 using Sequest HT and Percolator. It is crucial to only consider highly

confident peptide identifications. The aim for a false discovery rate should be  $FDR \leq 0.01$  using a SEQUEST HT workflow coupled with Percolator validation in Proteome Discoverer 2.2. For the comparative profiling of protein abundance, the determination of the peptide ions of interest should be based on the significance measure of ANOVA with a  $p$ -value of 0.05. The final determination of the human protein species of interest should also be based on the significance measure of ANOVA with a  $p$ -value of 0.05. Ideally, the identification of a particular proteoform should be based on sequence information from at least 2 peptides.

### ADVANTAGES

Mass spectrometry-based proteomics has developed into a robust and reliable bioanalytical tool for the large-scale identification of peptides and proteins of clinical interest (Mann et al., 2020). In contrast to focusing on individual proteins and their potentially preconceived pathophysiological role, the great advantage of proteomic surveys is the unbiased and technology-driven approach that can result relatively swiftly in the comprehensive establishment of proteome-wide changes in a particular disease. If used as part of clinical studies, proteomics can be employed for the systematic discovery of novel biomarker candidates for improving differential diagnosis, prognosis and therapy-monitoring.

### LIMITATIONS

Limitations of the proteomic analysis of extracts from clinical tissue specimens are related to potential bioanalytical issues with sample handling, mass spectrometry, single timepoint assaying, sample heterogeneity and inter-individual differences within patient populations. The systematic mass spectrometric survey of clinical tissue samples includes a variety of critical steps that may affect the quality of the proteomic data, including the method of surgical resection, as well as the initial preparation, transportation and potential preservation of biopsy material. Especially critical can be complications due to extended delays between initial sample retrieval and the start of tissue homogenization and subsequent biochemical analysis. This may result in the degradation of sensitive protein species and can thereby potentially introduce bioanalytical artefacts. It is also important to remember that the entirety of the diverse protein constituents of a specific cellular arrangement represents a highly dynamic system with constant changes in protein abundance, isoform expression patterns, protein interactions and

post-translational modifications. The cellular proteome in the human body is in a constant mode of adaptation to altered functional demands on the physiological, biochemical, metabolic and signaling level (Walther and Mann, 2010). Hence, the pathoproteomic profile of a particular clinical biopsy sample reflects only a single timepoint of protein expression at a specific disease stage. This issue should be taken into account when complex pathological protein changes are interpreted. In addition, the heterogeneity of human tissue specimens and considerable inter-individual genetic differences between patients require usually larger numbers of samples for reliable statistical analysis as compared to studies with cell cultures or animal models of human disease.

## OPTIMIZATION AND TROUBLESHOOTING

### Issues with small amounts of clinical biopsy material

The availability of sufficient amounts of starting material for the extraction of appropriate quantities of protein to be analyzed by mass spectrometry is a crucial factor for a successful proteome-wide identification of changes in distinct protein species. Small amounts of tissue are difficult to homogenize in a reproducible manner.

### Potential solution to optimize the procedure

Ideally at least 25 mg weight wet of individual tissue samples should be used as starting material for proper homogenization by grinding with a liquid nitrogen-cooled miniature mortar. In the case of biopsy sampling in the field of neuromuscular disorders, often more than one muscle specimen is taken per patient, so aliquots from several tissue samples originated from the same individual can be pooled for the reproducible extraction of total tissue protein. However, if proteomic studies are not employed for diagnostic, prognostic or therapy-monitoring purposes and the determination of altered protein expression levels or post-translational modifications at the level of individual patients, but in order to conduct novel basic research into pathoproteomic mechanisms, then sufficient amounts of tissue specimens can be pooled prior to homogenization.

Difficulties with low numbers of identified proteins of pathobiochemical interest

The proteomic analysis of skeletal muscle biopsy material at the initial stages of an acquired or genetic neuromuscular disease that exhibits only relatively mild symptoms may result in a low number of identified protein candidates that exhibit differential expression patterns.

Potential solution to optimize the procedure

In general, the increase in severity of human disease is usually reflected by a rise in altered protein expression patterns. Increased symptoms are often associated with elevated numbers of significant protein hits in the pathological phenotype. Thus, if the proteomic survey of biopsy material at an early disease stage does not result in a large enough number of protein changes for proper systems biological analyses, more advanced pathological stages should be studied. The proteomic profiling of neuromuscular disorders reveals routinely changes in the expression and/or post-translational modifications in hundreds of proteoforms.

Difficulties with poorly identified lists of proteins present in tissue specimens

Depending on search parameters, the systematic mass spectrometric analysis of tissue specimens can result in a poor list of proteomic hits with an unsatisfactory coverage of peptide sequences.

Potential solution to optimize the procedure

To avoid issues with poorly identified lists of proteins present in clinical tissue samples, it is important to strictly define suitable search parameters during the data analysis steps. For the establishment of a useful multi-consensus list of distinct proteoforms of biomedical interest, the usage of critical parameters should include acceptable values for (i) peptide mass tolerance, (ii) MS/MS mass tolerance, (iii) the allowable number of missed peptide cleavages, (iv) the minimum number of unique peptides used for protein identification, (v) a sufficient percent coverage of the total protein sequence for the unequivocal identification of distinct proteoforms, and (vi) the occurrence of certain chemical modifications, including methionine oxidation and carbamido-methylation of cysteine residues.

Issues with poor data alignment using proteomic analysis software

Potential problems with poor data alignment might arise during the usage of analysis software programs, such as Progenesis QI for proteomics.

Potential solution to optimize the procedure

Issues with data alignment can occur if the process of automatic alignment fails to properly align mass spectrometric runs during the initial round of analysis. In such a case, manual alignment vectors should be used and be included before automatic alignment is started for a second time. In general, an improvement of data alignment can be achieved by combining both manual and automatic vectors.

## SAFETY CONSIDERATIONS AND STANDARDS

National legal standards and international principles in research ethics should be adhered to during the sampling, processing, storage and analysis of clinical tissue specimens for both diagnostic and basic research purposes. Since human samples can be potentially harmful due to the presence of infectious material such as viruses or bacteria, as well as cytotoxic or radioactive material introduced to the body during diagnostic procedures or therapeutic interventions, health and safety regulations should be taken into account according to national law. For the utilization of human tissue material, such as diagnostic biopsy specimens, operational remnants or autopsy material, guidelines for anonymization of human specimens and the safe storage of patient data and research findings have to be introduced prior to starting a new project. Special safety considerations of the individual analytical steps outlined in this protocol are concerned with sodium dodecyl sulphate, dithiothreitol and liquid nitrogen. The detergent sodium dodecyl sulphate used in the sample homogenization buffer is an irritant of exposed skin, the eyes and the respiratory system. Therefore, during the handling of the powdered form of this detergent and the preparation of the sample buffer, proper eye and face protection, a mask and protective gloves and a lab coat, should be worn. The same is true for iodoacetamide, which is classified as an irritant and an acutely toxic health hazard. Special safety precautions have also to be arranged when handling liquid nitrogen. Potential cryogenic burns by direct eye or skin contact should be prevented by wearing a proper face shield, protective clothing and special cryo-gloves. Although the gaseous form of nitrogen is non-toxic, the fact that it is colorless, odorless and tasteless and may replace oxygen in the air makes it dangerous when present at high concentration in enclosed facilities. The displacement of sufficient amounts of oxygen in the air may induce initially drowsiness and a diminished state of mental alertness, which can be followed by loss of consciousness. Hence, liquid nitrogen should never be transported in a simple Dewar container in an elevator designed for passengers or used in a non-ventilated cold room. Evaporation of excess liquid nitrogen should only be carried out in a well-ventilated space or under a fume hood.

## ALTERNATIVE METHODS/PROCEDURES

The analytical workflow described in this protocol uses liquid nitrogen-based pulverization of tissue samples for homogenization followed by a bottom-up proteomic approach, reversed phase liquid chromatography for peptide separation and an Orbitrap type mass spectrometer for the identification of protein species of biomedical interest. A variety of alternative approaches can be employed to analyze biopsy material. For example, depending on the amounts of available tissue material, alternative methods of homogenization can be used. If a liquid nitrogen-cooled miniature mortar and pestle system is not available for tissue grinding and pulverization, a hand-held homogenizer that is capable of handling small tissue specimens can also be used. Various commercially available types of handheld devices are suitable for the homogenization of tissue samples in the mg range. Instead of bottom-up proteomics, a more targeted top-down proteomic method can be utilized for studying clinical tissue samples. This could involve the initial protein separation using one-dimensional gel electrophoresis in combination with liquid chromatography or two-dimensional gel electrophoresis with sensitive protein dyes or the application of differential fluorescent tagging of normal control versus diseased samples. If the digestion of extracted protein populations by routine trypsin protocols, as described here, does not result in a sufficient degree of proteolytic cleavage, alternative protocols using other enzymes such as chymotrypsin, LysC, LysN, GluC, ArgC or AspN can be used alone or in combination (LysC/trypsin; AspN/LysC/trypsin). Peptide sequencing and proteomic data analysis can also be carried out by a variety of alternative mass spectrometric methods and analysis software programs, respectively.

## References

Antharavally, B.S. (2012). Removal of detergents from proteins and peptides in a spin-column format. *Curr. Protoc. Protein Sci. Chapter 6, Unit 6.12.*

Antharavally, B.S., Mallia, K.A., Rangaraj, P., Haney, P. & Bell, P.A. (2009). Quantitation of proteins using a dye-metal-based colorimetric protein assay. *Anal. Biochem.*, 385, 342-345.

Barthelemy, F., Woods, J.D., Nieves-Rodriguez, S., Douine, E.D., Wang, R., Wanagat, J., Miceli, M.C. & Nelson, S.F. (2020). A well-tolerated core needle muscle biopsy process suitable for children and adults *Muscle Nerve*. 62, 688-698.

Capitano, D., Moriggi, M., Torretta, E., Barbacini, P., De Palma, S., Viganò, A., Lochmüller, H., Muntoni, F., Ferlini, A., Mora, M. & Gelfi, C. (2020). Comparative proteomic analyses of Duchenne muscular dystrophy and Becker muscular dystrophy muscles: changes contributing to preserve muscle function in Becker muscular dystrophy patients. *J. Cachexia Sarcopenia Muscle*. 11, 547-563.

Dapic, I., Baljeu-Neuman, L., Uwugiaren, N., Kers, J., Goodlett, D.R. & Corthals, G.L. (2019). Proteome analysis of tissues by mass spectrometry. *Mass Spectrom. Rev.* 38, 403-441.

Deshmukh, A.S., Steenberg, D.E., Hostrup, M., Birk, J.B., Larsen, J.K., Santos, A., Kjøbsted, R., Hingst, J.R., Schéele, C.C., Murgia, M., Kiens, B., Richter, E.A., Mann M. & Wojtaszewski J.F.P. (2021). Deep muscle-proteomic analysis of freeze-dried human muscle biopsies reveals fiber type-specific adaptations to exercise training. *Nat. Commun.* 12, 304.

Dias, P.R.F., Gandra, P.G., Brenzikofer, R. & Macedo, D.V. (2020). Subcellular fractionation of frozen skeletal muscle samples. *Biochem. Cell Biol.* 98, 293-298.

Dowling, P., Gargan, S., Zweyer, M., Henry, M., Meleady, P., Swandulla, D. & Ohlendieck, K. (2020). Protocol for the Bottom-Up Proteomic Analysis of Mouse Spleen. *STAR Protoc.* 1, 100196.

Dowling, P., Murphy, S., Zweyer, M., Raucamp, M., Swandulla, D. & Ohlendieck K. (2019). Emerging proteomic biomarkers of X-linked muscular dystrophy. *Expert Rev. Mol. Diagn.* 19, 739-755.

Dupree, E.J., Jayathirtha, M., Yorkey, H., Mihasan, M., Petre, B.A. & Darie, C.C. (2020). A Critical Review of Bottom-Up Proteomics: The Good, the Bad, and the Future of this Field. *Proteomes*. 8, E14.

Joyce, N.C, Oskarsson, B. & Jin L.W. (2012). Muscle biopsy evaluation in neuromuscular disorders. *Phys. Med. Rehabil. Clin. N. Am.* 23, 609-631.

Kang, L., Weng, N., & Jian, W. (2020). LC-MS bioanalysis of intact proteins and peptides. *Biomed. Chromatogr.* 34, e4633.

Macklin, A., Khan, S. & Kislinger, T. (2020). Recent advances in mass spectrometry based clinical proteomics: applications to cancer research. *Clin. Proteomics.* 17, 17.

Mann, S.P., Treit, P.V., Geyer, P.E., Omenn, G.S. & Mann, M. (2021). Ethical Principles, Constraints and Opportunities in Clinical Proteomics. *Mol. Cell. Proteomics.* 20, 100046.

Meola, G., Bugiardini, E. & Cardani, R. (2012). Muscle biopsy. *J. Neurol.* 259, 601-610.

Murphy S. & Ohlendieck, K. (2018). Protein Digestion for DIGE Analysis. *Methods Mol. Biol.* 1664, 223-232.

Nix, J.S. & Moore, S.A. (2020). What Every Neuropathologist Needs to Know: The Muscle Biopsy. *J. Neuropathol. Exp. Neurol.* 79, 719-733.

Sethi, S., Chourasia, D. & Parhar, I.S. (2015). Approaches for targeted proteomics and its potential applications in neuroscience. *J. Biosci.* 40, 607-627.

Shanely, R.A., Zwetsloot, K.A., Triplett, N.T., Meaney, M.P., Farris, G.E. & Nieman D.C. (2014). Human skeletal muscle biopsy procedures using the modified Bergström technique. *J. Vis. Exp.* 10, 51812.

Staron, R.S., Hagerman, F.C., Hikida, R.S., Murray, T.F., Hostler, D.P., Crill, M.T., Ragg, K.E. & Toma, K. (2000). Fiber type composition of the vastus lateralis muscle of young men and women. *J. Histochem. Cytochem.* 48, 623-629.

Staunton, L., Zweyer, M., Swandulla, D. & Ohlendieck, K. (2012). Mass spectrometry-based proteomic analysis of middle-aged vs. aged vastus lateralis reveals increased levels of carbonic anhydrase isoform 3 in senescent human skeletal muscle. *Int. J. Mol. Med.* 30, 723-733.

Uozie, A.C. & Aebersold, R. (2018). Advancing translational research and precision medicine with targeted proteomics. *J. Proteomics*. 189, 1-10.

Walther, T.C. & Mann, M. (2010). Mass spectrometry-based proteomics in cell biology. *J. Cell Biol.* 190, 491-500.

## Chapter 3

### Sample preparation and protein determination for 2D-DIGE proteomics

Published as Chapter 22 in ‘Difference Gel Electrophoresis: Methods and Protocols’, Volume 2596, Springer Protocols (2023).

Gargan, S., & Ohlendieck, K. (2023). Sample Preparation and Protein Determination for 2D-DIGE Proteomics. *Methods in molecular biology* (Clifton, N.J.), 2596, 325–337. [https://doi.org/10.1007/978-1-0716-2831-7\\_22](https://doi.org/10.1007/978-1-0716-2831-7_22).

#### Abstract

Fluorescence two-dimensional difference gel electrophoresis (2D-DIGE) is a widely employed method for efficient protein separation and the determination of abundance changes in distinct proteoforms. This makes this gel-based method a key technique of comparative approaches in top-down proteomics. For the appropriate screening of proteome-wide alterations, initial preparative steps involve sample handling, homogenization, subcellular fractionation and the determination of protein concentration, which makes the optimal application of these techniques a crucial part of a successful initiation of a new 2D-DIGE based analysis. This chapter describes sample homogenization and a standardized protein assay for the preparation of homogenates with a known protein concentration for subsequent differential fluorescent tagging and two-dimensional gel electrophoretic separation.

**Key words:** Difference gel electrophoresis, Homogenization, Protein assay, Proteomics, Top-down proteomics

#### 1. Introduction

Mass spectrometry-based proteomics is routinely used for protein expression profiling and the determination of abundance changes in distinct proteoforms due to physiological challenges or disease processes, as well as the systematic analysis of post-translational modifications, making it a key method of analytical biochemistry [1]. Proteins can be efficiently separated by gel electrophoretic techniques and/or liquid chromatography, whereby gel-based approaches

have the advantage of the direct visualization of a protein spot or band of interest to be isolated for top-down proteomics [2-4]. The differential tagging of proteins with fluorescent dyes following extraction from crude samples enables the direct comparison of different protein populations on the same two-dimensional gel system [5]. Fluorescence two-dimensional difference gel electrophoresis (2D-DIGE) has been widely applied to compare proteome-wide changes in biological fluids, cells, tissues, organs and organisms [6, 7], and been instrumental for biomarker discovery [8]. A crucial first step of the 2D-DIGE based proteomic workflow is presented by sample preparation. This might require a homogenization step, the dilution or concentration of samples depending on their protein content, and subcellular fractionation using differential centrifugation or affinity isolation methodology.

The need for the preparation of subcellular fractions depends both on the complexity of the specimen to be analysed and whether the bioanalytical focus of the 2D-DIGE experiment is on a particular proteome or distinct subproteomes. As outlined in **Figure 1**, the analytical workflow in 2D-DIGE based experiments usually involve the following steps: (i) sample extraction, transportation, initial preparation and possibly preservation for long-term storage prior to usage, (ii) a homogenization step in the case of cell or tissue samples, (iii) a dilution or concentration step in the case of biological fluids, (iv) resuspension of the homogenised or adjusted samples, (v) the determination of protein concentration in individual suspensions, (vi) the differential fluorescent tagging of distinct protein populations using 2- or 3-CyDye systems, (vii) the two-dimensional separation of differently labelled and co-migrating proteins using isoelectric focusing in the first dimension and sodium dodecyl sulphate polyacrylamide slab gel electrophoresis in the second dimension, (viii) the densitometric scanning of fluorescently tagged protein spots, (ix) image analysis of differently labelled protein spots, and finally (x) the biochemical identification of changed protein species using controlled proteolytic cleavage of extracted proteins from distinct two-dimensional spots followed by peptide mass spectrometry [9].

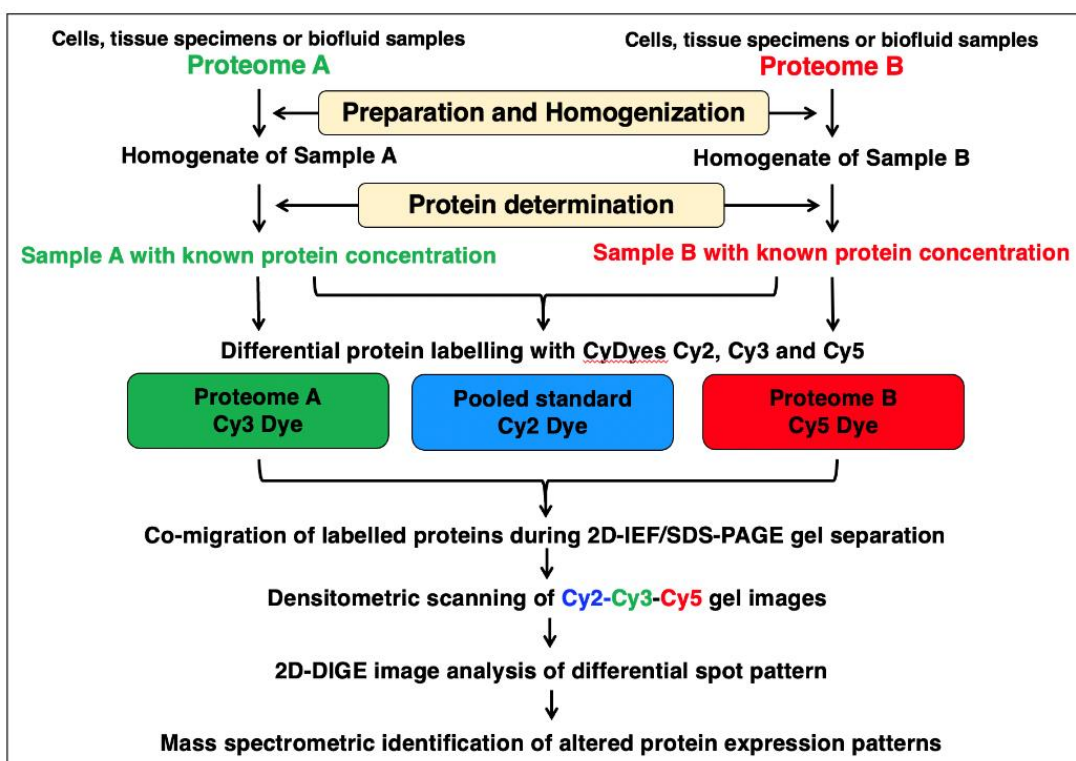


**Figure 1.** Overview of the preparation of samples for the comparative proteomic analysis using fluorescence difference gel electrophoresis. Cells and tissue specimens are homogenized and then their protein fraction extracted for mass spectrometric analysis. Prior to differential fluorescent tagging and two-dimensional gel electrophoretic separation, the protein concentration of the generated suspensions is determined by a colorimetric assay.

Here we outline the initial steps of 2D-DIGE analysis and describe in detail both sample homogenization and the determination of protein concentration. The application of these two standard methods of biochemistry achieves the preparation of a sample homogenate with a known protein concentration that can then subsequently be used for the pre-electrophoretic labelling with fluorescent dyes followed by two-dimensional gel electrophoresis. In the case of the proteomic analysis of biological fluids, an initial adjustment of the protein concentration in individual samples might be necessary. For example, very dilute biofluids such as urine often have to be concentrated prior to gel electrophoretic separation, which can be carried out by protein absorption devices or filtration techniques, and then undergo an immuno-depletion step to improve proteome resolution [10]. In contrast, serum or plasma samples might have to be diluted and then pre-treated with immunoaffinity methods to remove highly abundant proteins such as albumin [11]. Otherwise, two-dimensional gel images could become distorted making

it difficult to properly analyse low-abundance protein components within complex blood samples.

In the case of cell or tissue specimens as starting material, cell disruption can be carried out with a large number of methods and devices such as high-pressure French Press-type homogenizers, Potter-Elvehjem tissue grinders, bead-assisted mills, liquid nitrogen-cooled mortar and pestle systems, sonicators and cell disruption vessels [12-15]. The enrichment of particular protein fractions can be achieved by precipitation, differential centrifugation, ultrafiltration, density gradient ultracentrifugation, size exclusion chromatography, immunoaffinity isolation and asymmetric flow field-flow fractionation [16-18]. A summarizing scheme of tissue preparation for 2D-DIGE analysis is provided in **Figure 2**.

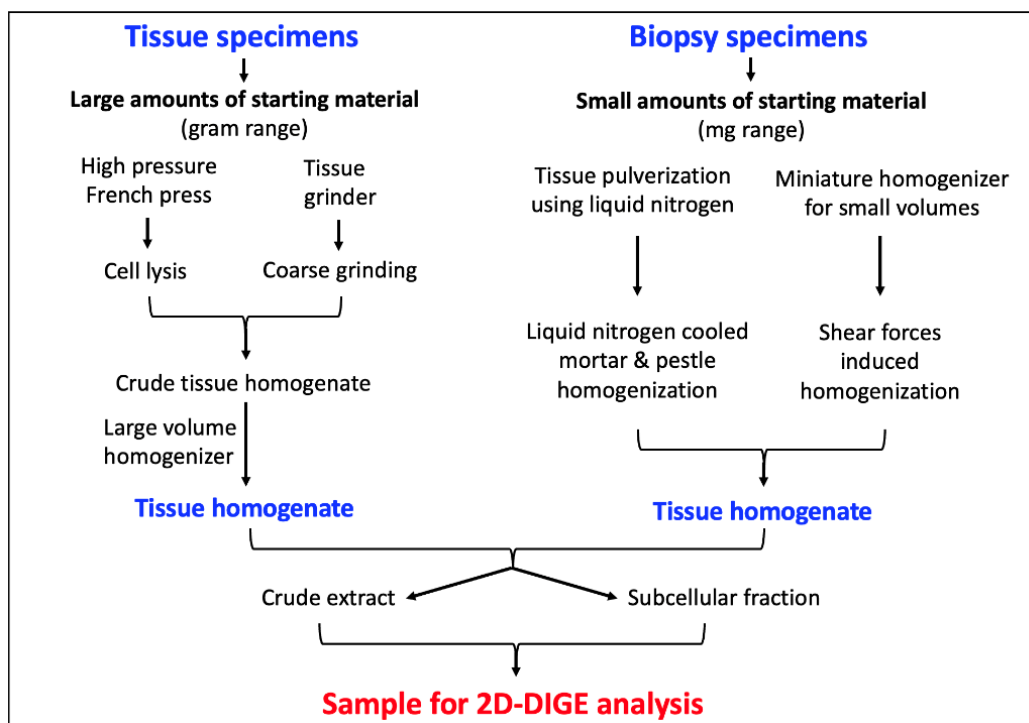


**Figure 2.** Summarizing scheme of tissue preparation for analysis by fluorescence two-dimensional difference gel electrophoresis (2D-DIGE). If large amounts of tissue specimens are available, samples can be conveniently homogenized by large-volume and high-pressure devices or tissue grinders and then be used as crude extracts or being further sub-fractionated by differential centrifugation or affinity isolation. Small specimens from biopsy material can be prepared by pulverization in a liquid nitrogen-cooled miniature mortar and pestle system or with the help of hand-held and small-scale homogenizers.

The protein concentration in suspensions can be determined by various standardized methods [20]. In the case of tissue homogenates and gel electrophoretic samples, it is crucial to take into account the potential interference by non-protein components during protein determination, such as detergents, chaotropic chemicals, reducing agents, ampholytes, salts and buffers [21]. The determination of protein concentration can be carried out with the Coomassie Brilliant Blue binding assay [21, 22], the bicinchoninic acid assay [23], the eosin dye binding assay [24], long-wave-absorbing cyanine probes [25], copper binding to protein [26], dye-metal binding systems [27], modified Lowry-type biuret assays [28], microbead-based protein binding assays [29] and protein determination by amino acid analysis [30].

This chapter describes a dye-metal based colorimetric assay for protein determination prior to 2D-DIGE analysis. **Figure 3** provides an overview of the various steps involved in this protein assay. The amount of protein present in individual samples is determined by a characteristic brown-to-green color change, which is measured in a spectrophotometer at 660 nm and compared to a standard curve with absorbance values generated by a dilution series of known protein concentration [27]. The assay is suitable for the accurate protein quantitation in extracted tissue fractions from a variety of samples, such as diaphragm, *gastrocnemius* muscle, brain and liver (**Figure 4**), prior to differential labelling with fluorescent dyes and two-dimensional gel electrophoretic separation.

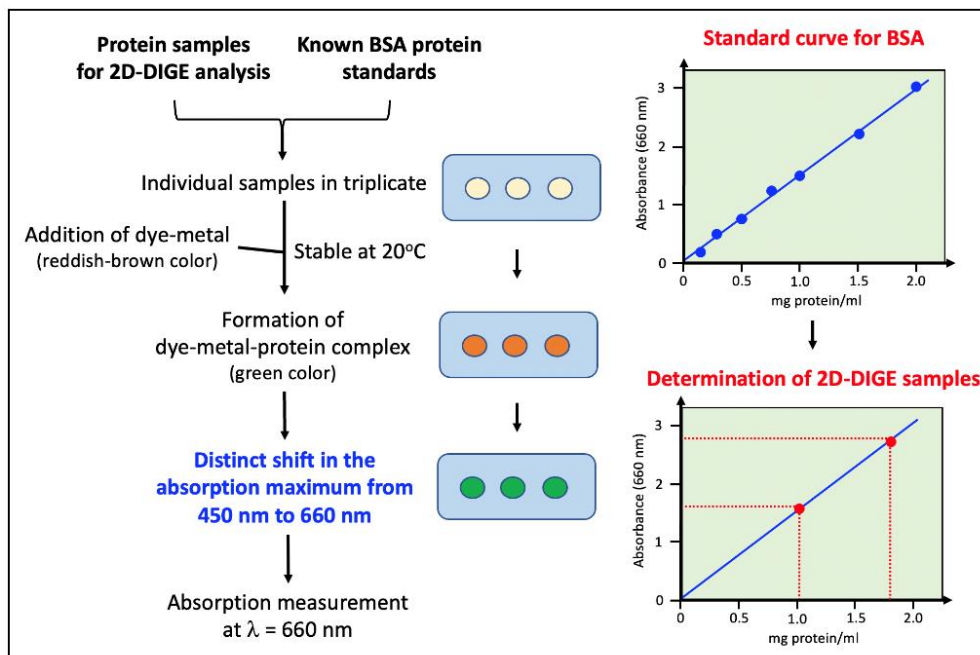


**Figure 3.** Overview of a standardized dye-metal based colorimetric assay for the determination of protein. The described assay is highly suitable for the determination of protein content in

samples prior to differential fluorescent tagging and gel electrophoretic separation. Shown is a flowchart of the main steps involved in this protein assay [27] and the usage of a standard curve for protein determination generated with bovine serum albumin (BSA).

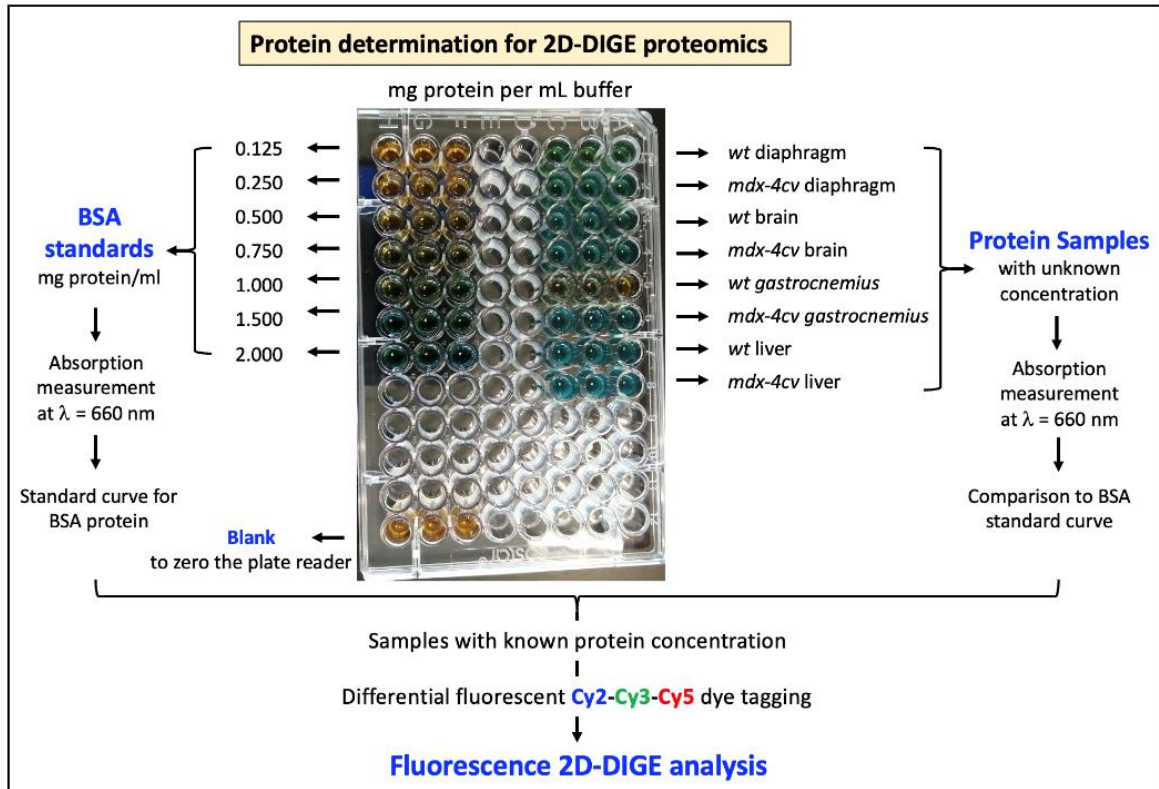


**Fig. 4** Determination of protein concentration in unknown samples to be used for two-dimensional difference gel electrophoresis (2D-DIGE) analysis. Shown is a flat-bottomed 96-well plate with individual samples in triplicate and their color change due to increasing amounts of bovine serum albumin (BSA) ranging from 0.125 to 2.000 mg protein per mL buffer as compared to wild type (*wt*) and dystrophic (*mdx-4cv*) samples (*wt* diaphragm, *mdx-4cv* diaphragm, *wt* brain, *mdx-4cv* brain, *wt* gastrocnemius muscle, *mdx-4cv* gastrocnemius muscle, *wt* liver and *mdx-4cv* liver). In addition, a blank is shown that is used to zero the microplate reader.

## 2. Materials

### 2.1. Equipment

Equipment for tissue homogenization and protein determination is available from various commercial sources.

1. Sterile medical gauze.
2. Analytical weighing scale.
3. Razor blades.
4. Hand-held tissue homogenizer.
5. Dewar for liquid nitrogen.
6. Thermomixer.
7. Sonicator.
8. Microcentrifuge.
9. Microplates (flat-bottomed 96-well plates).
10. Vortex.
11. Plate shaker.
12. Plate reader.
13. Accurate single channel pipettes.
14. Accurate cuvettes.

## 2.2. Solutions

**All solutions should be prepared with analytical grade chemicals and ultrapure water.**

1. Homogenization buffer: 7 M urea, 2 M thiourea, 4% (w/v) CHAPS, 2% (w/v) IPG buffer pH 3-10 ampholytes (Amersham/GE Healthcare), 2 % (w/v) dithiothreitol (*see Note 1*). Depending on the type of tissue to be analysed and the subsequent analytical steps, the buffer can be supplemented with protease inhibitors to prevent excess degradation of sensitive proteins (*see Note 2*).
2. 2D-DIGE rehydration buffer: Homogenization buffer (1 ml) supplemented with 0.002 % Bromphenol Blue dye and 12 ml Destreak reagent (Amersham/GE Healthcare).
3. Protein standards: Individual solutions containing 25, 50, 125, 250, 500, 750, 1000, 1500 and 2000 µg protein per mL homogenization buffer (*see Note 3*).

## 2.3. Mice

1. Wild type mice (12 months old; male); C57BL/6 (Jackson Laboratory) for the preparation of normal diaphragm, *gastrocnemius* muscle, brain and liver samples.
2. Dystrophic *mdx-4cv* mice (12 months old; male); B6Ros.Cg-*Dmd*<sup>*mdx-4Cv*</sup>/J (Jackson Laboratory) for the preparation of dystrophic diaphragm, *gastrocnemius* muscle, brain and liver samples.

### 3. Methods

#### 3.1. Preparation and homogenization of tissue extracts

1. Freshly dissect tissue samples of interest and transport them on sterile medical gauze in an appropriately cooled container to the laboratory for further processing (*see Note 4*).
2. For comparative studies, normal diaphragm, *gastrocnemius* muscle, brain and liver specimens are prepared from wild type mice, and dystrophic diaphragm, *gastrocnemius* muscle, brain and liver specimens are prepared from age-matched *mdx-4cv* mice.
3. Depending on the type of tissue under investigation, specimens can be briefly washed with phosphate-buffered saline to remove excess blood or interfering fatty or connective tissue.
4. For proper statistical analysis, use ideally 6 biological repeats and 2 technical repeats per condition to be studied by differential fluorescent tagging and two-dimensional gel electrophoretic separation (*see Note 5*).
5. Determine the wet weight of individual tissue samples, i.e. diaphragm, *gastrocnemius* muscle, brain and liver, to be compared by proteomic analysis.
6. Use a sharp razor blade to finely chop 100 mg of individual tissue specimens into small pieces.
7. Tissue pieces should then be transferred to a large and round-bottomed plastic tube.
8. Add 10 ml of ice-cold homogenization buffer to the plastic tube.
9. Homogenize the tissue pieces with the help of a handheld homogenizer (*see Note 6*). Several bursts of blending at 20 s intervals usually result in a homogeneous suspension (*see Note 7*).
10. Leave tubes with freshly homogenated samples for 10 min on ice, so that the suspension can settle down in case of foam-up during tissue blending.
11. Briefly sonicate samples that contain tough tissue specimens on ice. Usually, 6 bursts of 10 s with 1 min breaks give good results and properly suspend homogenates.
12. Transfer individual samples to pre-cooled 1.5 ml microcentrifuge tubes.
13. Gently mix samples for 1.5 h at 4°C on a Thermomixer.
14. Centrifuge the mixture for 20 min at 20,000 x g in a pre-cooled microcentrifuge at 4°C.
15. Collect the protein-containing middle layer of the supernatant fraction (*see Note 8*).
16. Transfer the supernatant to a fresh microcentrifuge tube (*see Note 9*).
17. If necessary, samples can be treated at this stage to remove potentially interfering chemicals. This can be carried out by commercially available clean-up kits for gel electrophoresis or acetone precipitation (*see Note 10*).

18. Following a suitable clean-up procedure, resuspend the protein fraction in 2D-DIGE rehydration buffer for fluorescent tagging and gel electrophoretic analysis (*see Note 11*).

### **3.2. Determination of protein concentration**

For a successful 2D-DIGE analysis, it is crucial to accurately determine the protein concentration in individual tissue extracts to be compared by gel-based proteomics using a reliable protein quantification method. A large variety of suitable protein assays are commercially available (*see Note 12*). This section describes a colorimetric assay based on color change from reddish-brown to green, which can be conveniently measured at 660 nm with a standard spectrophotometer.

1. Use bovine serum albumin (or another suitable protein) as a protein standard to generate a standard curve with a linear relationship between protein concentration and absorbance (*see Note 13*).
2. A standard graph can be established with 125, 250, 500, 750, 1000, 1500 and 2000  $\mu\text{g}$  protein per mL (*see Note 14*).
3. Transfer 10  $\mu\text{L}$  of each protein standard solution to individual wells in a flat-bottomed 96-well plate. Each standard concentration should be measured in triplicate.
4. Transfer 10  $\mu\text{L}$  of the tissue suspensions to individual wells on the same microplate. Each individual sample with unknown protein concentration should be measured in triplicate.
5. To generate a blank sample, transfer 10  $\mu\text{L}$  of a suitable buffer (such as 2D-DIGE rehydration buffer) into individual wells on the same microplate in triplicate.
6. Add 150  $\mu\text{L}$  of the protein assay reagent (i.e. Pierce 660 nm Protein Assay Reagent from ThermoFisher Scientific) that is supplemented with ionic detergent compatibility reagent (i.e. Ionic Detergent Compatibility Reagent for Pierce 660 nm Protein Assay Reagent from ThermoFisher Scientific) to each well in the microplate (*see Note 15*).
7. Cover the microplate and briefly mix the samples and the protein assay reagent on a plate shaker at medium speed (*see Note 16*).
8. Incubation of the dye-containing protein suspension should be carried out for 5 min at 20°C.
9. Zero the plate reader with the blank samples to generate an averaged baseline value.
10. Measure the absorbance of the various bovine serum albumin standards (125, 250, 500, 750, 1000, 1500 and 2000  $\mu\text{g}$  protein per mL) at a wavelength of 660 nm.
11. Take the 660 nm measurement for each bovine serum albumin standard and plot it against its known protein concentration in mg/mL.

12. Following the establishment of a protein standard curve, measure the absorbance of the tissue suspensions with unknown protein concentration at 660 nm.
13. Use graphical or mathematical methods to compare the absorbance values of the samples with unknown protein concentration with the standard curve.
14. Equalize the protein concentration in all samples to be analysed by 2D-DIGE using an appropriate buffer, such as 2D-DIGE rehydration buffer.

#### 4. Notes

1. Different types of cell lysis or tissue homogenization buffers can be used for the preparation of protein suspensions. Buffers can vary in their content of urea and detergents. Dependent on the subsequent analytical requirements, 2D-DIGE buffer systems might also differ in their ampholyte composition.
2. A variety of protease inhibitor mixtures are commercially available. In order to prevent excess protein degradation during individual tissue homogenization steps, the optimum composition of a protease inhibitor cocktail has to be determined for the preparation of fractions from specific tissues by trial-and-error experiments. Frequently used protease inhibitors are aprotinin, E-64, bestatin, 4-benzenesulfonyl fluoride hydrochloride, leupeptin and pepstatin A
3. Bovine serum albumin standards for the generation of a protein standard curve can be obtained from several commercial sources as convenient ampules with a 2 mg protein per mL stock solution or even pre-diluted protein solutions ranging from 0.125 to 2.0 mg protein per mL standard.
4. Following the harvesting of tissue specimens, samples should be kept in cooled transport containers. Most tissue samples can be quick-frozen at this stage and stored at  $-80^{\circ}\text{C}$  for future usage. Alternatively, individual samples can be homogenized by grinding them to a powder with a liquid nitrogen-cooled mortar and pestle system, followed by resuspension in a suitable buffer complemented with protease inhibitors. Aliquots of suspensions can then be quick-frozen in liquid nitrogen and kept at  $-80^{\circ}\text{C}$  for long-term storage.
5. The number of biological repeats needed for routine 2D-DIGE analyses depends heavily on the type of specimens to be studied. For example, the comparison of wild type versus genetic animal models of human disorders needs considerably less individual samples than studies with human biopsy material due to the considerable inter-individual differences in patient cohorts.
6. Following tissue extraction and transportation to the laboratory, it is crucial to use the most suitable homogenization approach for generating a protein suspension that can be used for differential fluorescent tagging and gel electrophoretic separation. Choosing an optimal cell lysis or tissue homogenization method is greatly dependent on the nature of the starting material, i.e. tough tissue versus soft tissue and/or the availability of small sample sizes versus large amounts of biological material. The most commonly used

techniques involve French Press-type homogenizers, Potter-Elvehjem tissue grinders, bead-assisted mills and liquid nitrogen-cooled mortar and pestle systems.

7. Tissue homogenization should ideally be carried out on ice in order to prevent the potential over-heating of samples, which might otherwise result in protein degradation.
8. Following centrifugation of the homogenate, a small pellet might appear that contains cellular debris and a thin uppermost fatty layer. Both fractions can be discarded. Focus your proteomic analysis on the protein-containing middle layer of the supernatant fraction.
9. At this stage of the preparation of tissue samples for 2D-DIGE analysis, the protein-containing supernatant fraction can be dispensed in 50 ml aliquots and then quick-frozen in liquid nitrogen for long-term storage at  $-80^{\circ}\text{C}$ .
10. For the clean-up step to remove interfering chemicals from the protein suspension, a variety of commercially available kits can be employed that improve the subsequent gel electrophoretic separation of the fluorescently tagged protein species.
11. If full resuspension of samples cannot be easily achieved, use vortexing and/or sonication to aid in the production of a homogeneous protein suspension.
12. It is crucial to accurately determine the protein concentration in samples to be used for comparative gel-based proteomic studies. An alternative method to the Pierce 660 nm Protein Assay used in this protocol is the 2-D Quant Kit from Amersham Biosciences/GE Healthcare, which is also highly suitable for the accurate protein quantification prior to gel electrophoretic separation and 2D-DIGE analysis.
13. Solution with protein standards can be dispensed into suitable aliquots and stored at  $-20^{\circ}\text{C}$ .
14. Ideally a four-parameter curve fit should be employed for the establishment of the protein standard curve to avoid potential problems with linearity across a limited range of concentration magnitudes.
15. The usage of a specific protein assay reagent and the ionic detergent compatibility reagent in this protocol are based on a commercial assay system. However, a great variety of alternative protein dye binding assays are available and can be used instead to determine the protein concentration in 2D-DIGE samples. If detergent is present in

protein suspensions, it is important to add ionic detergent compatibility reagent to the protein assay reagent.

16. Mixing of protein samples with the dye-containing protein assay reagent can usually be achieved by shaking for 1 min at approximately 600 rpm.

### **Acknowledgements**

Research in the author's laboratory has been supported by the Kathleen Lonsdale Institute for Human Health Research, Maynooth University.

### **References**

1. Uozie AC, Aebersold R (2018) Advancing translational research and precision medicine with targeted proteomics. *J Proteomics* 189:1-10.
2. Westermeier R (2014) Looking at proteins from two dimensions: a review on five decades of 2D electrophoresis. *Arch Physiol Biochem* 120:168-172.
3. Zhan X, Li B, Zhan X, Schlüter H, Jungblut PR, Coorsen JR (2019) Innovating the Concept and Practice of Two-Dimensional Gel Electrophoresis in the Analysis of Proteomes at the Proteoform Level. *Proteomes* 7:36.
4. Dowling P, Zweyer M, Swandulla D, Ohlendieck K (2019) Characterization of Contractile Proteins from Skeletal Muscle Using Gel-Based Top-Down Proteomics. *Proteomes* 7:25.
5. Arentz G, Weiland F, Oehler MK, Hoffmann P (2015) State of the art of 2D DIGE. *Proteomics Clin Appl* 9:277-288.
6. Timms JF, Cramer R (2008) Difference gel electrophoresis. *Proteomics* 8:4886-4897.
7. Minden JS, Dowd SR, Meyer HE, Stühler K (2009) Difference gel electrophoresis. *Electrophoresis* 30:S156-S161.
8. Kondo T (2019) Cancer biomarker development and two-dimensional difference gel electrophoresis (2D-DIGE). *Biochim Biophys Acta Proteins Proteom* 1867:2-8.
9. Carberry S, Zweyer M, Swandulla D, Ohlendieck K (2013) Application of fluorescence two-dimensional difference in-gel electrophoresis as a proteomic biomarker discovery tool in muscular dystrophy research. *Biology (Basel)* 2:1438-1464.

10. Magagnotti C, Fermo I, Carletti RM, Ferrari M, Bachi A (2010) Comparison of different depletion strategies for improving resolution of the human urine proteome. *Clin Chem Lab Med* 48:531-535.
11. Zhang AH, Sun H, Yan GL, Han Y, Wang XJ (2013) Serum proteomics in biomedical research: a systematic review. *Appl Biochem Biotechnol* 170:774-786.
12. Simpson RJ (2010) Homogenization of mammalian tissue. *Cold Spring Harb Protoc* 2010:pdb.prot5455.
13. DeCaprio J, Kohl TO (2019) Using Dounce Homogenization to Lyse Cells for Immunoprecipitation. *Cold Spring Harb Protoc* 2019(7).
14. Dias PRF, Gandra PG, Brenzikofer R, Macedo DV (2020) Subcellular fractionation of frozen skeletal muscle samples. *Biochem Cell Biol* 98:293-298.
15. Goldberg S (2021) Mechanical/Physical Methods of Cell Disruption and Tissue Homogenization. *Methods Mol Biol* 2261:563-585.
16. Lee YH, Tan HT, Chung MC (2010) Subcellular fractionation methods and strategies for proteomics. *Proteomics* 10:3935-3956.
17. Zhang H, Lyden D (2019) Asymmetric-flow field-flow fractionation technology for exomere and small extracellular vesicle separation and characterization. *Nat Protoc* 14:1027-1053.
18. Jalaludin I, Lubman DM, Kim J (2021) A guide to mass spectrometric analysis of extracellular vesicle proteins for biomarker discovery. *Mass Spectrom Rev* 8:e21749.
19. Noble JE, Bailey MJ (2009) Quantitation of protein. *Methods Enzymol* 463:73-95.
20. Goldring JPD (2019) Measuring Protein Concentration with Absorbance, Lowry, Bradford Coomassie Blue, or the Smith Bicinchoninic Acid Assay Before Electrophoresis. *Methods Mol Biol* 1855:31-39.
21. Bradford MM (1976) A rapid and sensitive method for the quantitation of microgram quantities of protein utilizing the principle of protein-dye binding. *Anal Biochem* 72:248-254.
22. Georgiou CD, Grintzalis K, Zervoudakis, Papapostolou I (2008) Mechanism of Coomassie brilliant blue G-250 binding to proteins: a hydrophobic assay for nanogram quantities of proteins. *Anal Bioanal Chem* 391:391-403
23. Walker JM (1994) The bicinchoninic acid (BCA) assay for protein quantitation. *Methods Mol Biol* 32:5-8.
24. Waheed AA, Rao KS, Gupta PD (2000) Mechanism of dye binding in the protein assay using eosin dyes. *Anal Biochem* 287:73-79.

25. Zheng H, Mao YX, Li DH, Zhu CQ (2003) Dye-binding protein assay using a long-wave-absorbing cyanine probe. *Anal Biochem* 318:86-90.
26. Wilkinson-White LE, Easterbrook-Smith SB (2008) A dye-binding assay for measurement of the binding of Cu(II) to proteins. *J Inorg Biochem* 102:1831-1838.
27. Antharavally BS, Mallia KA, Rangaraj P, Haney P, Bell PA (2009) Quantitation of proteins using a dye-metal-based colorimetric protein assay. *Anal Biochem* 385:342-345.
28. Shen YX, Xiao K, Liang P, Ma YW, Huang X (2013) Improvement on the modified Lowry method against interference of divalent cations in soluble protein measurement. *Appl Microbiol Biotechnol* 97:4167-78.
29. Snider EJ, Crowley AR, Raykin J, Kim RK, Splaine F, Ethier CR (2020) A flexible, robust microbead-based assay for quantification and normalization of target protein concentrations. *Anal Biochem* 590:113510.
30. May C, Serschnitzki B, Marcus K (2021) Good Old-Fashioned Protein Concentration Determination by Amino Acid Analysis. *Methods Mol Biol* 2228:21-28.

**Proteomic identification of markers of membrane repair, re-generation and fibrosis in the aged and dystrophic diaphragm**

Published on 22 October 2022

Gargan, S., Dowling, P., Zweyer, M., Henry, M., Meleady, P., Swandulla, D., & Ohlendieck, K. (2022). Proteomic Identification of Markers of Membrane Repair, Regeneration and Fibrosis in the Aged and Dystrophic Diaphragm. *Life (Basel, Switzerland)*, 12(11), 1679. <https://doi.org/10.3390/life12111679>.

**Abstract:** Deficiency in the membrane cytoskeletal protein dystrophin is the underlying cause of the progressive muscle wasting disease named Duchenne muscular dystrophy. In order to identify novel disease marker candidates and confirm the complexity of the pathobiochemical signature of dystrophinopathy, mass spectroscopic screening approaches represent ideal tools for comprehensive biomarker discovery studies. In this report, we describe the comparative proteomic analysis of young versus aged diaphragm muscles from wild type versus the dystrophic *mdx-4cv* mouse model of X-linked muscular dystrophy. The survey confirmed the drastic reduction of the dystrophin-glycoprotein complex in the *mdx-4cv* diaphragm muscle and concomitant age-dependent changes in key markers of muscular dystrophy, including proteins involved in cytoskeletal organization, metabolite transportation, the cellular stress response and excitation-contraction coupling. Importantly, proteomic markers of the regulation of membrane repair, tissue regeneration and reactive myofibrosis were identified by mass spectrometry and changes in key proteins were confirmed by immunoblotting. Potential disease marker candidates include various isoforms of annexin, the matricellular protein periostin and a large number of collagens. Alterations in these proteoforms can be useful to evaluate adaptive, compensatory and pathobiochemical changes in the intracellular cytoskeleton, myofiber membrane integrity and the extracellular matrix in dystrophin-deficient skeletal muscle tissues.

**Keywords:** annexin; biomarker; collagen; degeneration; dystrophinopathy; fibrosis; membrane repair; muscular dystrophy; periostin; regeneration

## 1. Introduction

Muscular dystrophies form a large group of progressive muscle wasting diseases in the domain of inherited neuromuscular disorders [1-3] and are triggered by a variety of primary abnormalities [4]. Mutations in the *DMD* gene cause dystrophinopathies, including severe Duchenne muscular dystrophy of early childhood and its more benign and later onset form named Becker's muscular dystrophy [5,6]. Dystrophinopathies are characterized by the almost complete loss or abnormal size of the dystrophin protein isoform Dp427-M in skeletal muscles [7,8]. The *DMD* gene is extremely large and contains several promoters [9]. Dystrophin proteins of 45 kDa to 427 kDa are expressed in a tissue-specific pattern [10]. Full-length isoforms of dystrophin are mostly found in muscular and neuronal tissues [11-13] with major cytoskeletal functions [14,15].

In skeletal muscles, dystrophin acts as a molecular anchor of a sarcolemmal glycoprotein complex that stabilizes the cellular periphery by indirectly linking extracellular merosin (laminin-211) of the basal lamina to cortical g-actin of the intracellular cytoskeleton [16-18]. The connection of the full-length dystrophin isoform to the microtubular network makes the Dp427-M protein a member of the family of giant cytolinkers in skeletal muscles [19]. The dystrophin complex also supports cellular signaling pathways and provides lateral force transmission at costamers [20]. The members of the core dystrophin-glycoprotein complex include the Dp427-M isoform of dystrophin,  $\alpha$ /b-dystroglycans,  $\alpha$ /b/g/d-sarcoglycans, sarcospan, a-dystrobrevin and  $\alpha$ /b-syntrophins [21,22].

Importantly, the expression of the dystrophin-glycoprotein complex is greatly reduced in dystrophinopathy [23-25] resulting in the loss of trans-plasmalemmal linkage in dystrophic skeletal muscles [26]. This was shown to impair sarcolemmal integrity and render dystrophin-deficient fibers more susceptible to membrane rupturing, which in turn triggers abnormal ion homeostasis and impaired signaling, affecting especially calcium handling and excitation-contraction coupling in muscular dystrophy [27-29]. Dystrophinopathies are mainly characterized by progressive skeletal muscle weakness, cognitive impairment in a subset of

Duchenne patients, articular deformities, scoliosis and the occurrence of cardio-respiratory failure, which represent the main cause of death [6,30,31]. In addition to skeletal muscle weakness, Duchenne muscular dystrophy is associated with a variety of less severe and body-wide complications affecting liver metabolism, the gastrointestinal tract, the immune system and kidney function [30-32]. This makes X-linked muscular dystrophy a multi-systems disease with a primary neuromuscular pathology, which is reflected by complex changes in the serum biomarker profile of Duchenne patients [33-35].

In order to improve the differential diagnosis, prognostic evaluation and therapeutic-monitoring of the complex pathophysiology of muscular dystrophy, a considerable number of systematic studies have been applied to screen both tissue and biofluid specimens [36-38]. Proteomic searches for novel biomarker candidates have included clinical samples from patients afflicted with Duchenne/Becker muscular dystrophy [39,40] and various animal models of dystrophinopathy, such as dystrophic mice, dogs and pigs [41-46]. Animal models play a key role in the initial identification of new biomarkers [47-50] that can then be utilized for the evaluation of novel therapeutic approaches to treat dystrophinopathies [51-54]. Proteome-wide changes in the skeletal musculature were established to occur in the contractile apparatus, signaling pathways, the cytoskeletal network, metabolite transportation, bioenergetic pathways, the cellular stress response and the extracellular matrix [29,55-57]. Building on these findings, the new study presented in this report aimed at studying the effects of aging on dystrophinopathy and establish a comprehensive biomarker signature of the advanced stages of X-linked muscular dystrophy.

The mass spectrometry-based proteomic screening of young versus aged *mdx-4cv* diaphragm muscle described in this report has revealed complex proteome-wide changes in relation to dystrophin deficiency. Especially interesting was the identification of drastic and age-related increases in crucial markers of membrane repair regulation, tissue regeneration and reactive myofibrosis, *i.e.* annexins [58-60], dysferlin [61-63], caveolins [64-66], integrins [67-69], cadherin [70-72], CD34 [73-75], periostin [76-78] and collagens [79-81]. Changes in annexin 2, periostin and collagen VI were independently confirmed by comparative immunoblot analysis.

This is of considerable biomedical interest since annexins are intrinsically involved in the regulation of membrane repair [82-84], and the extracellular collagen network and its associated components play a crucial role in the stabilization, force transmission and functioning of skeletal muscles [85-87]. Considerable crosstalk occurs between the extracellular matrix and contractile fibers in various myopathies [88-90]. Thus, the elevated

expression levels of these crucial markers of regeneration, membrane repair and reactive myofibrosis at advanced stages of X-linked muscular dystrophy could be useful for the establishment of robust and informative indicators of changes in the sarcolemma and extracellular matrix region during the progression of dystrophinopathy [91-93].

## **2. Materials and Methods**

### *2.1. Materials*

General materials and analytical reagents for the comparative proteomic survey of normal versus dystrophic diaphragm muscles were obtained from Bio-Rad Laboratories (Hemel-Hempstead, Hertfordshire, UK), GE Healthcare (Little Chalfont, Buckinghamshire, UK) and Sigma Chemical Company (Dorset, UK). Protease inhibitor cocktail tablets were from Roche (Mannheim, Germany). For digestion of protein samples, MS-grade trypsin protease was purchased from ThermoFisher Scientific (Dublin, Ireland). Filter-aided sample preparations were carried out with Vivacon 500 spin filters (VN0H22; 30,000 MWCO) from Sartorius (Göttingen, Germany). Precast Invitrogen Bolt 4-12% Bis-Tris gels and Whatman nitrocellulose transfer membranes were used for one-dimensional gel electrophoresis and immunoblotting, respectively, and obtained from Bio-Science Ltd. (Dun Laoghaire, Ireland). For the visualization of gel-separated protein bands, InstantBlue Coomassie Protein Stain was purchased from Expedeon (Heidelberg, Germany). Primary antibodies for immunoblotting were from Invitrogen, Waltham, MA, USA (mAb SD83-03 against collagen VI), Abcam, Cambridge, UK (pAb ab41803 to annexin ANXA2) and Novus Biologicals, Cambridge, UK (mAb NBP1-30042 against periostin). Secondary peroxidase-conjugated anti-IgG were purchased from Sigma Chemical Company (Dorset, UK). Chemiluminescence kits were from Roche (Mannheim, Germany). The Pierce 660 nm Protein Assay Reagent was purchased from ThermoFisher Scientific (Dublin, Ireland).

### *2.2. Wild Type and Dystrophic Diaphragm Muscle Specimens*

The dissection of freshly prepared *postmortem* diaphragm specimens from 3-month and 15-month old wild type C57BL6 mice and aged-matched samples from the *mdx-4cv* mouse model of Duchenne muscular dystrophy was performed according to institutional regulations. Normal controls and dystrophic mice were handled in strict adherence to local governmental and institutional animal care regulations and were approved by the Institutional Animal Care and

Use Committee (Amt für Umwelt, Verbraucherschutz und Lokale Agenda der Stadt Bonn, North Rhine-Westphalia, Germany). Frozen specimens were transported on dry ice to Maynooth University in accordance with the regulations of the Department of Agriculture (animal by-product register number 2016/16 to the Department of Biology, National University of Ireland, Maynooth). Comparative proteomic analyses were carried out with muscle samples from 6 wild type and 6 dystrophic mice. Verification analyses using immunoblotting were carried out with specimens derived from a minimum of 4 wild type and 4 dystrophic mice.

### 2.3. Preparation of Muscle Tissue Extracts

The preparation of tissue specimens and subsequent analysis of extracted proteins by bottom-up proteomics was performed by a standardized procedure, which has recently been described in a detailed methods paper [94]. Wild type C57BL6 and dystrophic *mdx-4cv* mice of differing age were sacrificed in the Bioresource Unit of the University of Bonn and diaphragm muscle specimens then quick-frozen in liquid nitrogen [45]. Frozen samples were transported on dry ice to Maynooth University and stored at -80°C prior to comparative proteomic analysis. Both, young and aged diaphragm samples were homogenized in a comparative way using lysis buffer containing 4% (w/v) sodium dodecyl sulfate, 0.1 M dithiothreitol and 100 mM Tris-Cl, pH 7.6, as well as a protease inhibitor cocktail [95]. Homogenization was carried out with a handheld homogenizer (Kimble Chase, Rockwood, TN, USA) [96]. Following homogenization, samples were briefly treated in a sonicating water bath, then heated for 3 min at 95°C and centrifuged at 16,000×g for 5 min. The protein-containing supernatant was extracted and used for subsequent proteomic studies [95]. The Pierce 660 nm Protein Assay system was used to determine protein concentration [97]. Extracted diaphragm proteins were further processed for mass spectrometric analysis. Samples were mixed with 200 µL of 8 M urea, 0.1 M Tris pH 8.9 in Vivacon 500 spin filter units and centrifuged at 14,000×g for 15 min. The filter-aided sample preparation (FASP) method, developed by Wiśniewski and co-workers [98], was used for sample processing, buffer switching and protein trypsination prior to mass spectrometric peptide analysis [94].

### 2.4. Mass Spectrometry and Proteomic Data Analysis

The comparative label-free liquid chromatography mass spectrometric analysis of young versus aged diaphragm muscles from wild type versus the dystrophic *mdx-4cv* mouse model of dystrophinopathy was performed with a Thermo Orbitrap Fusion Tribrid mass spectrometer from Thermo Fisher Scientific (Waltham, MA, USA). Details of the proteomic workflow

describing all preparative steps and analytical procedures using data-dependent acquisition, as well as bioinformatic data handling, were recently outlined in detail [94]. Reverse-phased capillary high-pressure liquid chromatography was carried out with a Thermo UltiMate 3000 nano system and directly coupled in-line with the Thermo Orbitrap Fusion Tribrid mass spectrometer. The UniProtKB-SwissProt *Mus musculus* database with Proteome Discoverer 2.2 using Sequest HT (Thermo Fisher Scientific) and Percolator were employed for the qualitative data analysis of mass spectrometric files. For the identification of diaphragm proteins, the following crucial search parameters were employed: (i) a value of 0.02 Da for MS/MS mass tolerance, (ii) a value of 10 ppm for peptide mass tolerance, (iii) variable modification settings for methionine oxidation, (iv) fixed modification settings in relation to carbamido-methylation and (v) tolerance for the occurrence of up to two missed cleavages. Peptide probability was set to high confidence. A minimum XCorr score of 1.5 for 1, 2.0 for 2, 2.25 for 3 and 2.5 for 4 charge state was employed for the filtering of peptides. The software analysis programme Progenesis QI for Proteomics (version 2.0; Nonlinear Dynamics, a Waters company, Newcastle upon Tyne, UK) was used to carry out quantitative label-free data analysis. Proteome Discoverer 2.2 using Sequest HT (Thermo Fisher Scientific) and a percolator were employed for the identification of peptides and proteins. Datasets were imported into Progenesis QI software for further analysis. Following the review of protein identifications, only those data that agreed with a crucial set of criteria were deemed as differentially expressed protein species between experimental groups based on statistical significance and high confidence. The criteria included an ANOVA p-value of  $\leq 0.01$  between experimental groups, and proteins with  $\geq 2$  unique peptides contributing to the identification. The Progenesis QI programme calculated the mean abundance for individual protein species in

each experimental condition to determine the maximum fold change for particular proteins. Condition-vs-condition matrixes with mean values were then used to determine the maximum fold change between any two condition's mean protein abundances [94]. The multi-consensus MS files and listings of altered proteins in wild type versus dystrophic diaphragm muscle that were generated by the comparative proteomic study shown in this report have been deposited under the title 'Proteomic analysis of aged *mdx-4cv* diaphragm' with the unique identifier 'qmtre' to the Open Science Foundation (<https://osf.io/qmtre/>). The standard bioinformatic analysis tool PANTHER [99] was utilized for the identification of protein classes.

### 2.5. Comparative Immunoblot Analysis

Primary antibodies to the matricellular protein periostin (POSTN), the extracellular matrix component collagen (COL-VI) and the Ca<sup>2+</sup>-dependent membrane repair protein annexin (ANXA2) were used for the independent verification of key findings from the mass spectrometry-based proteomic screening of young versus aged *mdx-4cv* diaphragm muscle preparations. One-dimensional gel electrophoresis and immunoblot analysis were carried out by standardized methodology [95]. Diaphragm samples were incubated in Laemmli-type sample buffer and heated for 30 min at 37°C. Per lane, 20µg of protein were ran on Invitrogen Bolt 4–12% Bis-Tris gels. Coomassie staining of protein gels was performed with InstantBlue Coomassie Protein Stain. Gel electrophoretically separated proteins were transferred to nitrocellulose membranes for immunoblot analysis. Blocking was performed with a fat-free milk solution and membrane sheets were incubated overnight with 1:1000 (v/v) diluted primary antibodies. Detection of labelled protein bands was carried out by incubation with 1:1000 (v/v) diluted peroxidase-conjugated secondary antibodies and enhanced chemiluminescence. Statistical analysis of immunoblots (n=4) was performed with ImageJ software (NIH, Bethesda, MD, USA), along with Microsoft Excel, in which statistical significance was based on a p-value ≤ 0.05.

## 3. Results

The comparative proteomic profiling of the dystrophin-deficient *mdx-4cv* diaphragm was carried out with a Thermo Orbitrap Fusion Tribrid mass spectrometer and multi-consensus analysis identified 2421 and 2790 protein species in wild type versus *mdx-4cv* preparations, respectively. Throughout the manuscript, names of proteins, protein subunits or protein isoforms that were identified by proteomics are abbreviated in capital letters. Differential protein expression patterns were analyzed by bioinformatics and are displayed in this report according to association with the (i) dystrophin-glycoprotein complex, (ii) the established marker signature of dystrophinopathy, (iii) excitation-contraction coupling, (iv) the annexin family, (v) the collagen family, and (vi) the extracellular matrix. The increased abundance of collagen COL-VI as marker of reactive myofibrosis, the multi-functional periostin (POSTN) as a prototype of a matricellular component and the membrane repair protein annexin ANXA2 were verified by immunoblotting.

### 3.1. Mass spectrometric analysis of young versus aged *mdx-4cv* diaphragm muscle

Overall changes in protein classes were determined by bioinformatic PANTHER analysis [99]. The findings are displayed in Figures 1 and 2, which show drastic alterations in a variety of protein types, including RNA metabolism proteins, cytoskeletal proteins, metabolite interconversion enzymes, protein modifiers and translational proteins. An interesting change between 3-month and 15-month old *mdx-4cv* diaphragm muscle is the drastic increase in the changed density of metabolite interconversion enzymes during aging (Figure 2).

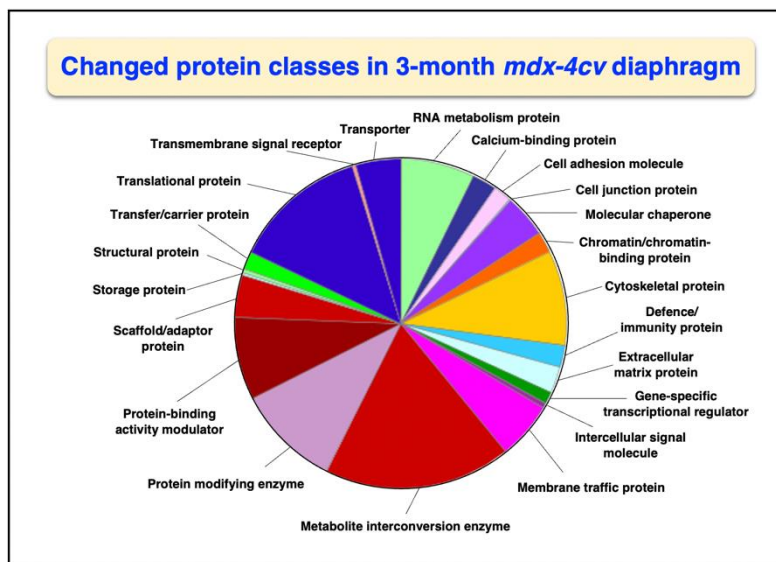


**Figure 1.** Bioinformatic analysis of changed protein classes in 3-month old *mdx-4cv* diaphragm muscle. The analysis was carried out with the PANTHER program [99].

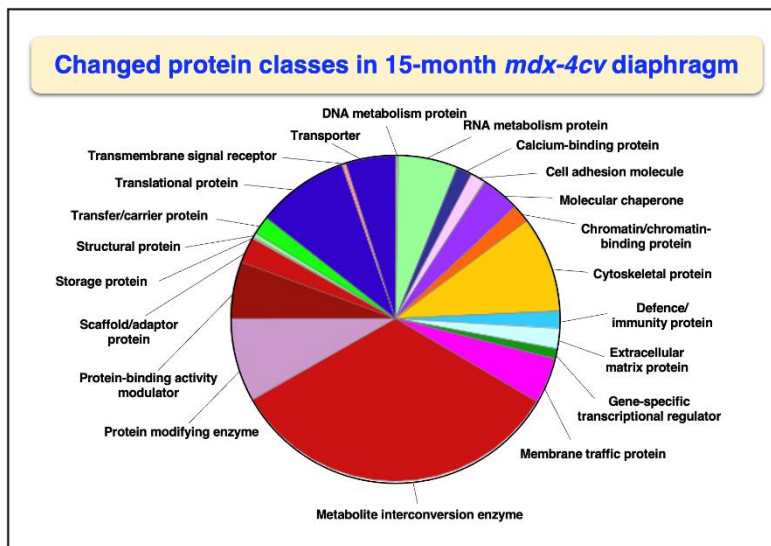


**Figure 2.** Bioinformatic analysis of changed protein classes in 15-month old *mdx-4cv* diaphragm muscle. The analysis was carried out with the PANTHER program [99].

### 3.2. Reduced dystrophin complex in *mdx-4cv* diaphragm muscle

Following the proteomic analysis of young versus aged *mdx-4cv* diaphragm muscle, the mutant status of the analyzed dystrophic muscle specimens was confirmed by comparison between wild type and *mdx-4cv* samples. As diagrammatically shown in Figure 3, the dystrophin complex consists of the cytoskeletal Dp427-M isoform of dystrophin, integral b-dystroglycan, extracellular  $\alpha$ -dystroglycan,  $\alpha/\beta/\gamma/\delta$ -sarcoglycans, sarcospan,  $\alpha$ -dystrobrevin and  $\alpha/\beta$ -syntrophins [20]. Error bars are not commonly used on proteomic diagrams such as these. Linkage to this sarcolemma-associated complex occurs to extracellular collagen isoforms via laminin-211, and intracellularly dystrophin binds to g-actin filaments and tubulins of the microtubular network.

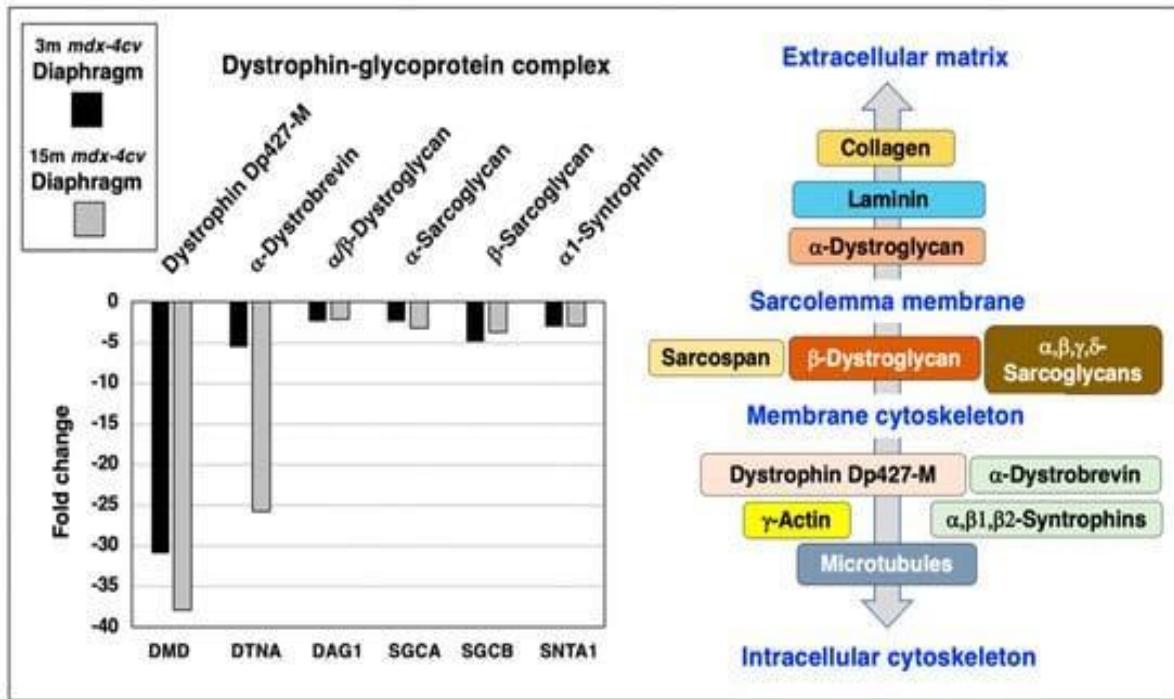


**Figure 3.** Proteomic analysis of the expression of the dystrophin-glycoprotein complex in 3-month (3m, black bars) versus 15-month (15m; grey bars) old *mdx-4cv* diaphragm muscle. On the left is shown a bar diagram of the fold change in abundance of representative members of the dystrophin-glycoprotein complex, as determined by comparative proteomics. Identified proteins included Dystrophin (DMD),  $\alpha/\beta$ -Dystroglycan (DAG1),  $\alpha$ -Sarcoglycan (SGCA),  $\beta$ -Sarcoglycan (SGCB),  $\alpha$ -Dystrobrevin (DTNA) and  $\alpha 1$ -Syntrophin (SNTA1). On the right side is shown a diagrammatic presentation of the dystrophin-glycoprotein complex [20].

Representative members of the core dystrophin-glycoprotein complex were identified by mass spectrometry, *i.e.* dystrophin (DMD),  $\alpha/\beta$ -dystroglycan (DAG1),  $\alpha$ -sarcoglycan (SGCA),  $\beta$ -sarcoglycan (SGCB),  $\alpha$ -dystrobrevin (DTNA) and  $\alpha 1$ -syntrophin (SNTA1), and shown to be greatly reduced in both young and aged *mdx-4cv* diaphragm (Figure 3). The most drastic change between young and old muscle specimens was observed for  $\alpha$ -dystrobrevin in 15-month old *mdx-4cv* diaphragm muscle.

### 3.3. Established changes of dystrophic biomarkers in *mdx-4cv* diaphragm muscle

In order to put this new study into perspective, a variety of established proteomic markers of X-linked muscular dystrophy were analyzed. As shown in Figure 4, increases in the intermediate filament component vimentin (VIM), the microtubular protein isoform tubulin-

alpha-1c (TUBA1C), the intracellular iron regulatory protein ferritin light chain (FTL1), heat shock protein A5 (HSPA5), small heat shock protein B7 (HSPB7), large heat shock protein 90AA1 (HSP90AA1) and nuclear lamin isoform B2 (LMNB2) were confirmed. Characteristic decreases were established for the cytosolic calcium-signaling protein parvalbumin (PVALB) and the metalloenzyme carbonic anhydrase isoform 3 (CA3).

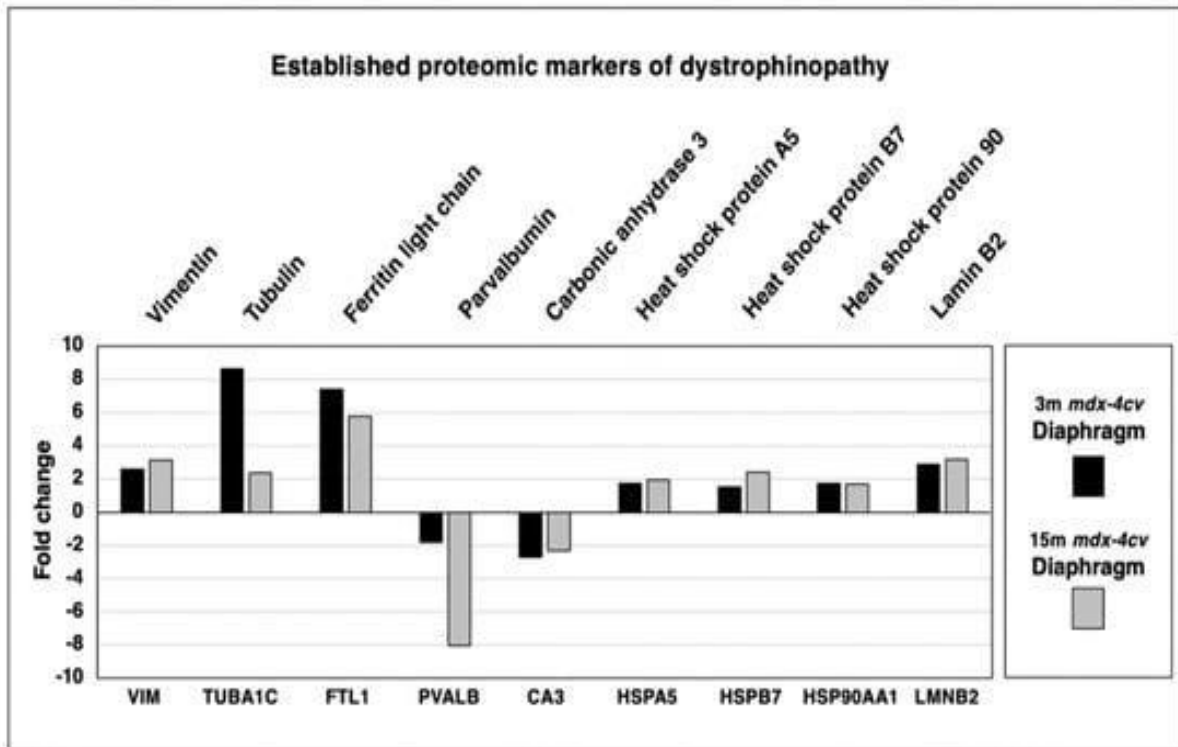


**Figure 4.** Proteomic analysis of the expression of established proteomic markers of X-linked muscular dystrophy in 3-month (3m, black bars) versus 15-month (15m; grey bars) old *mdx-4cv* diaphragm muscle. Identified proteins included Vimentin (VIM), Tubulin-alpha-1c (TUBA1C), Ferritin light chain (FTL1), Heat shock protein A5 (HSPA5), Heat shock protein B7 (HSPB7), Heat shock protein 90AA1 (HSP90AA1), Lamin isoform B2 (LMNB2), Parvalbumin (PVALB) and Carbonic anhydrase isoform 3 (CA3).

### 3.4. Proteomics of excitation-contraction coupling and calcium handling in *mdx-4cv* diaphragm

Since micro-rupturing of the dystrophin-deficient sarcolemma membrane causes disturbed calcium homeostasis and abnormal cellular signaling in X-linked muscular dystrophy, it was of interest to evaluate the status of proteins involved in excitation-contraction coupling and intracellular calcium handling. This included the mass spectrometric survey of the ryanodine receptor calcium-release channel (RYR1) of the sarcoplasmic reticulum, the transverse tubular

L-type calcium channel ( $Ca_v1.1$ ) with its voltage-sensing  $\alpha1S$ -subunit (CACNA1S) and the auxiliary subunits  $\beta1$  (CACNB1) and  $\alpha2/\delta$ (CACNA2D1), the calcium-binding protein calsequestrin (CASQ1) of the terminal cisternae region, the fast SERCA1 isoform of the sarco(endo)plasmic reticulum calcium-ATPase (ATP2A1), and the junctophilins 1 (JPH1) and 2 (JPH2) of the triad junction (Figure 5).

The principal ion channel-containing  $\alpha1S$ -subunit of the transverse tubular L-type calcium channel and its auxiliary  $\beta1$ -subunit were shown to be reduced in both young and aged dystrophic diaphragm muscle. In contrast, the ryanodine receptor, the  $\alpha2/\delta$ -subunit of the transverse tubular calcium channel, fast calsequestrin, the fast sarcoplasmic reticulum calcium ATPase SERCA1 and junctophilins exhibited a reduced expression level only in 15-month old *mdx-4cv* diaphragm.

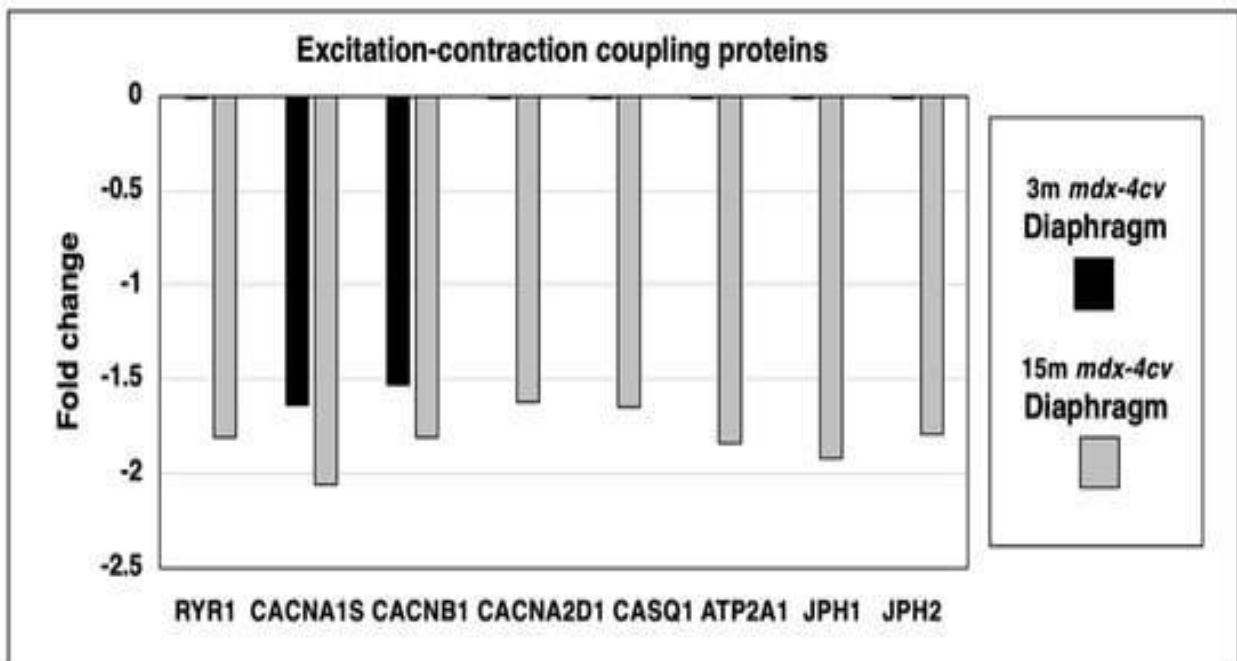


**Figure 5.** Proteomic identification of changes in the expression levels of key proteins involved in excitation-contraction coupling, calcium homeostasis and triad integrity in 3-month (3m, black bars) versus 15-month (15m; grey bars) old *mdx-4cv* diaphragm muscle. This included the Ryanodine receptor calcium-release channel (RYR1), the voltage-sensing L-type calcium channel with its  $\alpha1S$ -subunit (CACNA1S),  $\alpha1$ -subunit (CACNB1) and  $\alpha2/\gamma$ -subunits (CACNA2D1), fast Calsequestrin (CASQ1), the fast SERCA1 Calcium-ATPase (ATP2A1), Junctophilin 1 (JPH1) and Junctophilin 2 (JPH2).

### 3.5. Proteomics of membrane repair and calcium sensing in *mdx-4cv* diaphragm

A protein of central importance in the calcium-dependent membrane repair process of damaged skeletal muscles is dysferlin (DYSF). The mass spectrometric survey of wild type versus *mdx-4cv* diaphragm preparations revealed an increase of this sarcolemmal repair protein. Since the dysferlin/myoferlin system closely interacts with caveolins and annexins, the expression levels of these crucial components of the caveolae structures and calcium regulation, respectively, were also examined. The concentration of caveolin 1 (CAV1) and caveolin 2 (CAV2) increased drastically in aged and dystrophic diaphragm, while the muscle-specific caveolin-3 (CAV3) isoform showed elevated levels in 3-month old *mdx-4cv* diaphragm but only marginal changes in 15-month old dystrophic muscles. Integrins are useful markers of proliferation and the main type present in the skeletal muscle periphery,  $\alpha 7\beta 1$ -integrin (ITGA7/ITGB1), was identified to be increased in both young and aged *mdx-4cv* diaphragm. Interestingly, the expression of the myogenic markers cadherin-13 (CDH13) and CD34 were both elevated in muscular dystrophy. The calcium-dependent annexin isoforms A1 to A7 (ANXA1, ANXA2, ANXA3, ANXA4, ANXA5, ANXA7) of which some are involved in calcium-dependent and dysferlin-associated repair mechanisms of the muscle surface membrane system, were analyzed in 3-month versus 15-month old *mdx-4cv* diaphragm muscle preparations. The degree of increased expression levels in young versus aged *mdx-4cv* diaphragm was found to be relatively comparable (Figure 6).

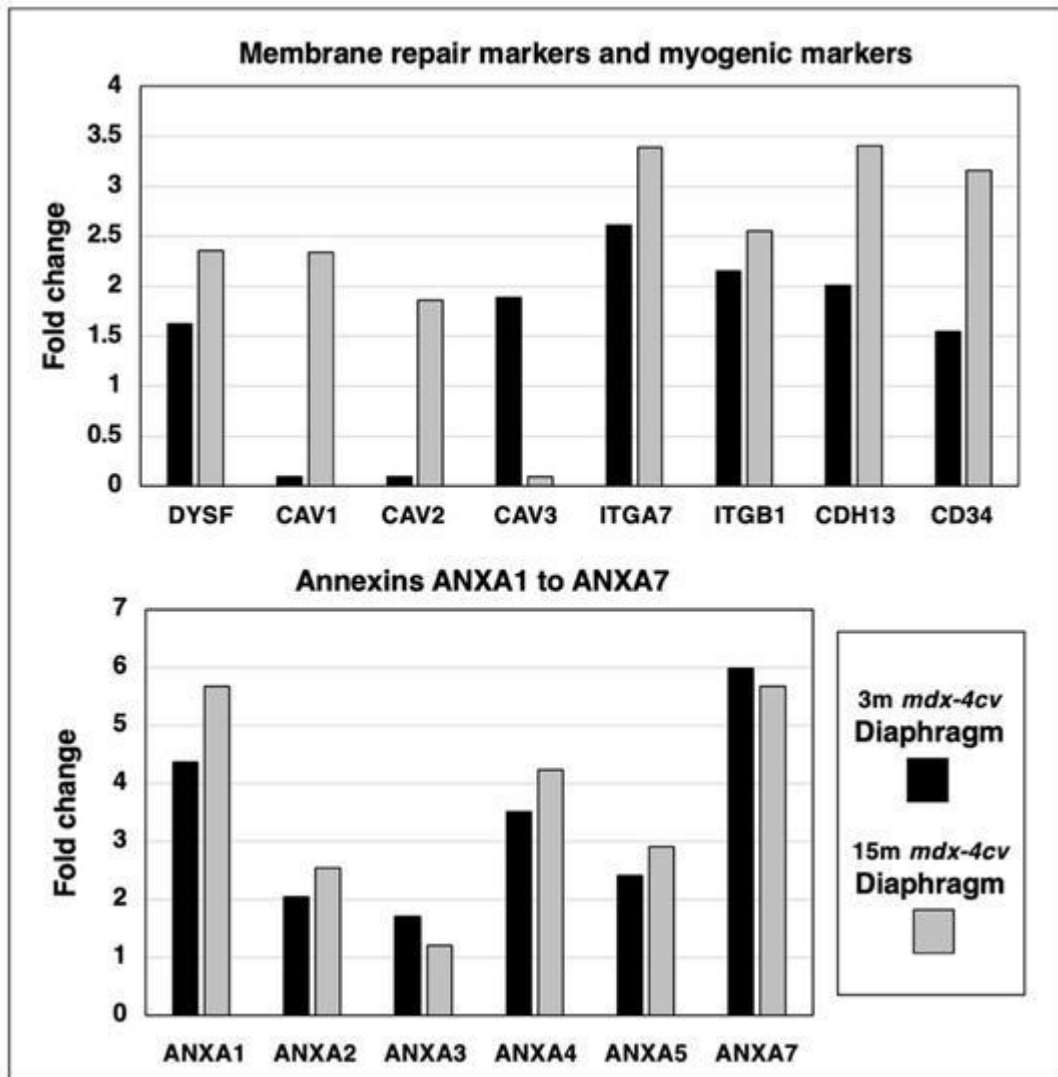


**Figure 6.** Proteomic identification of changes in the expression levels of key proteins involved in membrane repair and calcium sensing in 3-month (3m, black bars) versus 15-month (15m; grey bars) old *mdx-4cv* diaphragm muscle. This included the sarcolemmal membrane repair protein Dysferlin (DYSF), Caveolin 1 (CAV1), Caveolin 2 (CAV2), muscle-specific Caveolin 3 (CAV3), Integrin alpha-7 (ITGA7), Integrin beta-1 (ITGB1), Cadherin-13/T-cadherin (CDH13) and the myogenic marker CD34, as well as Annexin isoforms A1 (ANXA1), A2 (ANXA2), A3 (ANXA3), A4 (ANXA4), A5 (ANXA5) and A7 (ANXA7).

### 3.6. Proteomics of collagens and the extracellular matrix in *mdx-4cv* diaphragm muscle

Skeletal muscles contain a considerable number of collagen isoforms and its extracellular matrix is formed by a highly complex mesh of diverse proteins. The comparative proteomic analysis of 3-month versus 15-month old *mdx-4cv* diaphragm muscle revealed increases in collagen I (COL1A1 and COL1A2 chains), collagen IV (COL4A1, COL4A2 and COL4A3

chains), collagen V (COL5A1 and COL5A2 chains), collagen VI (COL6A1, COL6A2, COL6A5 and COL6A6 chains), collagen XII (COL12A1 chain), collagen XIV (COL14A chain), collagen XV (COL15A1 chain) and collagen XVIII (COL18A1 chain), as shown in Figure 7. Increased levels of crucial extracellular matrix proteins were identified in the case of the matricellular protein periostin (POSTN), the small leucine-rich proteoglycans asporin (ASPN), biglycan (BGN), lumican (LUM) and mimecan/osteoglycin (OGN), the adhesive glycoprotein fibronectin (FN1), the proteoglycan decorin (DCN), the tyrosine-rich acidic matrix protein dermatopontin (DPT), the hemopexin-type glycoprotein vitronectin (VTN) and the basal lamina component nidogen-2/osteonidogen (NID2). The most drastic differences in the degree of increased expression levels between young versus aged *mdx-4cv* diaphragm were found for the collagen chains COL5A1, COL5A2, COL6A5 and COL-XIV, as well as the matricellular protein periostin (Figure 7).

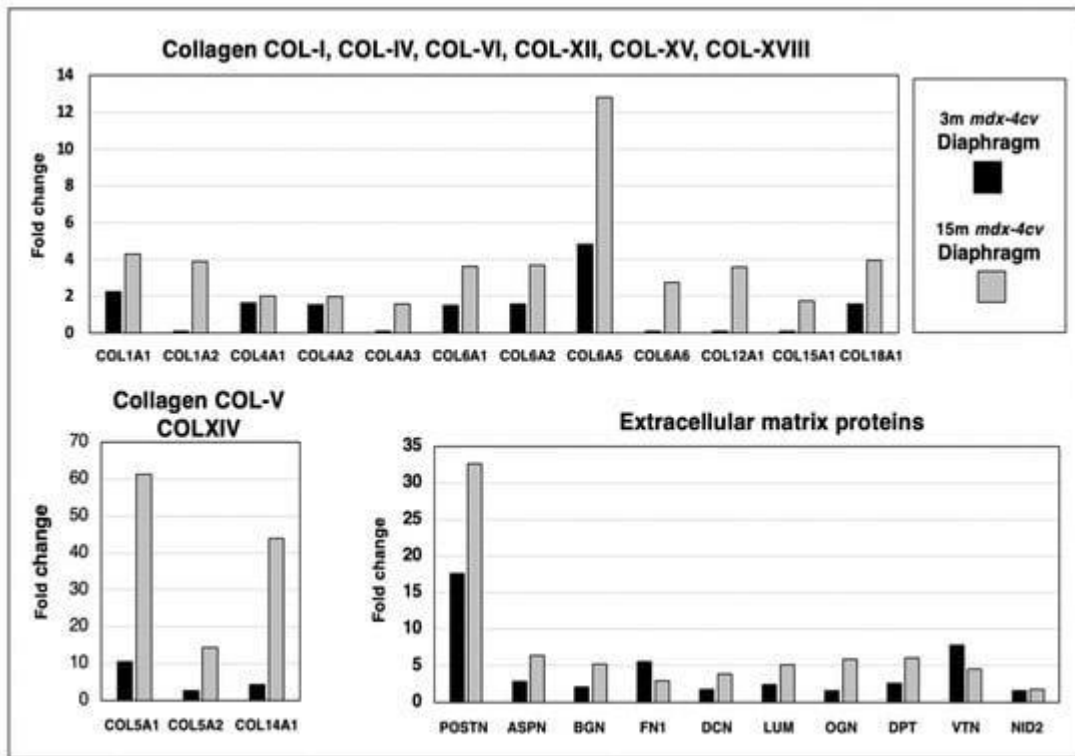


**Figure 7.** Proteomic identification of changes in the expression levels of collagens and related extracellular matrix proteins in 3-month (3m, black bars) versus 15-month (15m; grey bars) old *mdx-4cv* diaphragm muscle. This included Collagen I (COL1A1, COL1A2), Collagen IV (COL4A1, COL4A2, COL4A3), Collagen V (COL5A1, COL5A2), Collagen VI (COL6A1, COL6A2, COL6A5, COL6A6), Collagen XII (COL12A1), Collagen XIV (COL14A), Collagen XV (COL15A1), Collagen XVIII (COL18A1), Periostin (POSTN), Asporin (ASPN),

Biglycan (BGN), Lumican (LUM), Mimecan/osteoglycin (OGN), Fibronectin (FN1), Decorin (DCN), Dermatotin (DPT), Vitronectin (VTN) and Nidogen-2/osteonidogen (NID2).

### 3.7. Immunoblotting of collagen VI, periostin and annexin 2 in *mdx-4cv* diaphragm

Trends in changed protein expression pattern as determined by the above-described comparative mass spectrometric investigation of protein extracts from 3-month versus 15-month old *mdx-4cv* diaphragm muscle were independently verified by immunoblotting, as shown in Figures 8.

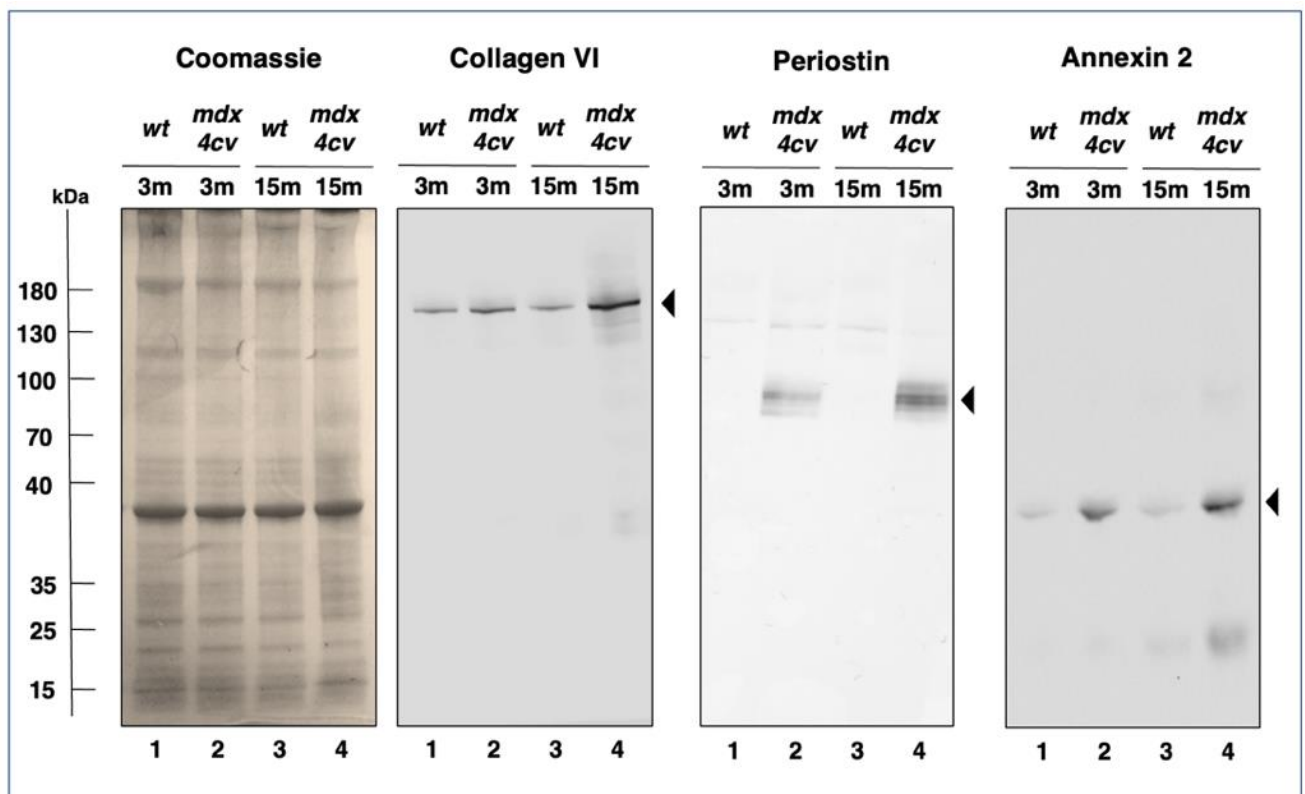


**Figure 8.** Immunoblot analysis of Collagen VI, Periostin and Annexin 2 in *mdx-4cv* diaphragm. Lanes 1 to 4 contain protein extracts from 3-month (3m) versus 15-month (15m) old wild type versus *mdx-4cv* diaphragm, respectively. Molecular weight standards are marked on the left.

Coomassie Blue staining of one-dimensionally separated diaphragm proteins revealed no major differences in the band pattern of 3-month versus 15-month old wild type versus *mdx-4cv* diaphragm preparations. However, immunoblotting with antibodies to collagen COL-VI, periostin and annexin isoform ANXA2 clearly showed a significant increase of these proteins in dystrophic diaphragm muscle. Both, collagen and periostin exhibited high expression levels in aged and dystrophin-deficient muscles (Figure 8).

#### 4. Discussion

The comparative proteomic analysis described in this report was carried out with young versus aged diaphragm muscles from wild type versus the dystrophic *mdx-4cv* mouse model of Duchenne muscular dystrophy. The *mdx*-type models of Duchenne muscular dystrophy are based on the spontaneous *mdx-23* mouse [100] which is characterized by a point mutation in exon 23 of the *DMD* gene [101]. This results in the almost complete deficiency of dystrophin isoform Dp427-M [47] and causes an X-linked myopathy in association with muscular hypotrophy, hypertrophy and hyperplasia in *mdx-23* fibres [102]. Especially the diaphragm muscle is severely affected in *mdx*-type mice and exhibits progressive fiber degeneration and reactive myofibrosis [103-105] making the dystrophin-deficient diaphragm a suitable tissue for studying the molecular and cellular pathogenesis of Duchenne muscular dystrophy [47,49]. An alternative model of dystrophinopathy is the *mdx-4cv* mouse [106] that has been generated by chemical mutagenesis with N-ethylnitrosourea which induced a C-to-T transition at position 7916 in exon 53 [107]. This nonsense point mutation results in the premature termination of translation and the production of a truncated and non-functional dystrophin protein [108]. Importantly, skeletal muscles from the *mdx-4cv* mouse display approximately 10-fold fewer revertant and dystrophin-positive contractile fibers as compared to the *mdx-23* mouse [109]. The drastically reduced presence of revertant fibers makes the *mdx-4cv* mouse an attractive model and has therefore been widely used for (i) the detailed analysis of dystrophic changes in the skeletal musculature [95,96,110-112], (ii) studying dystrophinopathy-related cardiomyopathy [113], (iii) evaluating the protective phenotype of extraocular muscle [114], (iv) surveying of bodily fluids for biomarker candidates including serum, urine and saliva [115-117], (v) the screening of body-wide changes in the multi-systems pathology of X-linked muscular dystrophy including proteome-wide alterations in liver, spleen, kidney, stomach and brain [118-122] and (vi) the testing of new therapeutic procedures to treat muscular dystrophy [123-125].

Building on these studies, we have used the aged *mdx-4cv* diaphragm muscle as a model system to study the advanced stages of X-linked muscular dystrophy. Crucial findings from the mass spectrometric survey include the identification of increased levels of key marker proteins that are involved in the regulation of membrane repair, tissue regeneration and reactive myofibrosis. Annexin isoform ANXA2 [58-60], the matricellular protein periostin [76-78] and collagen isoform COL-VI [79-81], as well as the caveolins CAV1 and CAV2 [64-66],  $\alpha$ 7b1-integrin

[67-69], cadherin-13/T-cadherin [70-72] and CD34 [73-75] were shown to be drastically increased in aged and dystrophin-lacking muscle preparations. Interestingly, the muscle-specific caveolin isoform CAV3 was only elevated in young and dystrophic diaphragm. Immunoblotting clearly verified the increased concentration of specific isoforms of annexin, periostin and collagen in muscular dystrophy. This suggests that these markers of membrane repair, tissue regeneration and myofibrosis are suitable to characterize muscle biopsy specimens from genetic animal models of dystrophinopathy. Since the spontaneous *mdx-23* mouse is the most frequently used animal model in muscular dystrophy research [47], it was of interest to compare the proteomic changes in the chemically induced *mdx-4cv* mouse [106-108] to the naturally occurring *mdx-23* mutant [100-102]. The proteome-wide changes identified in this report on established markers of X-linked muscular dystrophy, *i.e.* decreases in all members of the core dystrophin complex and concomitant increases in vimentin, tubulin, ferritin, various molecular chaperones and lamin, and decreases in parvalbumin and carbonic anhydrase isoform CA3, agree with previous studies of the dystrophic *mdx-23* mouse model [41-46, 126,127]. An increased abundance of collagen COL-VI was also observed in *mdx-23* muscle preparations using two-dimensional gel electrophoresis combined with staining by the fluorescent dye ruthenium II tris bathophenanthroline disulfonate [128].

New biomarker candidates can now be used to improve diagnostic procedures, the accuracy of prognosis, therapeutic-monitoring and the evaluation of potential side effects due to novel pharmacological treatments or new gene therapeutic approaches, such as gene substitution, exon-skipping or gene editing [51-54]. Proteomic biomarkers can be utilized in a variety of crucial biomedical and clinical applications and be useful to improve the evaluation of susceptibility to muscular dystrophy, differential diagnosis, prognostics, prediction of patient sensitivity, pharmacodynamics, monitoring of therapeutic success and drug safety [35]. Figure 9 summarizes some of the key findings of this proteomic survey of aged and dystrophin-deficient *mdx-4cv* diaphragm muscle.

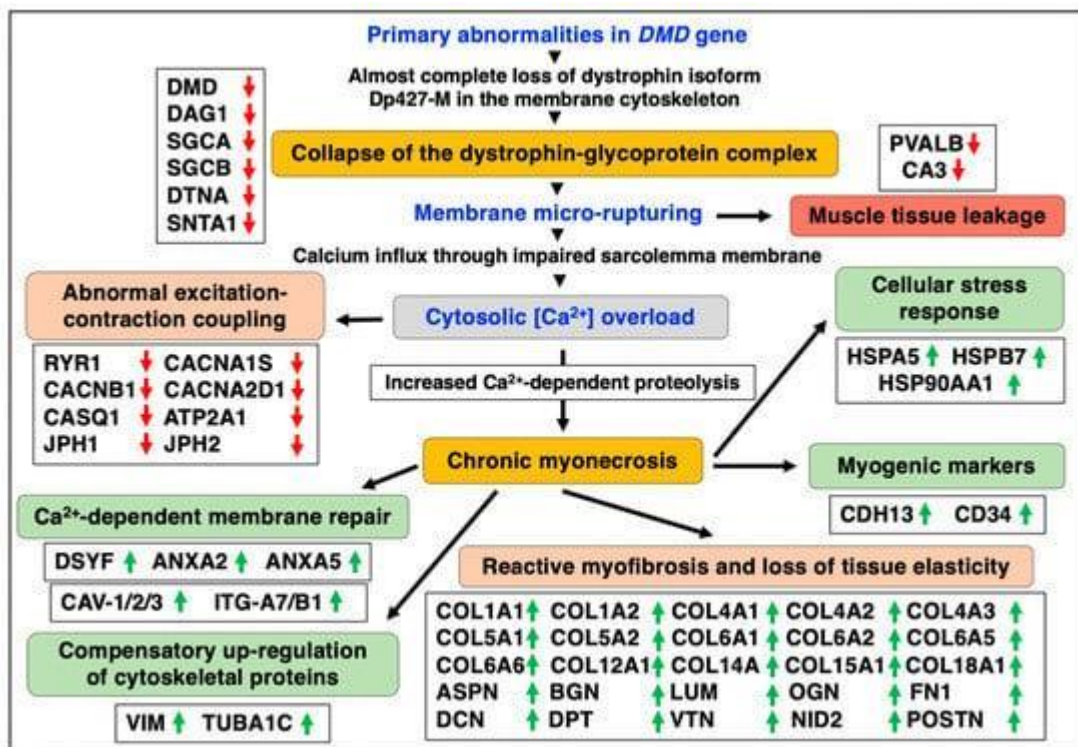


**Figure 9.** Overview of pathobiochemical and adaptive changes in the aged and dystrophin-deficient *mdx-4cv* diaphragm muscle as revealed by mass spectrometry-based proteomics. Listed are protein markers of crucial aspects of the molecular and cellular pathogenesis of dystrophinopathy, including the collapse of the dystrophin-glycoprotein complex, membrane rupturing, abnormal excitation-contraction coupling, reactive myofibrosis, calcium-dependent membrane repair, myogenic activation, the apparent compensatory up-regulation of cytoskeletal proteins, the cellular stress response and muscle tissue regeneration.

In relation to bioenergetic and metabolic enzymes, the bioinformatic PANTHER analysis of changed proteins revealed an extensive increase in the altered abundance of metabolite interconversion enzymes during aging of the dystrophic *mdx-4cv* diaphragm muscle. These considerable changes in the expression levels of muscle-associated enzymes included large numbers of hydrolases, isomerases, ligases, lyases, oxidoreductases and transferases. Within the protein class of hydrolases, this included proteins with amylase, deaminase, esterase, glucosidase, lipase, phosphatase, phosphodiesterase and pyrophosphatase activity. Isomerases were represented by epimerases, racemases and mutases. Lyases included aldolases, cyclases, dehydratases and hydratases. Alterations in the abundance of oxidoreductases encompassed dehydrogenases, oxidases, oxygenases, peroxidases and reductases. The protein family of transferases included acetyltransferases, acyltransferases, glycosyltransferases, kinases,

methyltransferases and transketolases. A comprehensive biomarker signature of these types of tissue-associated changes in combination with relevant alterations in biofluids, such as saliva, urine and serum/plasma, can be extremely helpful to advance the field of muscular dystrophy research [33-37] and (i) determine the risk for disease prior to the appearance of initial symptoms, (ii) detect the differential nature of specific and potentially sequential pathophysiological processes including progressive fiber degeneration, impaired excitation-contraction coupling, abnormal ion homeostasis, dysregulated cellular signaling, chronic inflammation with immune cell invasion, fat substitution and reactive myofibrosis [28-32,91-93], (iii) evaluate disease progression and potential adverse events during treatment, (iv) determine individual sensitivities towards drug treatment, (v) reflect the metabolic/biotransformation responses of detoxifying organs such as the liver and kidneys following exposure to a novel therapeutic agent, (vi) monitor (ideally repeatedly) alterations in the disease status due to therapeutic interventions [51-54], and (vii) assure the absence of cytotoxic side effects on whole-body physiology [37].

This gives proteomic markers of calcium-dependent membrane repair, tissue regeneration and myofibrosis, as identified in this study, great potential for future usage in disease evaluation and therapeutic-monitoring. The drastic changes in the collagen isoforms COL-V, COL-VI and COL-IV [79] in aged *mdx-4cv* diaphragm identify these proteins as suitable markers of reactive myofibrosis [91]. Skeletal muscles contain a variety of collagens ranging from COL-I to COL-XXII [79,86]. The comparative proteomic survey of the dystrophic diaphragm identified collagens COL-I, COL-IV, COL-V, COL-VI, COL-XII, COL-XIV, COL-XIV and COL-XVIII, which are located to differing degrees in the basal lamina, endomysium, perimysium, epimysium and myotendinous junctions [85-87]. Collagen COL-IV is the basic structural component of the basal lamina and characterized by a helical form [86]. COL-IV functions as the main linker to the dystrophin-glycoprotein complex via laminin-211 and the  $\alpha$ / $\beta$ -dystroglycan subcomplex [16,20,21]. Collagen COL-V forms fibrils and is mostly found in the endomysium where it controls the process of collagen fibrillogenesis [86]. The beaded filaments of collagen COL-VI interact with various cell surface receptors and are intrinsically involved in the maintenance of skeletal muscle integrity [80,81]. COL-XIV links fibrillar collagens to other components of the extracellular matrix and is mostly located in the endomysium and perimysium [87]. The increased levels of these collagens play a crucial role in reactive myofibrosis and are the underlying cause for the loss of tissue elasticity in X-linked muscular dystrophy [91-93]. In relation to the progressive nature of X-linked muscular

dystrophy, myofibrosis is an excellent indicator of overall muscle deterioration and correlates well with loss in motor functions in Duchenne patients [88,89].

Thus, protein markers of myofibrosis, such as collagen isoform COL-VI, in conjunction with elevated expression levels of other extracellular matrix components, represent excellent indicators of the progression of muscular dystrophy. Additional suitable proteins of the matrisome are the small leucine-rich proteoglycans asporin, biglycan, lumican and mimecan, as well as the proteoglycan decorin, fibronectin, dermatopontin, vitronectin and nidogen-2. The identified increased levels of the tyrosine-rich acidic matrix protein dermatopontin, the dystrophin-associated protein biglycan and the adhesive glycoprotein fibronectin in dystrophic skeletal muscles agree with previous proteomic studies using fluorescence two-dimensional difference in-gel electrophoresis [112,113]. Periostin is a crucial matricellular protein involved in tissue regeneration and cellular signaling events [76,78]. Previous studies indicate that periostin is only temporally expressed in the extracellular matrix during differentiation and regenerative processes [77], which agrees with the findings of the mass spectrometric study presented in this report. Expression levels of periostin are clearly affected by dystrophinopathy-associated changes in the extracellular matrix [91,93,129]. Of note, the deletion of periostin was shown to have a positive effect on X-linked muscular dystrophy by reducing myofibrosis via modulation of the signaling pathway that is associated with transforming growth factor TGF- $\beta$  [130]. Immunoblotting indicates that periostin exists only at very low levels in normal wild type diaphragm. This makes this component of the extracellular matrix an excellent candidate for evaluating progressive alterations in dystrophin-deficient skeletal muscles.

The proteomic evaluation of key proteins involved in the regulation of calcium homeostasis has shown elevated levels of calcium-sensing annexins and a decrease in regulatory components of excitation-contraction coupling. The calcium hypothesis of Duchenne muscular dystrophy assumes that abnormal calcium handling plays a major role in progressive myonecrosis [27]. Full-length dystrophin forms a lattice underneath the sarcolemma in normal muscles, which stabilizes the fiber periphery by linking the actin cytoskeleton to the extracellular matrix via the dystrophin-associated dystroglycan complex [18,20]. The almost complete loss of the Dp427-M isoform in dystrophinopathy weakens this trans-plasmalemmal linkage and renders dystrophic fibers more susceptible to membrane leakage during excitation-contraction-relaxation cycles [28]. The resulting influx of calcium ions, both through membrane tears and calcium leak channels, causes a drastic elevation of the sarcosolic calcium concentration. This in turn activates calcium-dependent proteolysis, which results in the enhanced destruction of muscle proteins [27]. The reduced levels of the voltage-sensing L-type

calcium channel of the transverse tubules, the ryanodine receptor calcium release channel and associated junctophilins of the triad junction, the luminal calcium-binding protein calsequestrin and the calcium-pumping ATPase of the sarcoplasmic reticulum agree with the pathophysiological concept of dysregulated calcium fluxes in dystrophin-deficient fibers [28]. The loss of key proteins involved in the temporal and spatial regulation of calcium movements through muscle membranes appears to be the underlying cause for impaired excitation-contraction coupling, decreased calcium buffering and abnormal calcium re-uptake into the lumen of the sarcoplasmic reticulum. These changes in ion-regulatory proteins might represent accumulating abnormalities and/or compensatory mechanisms in dystrophic diaphragm fibers [29]. Another interesting detection of altered expression levels is the mass spectrometric identification of increased levels of calcium-sensing annexins. This large family of proteins is involved in membrane repair [58] and annexin isoform ANXA2 was previously shown to be involved in myofiber repair in conjunction with inflammation and adipogenic replacement in injured contractile tissues [59]. Annexins are crucial facilitators of the accumulation of dysferlin, which is responsible for muscle fiber membrane repair [58-62]. Dysferlin, myoferlin and caveolins closely interact in dystrophic fibres [45,111]. This makes both the ANXA2 isoform of muscle annexin and elevated levels of dysferlin in damaged and dystrophin-deficient fibers [112,131] promising biomarker candidates of calcium-dependent and dysferlin/myoferlin-associated repair processes in X-linked muscular dystrophy.

Another interesting proteomic observation was the increase in integrins [67-69]. The  $\alpha7\beta1$ -integrin complex is developmentally regulated and important for sarcolemmal stability and prevention of exercise-induced injury [132] and increased levels of  $\alpha7\beta1$ -integrin were previously shown to counteract muscle degeneration [133-135]. Integrins play a key role in the reinforcement of crucial load-bearing structures at costamers and myotendinous junctions. Together with the dystrophin-complex, integrins provide structural integrity for lateral and longitudinal force transmission across the sarcolemma [136]. Thus, the increased expression of  $\alpha7\beta1$ -integrin might be part of the repair response in muscular dystrophy and represents a potential marker of cellular proliferation. Since this study was carried out with total extracts from crude muscle preparations, low-abundance markers were not detected. However, increases in the myogenic marker molecules CD34 [73-75] and cadherin-13 [71,72,137] were identified in the dystrophic *mdx-4cv* diaphragm by mass spectrometric analysis. The surface marker CD34 was recently shown to exhibit considerable potential as a satellite cell-linked biomarker of skeletal muscle aging [75]. Cadherin-13 (CDH13), also named heart cadherin (H-cadherin) or truncated cadherin (T-cadherin), attaches to the plasma membrane via a

glycosylphosphatidylinositol anchor. Importantly, T-cadherin interacts with integrin- $\alpha 7$  and is linked to signal transduction proteins within caveolae structures [70]. This makes the identified alterations in the abundance of specific isoforms of integrin, cadherin and caveolin in muscular dystrophy an interesting finding with potential for the establishment of a comprehensive biomarker signature of dystrophinopathy.

## 5. Conclusions

The mass spectrometry-based proteomic survey of 3-month versus 15-month old diaphragm muscles from wild type versus the dystrophic *mdx-4cv* mouse model of Duchenne muscular dystrophy has identified meaningful biomarker candidates of membrane repair, tissue regeneration and reactive myofibrosis. This included calcium-sensing annexins and caveolins that are involved in dysferlin-related membrane repair and the matricellular protein periostin which plays a crucial role in the extracellular matrix, as well as various isoforms of collagen that indicate the progression of fibrotic changes in the basal lamina, endomysium, perimysium, epimysium and myotendinous junctions of dystrophic skeletal muscles. Although not all of these proteomic candidate markers may be suitable as robust surrogate biomarkers that precisely correlate with a realistic clinical endpoint in therapeutic trials, they can nevertheless be useful for determining the complex pathogenesis of dystrophic muscles and might also be useful to evaluate the varied effects of novel treatments [138]. Biomarker signatures that have been established by omics-type screening processes, and properly verified for their effectiveness and reliability by patient-related analyses, should be able to reflect the pathobiochemical complexity of monogenetic disorders, such as Duchenne muscular dystrophy [57]. In the future, biomarker-guided diagnostics and therapeutic-monitoring will probably play a more central role in pre-clinical studies with animal disease models and patient screening during the main phases of clinical trials.

**Author Contributions:** Conceptualization, D.S., P.D. and K.O.; methodology, S.G. and P.D.; software, M.H. and P.M.; validation, S.G.; formal analysis, S.G., P.D., M.Z. and M.H.; resources, M.Z.; data curation, P.D., S.G. and M.H.; writing-original draft preparation, S.G., P.D. and K.O.; writing-review and editing, K.O., D.S., S.G. and P.D.; supervision, K.O., P.D. and P.M.; funding acquisition, K.O. and P.M. All authors have read and agreed to the published version of the manuscript.

**Funding:** Research was supported by the Kathleen Lonsdale Institute for Human Health Research at Maynooth University. The Orbitrap Fusion Tribrid mass spectrometer was funded under a Science Foundation Ireland Infrastructure Award to Dublin City University (SFI 16/RI/3701).

**Institutional Review Board Statement:** Animals were handled in strict adherence to local governmental and institutional animal care regulations and were approved by the Institutional Animal Care and Use Committee (Amt für Umwelt, Verbraucherschutz und Lokale Agenda der Stadt Bonn, North Rhine-Westphalia, Germany). Frozen specimens were transported on dry ice to Maynooth University in accordance with the Department of Agriculture (animal by-product register number 2016/16 to the Department of Biology, National University of Ireland, Maynooth).

**Data Availability Statement:** The multi-consensus MS files and listings of altered proteins in wild type versus dystrophic diaphragm muscle that were generated by the comparative proteomic study shown in this report have been deposited under the title ‘Proteomic analysis of aged mdx-4cv diaphragm’ with the unique identifier ‘qmtre’ to the Open Science Foundation (<https://osf.io/qmtre/>).

**Conflicts of Interest:** The authors declare no conflict of interest.

## References

1. Benarroch, L.; Bonne, G.; Rivier, F.; Hamroun, D. The 2020 version of the gene table of neuromuscular disorders. *Neuromuscul. Disord.* **2019**, *29*, 980-1018.
2. Thompson, R.; Spendiff, S.; Roos, A.; Bourque, P. R.; Warman Chardon, J.; Kirschner, J.; Horvath, V.; Lochmüller, H. Advances in the diagnosis of inherited neuromuscular diseases and implications for therapy development. *Lancet Neurol.* **2020**, *19*, 522-532.
3. Dowling, J.J.; Weihl, C.C.; Spencer, M.J. Molecular and cellular basis of genetically inherited skeletal muscle disorders. *Nat. Rev. Mol. Cell Biol.* **2021**, *22*, 713-732.
4. Mercuri, E.; Bönnemann, C.G.; Muntoni, F. Muscular dystrophies. *Lancet.* **2019**, *394*, 2025-2038.
5. Koenig, M.; Hoffman, E.P.; Bertelson, C.J.; Monaco, A.P.; Feener, C.; Kunkel, L.M. Complete cloning of the Duchenne muscular dystrophy (DMD) cDNA and

- preliminary genomic organization of the DMD gene in normal and affected individuals. *Cell*. **1987**, *50*, 509-517.
6. Duan, D.; Goemans, N.; Takeda, S.; Mercuri, E.; Aartsma-Rus, A. Duchenne muscular dystrophy. *Nat. Rev. Dis. Primers*. **2021**, *7*, 13.
  7. Bonilla, E.; Samitt, C.E.; Miranda, A.F.; Hays, A.P.; Salviati, G.; DiMauro, S.; Kunkel, L.M.; Hoffman, E.P.; Rowland, L.P. Duchenne muscular dystrophy: deficiency of dystrophin at the muscle cell surface. *Cell*. **1988**, *54*, 447-452.
  8. Hoffman, E.P. Causes of clinical variability in Duchenne and Becker muscular dystrophies and implications for exon skipping therapies. *Acta Myol*. **2020**, *39*, 179-186.
  9. Roberts, R.G. Dystrophin, its gene, and the dystrophinopathies. *Adv. Genet*. **1995**, *33*, 177-231.
  10. Blake, D.J.; Weir, A.; Newey, S.E.; Davies, K.E. Function and genetics of dystrophin and dystrophin-related proteins in muscle. *Physiol. Rev*. **2002**, *82*, 291-329.
  11. Hoffman, E.P.; Hudecki, M.S.; Rosenberg, P.A.; Pollina, C.M.; Kunkel, L.M. Cell and fiber-type distribution of dystrophin. *Neuron*. **1988**, *1*, 411-420.
  12. Delalande, O.; Czogalla, A.; Hubert, J.F.; Sikorski, A.; Le Rumeur, E. Dystrophin and Spectrin, Two Highly Dissimilar Sisters of the Same Family. *Subcell. Biochem*. **2017**, *82*, 373-403.
  13. Hoffman, E.P. The discovery of dystrophin, the protein product of the Duchenne muscular dystrophy gene. *FEBS J*. **2020**, *287*, 3879-3887.
  14. Ohlendieck, K.; Campbell, K.P. Dystrophin constitutes 5% of membrane cytoskeleton in skeletal muscle. *FEBS Lett*. **1991**, *283*, 230-234.
  15. Finn, D.M.; Ohlendieck, K. Rabbit brain and muscle isoforms containing the carboxy-terminal domain of 427 kDa skeletal muscle dystrophin exhibit similar biochemical properties. *Neurosci. Lett*. **1997**, *222*, 25-28.
  16. Ervasti, J.M.; Campbell, K.P. A role for the dystrophin-glycoprotein complex as a transmembrane linker between laminin and actin. *J. Cell Biol*. **1993**, *122*, 809-823.
  17. Ervasti, J.M.; Campbell, K.P. Dystrophin and the membrane skeleton. *Curr. Opin. Cell Biol*. **1993**, *5*, 82-87.
  18. Murphy, S.; Ohlendieck, K. The biochemical and mass spectrometric profiling of the dystrophin complexome from skeletal muscle. *Comput. Struct. Biotechnol. J*. **2015**, *14*, 20-27.

19. Prins, K.W.; Humston, J.L.; Mehta, A.; Tate, V.; Ralston, E.; Ervasti, J.M. Dystrophin is a microtubule-associated protein. *J. Cell Biol.* **2009**, *186*, 363-369.
20. Dowling, P.; Gargan, S.; Murphy, S.; Zweyer, M.; Sabir, H.; Swandulla, D.; Ohlendieck, K. The Dystrophin Node as Integrator of Cytoskeletal Organization, Lateral Force Transmission, Fiber Stability and Cellular Signaling in Skeletal Muscle. *Proteomes.* **2021**, *9*, 9.
21. Ervasti, J.M.; Campbell, K.P. Membrane organization of the dystrophin-glycoprotein complex. *Cell.* **1991**, *66*, 1121-1131.
22. Ohlendieck, K. Towards an understanding of the dystrophin-glycoprotein complex: linkage between the extracellular matrix and the membrane cytoskeleton in muscle fibers. *Eur. J. Cell Biol.* **1996**, *69*, 1-10.
23. Ervasti, J.M.; Ohlendieck, K.; Kahl, S.D.; Gaver, M.G.; Campbell, K.P. Deficiency of a glycoprotein component of the dystrophin complex in dystrophic muscle. *Nature.* **1990**, *345*, 315-319.
24. Ohlendieck, K.; Campbell, K.P. Dystrophin-associated proteins are greatly reduced in skeletal muscle from mdx mice. *J. Cell Biol.* **1991**, *115*, 1685-1694.
25. Ohlendieck, K.; Matsumura, K.; Ionasescu, V.V.; Towbin, J.A.; Bosch, E.P.; Weinstein, S.L.; Sernett, S.W.; Campbell, K.P. Duchenne muscular dystrophy: deficiency of dystrophin-associated proteins in the sarcolemma. *Neurology.* **1993**, *43*, 795-800.
26. Culligan, K.G.; Mackey, A.J.; Finn, D.M.; Maguire, P.B.; Ohlendieck, K. Role of dystrophin isoforms and associated proteins in muscular dystrophy (review). *Int. J. Mol. Med.* **1998**, *2*, 639-648.
27. Alderton, J.M.; Steinhardt, R.A. Calcium influx through calcium leak channels is responsible for the elevated levels of calcium-dependent proteolysis in dystrophic myotubes. *J. Biol. Chem.* **2000**, *275*, 9452-9460.
28. Allen, D.G.; Whitehead, N.P.; Froehner, S.C. Absence of Dystrophin Disrupts Skeletal Muscle Signaling: Roles of Ca<sup>2+</sup>, Reactive Oxygen Species, and Nitric Oxide in the Development of Muscular Dystrophy. *Physiol. Rev.* **2016**, *96*, 253-305.
29. Dowling, P.; Gargan, S.; Swandulla, D.; Ohlendieck, K. Proteomic profiling of impaired excitation-contraction coupling and abnormal calcium handling in muscular dystrophy. *Proteomics.* **2022** (in press) doi: 10.1002/pmic.202200003.

30. Ohlendieck, K.; Swandulla, D. Complexity of skeletal muscle degeneration: Multi-systems pathophysiology and organ crosstalk in dystrophinopathy. *Pflugers Arch.* **2021**, *473*, 1813-1839.
31. Schultz, T.I.; Raucci, F.J. Jr.; Salloum, F.N. Cardiovascular Disease in Duchenne Muscular Dystrophy: Overview and Insight Into Novel Therapeutic Targets. *JACC Basic Transl. Sci.* **2022**, *7*, 608-625.
32. Tripodi, L.; Villa, C.; Molinaro, D.; Torrente, Y.; Farini, A. The Immune System in Duchenne Muscular Dystrophy Pathogenesis. *Biomedicines.* **2021**, *9*, 1447.
33. Murphy, S.; Zweyer, M.; Mundegar, R.R.; Swandulla, D.; Ohlendieck, K. Proteomic serum biomarkers for neuromuscular diseases. *Expert Rev. Proteomics.* **2018**, *15*, 277-291.
34. Spitali, P.; Hettne, K.; Tsonaka, R.; Charrouf, M.; van den Bergen, J.; Koeks, Z.; Kan, H.E.; Hooijmans, M.T.; Roos, A.; Straub, V.; Muntoni, F.; Al-Khalili-Szigyarto, C.; Koel-Simmeling, M.J.A.; Teunissen, C.E.; Lochmüller, H.; Niks, E.H.; Aartsma-Rus, A. (2018). Tracking disease progression non-invasively in Duchenne and Becker muscular dystrophies. *J. Cachexia Sarcopenia Muscle.* **2018**, *9*, 715-726.
35. Al-Khalili Szigyarto, C. Duchenne muscular dystrophy: Recent advances in protein biomarkers and the clinical application. *Expert Rev. Proteomics.* **2020**, *17*, 365-375.
36. Carr, S.J.; Zahedi, R.P.; Lochmüller, H.; Roos, A. Mass spectrometry-based protein analysis to unravel the tissue pathophysiology in Duchenne muscular dystrophy. *Proteomics Clin. Appl.* **2018**, *12*, 1700071.
37. Dowling, P.; Murphy, S.; Zweyer, M.; Raucamp, M.; Swandulla, D.; Ohlendieck, K. Emerging proteomic biomarkers of X-linked muscular dystrophy. *Expert Rev. Mol. Diagn.* **2019**, *19*, 739-755.
38. Zweyer, M.; Sabir, H.; Dowling, P.; Gargan, S.; Murphy, S.; Swandulla, D.; Ohlendieck, K. Histopathology of Duchenne muscular dystrophy in correlation with changes in proteomic biomarkers. *Histol. Histopathol.* **2022**, *37*, 101-116.
39. Capitano, D.; Moriggi, M.; Torretta, E.; Barbacini, P.; Palma, S.D.; Viganò, A.; Lochmüller, H.; Muntoni, F.; Ferlini, A.; Mora, M.; Gelfi, C. Comparative proteomic analyses of Duchenne muscular dystrophy and Becker muscular dystrophy muscles: Changes contributing to preserve muscle function in Becker muscular dystrophy patients. *J. Cachexia Sarcopenia Muscle.* **2020**, *11*, 547-563.

40. Capitanio, D.; Moriggi, M.; Barbacini, P.; Torretta, E.; Moroni, I.; Blasevich, F.; Morandi, L.; Mora, M.; Gelfi, C. (2022). Molecular fingerprint of BMD patients lacking a portion in the rod domain of dystrophin. *Int. J. Mol. Sci.* **2020**, *23*, 2624.
41. Doran, P.; Martin, G.; Dowling, P.; Jockusch, H.; Ohlendieck, K. Proteome analysis of the dystrophin-deficient MDX diaphragm reveals a drastic increase in the heat shock protein cvHSP. *Proteomics.* **2006**, *6*, 4610-4621.
42. Guevel, L.; Lavoie, J.R.; Perez-Iratxeta, C.; Rouger, K.; Dubreil, L.; Feron, M.; Talon, S.; Brand, M.; Megeney, L.A. Quantitative proteomic analysis of dystrophic dog muscle. *J. Proteome Res.* **2011**, *10*, 2465-2478.
43. Rayavarapu, S.; Coley, W.; Cakir, E.; Jahnke, V.; Takeda, S.; Aoki, Y.; Grodish-Dressman, H.; Jaiswal, J.K.; Hoffman, E.P.; Brown, K.J.; Hathout, Y.; Nagaraju, K. Identification of disease specific pathways using in vivo SILAC proteomics in dystrophin deficient mdx mouse. *Mol. Cell. Proteomics.* **2013**, *12*, 1061-1073.
44. Fröhlich, T.; Kemter, E.; Flenkenthaler, F.; Klymiuk, N.; Otte, K.A.; Blutke, A.; Krause, S.; Walter, M.C.; Wanke, R.; Wolf, E.; Arnold, G.J. Progressive muscle proteome changes in a clinically relevant pig model of Duchenne muscular dystrophy. *Sci. Rep.* **2016**, *6*, 33362
45. Murphy, S.; Zweyer, M.; Mundegar, R.R.; Swandulla, D.; Ohlendieck, K. Comparative gel-based proteomic analysis of chemically crosslinked complexes in dystrophic skeletal muscle. *Electrophoresis.* **2018**, *39*, 1735-1744.
46. van Westering, T.L.E.; Johansson, H.J.; Hanson, B.; Coenen-Stass, A.M.L.; Lomonosova, Y.; Tanihata, J.; Motohashi, N.; Yokota, T.; Takeda, S.; Lehtiö, J.; Wood, M.J.A.; Andaloussi, S.E.; Aoki, Y.; Roberts, T.C. Mutation-independent proteomic signatures of pathological progression in murine models of Duchenne muscular dystrophy. *Mol. Cell. Proteomics.* **2020**, *19*, 2047-2068.
47. Partridge, T.A. The mdx mouse model as a surrogate for Duchenne muscular dystrophy. *FEBS J.* **2013**, *280*, 4177-4186.
48. Nghiem, P.P.; Kornegay, J.N. Gene therapies in canine models for Duchenne muscular dystrophy. *Hum. Genet.* **2019**, *138*, 483-489.
49. Zaynitdinova, M.I.; Lavrov, A.V.; Smirnikhina, S.A. Animal models for researching approaches to therapy of Duchenne muscular dystrophy. *Transgenic Res.* **2021**, *30*, 709-725.
50. Stirm, M.; Fonteyne, L.M.; Shashikadze, B.; Stöckl, J.B.; Kurome, M.; Keßler, B.; Zakhartchenko, V.; Kemter, E.; Blum, H.; Arnold, G.J.; Matiasek, K.; Wanke, R.;

- Wurst, W.; Nagashima, H.; Knieling, F.; Walter, M.C.; Kupatt, C.; Fröhlich, T.; Klymiuk, N.; Blutke, A.; Wolf, E. Pig models for Duchenne muscular dystrophy - from disease mechanisms to validation of new diagnostic and therapeutic concepts. *Neuromuscul. Disord.* **2022**, *32*, 543-556.
51. Markati, T.; Oskoui, M.; Farrar, M.A.; Duong, T.; Goemans, N.; Servais, L. Emerging therapies for Duchenne muscular dystrophy. *Lancet Neurol.* **2022**, *21*, 814-829.
52. Deng, J.; Zhang, J.; Shi, K.; Liu, Z. Drug development progress in duchenne muscular dystrophy. *Front. Pharmacol.* **2022**, *13*, 950651.
53. Eser G, Topaloğlu H. Current Outline of Exon Skipping Trials in Duchenne Muscular Dystrophy. *Genes (Basel)* **2022**, *13*, 1241.
54. Chung Liang, L.; Sulaiman, N.; Yazid, M.D. A Decade of Progress in Gene Targeted Therapeutic Strategies in Duchenne Muscular Dystrophy: A Systematic Review. *Front. Bioeng. Biotechnol.* **2022**, *10*, 833833.
55. Holland, A.; Carberry, S.; Ohlendieck, K. Proteomics of the dystrophin-glycoprotein complex and dystrophinopathy. *Curr. Protein Pept. Sci.* **2013**, *14*, 680-697.
56. Brinkmeier, H.; Ohlendieck, K. Chaperoning heat shock proteins: proteomic analysis and relevance for normal and dystrophin-deficient muscle. *Proteomics Clin. Appl.* **2014**, *8*, 875-895.
57. Grounds, M.D.; Terrill, J.R.; Al-Mshhdani, B.A.; Duong, M.N.; Radley-Crabb, H.G.; Arthur, P.G. Biomarkers for Duchenne muscular dystrophy: myonecrosis, inflammation and oxidative stress. *Dis. Model Mech.* **2020**, *13*, dmm043638.
58. Demonbreun, A.R.; Quattrocchi, M.; Barefield, D.Y.; Allen, M.V.; Swanson, K.E.; McNally, E.M. An actin-dependent annexin complex mediates plasma membrane repair in muscle. *J. Cell Biol.* **2016**, *213*, 705-718.
59. Defour, A.; Medikayala, S.; Van der Meulen, J.H.; Hogarth, M.W.; Holdreith, N.; Malatras, A.; Duddy, W.; Boehler, J.; Nagaraju, K.; Jaiswal, J.K. Annexin A2 links poor myofiber repair with inflammation and adipogenic replacement of the injured muscle. *Hum. Mol. Genet.* **2017**, *26*, 1979-1991.
60. Bittel, D.C.; Chandra, G.; Tirunagri, L.M.S.; Deora, A.B.; Medikayala, S.; Scheffer, L.; Defour, A.; Jaiswal, J.K. Annexin A2 Mediates Dysferlin Accumulation and Muscle Cell Membrane Repair. *Cells.* **2020**, *9*, 1919.
61. Lennon, N.J.; Kho, A.; Bacskai, B.J.; Perlmutter, S.L.; Hyman, B.T.; Brown, R.H. Jr. Dysferlin interacts with annexins A1 and A2 and mediates sarcolemmal wound-healing. *J. Biol. Chem.* **2003**, *278*, 50466-50473.

62. Han, R.; Campbell, K.P. Dysferlin and muscle membrane repair. *Curr. Opin. Cell Biol.* **2007**, *19*, 409-416.
63. Demonbreun, A.R.; Rossi, A.E.; Alvarez, M.G.; Swanson, K.E.; Deveaux, H.K.; Earley, J.U.; Hadhazy, M.; Vohra, R.; Walter, G.A.; Pytel, P.; McNally, E.M. Dysferlin and myoferlin regulate transverse tubule formation and glycerol sensitivity. *Am. J. Pathol.* **2014**, *184*, 248-259.
64. Couchoux, H.; Bichraoui, H.; Chouabe, C.; Altafaj, X.; Bonvallet, R.; Allard, B.; Ronjat, M.; Berthier, C. Caveolin-3 is a direct molecular partner of the Cav1.1 subunit of the skeletal muscle L-type calcium channel. *Int. J. Biochem. Cell Biol.* **2011**, *43*, 713-720.
65. Pradhan, B.S.; Prószyński, T.J. A Role for Caveolin-3 in the Pathogenesis of Muscular Dystrophies. *Int. J. Mol. Sci.* **2020**, *21*, 8736.
66. Matsunobe, M.; Motohashi, N.; Aoki, E.; Tominari, T.; Inada, M.; Aoki, Y. Caveolin-3 regulates the activity of Ca<sup>2+</sup>/calmodulin-dependent protein kinase II in C2C12 cells. *Am. J. Physiol. Cell Physiol.* **2022**, *323*, C1137-C1148.
67. Collo, G.; Starr, L.; Quaranta, V. A new isoform of the laminin receptor integrin alpha 7 beta 1 is developmentally regulated in skeletal muscle. *J. Biol. Chem.* **1993**, *268*, 19019-19024.
68. Burkin, D.J.; Wallace, G.Q.; Milner, D.J.; Chaney, E.J.; Mulligan, J.A.; Kaufman, S.J. Transgenic expression of {alpha}7{beta}1 integrin maintains muscle integrity, increases regenerative capacity, promotes hypertrophy, and reduces cardiomyopathy in dystrophic mice. *Am. J. Pathol.* **2005**, *166*, 253-263.
69. Liu, J.; Burkin, D.J.; Kaufman, S.J. Increasing alpha 7 beta 1-integrin promotes muscle cell proliferation, adhesion, and resistance to apoptosis without changing gene expression. *Am. J. Physiol. Cell Physiol.* **2008**, *294*, C627-640.
70. Philippova, M.P.; Bochkov, V.N.; Stambolsky, D.V.; Tkachuk, V.A.; Resink, T.J. T-cadherin and signal-transducing molecules co-localize in caveolin-rich membrane domains of vascular smooth muscle cells. *FEBS Lett.* **1998**, *429*, 207-210.
71. Tanaka, Y.; Kita, S.; Nishizawa, H.; Fukuda, S.; Fujishima, Y.; Obata, Y.; Nagao, H.; Masuda, S.; Nakamura, Y.; Shimizu, Y.; Mineo, R.; Natsukawa, T.; Funahashi, T.; Ranscht, B.; Fukada, S.I.; Maeda, N.; Shimomura, I. Adiponectin promotes muscle regeneration through binding to T-cadherin. *Sci. Rep.* **2019**, *9*, 16.
72. Nalbandian, M.; Zhao, M.; Sasaki-Honda, M.; Jonouchi, T.; Lucena-Cacace, A.; Mizusawa, T.; Yasuda, M.; Yoshida, Y.; Hotta, A.; Sakurai, H. Characterization of

- hiPSC-Derived Muscle Progenitors Reveals Distinctive Markers for Myogenic Cell Purification Toward Cell Therapy. *Stem Cell Reports*. **2021**, *16*, 883-898.
73. Beauchamp, J.R.; Heslop, L.; Yu, D.S.; Tajbakhsh, S.; Kelly, R.G.; Wernig, A.; Buckingham, M.E.; Partridge, T.A.; Zammit, P.S. Expression of CD34 and Myf5 defines the majority of quiescent adult skeletal muscle satellite cells. *J. Cell Biol.* **2000**, *151*, 1221-1234.
74. Jankowski, R.J.; Deasy, B.M.; Cao, B.; Gates, C.; Huard, J. The role of CD34 expression and cellular fusion in the regeneration capacity of myogenic progenitor cells. *J. Cell Sci.* **2002**, *115*, 4361-4374.
75. Fernández-Lázaro, D.; Garrosa, E.; Seco-Calvo, J.; Garrosa, M. Potential Satellite Cell-Linked Biomarkers in Aging Skeletal Muscle Tissue: Proteomics and Proteogenomics to Monitor Sarcopenia. *Proteomes*. **2022**, *10*, 29.
76. Ito, N.; Miyagoe-Suzuki, Y.; Takeda, S.; Kudo, A. Periostin Is Required for the Maintenance of Muscle Fibers during Muscle Regeneration. *Int. J. Mol. Sci.* **2021**, *22*, 3627.
77. Ozdemir, C.; Akpulat, U.; Sharafi, P.; Yıldız, Y.; Onbaşlar, I.; Kocaefe, C. Periostin is temporally expressed as an extracellular matrix component in skeletal muscle regeneration and differentiation. *Gene* **2014**, *553*, 130-139.
78. Wang, Z.; An, J.; Zhu, D.; Chen, H.; Lin, A.; Kang, J.; Liu, W.; Kang, X. Periostin: an emerging activator of multiple signaling pathways. *J. Cell Commun. Signal.* **2022**, doi: 10.1007/s12079-022-00674-2.
79. Ricard-Blum, S. The collagen family. *Cold Spring Harb. Perspect. Biol.* **2011**, *3*, a004978.
80. Cescon, M.; Gattazzo, F.; Chen, P.; Bonaldo, P. Collagen VI at a glance. *J. Cell Sci.* **2015**, *128*, 3525-3531.
81. Cescon, M.; Gregorio, I.; Eiber, N.; Borgia, D.; Fusto, A.; Sabatelli, P.; Scorzeto, M.; Megighian, A.; Pegoraro, E.; Hashemolhosseini, S.; Bonaldo, P. Collagen VI is required for the structural and functional integrity of the neuromuscular junction. *Acta Neuropathol.* **2018**, *136*, 483-499.
82. Dias, C.; Nylandsted, J. Plasma membrane integrity in health and disease: significance and therapeutic potential. *Cell Discov.* **2021**, *7*, 4.
83. Croissant, C.; Carmeille, R.; Brévar, C.; Bouter, A. Annexins and Membrane Repair Dysfunctions in Muscular Dystrophies. *Int. J. Mol. Sci.* **2021**, *22*, 5276.

84. Croissant, C.; Gounou, C.; Bouvet, F.; Tan, S.; Bouter, A. Trafficking of Annexins during Membrane Repair in Human Skeletal Muscle Cells. *Membranes (Basel)* **2022**, *12*, 153.
85. Mouw, J.K.; Ou, G.; Weaver, V.M. Extracellular matrix assembly: a multiscale deconstruction. *Nat. Rev. Mol. Cell Biol.* **2014**, *15*, 771-785.
86. Csapo, R.; Gumpenberger, M.; Wessner, B. Skeletal Muscle Extracellular Matrix - What Do We Know About Its Composition, Regulation, and Physiological Roles? A Narrative Review. *Front. Physiol.* **2020**, *11*, 253.
87. Zhang, W.; Liu, Y.; Zhang, H. Extracellular matrix: an important regulator of cell functions and skeletal muscle development. *Cell Biosci.* **2021**, *11*, 65.
88. Desguerre, I.; Mayer, M.; Leturcq, F.; Barbet, J.P.; Gherardi, R.K.; Christov, C. Endomysial fibrosis in Duchenne muscular dystrophy: a marker of poor outcome associated with macrophage alternative activation. *J. Neuropathol. Exp. Neurol.* **2009**, *68*, 762-773.
89. Klingler, W.; Jurkat-Rott, K.; Lehmann-Horn, F.; Schleip, R. The role of fibrosis in Duchenne muscular dystrophy. *Acta Myol.* **2012**, *31*, 184-195.
90. Ahmad, K.; Shaikh, S.; Ahmad, S.S.; Lee, E.J.; Choi, I. Cross-Talk Between Extracellular Matrix and Skeletal Muscle: Implications for Myopathies. *Front. Pharmacol.* **2020**, *11*, 142.
91. Holland, A.; Murphy, S.; Dowling, P.; Ohlendieck, K. Pathoproteomic profiling of the skeletal muscle matrisome in dystrophinopathy associated myofibrosis. *Proteomics* **2016**, *16*, 345-366.
92. Serrano, A.L.; Muñoz-Cánoves, P. Fibrosis development in early-onset muscular dystrophies: Mechanisms and translational implications. *Semin. Cell Dev. Biol.* **2017**, *64*, 181-190.
93. Ohlendieck, K.; Swandulla, D. Molecular pathogenesis of Duchenne muscular dystrophy-related fibrosis. *Pathologe* **2017**, *38*, 21-29.
94. Dowling, P.; Gargan, S.; Zweyer, M.; Henry, M.; Meleady, P.; Swandulla, D.; Ohlendieck, K. Protocol for the Bottom-Up Proteomic Analysis of Mouse Spleen. *STAR Protoc.* **2020**, *1*, 100196.
95. Murphy, S.; Zweyer, M.; Mundegar, R.R.; Henry, M.; Meleady, P.; Swandulla, D.; Ohlendieck, K. Concurrent Label-Free Mass Spectrometric Analysis of Dystrophin Isoform Dp427 and the Myofibrosis Marker Collagen in Crude Extracts from mdx-4cv Skeletal Muscles. *Proteomes* **2015**, *3*, 298-327.

96. Murphy, S.; Zweyer, M.; Raucamp, M.; Henry, M.; Meleady, P.; Swandulla, D.; Ohlendieck, K. Proteomic profiling of the mouse diaphragm and refined mass spectrometric analysis of the dystrophic phenotype. *J. Muscle Res. Cell. Motil.* **2019**, *40*, 9-28.
97. Antharavally, B.S.; Mallia, K.A.; Rangaraj, P.; Haney, P.; Bell, P.A. Quantitation of proteins using a dye-metal-based colorimetric protein assay. *Anal. Biochem.* **2009**, *385*, 342-345.
98. Wiśniewski, J.R.; Zougman, A.; Nagaraj, N.; Mann, M. Universal sample preparation method for proteome analysis. *Nat. Methods* **2009**, *6*, 359-362.
99. Mi, H.; Ebert, D.; Muruganujan, A.; Mills, C.; Albou, L.P.; Mushayamaha, T.; Thomas, P.D. PANTHER version 16: a revised family classification, tree-based classification tool, enhancer regions and extensive API. *Nucleic Acids Res.* **2021**, *49*, D394-D403.
100. Bulfield, G.; Siller, W.G.; Wight, P.A.; Moore, K.J. X chromosome-linked muscular dystrophy (mdx) in the mouse. *Proc. Natl. Acad. Sci. USA* **1984**, *81*, 1189-1192.
101. Sicinski, P.; Geng, Y.; Ryder-Cook, A.S.; Barnard, E.A.; Darlison, M.G.; Barnard, P.J. The molecular basis of muscular dystrophy in the mdx mouse: A point mutation. *Science* **1989**, *244*, 1578-1580.
102. Duddy, W.; Duguez, S.; Johnston, H.; Cohen, T.V.; Phadke, A.; Gordish-Dressman, H.; Nagaraju, K.; Gnocchi, V.; Low, S.; Partridge, T. Muscular dystrophy in the mdx mouse is a severe myopathy compounded by hypotrophy, hypertrophy and hyperplasia. *Skelet. Muscle* **2015**, *5*, 16.
103. Stedman, H.H.; Sweeney, H.L.; Shrager, J.B.; Maguire, H.C.; Panettieri, R.A.; Petrof, B.; Narusawa, M.; Leferovich, J.M.; Sladky, J.T.; Kelly, A.M. The mdx mouse diaphragm reproduces the degenerative changes of Duchenne muscular dystrophy. *Nature* **1991**, *352*, 536-539.
104. Sahani, R.; Wallace, C.H.; Jones, B.K.; Blemker, S.S. Diaphragm muscle fibrosis involves changes in collagen organization with mechanical implications in Duchenne muscular dystrophy. *J. Appl. Physiol.* **2022**, *132*, 653-672.
105. Giovarelli, M.; Arnaboldi, F.; Zecchini, S.; Cornaghi, L.B.; Nava, A.; Sommariva, M.; Clementi, E.G.I.; Gagliano, N. Characterisation of Progressive Skeletal Muscle Fibrosis in the Mdx Mouse Model of Duchenne Muscular Dystrophy: An In Vivo and In Vitro Study. *Int. J. Mol. Sci.* **2022**, *23*, 8735.

- 106.Im, W.B.; Phelps, S.F.; Copen, E.H.; Adams, E.G.; Slightom, J.L.; Chamberlain, J.S. Differential expression of dystrophin isoforms in strains of mdx mice with different mutations. *Hum. Mol. Genet.* **1996**, *5*, 1149-1153.
- 107.Chapman, V.M.; Miller, D.R.; Armstrong, D.; Caskey, C.T. Recovery of induced mutations for X chromosome-linked muscular dystrophy in mice. *Proc. Natl. Acad. Sci. USA* **1989**, *86*, 1292-1296.
- 108.Shin, J.H.; Hakim, C.H.; Zhang, K.; Duan, D. Genotyping mdx, mdx3cv, and mdx4cv mice by primer competition polymerase chain reaction. *Muscle Nerve* **2011**, *43*, 283-286.
- 109.Danko, I.; Chapman, V.; Wolff, J.A. The frequency of revertants in mdx mouse genetic models for Duchenne muscular dystrophy. *Pediatr. Res.* **1992**, *32*, 128-131.
- 110.Murphy, S.; Henry, M.; Meleady, P.; Zweyer, M.; Mundegar, R.R.; Swandulla, D.; Ohlendieck, K. Simultaneous Pathoproteomic Evaluation of the Dystrophin-Glycoprotein Complex and Secondary Changes in the mdx-4cv Mouse Model of Duchenne Muscular Dystrophy. *Biology (Basel)* **2015**, *4*, 397-423.
- 111.Murphy, S.; Zweyer, M.; Mundegar, R.R.; Swandulla, D.; Ohlendieck, K. Chemical crosslinking analysis of  $\beta$ -dystroglycan in dystrophin-deficient skeletal muscle. *HRB Open Res.* **2018**, *1*, 17.
- 112.Murphy, S.; Zweyer, M.; Henry, M.; Meleady, P.; Mundegar, R.R.; Swandulla, D.; Ohlendieck, K. Proteomic analysis of the sarcolemma-enriched fraction from dystrophic mdx-4cv skeletal muscle. *J. Proteomics* **2019**, *191*, 212-227.
- 113.Murphy, S.; Dowling, P.; Zweyer, M.; Mundegar, R.R.; Henry, M.; Meleady, P.; Swandulla, D.; Ohlendieck, K. Proteomic analysis of dystrophin deficiency and associated changes in the aged mdx-4cv heart model of dystrophinopathy-related cardiomyopathy. *J. Proteomics* **2016**, *145*, 24-36.
- 114.Gargan, S.; Dowling, P.; Zweyer, M.; Reimann, J.; Henry, M.; Meleady, P.; Swandulla, D.; Ohlendieck, K. Mass Spectrometric Profiling of Extraocular Muscle and Proteomic Adaptations in the mdx-4cv Model of Duchenne Muscular Dystrophy. *Life (Basel)* **2021**, *11*, 595.
- 115.Murphy, S.; Dowling, P.; Zweyer, M.; Henry, M.; Meleady, P.; Mundegar, R.R.; Swandulla, D.; Ohlendieck, K. Proteomic profiling of mdx-4cv serum reveals highly elevated levels of the inflammation-induced plasma marker haptoglobin in muscular dystrophy. *Int. J. Mol. Med.* **2017**, *39*, 1357-1370.

116. Murphy, S.; Zweyer, M.; Mundegar, R.R.; Swandulla, D.; Ohlendieck, K. Proteomic identification of elevated saliva kallikrein levels in the mdx-4cv mouse model of Duchenne muscular dystrophy. *Biochem. Biophys. Rep.* **2018**, *18*, 100541.
117. Gargan, S.; Dowling, P.; Zweyer, M.; Swandulla, D.; Ohlendieck, K. Identification of marker proteins of muscular dystrophy in the urine proteome from the mdx-4cv model of dystrophinopathy. *Mol. Omics* **2020**, *16*, 268-278.
118. Murphy, S.; Zweyer, M.; Henry, M.; Meleady, P.; Mundegar, R.R.; Swandulla, D.; Ohlendieck, K. Label-free mass spectrometric analysis reveals complex changes in the brain proteome from the mdx-4cv mouse model of Duchenne muscular dystrophy. *Clin. Proteomics* **2015**, *12*, 27.
119. Murphy, S.; Zweyer, M.; Henry, M.; Meleady, P.; Mundegar, R.R.; Swandulla, D.; Ohlendieck, K. Proteomic profiling of liver tissue from the mdx-4cv mouse model of Duchenne muscular dystrophy. *Clin. Proteomics* **2018**, *15*, 34.
120. Dowling, P.; Gargan, S.; Zweyer, M.; Henry, M.; Meleady, P.; Swandulla, D.; Ohlendieck, K. Proteome-wide Changes in the mdx-4cv Spleen due to Pathophysiological Cross Talk with Dystrophin-Deficient Skeletal Muscle. *iScience* **2020**, *23*, 101500.
121. Dowling, P.; Zweyer, M.; Raucamp, M.; Henry, M.; Meleady, P.; Swandulla, D.; Ohlendieck, K. Proteomic and cell biological profiling of the renal phenotype of the mdx-4cv mouse model of Duchenne muscular dystrophy. *Eur. J. Cell Biol.* **2020**, *99*, 151059.
122. Dowling, P.; Gargan, S.; Zweyer, M.; Sabir, H.; Henry, M.; Meleady, P.; Swandulla, D.; Ohlendieck, K. Proteomic profiling of the interface between the stomach wall and the pancreas in dystrophinopathy. *Eur. J. Transl. Myol.* **2021**, *31*, 9627.
123. Judge, L.M.; Haraguchiln, M.; Chamberlain, J.S. Dissecting the signaling and mechanical functions of the dystrophin-glycoprotein complex. *J. Cell Sci.* **2006**, *119*, 1537-1546.
124. Mitrpant, C.; Fletcher, S.; Iversen, P.L.; Wilton, S.D. By-passing the nonsense mutation in the 4 CV mouse model of muscular dystrophy by induced exon skipping. *J. Gene Med.* **2009**, *11*, 46-56.
125. Kimura, E.; Li, S.; Gregorevic, P.; Fall, B.M.; Chamberlain, J.S. Dystrophin delivery to muscles of mdx mice using lentiviral vectors leads to myogenic progenitor targeting and stable gene expression. *Mol. Ther.* **2010**, *18*, 206-213.

- 126.Holland, A.; Henry, M.; Meleady, P.; Winkler, C.K.; Krautwald, M.; Brinkmeier, H.; Ohlendieck, K. Comparative Label-Free Mass Spectrometric Analysis of Mildly versus Severely Affected mdx Mouse Skeletal Muscles Identifies Annexin, Lamin, and Vimentin as Universal Dystrophic Markers. *Molecules* **2015**, *20*, 11317-11344.
- 127.Murphy, S.; Brinkmeier, H.; Krautwald, M.; Henry, M.; Meleady, P.; Ohlendieck, K. Proteomic profiling of the dystrophin complex and membrane fraction from dystrophic mdx muscle reveals decreases in the cytolinker desmoglein and increases in the extracellular matrix stabilizers biglycan and fibronectin. *J. Muscle Res. Cell. Motil.* **2017**, *38*, 251-268.
- 128.Carberry, S.; Zweyer, M.; Swandulla, D.; Ohlendieck, K. Proteomics reveals drastic increase of extracellular matrix proteins collagen and dermatopontin in the aged mdx diaphragm model of Duchenne muscular dystrophy. *Int. J. Mol. Med.* **2012**, *30*, 229-234.
- 129.Holland, A.; Dowling, P.; Meleady, P.; Henry, M.; Zweyer, M.; Mundegar, R.R.; Swandulla, D.; Ohlendieck, K. Label-free mass spectrometric analysis of the mdx-4cv diaphragm identifies the matricellular protein periostin as a potential factor involved in dystrophinopathy-related fibrosis. *Proteomics* **2015**, *15*, 2318-2331.
- 130.Lorts, A.; Schwanekamp, J.A.; Baudino, T.A.; McNally, E.M.; Molkentin, J.D. Deletion of periostin reduces muscular dystrophy and fibrosis in mice by modulating the transforming growth factor- $\beta$  pathway. *Proc. Natl. Acad. Sci. USA.* **2012**, *109*, 10978-10983.
- 131.Vontzalidis, A.; Terzis, G.; Manta, P. Increased dysferlin expression in Duchenne muscular dystrophy. *Anal. Quant. Cytopathol. Histopathol.* **2014**, *36*, 15-22.
- 132.Boppart, M.D.; Mahmassani, Z.S. Integrin signaling: linking mechanical stimulation to skeletal muscle hypertrophy. *Am. J. Physiol. Cell Physiol.* **2019**, *317*, C629-C641.
- 133.Burkin, D.J.; Wallace, G.Q.; Nicol, K.J.; Kaufman, D.J.; Kaufman, S.J. Enhanced expression of the alpha 7 beta 1 integrin reduces muscular dystrophy and restores viability in dystrophic mice. *J. Cell Biol.* **2001**, *152*, 1207-1218.
- 134.Rooney, J.E.; Gurpur, P.B.; Burkin, D.J. Laminin-111 protein therapy prevents muscle disease in the mdx mouse model for Duchenne muscular dystrophy. *Proc. Natl. Acad. Sci. USA.* **2009**, *106*, 7991-7996.
- 135.Heller, K.N.; Montgomery, C.L.; Janssen, P.M.; Clark, K.R.; Mendell, J.R.; Rodino-Klapac, L.R. AAV-mediated overexpression of human  $\alpha 7$  integrin leads to histological and functional improvement in dystrophic mice. *Mol. Ther.* **2013**, *21*, 520-525.

136. Marshall, J.L.; Oh, J.; Chou, E.; Lee, J.A.; Holmberg, J.; Burkin, D.J.; Crosbie-Watson, R.H. Sarcospan integration into laminin-binding adhesion complexes that ameliorate muscular dystrophy requires utrophin and  $\alpha 7$  integrin. *Hum. Mol. Genet.* **2015**, *24*, 2011-2022.
137. Kim, H.; Perlingeiro, R.C.R. Generation of human myogenic progenitors from pluripotent stem cells for in vivo regeneration. *Cell. Mol. Life Sci.* **2022**, *79*, 406.
- Szigyarto, C.A.; Spitali, P. Biomarkers of Duchenne muscular dystrophy: current findings. *Degener. Neurol. Neuromuscul. Dis.* **2018**, *8*, 1-13.

## Chapter 5

### Mass spectrometric profiling of extraocular muscle and proteomic adaptations in the *mdx-4cv* model of Duchenne muscular dystrophy

Published on 22 June 2021

Gargan, S., Dowling, P., Zweyer, M., Reimann, J., Henry, M., Meleady, P., Swandulla, D., & Ohlendieck, K. (2021). Mass Spectrometric Profiling of Extraocular Muscle and Proteomic Adaptations in the *mdx-4cv* Model of Duchenne Muscular Dystrophy. *Life (Basel, Switzerland)*, 11(7), 595. <https://doi.org/10.3390/life11070595>.

**Abstract:** Extraocular muscles (EOMs) represent a specialized type of contractile tissue with unique cellular, physiological and biochemical properties. In Duchenne muscular dystrophy, EOMs stay functionally unaffected in the course of disease progression. Therefore, it was of interest to determine its proteomic profile in dystrophinopathy. The proteomic survey of wild type mice and the dystrophic *mdx-4cv* model revealed a broad spectrum of sarcomere-associated proteoforms, including components of the thick filament, thin filament, M-band and Z-disk, as well as a variety of muscle-specific markers. Interestingly, the mass spectrometric analysis revealed unusual expression levels of contractile proteins, especially isoforms of myosin heavy chain. As compared to diaphragm muscle, both proteomics and immunoblotting established isoform MyHC14 as a new potential marker in wild type EOMs, in addition to the previously identified isoforms MyHC13 and MyHC15. Comparative proteomics was employed to establish alterations in the protein expression profile between normal EOMs and dystrophin-lacking EOMs. The analysis of *mdx-4cv* EOMs identified elevated levels of glycolytic enzymes and molecular chaperones, as well as decreases in mitochondrial enzymes. These findings suggest a process of adaptation in dystrophin-deficient EOMs via a bioenergetic shift to more glycolytic metabolism, as well as an efficient cellular stress response in EOMs in dystrophinopathy.

**Keywords:** Duchenne muscular dystrophy; dystrophinopathy; extraocular muscle; glyceraldehyde-3-phosphate dehydrogenase; myosin-14; myosin heavy chain

## 1. Introduction

One of the most abundant cellular entities in the human body, the diverse types of skeletal muscle fibres, form the contractile units of over 650 individual muscles. Voluntary striated muscles differ considerably in their histological, anatomical, metabolic, biochemical and physiological specialization between predominantly slow-twitching versus fast-twitching phenotypes [1]. A distinctly different subtype of skeletal muscles, as compared to non-craniofacial muscles, is presented by extraocular muscles (EOMs) [2,3], which control the movements of the eyes [4]. The finely tuned and highly coordinated actions of six EOMs, i.e. *M. obliquus superior*, *M. obliquus inferior*, *M. rectus medialis*, *M. rectus lateralis*, *M. rectus superior*, and *M. rectus inferior* [5], enable the eyeball a wide range of complex movements about its horizontal and vertical axis. This includes a diverse range of eye movements ranging from gaze-holding, slow vergence, smooth pursuit convergence, optokinetic responses, vestibulo-ocular reflexes to rapid saccades [6].

Characteristic biological features of EOMs include (i) unique developmental processes with specific upstream activators [7,8], (ii) longitudinal dispersion of multiterminal neuromuscular junctions [9-11], (iii) morphologically distinct muscle spindles as compared to conventional somatic spindles [12], (iv) an unusually high capacity for cellular remodelling and fibre regeneration [13,14], (v) an efficient calcium handling and extrusion system [15], (vi) high levels of fatigue resistance even in extremely fast-twitching fibres [16] and (vii) distinguishing combinations of contractile protein isoform expression patterns [17]. Another striking biomedical feature of EOMs is their apparent resistance to degeneration in X-linked muscular dystrophy [18-20].

Duchenne muscular dystrophy is an X-chromosomally inherited and severely debilitating disorder of early childhood that primarily affects contractile tissues [21]. Mutations in the *DMD* gene result in the almost complete loss of the full-length isoform of dystrophin, which exhibits high levels of sequence similarity with membrane cytoskeletal proteins, and the concomitant reduction of a variety of sarcolemmal glycoproteins [22]. The extremely large *DMD* gene contains 7 different promoters that are involved in the tissue-specific expression of several small dystrophin isoforms, i.e. Dp45 (central nervous system), Dp71-G (ubiquitous), Dp116-S

(Schwann cells), Dp140-B/K (brain and kidney) and Dp260-R (retina), as well as the large dystrophins, i.e. Dp427-M (skeletal muscle, heart muscle, smooth muscle), Dp427-B (brain) and Dp427-P (Purkinje cells) [23]. The collapse of the dystrophin-associated glycoprotein complex, which acts as a key signaling hub in normal muscles [23,24], causes weakening of the actin cytoskeleton-sarcolemma-extracellular matrix axis. This results in micro-rupturing events at the level of the sarcolemmal membrane system and triggers abnormal lateral force transmission, impaired cellular signaling and enhanced levels of calcium-induced proteolysis [25,27]. These pathophysiological changes affect the majority of the skeletal musculature, which undergoes cellular degeneration, partial replacement by fatty tissue, severe fibrotic scarring and chronic inflammation [24,25,28]. In addition, respiratory deficiencies, late-onset cardiomyopathy and scoliosis, as well as neuronal and metabolic complications, are characteristic features of the complex pathology of X-linked muscular dystrophy [26,29,30]. In contrast to other types of skeletal muscles, as previously reviewed in detail [31-33], relatively limited numbers of studies on the normal EOM proteome [34-36] or proteome-wide changes in dystrophin-deficient EOMs [37,38] have been carried out. We therefore performed a systematic mass spectrometric analysis of EOM preparations and potential adaptations in the dystrophic *mdx-4cv* phenotype, as compared to the recently established proteomic changes in the severely affected *mdx-4cv* diaphragm [39]. Initially the proteomic profile of wild type EOMs was determined with the help of an Orbitrap Fusion Tribrid mass spectrometer, which identified unusual expression levels of contractile proteins, especially isoforms of myosin heavy chain. Subsequently, comparative proteomics was used to identify changes in the protein expression profile between unaffected EOMs and dystrophin-lacking EOMs. The mass spectrometric characterization of *mdx-4cv* EOMs showed increases in a variety of proteins, including glycolytic enzymes and molecular chaperones.

## **2. Materials and Methods**

### **2.1. Materials**

For the mass spectrometric analysis of extraocular muscle preparations, analytical grade reagents and general materials were obtained from Sigma Chemical Company (Dorset, UK), GE Healthcare (Little Chalfont, Buckinghamshire, UK) and Bio-Rad Laboratories (Hemel-Hempstead, Hertfordshire, UK). MS Grade trypsin protease was obtained from ThermoFisher Scientific (Dublin, Ireland), as was the Pierce 660nm Protein Assay Reagent. Spin filters of the type Vivacon 500 (VNOH22; 30 000 MWCO) were purchased from Sartorius (Göttingen,

Germany) for carrying out filter-aided sample preparations. Gel electrophoretic separation and immunoblotting was performed with precast Invitrogen Bolt 4-12% Bis-Tris gels and Whatman nitrocellulose transfer membranes from Bio-Science Ltd (Dun Laoghaire, Ireland), respectively. InstantBlue Coomassie Protein Stain was obtained from Expedeon (Heidelberg, Germany). For immunoblot analysis and immunofluorescence microscopy, primary antibodies were obtained from R&D Systems, Minneapolis, MN, USA (MAB5718 against glyceraldehyde-3-phosphate dehydrogenase), ProteinTech, Rosemont, IL, USA (20716-1-AP against myosin heavy chain 14) and Abcam, Cambridge, UK (ab2413 against fibronectin). Secondary peroxidase-conjugated anti-mouse IgG and anti-rabbit IgG were purchased from Sigma Chemical Company (Dorset, UK) and Cell Signalling Technology (Danvers, MA, USA), respectively.

## **2.2. Extraocular muscle specimens**

The harvesting of *post-mortem* EOMs and diaphragm muscle specimens from 12-month old wild type mice and the *mdx-4cv* mouse model of dystrophinopathy, which is lacking the dystrophin isoforms Dp140, Dp260 and Dp427 due to a point mutation in exon 53, was carried out according to institutional regulations. The eyeball and its surrounding tissues were carefully removed from the ocular cavity by bulbar exenteration. The entire EOM cone was then dissected out and extracted for the isolation of the combined EOM proteome. The establishment of multi-consensus files was carried out with muscle samples from 6 wild type and 6 dystrophic mice. Comparative proteomics was performed with specimens from 3 wild type versus 3 dystrophic mice. Verification analyses were carried out with samples derived from a minimum of 4 wild type and 4 dystrophic mice. Comparative tissue proteomics was carried out by standardized procedures, as previously described in detail [40,41]. Mice were sacrificed in the Bioresource Unit of the University of Bonn and muscle specimens quick-frozen in liquid nitrogen and then transported on dry ice to Maynooth University [42]. Samples were stored at -80°C prior to proteomic analysis. Muscle samples were homogenised in lysis buffer (4% SDS, 100mM Tris-Cl pH 7.6, 0.1M dithiothreitol) using a handheld homogeniser from Kimble Chase (Rockwood, TN, USA), briefly treated in a sonicating water bath and then heated for 3 min at 95°C. Suspensions were centrifuged at 16,000xg for 5 min and the protein-containing supernatant extracted for subsequent analysis [43]. The Pierce 660nm Protein Assay system was used to determine protein concentration [44]. EOM extracts were further processed for mass spectrometric analysis. Samples were mixed with 200µl of 8M urea, 0.1M Tris pH

8.9 in filter units and centrifuged at 14,000xg for 15 min. For filter-aided sample preparation, processing was carried out according to the standardized FASP protocol [45].

### ***2.3. Label-free liquid chromatography mass spectrometry and proteomic data analysis***

The label-free liquid chromatography mass spectrometric analysis of EOMs from wild type versus *mdx-4cv* mice was carried out using a Thermo Orbitrap Fusion Tribrid mass spectrometer (Thermo Fisher Scientific, Waltham, MA, USA). Details of the proteomic workflow describing all preparative steps and analytical procedures using data-dependent acquisition, as well as bioinformatic data handling, were recently outlined in detail [41]. A Thermo UltiMate 3000 nano system was used for reverse-phased capillary high-pressure liquid chromatography and directly coupled in-line with the Thermo Orbitrap Fusion Tribrid mass spectrometer. The qualitative data analysis of mass spectrometric files was carried out with the help of the UniProtKB-SwissProt *Mus musculus* database with Proteome Discoverer 2.2 using Sequest HT (Thermo Fisher Scientific) and Percolator. For protein identification, the following crucial search parameters were employed: (i) a value of 0.02 Da for MS/MS mass tolerance, (ii) a value of 10 ppm for peptide mass tolerance, (iii) variable modification settings for methionine oxidation, (iv) fixed modification settings in relation to carbamido-methylation and (v) tolerance for the occurrence of up to two missed cleavages. Peptide probability was set to high confidence. A minimum XCorr score of 1.5 for 1, 2.0 for 2, 2.25 for 3 and 2.5 for 4 charge state was employed for filtering of peptides [40]. The software analysis programme Progenesis QI for Proteomics (version 2.0; Nonlinear Dynamics, a Waters company, Newcastle upon Tyne, UK) was used to carry out quantitative label-free data analysis. Proteome Discoverer 2.2 using Sequest HT (Thermo Fisher Scientific) and Percolator were employed for the identification of peptides and proteins. Data sets were imported into Progenesis QI software for further analysis. Following the review of protein identifications, only those data that agreed with a crucial set of criteria were deemed as

differentially expressed species between experimental groups based on statistical significance and high confidence. Criteria included an ANOVA p-value of  $\leq 0.01$  between experimental groups, and proteins with  $\geq 2$  unique peptides contributing to the identification. The Progenesis QI programme calculates the mean abundance for individual protein species in each experimental condition to determine the maximum fold change for particular proteins. Condition-vs-condition matrixes with mean values are then used to determine the maximum fold change between any two condition's mean protein abundances [41]. The raw MS files generated by this proteomic study have been deposited under the unique identifier 'j4867' to the Open Science Foundation (<https://osf.io/j4867/>). The standard bioinformatic analysis tools PANTHER [46] and STRING [47] were utilized for the identification of protein classes and for the characterisation of potential protein interaction patterns, respectively.

#### ***2.4. Comparative immunoblot analysis***

For the independent evaluation of the differential expression levels of myosin isoform MyHC14 in wild type EOM versus wild type diaphragm, as identified by mass spectrometry, comparative immunoblotting was carried out under standard conditions [48]. Labelling of glyceraldehyde-3-phosphate dehydrogenase was used to evaluate concentration levels in *mdx-4cv* EOM as compared to wild type EOM preparations. EOM and diaphragm samples were prepared in Laemmli-type sample buffer and heated for 30 min at 37°C. For gel electrophoresis and immunoblotting analysis, 20µg protein per lane were ran on Invitrogen Bolt 4-12% Bis-Tris gels. Coomassie staining of protein gels was performed with InstantBlue Coomassie Protein Stain [39]. For immunoblotting, gel electrophoretically separated proteins were transferred to nitrocellulose membranes, blocked in fat-free milk solution and incubated in 1:1000 diluted primary antibody overnight. The subsequent detection with 1:1000 diluted

peroxidase-conjugated secondary antibodies was carried out with the enhanced chemiluminescence method [40]. Statistical analysis of immunoblots was carried out using ImageJ software (NIH, Bethesda, MD, USA), along with Microsoft Excel in which statistical significance was based on a  $p$ -value  $\leq 0.05$ .

### **2.5. Immunofluorescence microscopy**

In order to evaluate the expression of glyceraldehyde-3-phosphate dehydrogenase in wild type versus *mdx-4cv* EOM muscle, immunofluorescence microscopy was carried out by standardized methodology in combination with histological staining [49]. Freshly dissected skeletal muscle specimens from mice were quick-frozen in liquid nitrogen-cooled isopentane and 10  $\mu\text{m}$  sections cut in a cryostat [50]. Tissue sections were fixed in a 1:1 (v/v) mixture of methanol and acetone for 10 min at room temperature and then blocked with 1:20 diluted normal goat serum for 30 min at room temperature. Primary antibodies to myosin heavy chain MyHC14 and glyceraldehyde-3-phosphate dehydrogenase were diluted 1:200 and 1:400, respectively, in carrageenan-containing and phosphate-buffered saline for overnight incubation at 4°C. The buffer was made by mixing 100 ml phosphate-buffered saline with 0.7 g carrageenan and 10 mg sodium azide. Tissue specimens were carefully washed and then incubated with fluorescently labelled secondary antibodies, using 1:500 diluted anti-mouse RRX antibody for 45 min at room temperature [40]. Nuclei were counter-stained with 1  $\mu\text{g}/\text{ml}$  bis-benzimide Hoechst 33,342. Antibody-labelled EOM sections were embedded in Fluoromount G medium and viewed under a Zeiss Axioskop 2 epifluorescence microscope equipped with a digital Zeiss AxioCam HRc camera (Carl Zeiss Jena GmbH, Jena, Germany).

## **3. Results and Discussion**

In order to elucidate the unique cell biological and biochemical status of EOMs among other types of skeletal muscles [2], this study has focused on the refined proteomic analysis of this subtype of contractile tissue using an Orbitrap Fusion Tribrid mass spectrometer. Based on the mass spectrometric identification of the accessible EOM proteome, the comparative analysis of wild type versus dystrophic *mdx-4cv* muscle preparations was carried out to investigate the underlying protein expression profile of the relatively mild phenotype of dystrophin-deficient EOMs in dystrophinopathy [19].

### 3.1. The proteomic profile of extraocular muscle

The analytical workflow used in this study is outlined in Figure 1. The mass spectrometry-based proteomic profiling of crude extracts from the EOM cone resulted in the identification of a large number of both muscle-specific marker proteins and core proteins of the sarcomere-associated contractile apparatus [51]. The multi-consensus file of unequivocally identified proteoforms has been submitted to a public data repository (Open Science Foundation, OSF Facility, Frankfurt, Germany), under the unique identifier ‘j4867’ (<https://osf.io/j4867/>).

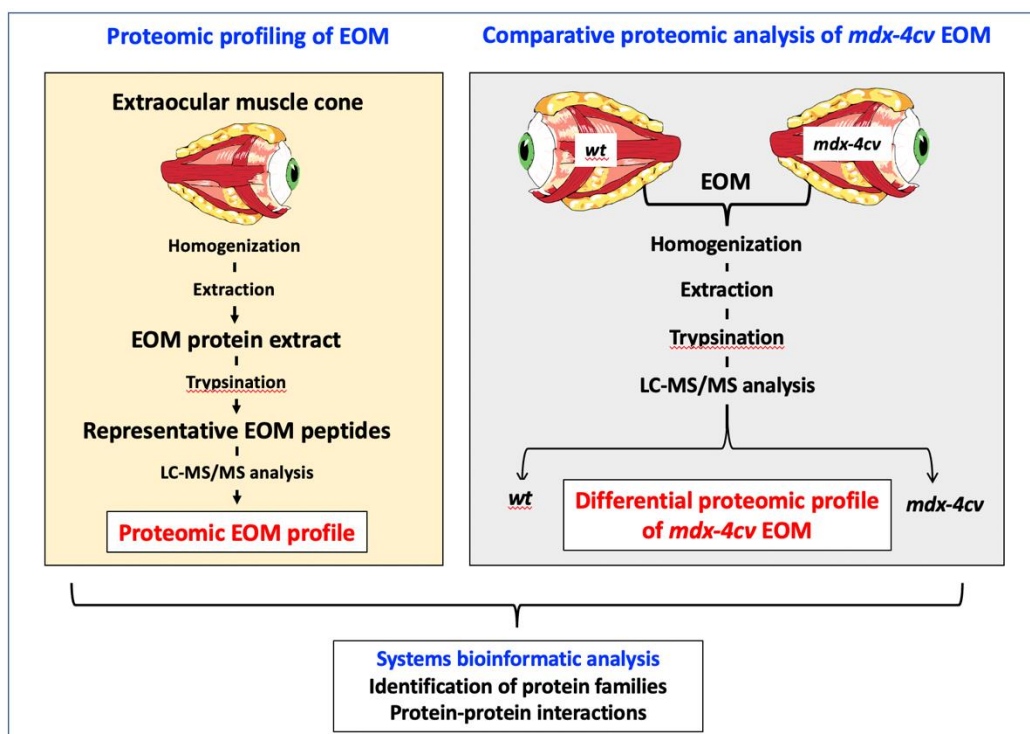


**Figure 1.** Overview of the proteomic profiling approach to characterize extraocular muscle (EOM), as well as determine changes in the *mdx-4cv* mouse model of Duchenne muscular dystrophy.

The proteomic analysis presented in this report identified 2521 protein species in wild type EOM samples and 2331 protein species in *mdx-4cv* EOM samples. Table 1 lists the proteomic identification of sarcomeric proteins and related isoforms in EOM preparations from wild type mice. General marker proteins that exhibit the highest level of enriched expression in skeletal muscles according to the Human Protein Atlas [52], were identified as myosin heavy chain MyHC-IIa (MYH2), myosin-binding protein C (MYBPC1), the Z-disk component myotilin (MYOT), the M-band associated enzyme beta-enolase (ENO3), the half-sarcomere spanning giant protein titin (TTN), the actin-binding protein nebulin (NEB) of the thin filament and the

skeletal muscle LIM-protein 1 (FHL1) (Table 1). Additional muscle-associated markers included the fast sarcoplasmic reticulum Ca<sup>2+</sup>-ATPase SERCA1 (Q8R429; Atp2a1 gene; 27.5% coverage; 19 unique peptides; 109.4 kDa), the slow sarcoplasmic reticulum Ca<sup>2+</sup>-ATPase SERCA2 (O55143; Atp2a2 gene; 16.4% coverage; 12 unique peptides; 114.8 kDa), the muscle-type glycolytic enzyme phosphofructokinase (P47857; Pfk gene; 3.9% coverage; 2 unique peptides; 85.2 kDa) and the muscle-specific oxygen transporter myoglobin (P04247; Mb gene; 28.6% coverage; 5 unique peptides; 17.1 kDa) [39,53,54].

**Table 1.** Proteomic identification of sarcomere-associated proteins and related isoforms in mouse extraocular muscle.

Accession	Protein	Gene	Score	Coverage %	Peptides	Molecular mass (kDa)
E9Q8K5	Titin, muscle-specific	TTN	171.5	2.14	52	3713.7
Q5SX40	Myosin-1 heavy chain, MyHC-IId, fast muscle	MYH1	459.6	31.10	63	223.2
G3UW82	Myosin-2 heavy chain, MyHC-IIa, fast muscle	MYH2	382.7	31.15	60	223.1
P13541	Myosin-3 heavy chain, MyHC-embryonic, muscle	MYH3	125.1	11.70	24	223.7
Q5SX39	Myosin-4, MyHC-IIb, fast muscle	MYH4	472.9	32.75	68	222.7
Q91Z83	Myosin-7 heavy chain, MyHC-I, slow muscle	MYH7	96.04	10.70	20	222.7

---

P13542	Myosin-8 heavy	MYH8	277.9	24.68	47	222.6
	chain, MyHC-					
	perinatal, muscle					
Q8VDD5	Myosin-9 heavy	MYH9	87.81	10.61	20	226.2
	chain, MyHC-					
	cellular, type A					
Q61879	Myosin-10 heavy	MYH10	20.79	2.68	5	228.8
	chain, MyHC-					
	cellular, type B					
A0A2R8VHF9	Myosin-11 heavy	MYH11	255.1	20.07	44	223.2
	chain, smooth					
	muscle					
B1AR69	Myosin-13 heavy	MYH13	217.41	17.03	31	223.4
	chain,					
	extraocular					
	muscle					
K3W4R2	Myosin-14 heavy	MYH14	25.40	3.45	6	228.4
	chain, MyHC-					
	eom,					
	developmental					
E9Q264	Myosin-15 heavy	MYH15	10.20	1.56	3	221.7
	chain,					
	extraocular					
	muscle					
P05977	Myosin light	MYL1	74.36	45.21	8	20.6
	chain MLC-1/3,					
	muscle					
A0A0U1RP93	Myosin light	MYLPF	28.02	10.07	1	16.9
	chain MLC-2,					
	muscle					
Q60605	Myosin light	MYL6	56.91	54.30	7	16.9
	chain MLC-3,					
	muscle					

---

D3YU50	Myosin-binding protein C, slow	MYBPC1	20.96	5.24	4	126.5
A0A571BF46	Nebulin	NEB	15.55	1.32	8	866.5
P68033	Actin, alpha, skeletal muscle	ACTC1	382.05	66.84	26	42.0
P60710	Actin, beta, cytoplasmic	ACTB	384.11	52.53	25	41.7
E9Q452	Tropomyosin alpha-1	TPM1	119.92	40.93	14	32.5
A2AIM4	Tropomyosin beta	TPM2	112.31	41.55	16	33.0
D3Z6I8	Tropomyosin alpha-3	TPM3	47.89	43.72	12	28.7
A0A571BEU1	Tropomyosin alpha-4	TPM4	4.33	14.56	3	18.4
P20801	Troponin muscle	C,TNNC2	3.99	11.88	2	18.1
A0A1B0GRY8	Troponin I, muscle	fastTNNI2	23.66	13.95	2	20.2
A2A6I8	Troponin T, muscle	fastTNNT3	8.66	20.08	4	28.3
A1BN54	Alpha-actinin-1	ACTN1	36.58	8.34	6	102.7
Q9JI91	Alpha-actinin-2	ACTN2	13.09	7.83	6	103.8
O88990	Alpha-actinin-3	ACTN3	11.30	5.11	4	103.0
P57780	Alpha-actinin-4	ACTN4	65.92	20.39	14	104.9
P31001	Desmin	DES	27.89	15.99	8	53.5
P20152	Vimentin	VIM	72.37	24.89	8	53.7
E9Q3W4	Plectin	PLEC	22.89	3.17	12	498.8
P23927	Alpha-B- crystallin	CRYAB	14.36	36.57	7	20.1
E9PYJ9	LIM domain- binding protein 3	LDB3	10.34	3.98	2	72.3
Q9JIF9	Myotilin	MYOT	10.23	6.45	3	55.3

A0A1L1STC	Nesprin-1	SYNE1	4.29	0.31	2	1009.3
6						
A0A571BDS	Xin actin-binding	XIRP1	2.03	1.05	2	196.6
0	repeat-containing					
	protein 1					
Q8VHX6	Filamin-C,	FNLC	21.04	2.53	6	290.9
	muscle-specific					
Z4YJF5	Myomesin-1	MYOM	2.09	0.83	1	175.4
		1				
A2ABU4	Myomesin-3,	MYOM	5.42	2.08	2	161.7
	slow, extraocular	3				
	muscle					
P07310	Creatine kinase,	CKM	48.98	29.92	11	43.0
	muscle-type					
Q9R0Y5	Adenylate	AK1	17.30	16.49	2	21.5
	kinase, AK1					
P97447	Skeletal muscle	FHL1	10.47	5.89	2	61.8
	LIM-protein 1					
P21550	Beta-enolase,	ENO3	152.38	42.63	18	47.0
	muscle-specific					

### 3.2. Proteomic profile of the sarcomere from extraocular muscle

An extensive list of sarcomeric proteins found in wild type EOM is listed in Table 1, including proteins of the thick myosin filament, the thin actin filament, the Z-disk, the M-band region, the titin filament and the auxiliary nebulin filament [22,55], as well as components of the sarcomere-attached cytoskeletal network [56]. The general arrangement of these components in the sarcomere is diagrammatically shown in Figure 2a. In total, this study established 15 different myosin heavy chains [17] to be associated with EOMs. This included the sarcomeric forms myosin-1 (MyHC-II<sub>d</sub>, muscle), myosin-2 (MyHC-II<sub>a</sub>, muscle), myosin-3 (MyHC-embryonic), myosin-4 (MyHC-II<sub>b</sub>, muscle), myosin-7 (MHyC-I, slow) and myosin-8 (MyHC-

perinatal), as well as the specialized myosins named myosin-13, myosin-14 and myosin-15 [57,58].

The crucial myosin-binding protein being present in EOMs was determined to be the slow-type MYBP-C1. Identified cytoskeletal myosins included the MyHC-cellular types A (myosin-9) and B (myosin-10). Besides smooth muscle myosin-11 heavy chain, 4 unconventional myosins were also identified by mass spectrometry, i.e. myosin-6 (E9Q175, Myo6, 144.7 kDa), myosin VC (E9Q1F5, Myo5c, 202.6 kDa), myosin XVIIIa (K3W4L0, Myo18a, 230.8 kDa) and myosin XVIIIb (E9PV66, Myo18b, 288.7 kDa). Myosin light chains included the muscle-specific isoforms MLC-1/3, MLC-2 and MLC-3 [36,59].

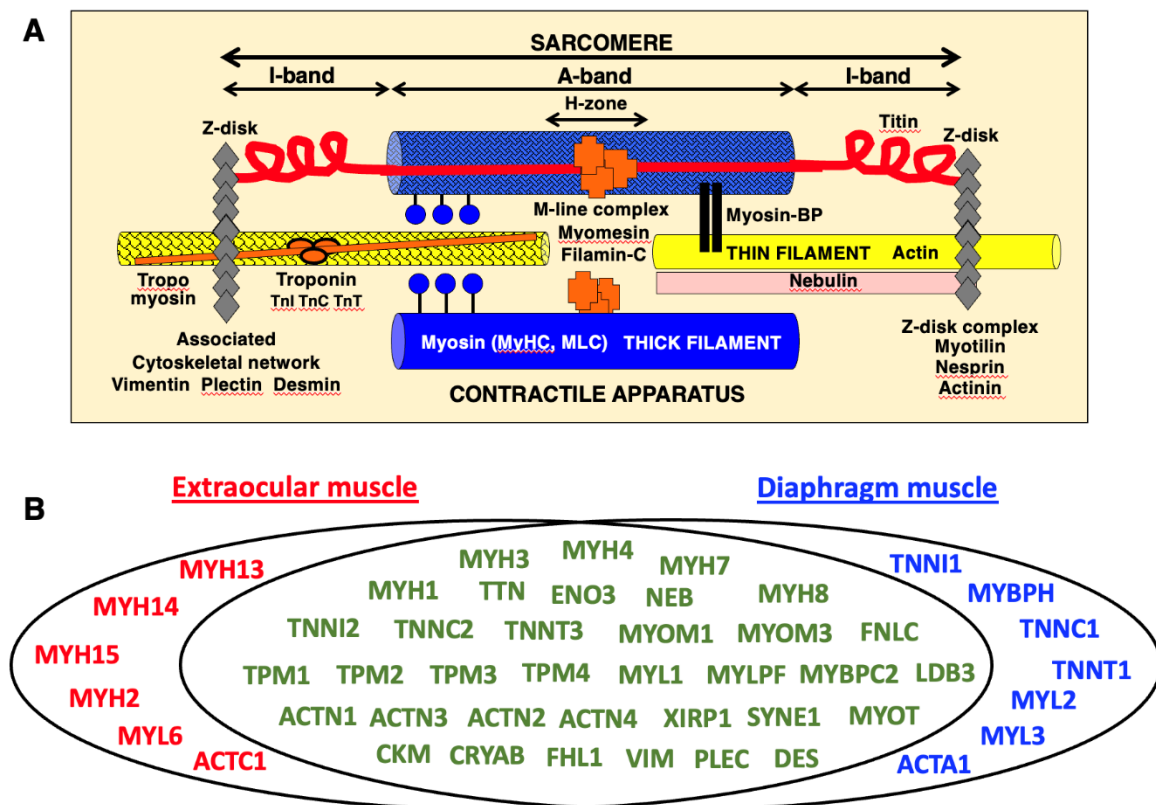


**Figure 2.** Comparative display of mass spectrometrically identified proteins of the sarcomere in extraocular muscle versus diaphragm from wild type mice. Shown is in panel (a) a diagram of the main components of the contractile apparatus and in panel (b) a Venn diagram with the proteomic profile of the two types of investigated skeletal muscles.

Mass spectrometric analysis established major proteins of the thin filament in EOMs, including alpha-actin (ACTC1), nebulin, the tropomyosins TPM1 (alpha-1), TPM2 (beta), TPM3 (alpha-

3) and TPM4 (alpha-4) and the troponin subunits TnC (TNNC2), TnI (TNNI2) and TnT (TNNT3) [58]. In agreement with a previous study [34], a large number of Z-disk associated proteins were identified in EOMs, including the alpha-actinins ACTN1, ACTN2, ACTN3 and ACTN4, desmin, vimentin, plectin, alphaB-crystallin, LIM domain-binding protein LDB3, myotilin, nesprin-1 and xin actin-binding repeat-containing protein 1, as well as muscle-specific filamin-C [60]. Established markers of the M-band region in EOMs included muscle-type creatine kinase, myomesin-1, myomesin-3, adenylate kinase AK1, skeletal muscle LIM-protein FHL1 and muscle-specific beta-enolase [61].

### *3.3. Mass spectrometric identification of proteins specifically expressed in extraocular muscle*

In order to determine enriched expression levels of specific sarcomere-associated proteins in EOMs, the proteomic analysis of extracts from the wild type EOM cone was compared to the recently established proteome of wild type diaphragm muscle [39]. Figure 2b shows a Venn diagram of EOM versus diaphragm and illustrates the large cohort of overlapping expression of proteins belonging to the thick filament, the thin filament, the Z-disk, the M-band, auxiliary filaments and the sarcomere-associated cytoskeletal network [22,55,56]. Interestingly, elevated protein levels in EOMs included the myosin heavy chain isoforms myosin-2 (fast MyHC-IIa; MYH2) [51], myosin-13 (MyHC13; MYH13) [62], myosin-14 (MyHC14; MYH14) [57,58] and myosin-15 (MyHC15; MYH15) [57,58], as well as myosin light polypeptide 6 (MYL6; MLC-3 isoform) [59] and slow cardiac alpha-actin-1 (ACTC1) [63]. In contrast, diaphragm muscle contained apparently higher concentrations of myosin light chains MLC-2 (MYL2) and MLC-3 (MYL3), muscle alpha-actin-1 (ACTA1), the troponin isoforms TNNI1, TNNC1 and TNNT1 and myosin-binding protein MYBP-H [36,39]. These findings confirm that MyHC13 (myosin-13) represents an excellent marker of EOMs [17,34], and additionally establishes the two ancient myosins MyHC14 (myosin-14) and MyHC15 (myosin-15) as highly enriched components of this type of skeletal muscle [57,58]. Immunoblotting confirmed the differential expression pattern of myosin MyHC14 in wild type EOM versus diaphragm muscle. In contrast to comparable concentration levels of glyceraldehyde-3-phosphate dehydrogenase, the immunoblot analysis of MyHC14 demonstrated a significant elevation of this myosin isoform in EOMs as compared to diaphragm muscle (Figure 3).

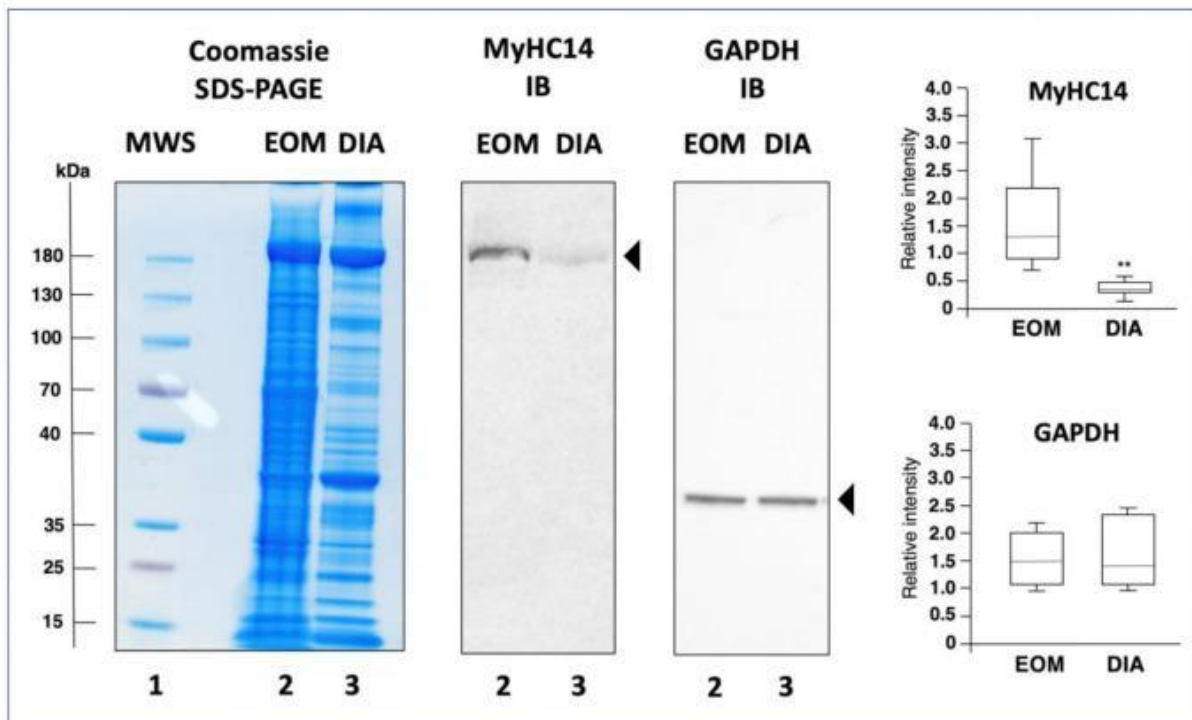


**Figure 3.** Immunoblot analysis of extraocular muscle (EOM) versus diaphragm (DIA) muscle from wild type mice. Shown is an InstantBlue Coomassie stained protein gel using sodium dodecyl sulphate polyacrylamide gel electrophoresis (SDS-PAGE) with molecular weight standards (lane 1; MWS), wild type EOM (lane 2) and wild type DIA (lane 3) samples, as well as identical nitrocellulose replicas used for immunoblotting (IB) and labelled with antibodies to myosin heavy chain MyHC14 and glyceraldehyde-3-phosphate dehydrogenase (GAPDH). In the adjacent panels are shown the statistical analysis of immunoblotting (Mann-Whitney U test;  $n=8$ ;  $**p<0.01$ ). The value of molecular mass standards ( $\times 10^{-3}$  kDa) is marked on the left side of the gel.

The EOM-specific expression and distribution of specialized types of myosin heavy chains, such as MyHC13, MyHC14 and MyHC15 [17], which surround the globe structure within the ocular cavity, could be related to the unusual physiological properties of this type of muscle. In addition, the broad isoform expression pattern in EOMs including both slow and fast myosin isoforms, i.e. slow MyHC-I, fast MyHC-IIa, fast MyHC-IIb and fast MyHC-IIc, as well as embryonic MyHC3 and perinatal MyHC8, form probably the functional basis for an extremely wide range of possible eye movements. This allows complex movements of the eyeball in relation to its horizontal and vertical axis ranging from slow vergence to rapid saccades [6]. EOMs are capable of both considerable eccentric contraction patterns and fibre twitching at high frequency without tetanus, and this is at least partially provided by the kinetic properties

of the unique combination of myosins and their distribution in EOMs. For example, the embryonic MyHC3 isoform is located to the terminal region of contractile fibres, while the super-fast MyHC13 isoform is positioned at the central endplate [62].

#### *3.4. Comparative proteomic profiling of extraocular muscle from the dystrophic mdx-4cv model of Duchenne muscular dystrophy*

Dystrophinopathy is the most frequently inherited neuromuscular disease of early childhood and characterized by progressive skeletal muscle degeneration [21,26], in combination with reactive myofibrosis [28] and sterile inflammation [40]. Genetic rearrangements in the *DMD* gene cause the almost complete loss of the full-length dystrophin isoform Dp427-M [21] and the simultaneous disintegration of the dystrophin-glycoprotein complex [22]. Established genetic animal models of dystrophinopathy, such as the *mdx-4cv* mouse [64-66], reflect many of the multifaceted and body-wide alterations seen in Duchenne patients, including necrosis, fibrosis and inflammation in the diaphragm muscle [39, 67], cardiomyopathic changes [68] and neuronal deficiencies [69], as well as secondary abnormalities in the liver [70], kidney [48] and spleen [40]. The molecular and cellular pathogenesis of muscular dystrophy is also mirrored by characteristic protein changes in biofluids, such as *mdx-4cv* serum, urine and saliva [71-73]. Building on the well-established muscle degeneration and accompanying effects on multiple other organ systems in the *mdx-4cv* mouse model, it was of interest to determine the pathobiochemical signature of apparently spared EOMs [74].

Detailed histological, cell biological and biochemical studies of dystrophin-deficient EOM have been carried out [75-80] and are supplemented here with findings on proteome-wide changes. Table 2 lists significantly altered proteins in *mdx-4cv* EOM. This includes characteristic increases in the glycolytic enzymes glyceraldehyde-3-phosphate dehydrogenase, enolase and lactate dehydrogenase [81], as well as the molecular chaperones heat shock protein 1 beta (HspB1) and heat shock cognate 71 kDa protein (HspA8) [82]. Findings from previous immunoblotting and mass spectrometric surveys of EOMs that were extracted from the spontaneously mutated *mdx-23* mouse model of dystrophinopathy agree with these changes in distinct protein families [37,38]. In contrast to comparable expression levels of the dystrophin-associated glycoprotein beta-dystroglycan, higher levels of the molecular chaperones alphaB-crystallin, cvHsp/HspB7, Hsp25/HspB1 and Hsp90 were previously demonstrated to exist in dystrophin-deficient EOMs. The apparent up-regulation of heat shock proteins in both *mdx* and *mdx-4cv* EOMs is an indication of a robust cellular stress response in dystrophin-deficient

EOMs [83]. Changes in HspB1 might be suitable to establish this small heat shock protein as a marker of the stress response in EOMs in the dystrophic phenotype [37].

The relatively mild phenotype of EOMs in X-linked muscular dystrophy [19,20] is probably closely related to the special biochemical and physiological features of the muscles surrounding the eyeball, such as the longitudinal distribution of neuromuscular junctions [9-11], the considerable capacity for fibre regeneration [13,14], exceptional fatigue resistance even in fast-twitching fibre populations [16] and an extensive calcium extrusion system [15]. In most skeletal muscles, dystrophin deficiency causes a collapse of sarcolemmal integrity and a concomitant increase in micro-rupturing of the surface membrane, which triggers influx of  $Ca^{2+}$ -ions into myofibres and associated enhanced  $Ca^{2+}$ -dependent proteolytic activity in the sarcosol [25,27]. The efficient and swift removal of cytosolic calcium from EOM fibres and the enhanced ion buffering capacity of EOMs might therefore play a key role in the protection from dystrophic changes [18,75,78]. Another important factor might be the relatively low concentration of dystrophin isoform Dp427-M in EOMs. The sub-sarcolemmal dystrophin lattice might not play the same crucial role in the membrane cytoskeleton and linkage of the intracellular actin filaments to extracellular laminin via the dystrophin-glycoprotein complex in EOMs as compared to other skeletal muscles [36]. Importantly, previous studies have established an up-regulation of the autosomal dystrophin homologue named utrophin Up-395 and associated rescue of sarcolemmal glycoproteins such as beta-dystroglycan in dystrophin-deficient EOMs [37,76,77]. Thus, full-length utrophin might substitute for dystrophin in EOMs and thereby stabilize its trans-sarcolemmal cytolinker function and prevent secondary damage to myofibres.

**Table 2.** Comparative proteomic analysis of the *mdx-4cv* extraocular muscle cone.

Accession	Protein	Gene	Peptides	Annova (p)	Fold change
P16858	Glyceraldehyde-3-phosphate dehydrogenase	GAPDH	14	0.01427	+18.45
P14602	Heat shock protein 1, beta	HSPB1	25	0.04444	+15.62

---

P63017	Heat shock cognate 71HSPA8 kDa protein		24	0.00894 +10.22
G3XA25	Acetyl-CoA acetyltransferase 2	ACAT2	24	0.04001 +7.56
P06151	Lactate dehydrogenaseLDHA 1, A chain		14	0.02856 +5.93
P19536	Hydroxyacyl- coenzyme dehydrogenase	HADH A	22	0.04369 +3.38
P17182	Alpha-enolase	ENO1	19	0.04825 +3.13
P47740	Aldehyde dehydrogenase family 3 member A2	ALDH3A2	15	0.04301 +2.94
E9QNH7	Acyl-CoA-binding domain-containing protein 5	ACBD5	6	0.03134 +2.43
P07724	Albumin	ALB	45	0.03520 +1.76
P19096	Fatty acid synthase	FASN	119	0.02425 +1.69
G5E8R1	Tropomyosin alpha-1TPM1 chain		11	0.03985 -1.98
Q9DB20	ATP synthase subunitATP5PO O, mitochondrial		7	0.03449 -2.07
P37040	NADPH-cytochrome P450 reductase	POR	12	0.04813 -2.45
Q9R0P5	Dextrin	DSTN	9	0.03484 -2.66
Q9D3D9	ATP synthase subunitATP5F1D delta, mitochondrial		4	0.04228 -2.71
Q9CRB9	MICOS complex subunit Mic19	CHCHD3	11	0.04353 -2.90
Q9DBC7	cAMP-dependent protein kinase type I- alpha	PRKAR1A	2	0.02217 -2.91

---

The bioinformatic analysis of the proteomic survey of *mdx-4cv* EOMs is summarized in Figure 4, which displays the PANTHER analysis of the overall protein profile [46], the heat map of proteomic changes and the findings from the STRING analysis of potentially altered protein interaction hubs [47]. The overall distribution of protein families was shown not to be majorly different between wild type and dystrophic *mdx-4cv* EOM and agrees with previous mass spectrometric surveys [37,38]. The heat map illustrates the distribution pattern of changes between normal and dystrophic specimens. In contrast to other sub-types of dystrophin-deficient skeletal muscles [31,39,42,84-86], Dp427-lacking EOMs seem to exhibit relatively minor proteome-wide changes.

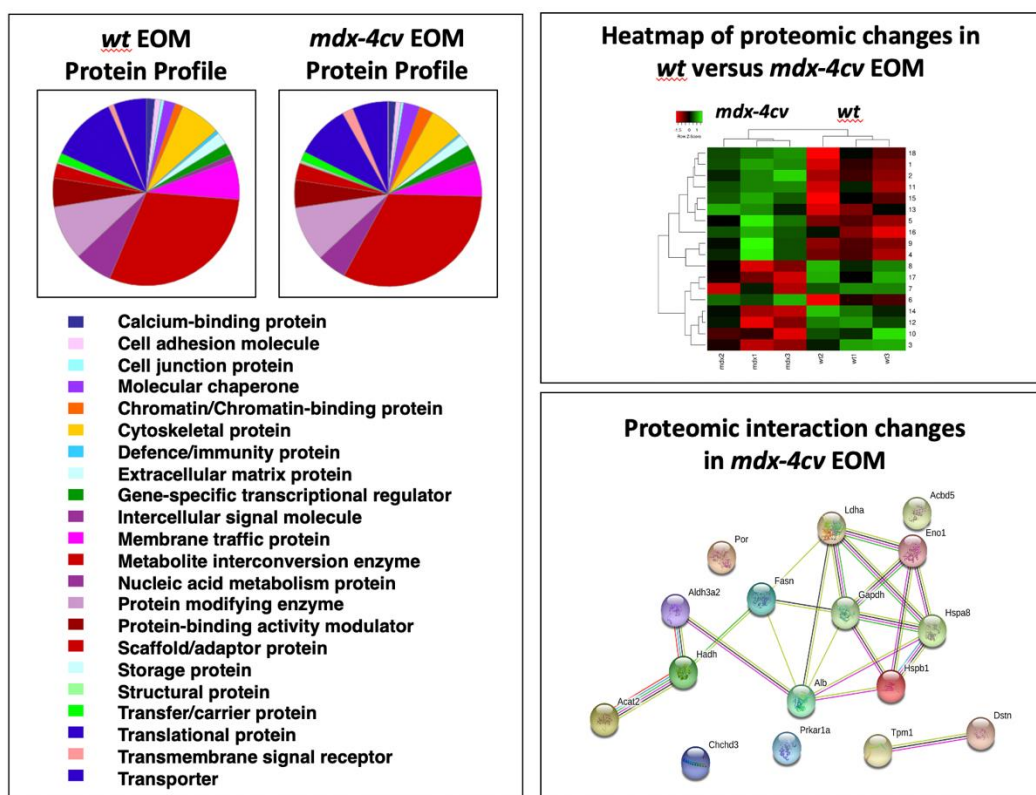


**Figure 4.** Bioinformatic analysis of the comparative proteomic profiling of extraocular muscle (EOM) from wild type (*wt*) versus the *mdx-4cv* model of X-linked muscular dystrophy. Shown is the result of the bioinformatic PANTHER analysis [46] of the distribution of protein classes within the EOM proteome from normal versus dystrophic mice. In addition, the heat map of the comparative proteomic analysis of *wt* versus *mdx-4cv* EOM is displayed, which shows the findings from hierarchical clustering of the mean protein expression values of statistically significant differentially abundant EOM proteins. Potential changes in protein-protein interaction patterns in *mdx-4cv* EOMs were determined with the help of the bioinformatics software programme STRING [47].

The STRING interaction network indicates that the drastically increased enzyme glyceraldehyde-3-phosphate dehydrogenase is positioned centrally within an altered protein hub in dystrophic EOMs. Immunofluorescence microscopy and immunoblotting was employed to compare the expression of glyceraldehyde-3-phosphate dehydrogenase. As illustrated in Figure 5, immunofluorescence labelling of this glycolytic enzyme shows elevated levels in dystrophin-deficient EOMs, as compared to relatively comparable levels of myosin MyHC14. Immunoblotting also indicates increased levels of glyceraldehyde-3-phosphate dehydrogenase in *mdx-4cv* EOMs, as compared to comparable expression of fibronectin. An approximately 2-fold increase in the expression of glyceraldehyde-3-phosphate dehydrogenase has previously been identified in dystrophic *mdx-23* diaphragm preparations [86]. Thus, a potential shift to more glycolytic metabolism appears to be associated with the dystrophic phenotype, and this seems to be especially striking in *mdx-4cv* EOMs, suggesting these types of metabolic enzymes as biomarker candidates for studying dystrophinopathy-related changes in bioenergetic pathways. The comparable levels of fibronectin in wild type versus dystrophin-deficient EOMs indicates the lack of reactive myofibrosis in this type of muscle, which is otherwise seen in most contractile tissues affected in the dystrophic phenotype [28,33,67].

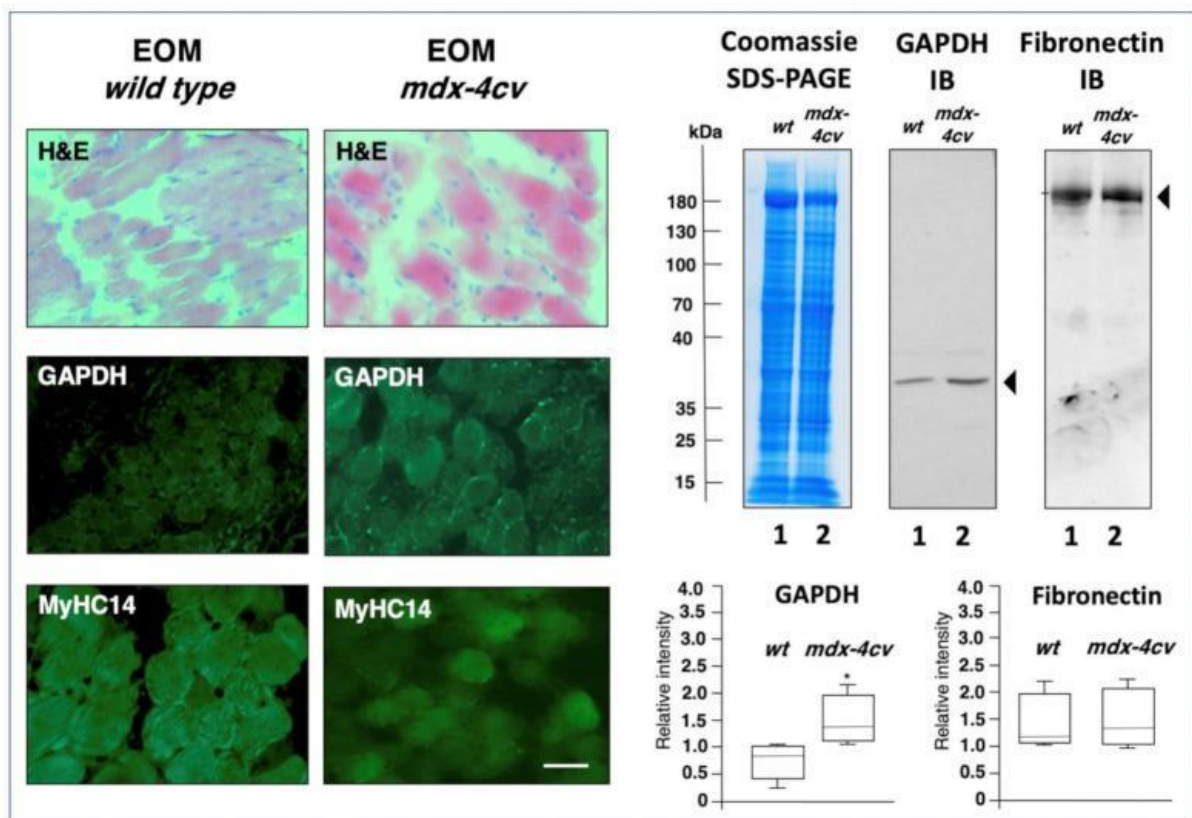


**Figure 5.** Histological and immunofluorescence microscopical characterization, as well as immunoblot analysis, of extraocular muscle (EOM) from the *mdx-4cv* mouse model of Duchenne muscular dystrophy. Shown are transverse cryosections of wild type (*wt*) and *mdx-4cv* EOMs stained with haematoxylin and eosin (H&E) and labelled with antibodies to glyceraldehyde-3-phosphate dehydrogenase (GAPDH) and myosin heavy chain MyHC14. Bar equals 30µm. Shown is an InstantBlue Coomassie (CBB) stained protein gel with wild type EOM (lane 1) and *mdx-4cv* EOM (lane 2) samples, as well as identical nitrocellulose replicas used for immunoblotting and labelled with antibodies to glyceraldehyde-3-phosphate dehydrogenase (GAPDH) and fibronectin (FN). In the below panels are shown the statistical analysis of immunoblotting (Mann-Whitney U test; n=4; \*p<0.05). The value of molecular mass standards ( $\times 10^{-3}$  kDa) is marked on the left side of the gel.

In addition, elevated expression levels were shown for cytosolic acetyl-CoA acetyltransferase ACAT2, aldehyde dehydrogenase family 3 member A2 and acyl-CoA-binding domain-containing protein 5, albumin, hydroxyacyl-coenzyme A dehydrogenase and fatty acid synthase. The proteomic changes in key enzymes of the glycolytic pathway and anaerobic metabolism suggest a potential metabolic shift in *mdx-4cv* EOMs [87]. A concomitant decrease was observed in certain mitochondrial proteins including the ATP synthase subunit O, NADPH-cytochrome P450 reductase, ATP synthase subunit delta and MICOS complex subunit Mic19. Decreased proteins also included Tropomyosin alpha-1 chain, the actin-depolymerizing protein destrin and cAMP-dependent protein kinase type I-alpha.

A potential weakness and bioanalytical limitations of this report relate to the usage of an animal model of Duchenne muscular dystrophy instead of patient samples, and the focus on changed protein concentration using peptide mass spectrometry. With the exception of the diaphragm, the *mdx-4cv* mouse exhibits relatively mild symptoms of fibre wasting in its general musculature. Thus, findings from this study should ideally be extended to characterize muscle specimens from Duchenne patients, which is however extremely difficult in the case of EOMs. Proteomics focuses on the mass spectrometric identification of individual proteoforms and can be routinely employed for comparative studies. However, it is important to realize that the establishment of abundance changes in individual proteins does not provide detailed information on the underlying regulatory mechanisms. It will therefore be important to supplement the new proteomic data sets with future analyses on the biochemical, physiological and cell biological properties of dystrophin-deficient EOMs.

#### 4. Conclusions

The systematic mass spectrometry-based proteomic survey of EOM specimens has established distinct myosin isoforms of the MyHC category as new sarcomeric marker candidates of this specialized type of skeletal muscle, i.e. MyHC14 and MyHC15, besides confirming MyHC13 as an EOM enriched component. The drastically elevated levels of MyHC14 in wild type EOMs as compared to wild type diaphragm muscle were clearly confirmed by immunoblotting. This makes MyHC14 a suitable biomarker of EOMs and it remains to be elucidated what exact physiological role this particular proteoform of the myosin complex plays in the contractile kinetics and functional adaptability of EOMs. Comparative proteomics of wild type versus dystrophic specimens indicates that an apparent metabolic shift from oxidative metabolism to more glycolytic pathway and heightened cellular stress response exists in *mdx-4cv* EOM. Elevated levels of the glycolytic enzyme glyceraldehyde-3-phosphate dehydrogenase appear to be associated with dystrophic alterations in mildly affected EOMs. These alterations in the cellular homeostasis may serve as mechanisms to compensate for deficits induced by the dystrophin loss in this model of Duchenne muscular dystrophy.

**Supplementary Materials:** The raw MS files generated by this proteomic study have been deposited under the unique identifier ‘j4867’ to the Open Science Foundation (<https://osf.io/j4867/>).

**Author Contributions:** Conceptualization, D.S., P.D. and K.O.; methodology, S.G. and P.D.; software, M.H., P.M.; validation, S.G., P.D. and M.Z.; formal analysis, S.G., P.D., M.Z. and M.H.; resources, J.R.; data curation, P.D., S.G. and M.H.; writing—original draft preparation, S.G., P.D. and K.O.; writing—review and editing, K.O., D.S., S.G. and P.D.; supervision, K.O., P.D., J.R. and P.M.; funding acquisition, K.O. and P.M. All authors have read and agreed to the published version of the manuscript.

**Funding:** Research was supported by the Kathleen Lonsdale Institute for Human Health Research at Maynooth University. The Orbitrap Fusion Tribrid mass spectrometer was funded under a Science Foundation Ireland Infrastructure Award to Dublin City University (SFI 16/RI/3701).

**Institutional Review Board Statement:** Animals were handled in strict adherence to local governmental and institutional animal care regulations and were approved by the Institutional Animal Care and Use Committee (Amt für Umwelt, Verbraucherschutz und Lokale Agenda der Stadt Bonn, North Rhine-Westphalia, Germany). Frozen specimens were transported on dry ice to Maynooth University in accordance with the Department of Agriculture (animal by-product register number 2016/16 to the Department of Biology, National University of Ireland, Maynooth).

**Data Availability Statement:** The raw MS files generated by this proteomic study have been deposited under the unique identifier ‘j4867’ to the Open Science Foundation (<https://osf.io/j4867/>).

**Acknowledgments:** We would like to thank Drs. Hemmen Sabir and Stephan Baader (University of Bonn) for their support of this project.

**Conflicts of Interest:** The authors declare no conflict of interest.

## References

1. Blaauw, B.; Schiaffino, S.; Reggiani, C. Mechanisms modulating skeletal muscle phenotype. *Compr. Physiol.* 2013, 3, 1645-1687, doi: 10.1002/cphy.c130009
2. Verma, M.; Fitzpatrick, K.; McLoon, L.K. Extraocular Muscle Repair and Regeneration. *Curr. Ophthalmol. Rep.* 2017, 5, 207-215, doi: 10.1007/s40135-017-0141-4
3. Haladaj, R.; Polgaj, M.; Tubbs, R.S. Comparison of the Superior and Inferior Rectus Muscles in Humans: An Anatomical Study with Notes on Morphology, Anatomical Variations, and Intramuscular Innervation Patterns. *Biomed. Res. Int.* 2020, 2020, 9037693, doi: 10.1155/2020/9037693
4. Spencer, R.F.; Porter, J.D. Biological organization of the extraocular muscles. *Prog. Brain Res.* 2006, 151, 43-80, doi: 10.1016/S0079-6123(05)51002-1.
5. van der Pol, C.B.; Chakraborty, S.; Gao, J.; Nguyen, T.; Torres, C.; Glikstein, R. Imaging anatomy and pathology of extraocular muscles in adults. *Can. Assoc. Radiol. J.* 2014, 65, 366-371, doi: 10.1016/j.carj.2014.05.001
6. Büttner-Ennever, J.A. Anatomy of the oculomotor system. *Dev. Ophthalmol.* 2007, 40, 1-14, doi: 10.1159/000100345

7. Sambasivan, R.; Gayraud-Morel, B.; Dumas, G., Cimper, C.; Paisant, S.; Kelly, R.G.; Tajbakhsh, S. Distinct regulatory cascades govern extraocular and pharyngeal arch muscle progenitor cell fates. *Dev. Cell.* 2009, *16*, 810-821, doi: 10.1016/j.devcel.2009.05.008
8. Zacharias, A.L.; Lewandoski, M.; Rudnicki, M.A.; Gage, P.J. Pitx2 is an upstream activator of extraocular myogenesis and survival. *Dev. Biol.* 2011, *349*, 395-405, doi: 10.1016/j.ydbio.2010.10.028
9. Jacoby, J.; Chiarandini, D.J.; Stefani, E. Electrical properties and innervation of fibers in the orbital layer of rat extraocular muscles. *J. Neurophysiol.* 1989, *61*, 116-125, doi: 10.1152/jn.1989.61.1.116
10. Hernández, R.G.; Calvo, P.M.; Blumer, R.; de la Cruz, R.R.; Pastor, A.M. Functional diversity of motoneurons in the oculomotor system. *Proc Natl Acad Sci USA.* 2019, *116*, 3837-3846. doi: 10.1073/pnas.1818524116
11. Liu, J.X.; Domellöf, F.P. A Novel Type of Multiterminal Motor Endplate in Human Extraocular Muscles. *Invest. Ophthalmol. Vis. Sci.* 2018, *59*, 539-548. doi: 10.1167/iovs.17-22554
12. Bruenech, J.R.; Kjellevold Haugen, I.B. How does the structure of extraocular muscles and their nerves affect their function? *Eye (Lond).* 2015, *29*, 177-183, doi: 10.1038/eye.2014.269
13. McLoon, L.K.; Rowe, J.; Wirtschafter, J.; McCormick, K.M. Continuous myofiber remodeling in uninjured extraocular myofibers: myonuclear turnover and evidence for apoptosis. *Muscle Nerve* 2004, *29*, 707-715, doi: 10.1002/mus.20012
14. Hebert, S.L.; Daniel, M.L.; McLoon, L.K. The role of Pitx2 in maintaining the phenotype of myogenic precursor cells in the extraocular muscles. *PLoS One.* 2013, *8*, e58405, doi: 10.1371/journal.pone.0058405
15. Sekulic-Jablanovic, M.; Ullrich, N.D.; Goldblum, D.; Palmowski-Wolfe, A.; Zorzato, F.; Treves, S. Functional characterization of orbicularis oculi and extraocular muscles. *J. Gen. Physiol.* 2016, *147*, 395-406, doi: 10.1085/jgp.201511542
16. Asmussen, G.; Punkt, K.; Bartsch, B.; Soukup, T. Specific metabolic properties of rat oculorotatory extraocular muscles can be linked to their low force requirements. *Invest. Ophthalmol. Vis. Sci.* 2008, *49*, 4865-4871, doi: 10.1167/iovs.07-1577
17. Hoh, J.F.Y. Myosin heavy chains in extraocular muscle fibres: distribution, regulation and function. *Acta Physiol (Oxf).* 2021, *231*, e13535, doi: 10.1111/apha.13535

18. Khurana, T.S.; Prendergast, R.A.; Alameddine, H.S.; Tome, F.M.; Fardeau, M.; Arahata, K.; Sugita, H.; Kunkel, L.M. Absence of extraocular muscle pathology in Duchenne's muscular dystrophy: role for calcium homeostasis in extraocular muscle sparing. *J. Exp. Med.* 1995, *182*, 467-475, doi: 10.1084/jem.182.2.467
19. Andrade, F.H.; Porter, J.D.; Kaminski, H.J. Eye muscle sparing by the muscular dystrophies: lessons to be learned? *Microsc. Res. Tech.* 2000, *48*, 192-203, doi: 10.1002/(SICI)1097-0029(20000201/15)48:3/4<192::AID-JEMT7>3.0.CO;2-J
20. Kallestad, K.M.; Hebert, S.L.; McDonald, A.A.; Daniel, M.L.; Cu, S.R.; McLoon, L.K. Sparing of extraocular muscle in aging and muscular dystrophies: a myogenic precursor cell hypothesis. *Exp. Cell Res.* 2011, *317*, 873-885, doi: 10.1016/j.yexcr.2011.01.018
21. Thompson, R.; Spendiff, S.; Roos, A.; Bourque, P.R.; Warman Chardon, J.; Kirschner, J.; Horvath, R., Lochmüller, H. Advances in the diagnosis of inherited neuromuscular diseases and implications for therapy development. *Lancet Neurol.* 2020, *19*, 522-532, doi: 10.1016/S1474-4422(20)30028-4
22. Murphy, S.; Ohlendieck, K. Proteomic profiling of large myofibrillar proteins from dried and long-term stored polyacrylamide gels. *Anal. Biochem.* 2018, *543*, 8-11, doi: 10.1016/j.ab.2017.11.022
23. Dowling, P.; Gargan, S.; Murphy, S.; Zweyer, M.; Sabir, H.; Swandulla, D.; Ohlendieck, K. The Dystrophin Node as Integrator of Cytoskeletal Organization, Lateral Force Transmission, Fiber Stability and Cellular Signaling in Skeletal Muscle. *Proteomes* 2021, *9*, 9, doi: 10.3390/proteomes9010009
24. Allen, D.G.; Whitehead, N.P.; Froehner, S.C. Absence of Dystrophin Disrupts Skeletal Muscle Signaling: Roles of Ca<sup>2+</sup>, Reactive Oxygen Species, and Nitric Oxide in the Development of Muscular Dystrophy. *Physiol. Rev.* 2016, *96*, 253-305, doi: 10.1152/physrev.00007.2015
25. Shin, J.; Tajrishi, M.M.; Ogura, Y.; Kumar, A. Wasting mechanisms in muscular dystrophy. *Int. J. Biochem. Cell Biol.* 2013, *45*, 2266-2279, doi: 10.1016/j.biocel.2013.05.001
26. Mercuri, E.; Bönnemann, C.G.; Muntoni, F. Muscular dystrophies. *Lancet* 2019, *394*, 2025-2038, doi: 10.1016/S0140-6736(19)32910-1
27. Starosta, A.; Konieczny, P. Therapeutic aspects of cell signaling and communication in Duchenne muscular dystrophy. *Cell. Mol. Life Sci.* 2021, in press, doi: 10.1007/s00018-021-03821-x

28. Ohlendieck, K.; Swandulla, D. Molecular pathogenesis of Duchenne muscular dystrophy-related fibrosis. *Pathologie* 2017, *38*, 21-29, doi: 10.1007/s00292-017-0265-1
29. Birnkrant, D.J.; Bushby, K.; Bann, C.M.; Apkon, S.D.; Blackwell, A.; Brumbaugh, D.; Case, L.E.; Clemens, P.R.; Hadjiyannakis, S.; Pandya, S.; Street, N.; Tomezsko, J.; Wagner, K.R.; Ward, L.M.; Weber, D.R.; DMD Care Considerations Working Group. Diagnosis and management of Duchenne muscular dystrophy, part 1: diagnosis, and neuromuscular, rehabilitation, endocrine, and gastrointestinal and nutritional management. *Lancet Neurol.* 2018, *17*, 251-267, doi: 10.1016/S1474-4422(18)30024-3
30. Meyers, T.A.; Townsend, D. Cardiac Pathophysiology and the Future of Cardiac Therapies in Duchenne Muscular Dystrophy. *Int. J. Mol. Sci.* 2019, *20*, 4098, doi: 10.3390/ijms20174098
31. Carr, S.J.; Zahedi, R.P.; Lochmüller, H.; Roos, A. Mass spectrometry-based protein analysis to unravel the tissue pathophysiology in Duchenne muscular dystrophy. *Proteomics Clin. Appl.* 2018, *12*(2), doi: 10.1002/prca.201700071
32. Dowling, P.; Murphy, S.; Zweyer, M.; Raucamp, M.; Swandulla, D.; Ohlendieck, K. Emerging proteomic biomarkers of X-linked muscular dystrophy. *Expert Rev. Mol. Diagn.* 2019, *19*, 739-755, doi: 10.1080/14737159.2019.1648214
33. Holland, A.; Murphy, S.; Dowling, P.; Ohlendieck, K. Pathoproteomic profiling of the skeletal muscle matrisome in dystrophinopathy associated myofibrosis. *Proteomics* 2016, *16*, 345-366, doi: 10.1002/pmic.201500158
34. Fraterman, S.; Zeiger, U.; Khurana, T.S.; Wilm, M.; Rubinstein, N.A. Quantitative proteomics profiling of sarcomere associated proteins in limb and extraocular muscle allotypes. *Mol. Cell. Proteomics* 2007, *6*, 728-737, doi: 10.1074/mcp.M600345-MCP200
35. Fraterman, S.; Zeiger, U.; Khurana, T.S.; Rubinstein, N.A.; Wilm, M. Combination of peptide OFFGEL fractionation and label-free quantitation facilitated proteomics profiling of extraocular muscle. *Proteomics* 2007, *7*, 3404-3416, doi: 10.1002/pmic.200700382
36. Zhang, S.Z.; Xie, H.Q.; Xu, Y.; Li, X.Q.; Wei, R.Q.; Zhi, W.; Deng, L.; Qiu, L.; Yang, Z.M. Regulation of cell proliferation by fast Myosin light chain 1 in myoblasts derived from extraocular muscle, diaphragm and gastrocnemius. *Exp. Biol. Med. (Maywood)*. 2008, *233*, 1374-1384, doi: 10.3181/0804-RM-134

37. Lewis, C.; Ohlendieck, K. Proteomic profiling of naturally protected extraocular muscles from the dystrophin-deficient mdx mouse. *Biochem. Biophys. Res. Commun.* 2010, *396*, 1024-1029, doi: 10.1016/j.bbrc.2010.05.052
38. Matsumura, C.Y.; Menezes de Oliveira, B.; Durbeej, M.; Marques, M.J. Isobaric Tagging-Based Quantification for Proteomic Analysis: A Comparative Study of Spared and Affected Muscles from mdx Mice at the Early Phase of Dystrophy. *PLoS One.* 2013, *8*, e65831, doi: 10.1371/journal.pone.0065831
39. Murphy, S.; Zweyer, M.; Raucamp, M.; Henry, M.; Meleady, P.; Swandulla, D.; Ohlendieck, K. Proteomic profiling of the mouse diaphragm and refined mass spectrometric analysis of the dystrophic phenotype. *J. Muscle Res. Cell. Motil.* 2019, *40*, 9-28, doi: 10.1007/s10974-019-09507-z
40. Dowling, P.; Gargan, S.; Zweyer, M.; Henry, M.; Meleady, P.; Swandulla, D.; Ohlendieck, K. Proteome-wide Changes in the mdx-4cv Spleen due to Pathophysiological Cross Talk with Dystrophin-Deficient Skeletal Muscle. *iScience* 2020, *23*, 101500, doi: 10.1016/j.isci.2020.101500
41. Dowling, P.; Gargan, S.; Zweyer, M.; Henry, M.; Meleady, P.; Swandulla, D.; Ohlendieck, K. Protocol for the Bottom-Up Proteomic Analysis of Mouse Spleen. *STAR Protoc.* 2020, *1*, 100196, doi: 10.1016/j.xpro.2020.100196
42. Murphy, S.; Zweyer, M.; Henry, M.; Meleady, P.; Mundegar, R.R.; Swandulla, D.; Ohlendieck, K. Proteomic analysis of the sarcolemma-enriched fraction from dystrophic mdx-4cv skeletal muscle. *J. Proteomics* 2019, *191*, 212-227, doi: 10.1016/j.jprot.2018.01.015.
43. Dowling, P.; Gargan, S.; Zweyer, M.; Sabir, H.; Henry, M.; Meleady, P.; Swandulla, D.; Ohlendieck, K. Proteomic profiling of the interface between the stomach wall and the pancreas in dystrophinopathy. *Eur. J. Transl. Myol.* 2021, *31*, 9627, doi: 10.4081/ejtm.2020.9627.
44. Antharavally, B.S.; Mallia, K.A.; Rangaraj, P.; Haney, P.; Bell, P.A. Quantitation of proteins using a dye-metal-based colorimetric protein assay. *Anal. Biochem.* 2009, *385*, 342-345, doi: 10.1016/j.ab.2008.11.024
45. Wiśniewski, J.R.; Zougman, A.; Nagaraj, N.; Mann, M. Universal sample preparation method for proteome analysis. *Nat. Methods* 2009, *6*, 359-362, doi: 10.1038/nmeth.1322
46. Mi, H.; Ebert, D.; Muruganujan, A.; Mills, C.; Albou, L.P.; Mushayamaha, T.; Thomas, P.D. PANTHER version 16: a revised family classification, tree-based classification

- tool, enhancer regions and extensive API. *Nucleic Acids Res.* 2021, *49(D1)*, D394-D403, doi: 10.1093/nar/gkaa1106
47. Szklarczyk, D.; Gable, A.L.; Nastou, K.C.; Lyon, D.; Kirsch, R.; Pyysalo, S.; Doncheva, N.T.; Legeay, M.; Fang, T.; Bork, P.; Jensen, L.J.; von Mering, C. The STRING database in 2021: customizable protein-protein networks, and functional characterization of user-uploaded gene/measurement sets. *Nucleic Acids Res.* 2021, *49(D1)*, D605-D612, doi: 10.1093/nar/gkaa1074
  48. Dowling, P.; Zweyer, M.; Raucamp, M.; Henry, M.; Meleady, P.; Swandulla, D.; Ohlendieck, K. Proteomic and cell biological profiling of the renal phenotype of the mdx-4cv mouse model of Duchenne muscular dystrophy. *Eur. J. Cell Biol.* 2020, *99*, 151059, doi: 10.1016/j.ejcb.2019.151059
  49. Murphy, S.; Zweyer, M.; Mundegar, R.R.; Henry, M.; Meleady, P.; Swandulla, D.; Ohlendieck, K. Concurrent Label-Free Mass Spectrometric Analysis of Dystrophin Isoform Dp427 and the Myofibrosis Marker Collagen in Crude Extracts from mdx-4cv Skeletal Muscles. *Proteomes* 2015, *3*, 298-327, doi: 10.3390/proteomes3030298
  50. Stuelsatz, P.; Yablonka-Reuveni, Z. Isolation of Mouse Periocular Tissue for Histological and Immunostaining Analyses of the Extraocular Muscles and Their Satellite Cells. *Methods Mol. Biol.* 2016, *1460*, 101-127, doi: 10.1007/978-1-4939-3810-0\_9
  51. Holland, A.; Ohlendieck, K. Proteomic profiling of the contractile apparatus from skeletal muscle. *Expert Rev. Proteomics* 2013, *10*, 239-257, doi: 10.1586/epr.13.20
  52. Thul, P.J.; Lindskog, C. The human protein atlas: A spatial map of the human proteome. *Protein Sci.* 2018, *27*, 233-244, doi: 10.1002/pro.3307
  53. Deshmukh, A.S.; Murgia, M.; Nagaraj, N.; Treebak, J.T.; Cox, J.; Mann, M. Deep proteomics of mouse skeletal muscle enables quantitation of protein isoforms, metabolic pathways, and transcription factors. *Mol. Cell. Proteomics* 2015, *14*, 841-853, doi: 10.1074/mcp.M114.044222.
  54. Deshmukh, A.S.; Steenberg, D.E.; Hostrup, M.; Birk, J.B.; Larsen, J.K.; Santos, A.; Kjøbsted, R.; Hingst, J.R.; Schéele, C.C.; Murgia, M.; Kiens, B.; Richter, E.A; Mann, M.; Wojtaszewski, J.F.P. Deep muscle-proteomic analysis of freeze-dried human muscle biopsies reveals fiber type-specific adaptations to exercise training. *Nat. Commun.* 2021, *12*, 304, doi: 10.1038/s41467-020-20556-8.

55. Dowling, P.; Zweyer, M.; Swandulla, D.; Ohlendieck, K.; Characterization of Contractile Proteins from Skeletal Muscle Using Gel-Based Top-Down Proteomics. *Proteomes* 2019, 7, 25, doi: 10.3390/proteomes7020025
56. Henderson, C.A.; Gomez, C.G.; Novak, S.M.; Mi-Mi, L.; Gregorio, C.C. Overview of the Muscle Cytoskeleton. *Compr. Physiol.* 2017, 7, 891-944, doi: 10.1002/cphy.c160033
57. Rossi, A.C.; Mammucari, C.; Argentini, C.; Reggiani, C.; Schiaffino, S. Two novel/ancient myosins in mammalian skeletal muscles: MYH14/7b and MYH15 are expressed in extraocular muscles and muscle spindles. *J. Physiol.* 2010, 588, 353-364, doi: 10.1113/jphysiol.2009.181008
58. Lee, L.A.; Karabina, A.; Broadwell, L.J.; Leinwand, L.A. The ancient sarcomeric myosins found in specialized muscles. *Skelet. Muscle* 2019, 9, 7, doi: 10.1186/s13395-019-0192-3
59. Sitbon, Y.H.; Yadav, S.; Kazmierczak, K.; Szczesna-Cordary, D. Insights into myosin regulatory and essential light chains: a focus on their roles in cardiac and skeletal muscle function, development and disease. *J. Muscle Res. Cell. Motil.* 2020, 41, 313-327, doi: 10.1007/s10974-019-09517-x
60. Leber, Y.; Ruparelia, A.A.; Kirfel, G.; van der Ven, P.F.; Hoffmann, B.; Merkel, R.; Bryson-Richardson, R.J.; Fürst, D.O. Filamin C is a highly dynamic protein associated with fast repair of myofibrillar microdamage. *Hum. Mol. Genet.* 2016, 25, 2776-2788, doi: 10.1093/hmg/ddw135
61. Hu, L.Y.; Ackermann, M.A.; Kontrogianni-Konstantopoulos, A. The sarcomeric M-region: a molecular command center for diverse cellular processes. *Biomed. Res. Int.* 2015, 2015, 714197, doi: 10.1155/2015/714197
62. Briggs, M.M.; Schachat, F. The superfast extraocular myosin (MYH13) is localized to the innervation zone in both the global and orbital layers of rabbit extraocular muscle. *J. Exp. Biol.* 2002, 205, 3133-3142. PMID: 12235193
63. Squire, J. Special Issue: The Actin-Myosin Interaction in Muscle: Background and Overview. *Int. J. Mol. Sci.* 2019, 20, 5715.
64. Banks, G.B.; Combs, A.C.; Chamberlain, J.S. Sequencing protocols to genotype mdx, mdx(4cv), and mdx(5cv) mice. *Muscle Nerve* 2010, 42, 268-270, doi: 10.1002/mus.21700
65. Bengtsson, N.E.; Hall, J.K.; Odom, G.L.; Phelps, M.P.; Andrus, C.R.; Hawkins, R.D.; Hauschka, S.D.; Chamberlain, J.R.; Chamberlain, J.S. Muscle-specific CRISPR/Cas9

- dystrophin gene editing ameliorates pathophysiology in a mouse model for Duchenne muscular dystrophy. *Nat. Commun.* 2017, 8, 14454, doi: 10.1038/ncomms14454
66. Tichy, E.D.; Mourkioti, F. A new method of genotyping MDX4CV mice by PCR-RFLP analysis. *Muscle Nerve* 2017, 56, 522-524, doi: 10.1002/mus.25566
67. Holland, A.; Dowling, P.; Meleady, P.; Henry, M.; Zweyer, M.; Mundegar, R.R.; Swandulla, D.; Ohlendieck, K. Label-free mass spectrometric analysis of the mdx-4cv diaphragm identifies the matricellular protein periostin as a potential factor involved in dystrophinopathy-related fibrosis. *Proteomics* 2015, 15, 2318-2331, doi: 10.1002/pmic.201400471.
68. Murphy, S.; Dowling, P.; Zweyer, M.; Mundegar, R.R.; Henry, M.; Meleady, P.; Swandulla, D.; Ohlendieck, K. Proteomic analysis of dystrophin deficiency and associated changes in the aged mdx-4cv heart model of dystrophinopathy-related cardiomyopathy. *J. Proteomics* 2016, 145, 24-36, doi: 10.1016/j.jprot.2016.03.011
69. Murphy, S.; Zweyer, M.; Henry, M.; Meleady, P.; Mundegar, R.R.; Swandulla, D.; Ohlendieck, K. Label-free mass spectrometric analysis reveals complex changes in the brain proteome from the mdx-4cv mouse model of Duchenne muscular dystrophy. *Clin. Proteomics* 2015, 12, 27, doi: 10.1186/s12014-015-9099-0
70. Murphy, S.; Zweyer, M.; Henry, M.; Meleady, P.; Mundegar, R.R.; Swandulla, D.; Ohlendieck, K. Proteomic profiling of liver tissue from the mdx-4cv mouse model of Duchenne muscular dystrophy. *Clin. Proteomics* 2018, 15, 34, doi: 10.1186/s12014-018-9212-2
71. Murphy, S.; Dowling, P.; Zweyer, M.; Henry, M.; Meleady, P.; Mundegar, R.R.; Swandulla, D.; Ohlendieck, K. Proteomic profiling of mdx-4cv serum reveals highly elevated levels of the inflammation-induced plasma marker haptoglobin in muscular dystrophy. *Int. J. Mol. Med.* 2017, 39, 1357-1370, doi: 10.3892/ijmm.2017.2952
72. Murphy, S.; Zweyer, M.; Mundegar, R.R.; Swandulla, D.; Ohlendieck, K. Proteomic identification of elevated saliva kallikrein levels in the mdx-4cv mouse model of Duchenne muscular dystrophy. *Biochem. Biophys. Rep.* 2018, 18, 100541, doi: 10.1016/j.bbrep.2018.05.006
73. Gargan, S.; Dowling, P.; Zweyer, M.; Swandulla, D.; Ohlendieck, K. Identification of marker proteins of muscular dystrophy in the urine proteome from the mdx-4cv model of dystrophinopathy. *Mol. Omics*. 2000, 16, 268-278, doi: 10.1039/c9mo00182d

74. Formicola, L.; Marazzi, G.; Sassoon, D.A. The extraocular muscle stem cell niche is resistant to ageing and disease. *Front. Aging Neurosci.* 2014, 6, 328, doi: 10.3389/fnagi.2014.00328
75. Zeiger, U.; Mitchell, C.H.; Khurana, T.S. Superior calcium homeostasis of extraocular muscles. *Exp. Eye Res.* 2010, 91, 613-622. doi: 10.1016/j.exer.2010.07.019
76. Dowling, P.; Culligan, K.; Ohlendieck, K. Distal mdx muscle groups exhibiting up-regulation of utrophin and rescue of dystrophin-associated glycoproteins exemplify a protected phenotype in muscular dystrophy. *Naturwissenschaften* 2002, 89, 75-78, doi: 10.1007/s00114-001-0289-4
77. Dowling, P.; Lohan, J.; Ohlendieck, K. Comparative analysis of Dp427-deficient mdx tissues shows that the milder dystrophic phenotype of extraocular and toe muscle fibres is associated with a persistent expression of beta-dystroglycan. *Eur. J. Cell Biol.* 2003, 82, 222-230, doi: 10.1078/0171-9335-00315
78. Pertille, A.; de Carvalho, C.L; Matsumura, C.Y.; Neto, H.S.; Marques, M.J. Calcium-binding proteins in skeletal muscles of the mdx mice: potential role in the pathogenesis of Duchenne muscular dystrophy. *Int. J. Exp. Pathol.* 2010, 91, 63-71, doi: 10.1111/j.1365-2613.2009.00688.x
79. McDonald, A.A.; Kunz, M.D.; McLoon, L.K. Dystrophic changes in extraocular muscles after gamma irradiation in mdx:utrophin(+/-) mice. *PLoS One.* 2014, 9, e86424, doi: 10.1371/journal.pone.0086424
80. McDonald, A.A.; Hebert, S.L.; McLoon, L.K. Sparing of the extraocular muscles in mdx mice with absent or reduced utrophin expression: A life span analysis. *Neuromuscul. Disord.* 2015, 25, 873-887, doi: 10.1016/j.nmd.2015.09.001
81. Ohlendieck, K. Proteomics of skeletal muscle glycolysis. *Biochim. Biophys. Acta* 2010, 1804, 2089-2101. doi: 10.1016/j.bbapap.2010.08.001
82. Brinkmeier, H.; Ohlendieck, K. Chaperoning heat shock proteins: proteomic analysis and relevance for normal and dystrophin-deficient muscle. *Proteomics Clin. Appl.* 2014, 8, 875-895, doi: 10.1002/prca.201400015
83. Doran, P.; Martin, G.; Dowling, P.; Jockusch, H.; Ohlendieck, K. Proteome analysis of the dystrophin-deficient MDX diaphragm reveals a drastic increase in the heat shock protein  $\alpha$ HSP. *Proteomics* 2006, 6, 4610-4621, doi: 10.1002/pmic.200600082
84. van Westering, T.L.E.; Johansson, H.J.; Hanson, B.; Coenen-Stass, A.M.L.; Lomonosova, Y.; Tanihata, J.; Motohashi, N.; Yokota, T.; Takeda, S.; Lehtiö, J.; Wood, M.J.A.; El Andaloussi, S.; Aoki, Y.; Roberts, T.C. Mutation-independent Proteomic

- Signatures of Pathological Progression in Murine Models of Duchenne Muscular Dystrophy. *Mol. Cell. Proteomics* 2020, 19, 2047-2068, doi: 10.1074/mcp.RA120.002345
85. Van Pelt, D.W.; Kharaz, Y.A.; Sarver, D.C.; Eckhardt, L.R.; Dzierzawski, J.T.; Disser, N.P.; Piacentini, A.N.; Comerford, E.; McDonagh, B.; Mendias, C.L. Multiomics analysis of the mdx/mTR mouse model of Duchenne muscular dystrophy. *Connect. Tissue Res.* 2021, 62, 24-39, doi: 10.1080/03008207.2020.1791103
86. Capitanio, D.; Moriggi, M.; Torretta, E.; Barbacini, P.; De Palma, S.; Viganò, A.; Lochmüller, H.; Muntoni, F.; Ferlini, A.; Mora, M.; Gelfi, C. Comparative proteomic analyses of Duchenne muscular dystrophy and Becker muscular dystrophy muscles: changes contributing to preserve muscle function in Becker muscular dystrophy patients. *J. Cachexia Sarcopenia Muscle* 2020, 11, 547-563, doi: 10.1002/jcsm.12527
87. Porter, J.D.; Merriam, A.P.; Khanna, S.; Andrade, F.H.; Richmonds, C.R.; Leahy, P.; Cheng, G.; Karathanasis, P.; Zhou, X.; Kusner, L.L.; Adams, M.E.; Willem, M.; Mayer, U.; Kaminski, H.J. Constitutive properties, not molecular adaptations, mediate extraocular muscle sparing in dystrophic mdx mice. *FASEB J.* 2003, 17, 893-895, doi: 10.1096/fj.02-0810fje

**Identification of marker proteins of muscular dystrophy in the urine proteome from the *mdx-4cv* model of dystrophinopathy**

Published on 1 June 2020

Gargan, S., Dowling, P., Zweyer, M., Swandulla, D., & Ohlendieck, K. (2020). Identification of marker proteins of muscular dystrophy in the urine proteome from the *mdx-4cv* model of dystrophinopathy. *Molecular omics*, *16*(3), 268–278.

<https://doi.org/10.1039/c9mo00182d>.

**Abstract**

Since the protein constituents of urine present a dynamic proteome that can reflect a variety of disease-related alterations in the body, the mass spectrometric survey of proteome-wide changes in urine promises new insights into pathogenic mechanisms. Urine can be investigated in a completely non-invasive way and provides valuable biomedical information on body-wide changes. In this report, we have focused on the urine proteome in X-linked muscular dystrophy using the established *mdx-4cv* mouse model of dystrophinopathy. In order to avoid potential artefacts due to the manipulation of the biofluid proteome prior to mass spectrometry, crude urine specimens were analyzed without the prior usage of centrifugation steps or concentration procedures. Comparative proteomics revealed 21 increased and 8 decreased proteins out of 870 identified urinary proteoforms using 50µl of biofluid per investigated sample, i.e. 14 wild type versus 14 *mdx-4cv* specimens. Promising marker proteins that were almost exclusively found in *mdx-4cv* urine included nidogen, parvalbumin and titin. Interestingly, the mass spectrometric identification of urine-associated titin revealed a wide spread of peptides over the sequence of this giant muscle protein. The newly established urinomic signature of dystrophinopathy might be helpful for the design of non-invasive assays to improve diagnosis, prognosis, therapy-monitoring and evaluation of potential harmful side effects of novel treatments in the field of muscular dystrophy research.

**Keywords:** Duchenne; Nidogen; Parvalbumin; Proteomics; Titin; Urine

## 1. Introduction

Measuring temporal changes in the protein composition of body fluids can be helpful for the systematic assessment and monitoring of body-wide effects due to physiological adaptations or pathological alterations. Biofluids present therefore an excellent starting point for the pathoproteomic analysis of disease processes, as long as the passive shedding or active secretion of tissue-associated proteins into the circulatory system can be measured by distinct variations in select protein species. In this respect, the increased usage of quantitative body fluid proteomics has greatly improved the scope of the bioanalytical analysis of protein release due to cellular damage.<sup>1</sup> Besides serum and plasma samples, urine is one of the most frequently employed body fluids for the purpose of clinical diagnosis.<sup>2</sup> The advantage of using urine as a source of clinical marker molecules is the fact that this abundant biofluid can be obtained non-invasively and be sampled in a continuous way. The majority of urinary proteins originate from plasma components that pass through the glomerular filtration barrier, as well as liberated proteins from the kidney and urinary tract.<sup>3-5</sup>

Thus, in the absence of primary urological disease, the marked increase in distinct types of cellular proteins (that usually only exist in extremely low concentration in urine) presents an excellent way to identify novel proteomic biomarker candidates of body-wide tissue degeneration.<sup>6</sup> This is the reason why the protein composition of urine is an appropriate mirror of general health status and advanced urine protein analysis has an excellent potential to develop into an even more important diagnostic tool in modern medicine.<sup>7</sup> In the future, the optimum integration of highly sensitive and urine-based liquid biopsy techniques will ideally eliminate the need for invasive and potentially harmful tissue biopsy procedures or expensive imaging approaches in routine diagnostic, prognostic and therapy-monitoring methodologies.<sup>8</sup> Mass spectrometry-based proteomics has been instrumental for the establishment of the normal urinary proteome using a variety of protein separation and detection methods.<sup>9-12</sup> Several thousand urine-associated proteoforms have been cataloged.<sup>10</sup> The most abundant urinary proteins encompass 20 protein species, including the MUP class of major urinary proteins, albumin, serum enzymes and uromodulin. Approximately 200 proteins represent 95% of the urine proteome.<sup>13</sup> It therefore requires sophisticated mass spectrometric techniques to cover the considerable number of urine proteins with lower abundance.<sup>14,15</sup> In human urinomics,

physiological parameters, gender and age are important parameters that have to be taken into account for the establishment of urinary protein signatures of diseases.<sup>13,16,17</sup>

In the field of muscular dystrophy research<sup>18</sup>, there is an urgent drive to identify novel biofluid markers for establishing improved diagnostic and therapy-monitoring approaches.<sup>19-21</sup> Duchenne muscular dystrophy, the most frequently inherited muscle wasting disease of early childhood<sup>22</sup>, is characterized by fibre necrosis, reactive myofibrosis and sterile inflammation in the skeletal musculature.<sup>23-25</sup> In addition to primary muscle weakness, dystrophinopathy is complicated by late-onset cardiomyopathy, respiratory impairments, neurological deficiencies, scoliosis and metabolic disturbances.<sup>26-28</sup> The genetic disorder is due to primary abnormalities in the extremely large *Dmd* gene, which encodes several isoforms of the protein dystrophin.<sup>29</sup> The full-length isoform of dystrophin, Dp427-M, functions in contractile fibres as a membrane cytoskeletal component and forms a supramolecular assembly with a variety of sarcolemma-associated proteins.<sup>30</sup> The dystrophin core complex, consisting of Dp427-M, dystroglycans, sarcoglycans, dystrobrevins, syntrophins and sarcospan, links the extracellular matrix component laminin to the intracellular actin cytoskeleton.<sup>31</sup> This trans-plasmalemmal structure plays a key role in lateral force transmission and the stabilization of the fibre surface during excitation-contraction-relaxation cycles.<sup>32</sup> In dystrophinopathy, the almost complete loss of Dp427-M causes a drastic reduction in the members of the dystrophin-associated glycoprotein complex<sup>33,34</sup>, which in turn triggers sarcolemmal micro-rupturing and calcium-induced proteolytic degradation.<sup>35</sup>

The proteomic screening of urine samples from dystrophic patients revealed the presence of N- and C-terminal fragments of the giant muscle protein titin.<sup>36</sup> Since X-linked muscular dystrophy is due to primary abnormalities in the membrane cytoskeletal protein dystrophin, changes in the sarcomeric protein titin might be linked to down-stream effects of the collapse of the dystrophin-glycoprotein complex.<sup>30</sup> The drastic elevation of urinary titin fragments was confirmed by immunoassays<sup>37-39</sup> and suggests that these protein species have a high potential as novel diagnostic markers and non-invasive screening tools.<sup>21,40,41</sup> Building on these findings, it was of interest to carry out a comprehensive proteomic comparison of urine and evaluate the body-wide effects of the dystrophic phenotype. In this report, we have used the established genetic *mdx-4cv* model of Duchenne muscular dystrophy<sup>42-44</sup>, which allows detailed comparisons of changes in the urine proteome due to primary or secondary pathological alterations in the dystrophic phenotype.<sup>45-47</sup>

## 2. Results and discussion

In order to improve our understanding of the molecular pathogenesis of dystrophinopathy and to identify novel protein candidates for the establishment of a proteomic biofluid signature of X-linked muscular dystrophy<sup>19-21</sup>, this study has focused on the mass spectrometric survey of the urine proteome from the dystrophic *mdx-4cv* mouse.

### Dystrophin deficiency in the *mdx-4cv* model of dystrophinopathy

Prior to the proteomic profiling of urine samples, the mutant status of *mdx-4cv* skeletal muscle fibres was confirmed by immunofluorescence microscopy. As shown in Figure 1, immunolabelling with an antibody to full-length dystrophin isoform Dp427-M demonstrated sarcolemmal localization in normal diaphragm and an almost complete absence of this membrane cytoskeletal protein in the dystrophic *mdx-4cv* diaphragm.

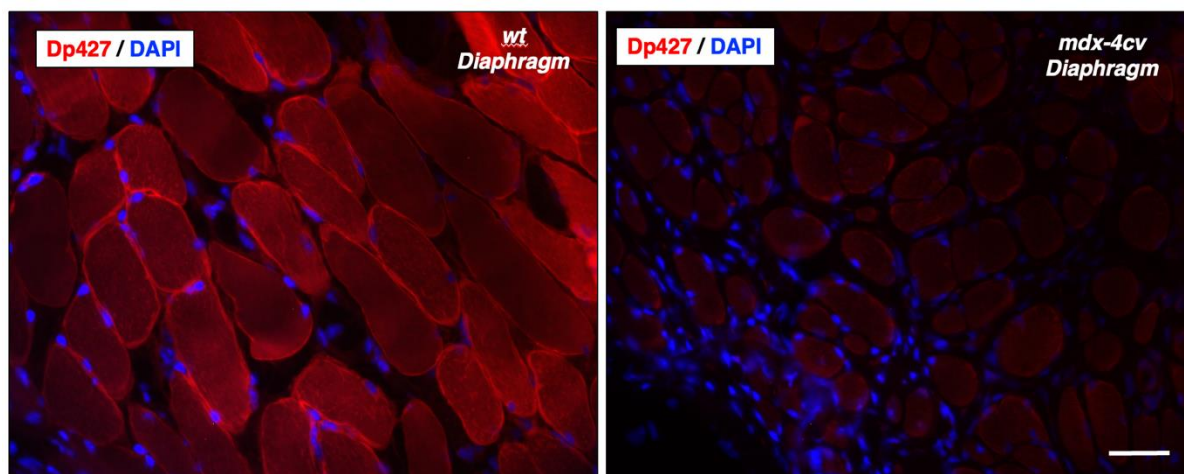


**Figure 1.** Immunofluorescence microscopical characterization of the dystrophic diaphragm from the *mdx-4cv* mouse model of dystrophinopathy. Shown are transverse cryo-sections of wild type (*wt*) versus dystrophic *mdx-4cv* diaphragm muscle labelled with an antibody to the Dp427-M isoform of the membrane cytoskeletal dystrophin. Nuclei were counter-stained with the blue-fluorescent DNA dye 4',6-diamidino-2-phenylindole (DAPI). The *mdx-4cv* muscle fibres are almost completely deficient of dystrophin at the sarcolemma. Bar equals 50µm.

### Proteomic profiling of urine

Urine contains a complex mixture of proteoforms over a wide dynamic concentration range.<sup>5,9-</sup>

<sup>11</sup> In order to avoid the potential introduction of bioanalytical artefacts due to differential

centrifugation procedures or extensive protein concentration steps, which are often used in urinomic investigations<sup>36</sup>, in this study neat urine specimens were analysed without any manipulation prior to mass spectrometry. The proteomic survey of wild type and *mdx-4cv* mouse urine samples identified 1010 and 870 protein species, respectively. Detailed information on proteomic multi-consensus data (4 files) and the raw data (28 files) of all identified urine proteins is available through the public repository Open Science Framework under the project title ‘Proteomic profiling of mouse urine’ (data identification number: 7dyqc; direct URL to data: <https://osf.io/7dyqc/>). The most abundant proteins in mouse urine that were mass spectrometrically identified in this study are listed in supplementary Table S1, including isoforms of major urinary protein, alpha-1-antitrypsin and alpha-amylase, as well as albumin, kallikrein, haptoglobin, serotransferrin, uromodulin and complement C3.

**Supplementary Table S1:** Mass spectrometric identification of abundant proteins in mouse urine.

Accession	Protein name	Gene	Coverage %	Unique Peptides	Peptides	Molecular mass (kDa)
P11588	Major urinary protein 1	Mup1	82.22	6	30	20.6
P11589	Major urinary protein 2	Mup2	79.44	3	28	20.7
P04939	Major urinary protein 3	Mup3	72.28	14	22	21.5
P11590	Major urinary protein 4	Mup4	58.43	8	12	20.5
P11591	Major urinary protein 5	Mup5	67.78	12	15	20.9
B5X0G2	Major urinary protein 17	Mup17	82.22	6	25	20.6
Q5FW60	Major urinary protein 20	Mup20	80.11	16	22	20.9
P07758	Alpha-1-antitrypsin 1-1	Serpina1a	51.33	6	18	46.0
P22599	Alpha-1-antitrypsin 1-2	Serpina1b	53.51	6	20	45.9
Q00897	Alpha-1-antitrypsin 1-4	Serpina1d	61.50	8	22	46.0
Q00898	Alpha-1-antitrypsin 1-5	Serpina1e	37.29	7	16	45.9
P07724	Serum albumin	Alb	57.40	33	33	68.6
P00687	Alpha-amylase 1	Amy1	41.29	12	17	57.6
P00688	Alpha-amylase 2	Amy2	53.15	15	20	57.3
P15947	Kallikrein-1	Klk1	49.81	6	12	28.8

Q61646	Haptoglobin	Hp	37.18	16	16	38.7
Q921I1	Serotransferrin	Tf	31.13	23	23	76.7
Q91X17	Uromodulin	Umod	26.64	13	13	70.8
P01027	Complement C3	C3	11.12	14	14	186.4

The proteomic fingerprint of abundant urine-associated proteins is provided in supplementary Figure S1, including the major urinary protein isoforms MUP1 to MUP20, isoforms of alpha-1-antitrypsin, alpha-amylase, haptoglobin and kallikrein.<sup>10-13</sup> The bioinformatic PANTHER analysis of protein families that were identified in mouse urine using mass spectrometry are presented in form of a pie chart in Figure 2. This included a considerable number of cellular proteins, transporters, receptors, structural components, signalling proteins and various classes of enzymes, such as hydrolases, isomerases and oxidoreductases. The STRING-based interaction map of identified urine proteins is provided in supplementary Figure S2.

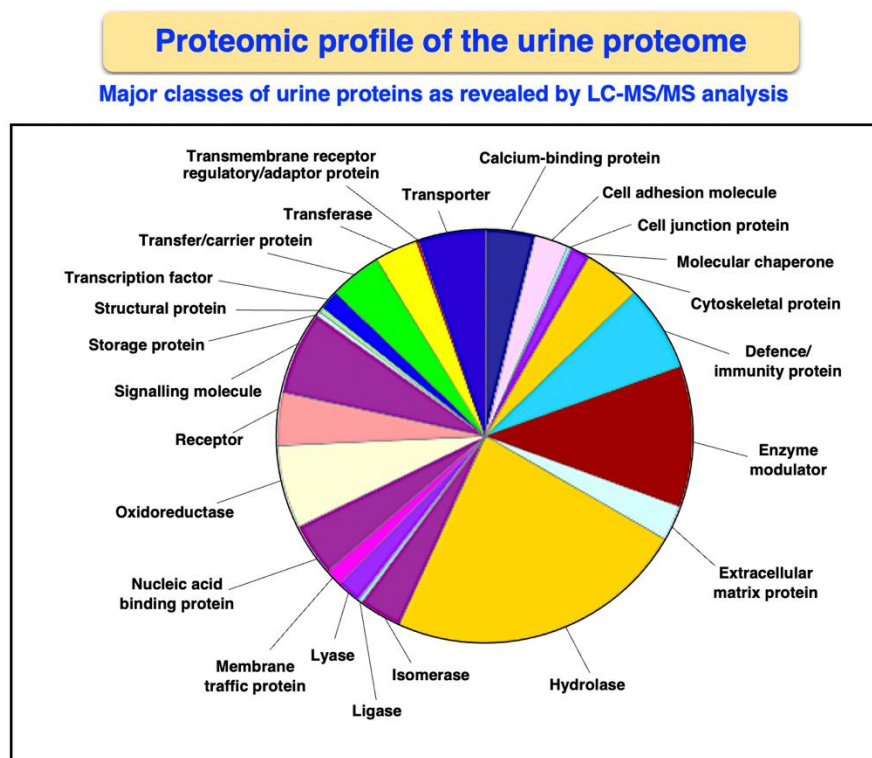
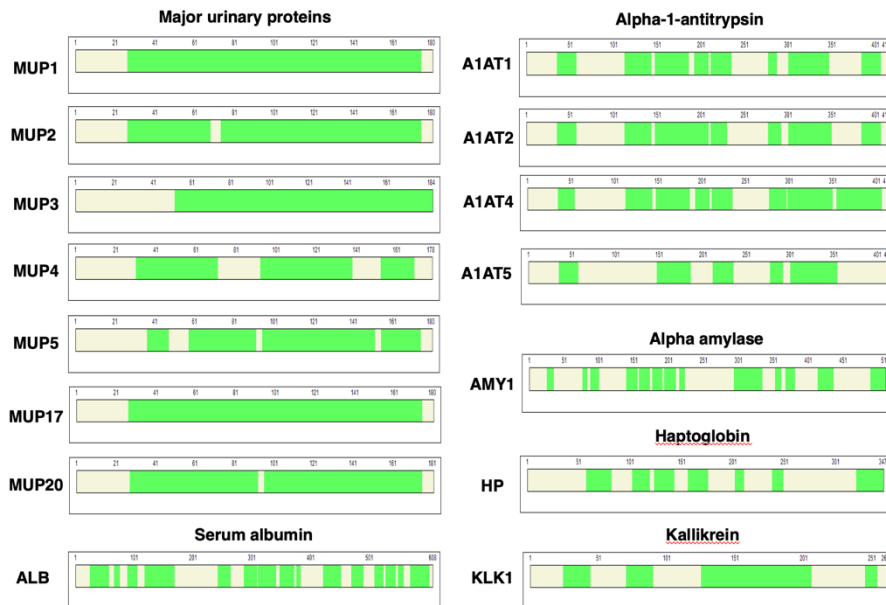
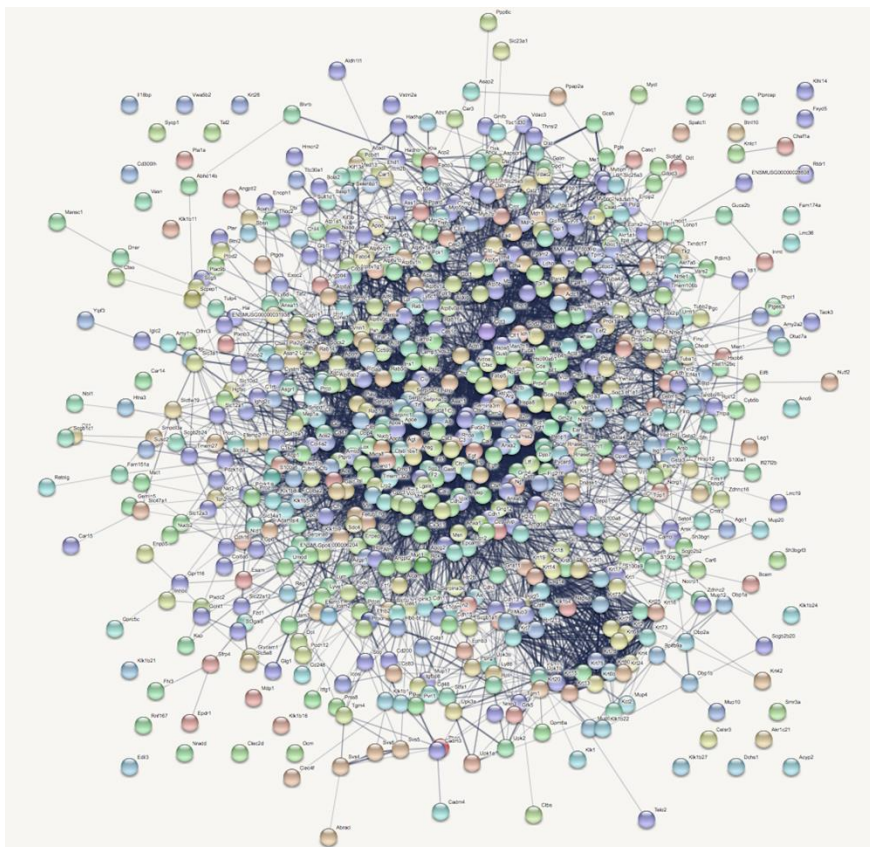


**Figure 2.** Distribution of protein classes within the mouse urine proteome as determined by mass spectrometry-based proteomics and bioinformatic PANTHER analysis.



**Supplementary Figure S1.** Proteomic fingerprints of abundant urine-associated proteins. The green bars represent peptide sequences that were identified by the proteomic analysis of urine from the *mdx-4cv* mouse model of dystrophinopathy.



**Supplementary Figure S2.** Bioinformatic STRING analysis of mass spectrometrically identified components of the mouse urine proteome.

### **Comparative proteomic profiling of urine from the *mdx-4cv* mouse model of dystrophinopathy**

The comparative mass spectrometric profiling of *mdx-4cv* urine revealed 21 increased proteins (Table 1) and 8 decreased protein species (Table 2), whereby the extent of protein elevation was drastically higher as compared to the degree of a lowered abundance in specific proteins. The heat map of the urinomic analysis is provided in Figure 3 and illustrates the differential expression pattern of changed proteins in wild type versus the dystrophic phenotype. There exists a slight discrepancy between the number of proteins featured in the heat map, and those listed in the tables below. This error was due to the usage of different cutoffs of abundance changes. Increased levels of the giant muscle protein titin in *mdx-4cv* urine, as previously reported in dystrophic patients and the conventional *mdx-23* mouse<sup>36-41</sup>, were clearly confirmed (Table 2).

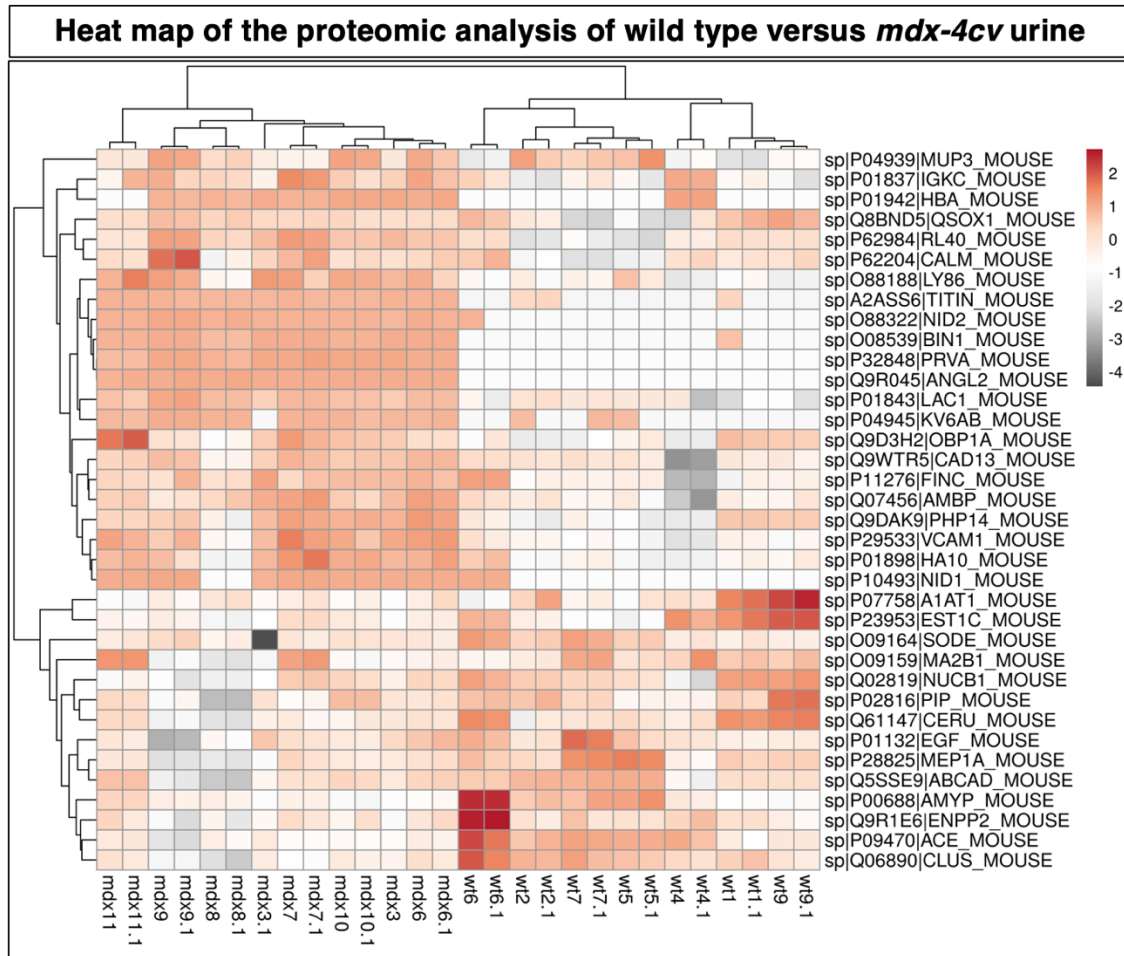


**Figure 3:** Heat map of the urinomic analysis of changed proteins in wild type versus the *mdx-4cv* mouse model of dystrophinopathy. The comparative proteomic survey was carried out with 28 urine samples from *mdx-4cv* (n=7 biological repeats; n=2 technical repeats) versus wild type (n=7 biological repeats; n=2 technical repeats) mice.

**Table 1: Proteomic identification of increased proteins in urine from the *mdx-4cv* mouse model of Duchenne muscular dystrophy.** The comparative proteomic survey was carried out with 28 urine samples from *mdx-4cv* (n=7 biological repeats; n=2 technical repeats) versus wild type (n=7 biological repeats; n=2 technical repeats) mice.

Accession	Protein name	Gene	Coverage %	Unique peptides	ANOVA (p)	Fold change
-----------	--------------	------	---------------	--------------------	--------------	----------------

A2ASS6	Titin	TTN	2.6	65	-	Detected only in <i>mdx</i>
O08539	Myc box-dependent-interacting protein 1	BIN1	17.7	6	-	Detected only in <i>mdx</i>
O88322	Nidogen-2	NID2	8.4	7	-	Detected only in <i>mdx</i>
P01942	Haemoglobin subunit alpha	HBA	36.6	5	-	Detected only in <i>mdx</i>
P04945	Ig kappa chain V-VI region	KV6AB	14.8	1	-	Detected only in <i>mdx</i>
P10493	Nidogen-1	NID1	10.3	10	-	Detected only in <i>mdx</i>
P32848	Parvalbumin alpha	PVALB	73.6	14	-	Detected only in <i>mdx</i>
Q9R045	Angiopoietin-related protein 2	ANGPTL2	18.3	10	-	Detected only in <i>mdx</i>
Q9DAK9	14 kDa phosphohistidine phosphatase	PHP14	45.9	6	0.000417	16.1
Q9D3H2	Odorant-binding protein 1a	OBP1A	49.7	8	0.002973	5.8
P62984	Ubiquitin-60S ribosomal protein L40	UBA52	43.0	9	3.21E-05	4.4
P01843	Ig lambda-1 chain C region	LAC1	61.9	4	4.59E-07	4.3
P01864	Ig gamma-2A chain C region	GCAB	17.3	5	0.040519	4.1
P29533	Vascular cell adhesion protein 1	VCAM1	33.3	2	4.81E-07	2.6
O88188	Lymphocyte antigen 86	LY86	33.3	4	1.26E-06	2.4
Q9WTR5	Cadherin-13	CDH13	26.2	12	0.005748	2.2

P01837	Immunoglobulin kappa constant	IGKC	38.7	6	0.001230	2.1
P01898	H-2 class I histocompatibility antigen, Q10 alpha chain	H2-Q10	43.4	10	0.000233	2.1
P11276	Fibronectin	FN1	17.8	27	0.000837	1.7
Q07456	Protein AMBP	AMBP	41.3	15	0.000129	1.7
P04939	Major urinary protein 3	MUP3	72.3	14	0.039672	1.6

Table 2: **Proteomic identification of decreased proteins in urine from the *mdx-4cv* mouse model of Duchenne muscular dystrophy.** The comparative proteomic survey was carried out with 28 urine samples from *mdx-4cv* (n=7 biological repeats; n=2 technical repeats) versus wild type (n=7 biological repeats; n=2 technical repeats) mice.

Accession	Protein name	Gene	Coverage %	Unique peptides	ANOVA (p)	Fold change
Q02819	Nucleobindin-1	NUCB1	46.84	17	0.018151	2.9
P23953	Carboxylesterase 1C	CES1C	31.59	12	0.011188	2.2
P09470	Angiotensin-converting enzyme	ACE	19.66	19	1.61E-05	2.1
O09159	Lysosomal alpha-mannosidase	MAN2B1	16.29	14	0.037992	2.1
Q5SSE9	ATP-binding cassette sub-family A member 13	ABCA13	11.25	33	0.042472	1.7
Q61147	Ceruloplasmin	CP	21.77	15	0.002404	1.7
Q06890	Clusterin	CLU	33.48	18	1.36E-05	1.7
P00688	Pancreatic alpha-amylase	AMY2	53.15	15	0.007610	1.6

The proteomic screening study by Rouillon et al<sup>36</sup>, which was carried out with urine samples from 5 Duchenne patients and 5 healthy subjects, lists 8 increased proteins (titin, uromodulin, nuclear transport factor NTF2, TNF receptor, myosin-1, fibulin-2, complement C1r, aminopeptidase) and 2 decreased proteins (cubulin, beta-galactosidase). Proteins in the study presented here were identified by a considerably higher number of unique peptides, especially in the case of titin. As shown in the diagrammatic presentation of the proteomic fingerprints of a select number of elevated proteins in *mdx-4cv* urine (supplementary Figure S3; Figure 4a), the mass spectrometric analysis of urine-associated titin revealed a widespread presence of 65 unique peptides over the entire sequence of this giant muscle protein (supplementary Figure S4). Immunoblotting confirmed the drastic increase of titin fragments in *mdx-4cv* urine as shown in Figure 4c-e. Titin is one of the most abundant sarcomeric muscle proteins and despite its extremely large size is routinely identified by a sequence coverage of above 50% in crude muscle extracts (Figure 4b) using proteomics.<sup>48</sup> Increased titin levels in *mdx-4cv* urine correlate well with the previous proteomic identification of a higher concentration of titin in *mdx-4cv* and *mdx-23* serum.<sup>19,49</sup>

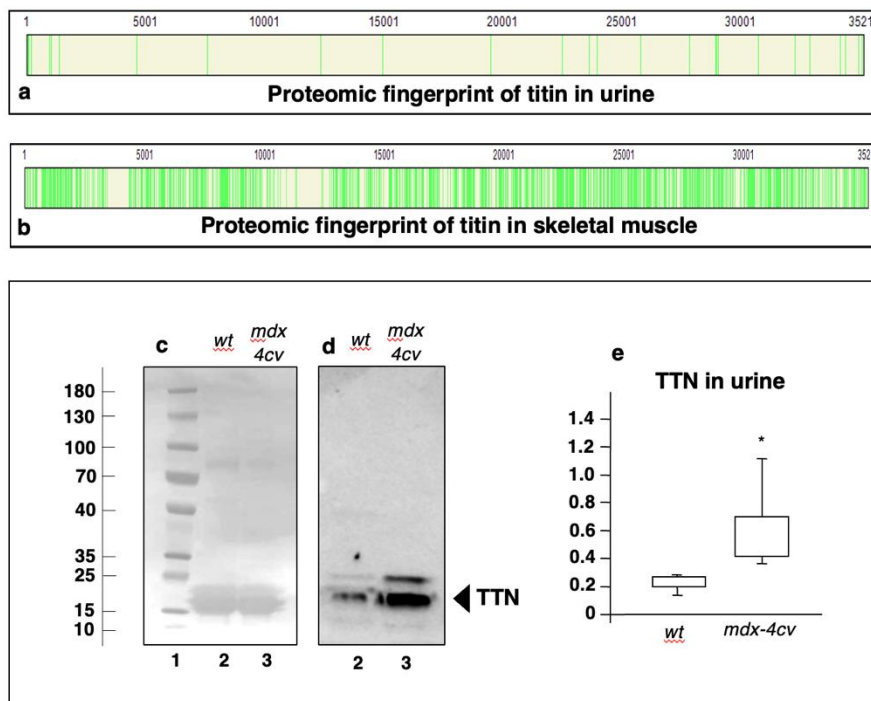
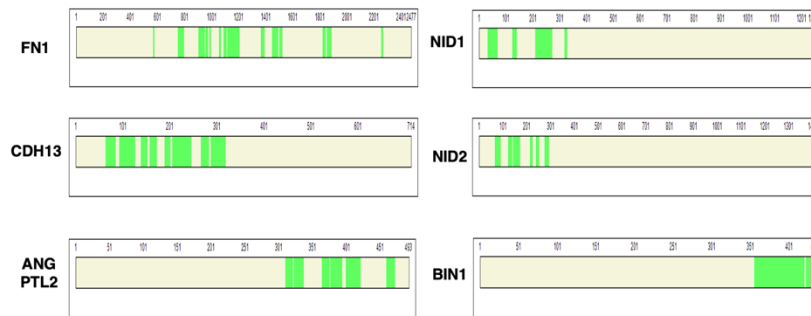


**Figure 4.** Proteomic fingerprint and immunoblot analysis of titin in urine from wild type versus dystrophic mice. Shown are the proteomic fingerprints of the giant protein species titin (TTN) in urine (a) versus skeletal muscle (b). The green bars represent peptide sequences that were

identified by mass spectrometry-based proteomics. In the lower panels are shown protein blots of wild type versus *mdx-4cv* urine samples stained with Ponceau Red (c) and an immunoblot labelled with an antibody to titin (d). Lanes 1-3 contain molecular mass standards, wild type urine and *mdx-4cv* urine, respectively. In panel (e) is shown the statistical analysis of titin immunoblotting (Mann-Whitney U test;  $p=0.01208$ ;  $n=5$ ). The value of molecular mass standards ( $\times 10^{-3}$  kDa) is marked on the left side of the blots.



**Supplementary Figure S3:** Proteomic fingerprints of urine proteins with an increased abundance in the *mdx-4cv* mouse model of dystrophinopathy. The green bars represent peptide sequences that were identified by the proteomic analysis of urine.

## Proteomic fingerprint of titin

TTN Residues	Sequence
42-62	DGQVISTSLPGVQISFSDGR
65-72	LMIPAVTK
82-116	ATNGSQATSTAELLVTAETAPPNFSQR
110-116	LQSMTVR
127-136	VTGIPTPVVK
185-202	ATSTAEVVQGEEVPPAK
185-203	ATSTAEVVQGEEVPPAKK
935-953	VPAPAEVPTPPTLVSLGK
954-976	NVTVIEGESVTLCHISGYSPK
958-969	DNDAIFEIDIK
1016-1050	FTCSAVNEAGTVSTSCYLAVQVSEEFDKETTLTEK
1120-1129	SGVPLTTGYR
1172-1184	NKHGETSASASLLEEADYEALVK
1174-1184	HGETSASASLLEEADYEALVK
1240-1255	TFVEDQEFHISFEER
1353-1372	IPVVLPEDEGIYAFASNIK
2090-2104	IQSQTVGGQSDAHFR
4630-4644	KVDPSYMLPGESAR
4673-4689	MSFVNSEAILDITDK
7099-7121	DGVLLRDDENLQMSFVDNVATLK
7105-7121	DDENLQMSFVDNVATLK
7601-7610	GLYTFEVENR
9628-9637	LTVIEPAWER
12356-12367	VTEPPKKPVPEK
14959-14974	VGTGEPVETDSPVEAR
19500-19527	FSPPSPGKPVVTDITENAATVSWTLPK
19553-19565	VTGLYEGNTYEFR
22508-22520	ITQFVVDLQTK
23602-23617	ATSYTITSLIENQEQYK
23620-23639	IYAMNSEGLGEPALVPGTPK
23644-23656	MLPPEIELDADLR
23852-23868	NSVSLSWEKPEHDGGSR
23983-23997	VNAESTENNSLLTIK
24702-27411	LLEKHEYNFR
25750-25765	ADEEEWQIVTPQTGLR
25790-25807	VGLGEAASVPGTVKPEDK
25790-25820	VGLGEAASVPGTVKPEDKLEAPELDLSELR
27866-27880	AEDPVFLSPSPKPK
27921-27927	VAIQSFR
28949-28961	AADPIDPPGPPAK
28970-28994	SSITLGSKPVYDGGSDVTGYVEMK
28995-2908	QGDEEEWTVSTR
29074-29085	AGEDVQLLIPFK
30759-30766	VVGYIIR
31188-31197	NNEFTVPDLK
32250-32259	EILGYWVEYR
32294-32306	VFAENETGLSRPR
32316-32325	LTSGEAPGVR
32902-32915	TVELDVADVPDPPR
32925-32941	DSVNLWTPEASDGGSK
32942-32949	VTNYIVEK
32968-32976	YTVINLFGK
33488-33496	TAYVGENVR
34182-34195	FILNVQSKPTAEVK
34209-34234	IHYTNTSGVLTLEILDQCQTEDGGTYR
34369-34385	FSCDTDGEVPTVTWLR
34431-34440	QEAQFTLTQK
34959-34973	NNLPISISSNISVSR
34976-34983	NVYTLDIR
35115-35133	GIPPKIEALPSDISIDEGK
35120-35133	IEALPSDISIDEGK
35134-35157	VLTVACAFTEPTPEITWSCGGR
35134-35158	VLTVACAFTEPTPEITWSCGGRK
35167-35185	FHIENTDDLTLIIMDVQK
35186-35211	QDGGLYTSLGNEFGSDSATVNIIR

urine

Ca<sup>2+</sup>-

direct

## Supplementary

**Figure S4.** Proteomic fingerprint of titin in from the *mdx-4cv* mouse model of dystrophinopathy.

Therefore, the loss of dystrophin and its associated glycoprotein complex appears to destabilize contractile fibres by impairing the trans-sarcolemmal linkage between the intracellular actin cytoskeleton and the extracellular matrix component laminin.<sup>30</sup> induced protein degradation and progressive weakening of the cytoskeletal network appear to have a effect on the structural and

functional integrity of the sarcomeric apparatus and cause the release of titin fragments. In normal muscle, the half-sarcomere spanning titin isoforms with a molecular mass of over 3 MDa were shown to interact with their carboxy-terminus at the M-band and the amino-terminal

region extends this tight molecular coupling to the Z-disk. Titin is intrinsically involved in sarcomeric protein scaffolding and cellular signalling mechanisms. This includes the critical cellular processes of myofibrillar assembly during myogenesis and the functioning as a molecular spring that determines passive stretch within myocytes, as well as critical aspects of signal integration and mechano-sensing as a regulatory node of contractile fibres.<sup>48</sup> These processes appear to be interrupted in X-linked muscular dystrophy due to the deficiency in dystrophin and the accompanying degradation of sarcomeric titin. The subsequent release of titin fragments into circulation is reflected by elevated levels of titin peptides in *mdx-4cv* urine. In addition to titin, promising marker proteins that are possibly linked to muscle degeneration and were shown here to be drastically increased in *mdx-4cv* urine, include parvalbumin, nidogen isoforms NID1 and NID2, the myc box-dependent interacting protein BIN1, angiotensin-related protein 2, cadherin-13 and fibronectin (Table 1, supplementary Figure S3). Parvalbumin was also shown to be elevated in *mdx-23* serum<sup>49</sup> and greatly reduced in various muscle types, including *flexor digitorum brevis*, *interosseous* and the highly fibrotic diaphragm in the *mdx-23* and *mdx-4cv* mouse.<sup>51-53</sup> Hence, the changes in this cytosolic Ca<sup>2+</sup>-binding protein that exists predominantly in mature fast-twitching fibers, might be due to a dystrophin-deficient and leaky sarcolemma membrane. Micro-rupturing of the plasma membrane appears to trigger a substantial release of parvalbumin into the circulation.<sup>49,54</sup> and this might explain the greatly increased presence of this muscle-derived protein in *mdx-4cv* urine. Interestingly, the nidogen isoform NID1, which is a laminin-associated glycoprotein of the basement membrane, was previously shown to be increased in *mdx-23* serum<sup>55</sup> and decreased in *mdx-23* heart.<sup>56</sup> Thus, the elevated concentration of nidogen in *mdx-4cv* urine might be related to shedding of this extracellular protein from fibrotic heart cells in association with dystrophinopathy-related cardiomyopathy. Of note, increased levels of fibronectin were also established in dystrophic and fibrotic *mdx-4cv* diaphragm muscle<sup>57</sup> and serum specimens from Duchenne patients<sup>58</sup>. Reactive myofibrosis might therefore be linked to increased release of fibronectin into the circulatory system and explain its elevated concentration in *mdx-4cv* urine.

Interesting urine-associated proteins with a decreased abundance were identified as the Ca<sup>2+</sup>-binding protein nucleobindin of the Golgi apparatus and carboxylesterase, angiotensin-converting enzyme and lysosomal alpha-mannosidase. Potential protein-protein interaction patterns of identified proteins are illustrated in the bioinformatic STRING analysis of Figure 5. Protein clusters of interest are represented by increases in the titin-parvalbumin hub and the extracellular fibronectin-nidogen axis, as well as decreases in the alpha-1-antitrypsin-

epidermal growth factor-ceruloplasmin hub. The mass spectrometric survey of proteome-wide changes in *mdx-4cv* urine has therefore provided (i) new insights into pathogenic mechanisms of muscular dystrophy, (ii) confirmed the drastically elevated levels of titin and fibronectin in urine from the dystrophic phenotype, and (iii) identified novel potential disease markers in an easily accessible biofluid, including the cytosolic protein parvalbumin and the extracellular matrix component nidogen.

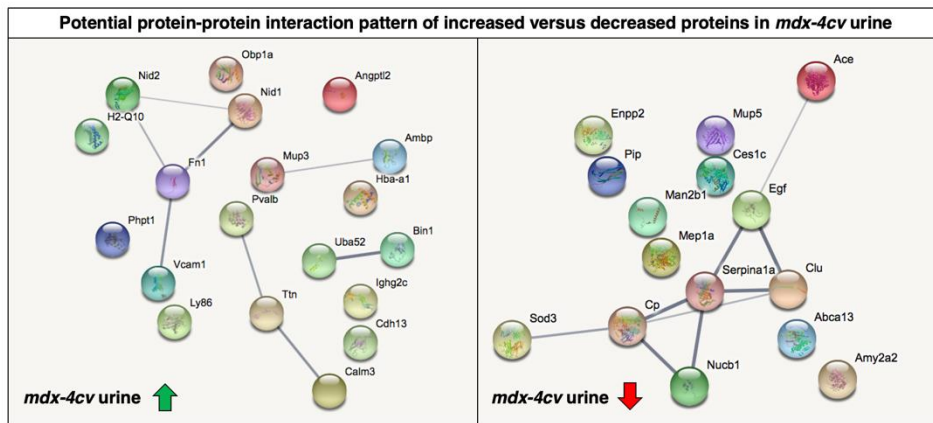


**Figure 5:** Bioinformatic STRING analysis of potential protein-protein interactions of increased versus decreased proteins in urine from the *mdx-4cv* mouse model of dystrophinopathy, as summarized in the heat map of Figure 3.

### The potential of urine as a biofluid for non-invasive and systemic sampling approaches in muscular dystrophy research

Urine is characterized by a complex set of protein constituents with a wide concentration range.<sup>5,10</sup> Dynamic changes in the urine proteome may reflect a variety of physiological adaptations or disease-associated alterations in the body<sup>6-8</sup>, making this abundant biofluid an excellent starting point for detailed omics-type investigations. Proteome-wide changes in urine are an ideal source for a better understanding of the complex molecular and cellular pathogenesis of inherited diseases, such as Duchenne muscular dystrophy.<sup>21</sup> One of the great advantages of urine over invasive tissue biopsy procedures or minimally invasive serum sampling is the fact that this biofluid can be harvested in a completely non-invasive way to provide meaningful biomedical information on body-wide changes in a continuous manner.<sup>11-13</sup> For example, in cases of acute muscle damage that results in rhabdomyolysis<sup>59</sup>, the release of the contents of injured myofibers into the circulatory system is reflected by a marked

elevation of urine myoglobin<sup>60</sup>. In analogy to urine myoglobin as a muscle damage marker for the risk assessment of acute renal failure following rhabdomyolysis, dystrophinopathy-related changes in the urine protein profile established in this report might serve as a useful addition to the biofluid marker signature of X-linked muscular dystrophy.

### **3. Conclusion**

The systematic mass spectrometric survey of the urine proteome from wild type versus dystrophic *mdx-4cv* mice has identified a considerable number of changed protein species. Especially the elevated levels of titin, parvalbumin, nidogen, cadherin and fibronectin present interesting biomarker candidates in association with chronic muscle wasting and reactive myofibrosis. Thus, in the absence of urological pathology, urine sampling presents an ideal source for carrying out non-invasive liquid biopsies as an alternative to highly invasive muscle biopsy procedures. In the long-term, the newly established proteomic signature of urine-associated changes in association with X-linked muscular dystrophy might be helpful for the improved design of simplified assays for diagnostic and prognostic purposes, as well as therapy-monitoring and the continuous evaluation of potential side effects of novel treatments of dystrophinopathy, such as exon skipping, stop codon read-through, viral gene transfer, stem cell/myoblast transfer, utrophin replacement or CRISPR/Cas9 genome editing.<sup>61-64</sup> Since novel treatment protocols, such as gene therapy, are routinely tested in genetic mouse models prior to clinical trials<sup>44</sup>, the findings from our new study on the *mdx-4cv* model should be a helpful addition to the class of non-invasive marker proteins to evaluate new approaches to treat dystrophinopathy. Ideally, combinations of proteomic and metabolomic urine-based biomarkers<sup>65</sup> would be used for the systems biological assessment of the molecular pathogenesis of dystrophinopathy.

### **Acknowledgements**

Research was supported by funding from the Kathleen Lonsdale Institute for Human Health Research at Maynooth University. The Q-Exactive quantitative mass spectrometer was funded under the Research Infrastructure Call 2012 by Science Foundation Ireland (SFI-12/RI/2346/3).

## 4. Materials and methods

### Materials

Materials and general analytical-grade reagents were obtained from GE Healthcare (Little Chalfont, Buckinghamshire, UK), BioRad Laboratories (Hemel-Hempstead, Hertfordshire, UK) and Sigma Chemical Company (Dorset, UK). For the filter-aided sample preparation method FASP, Vivacon 500 (30,000 MWCO, product number: VN0H22) spin filters were acquired from Sartorius (Göttingen, Germany). Sequencing grade-modified trypsin, Lys-C and Protease Max Surfactant Trypsin Enhancer were obtained from Promega (Madison, WI, USA). Protease inhibitors were purchased from Roche Diagnostics (Mannheim, Germany). The Pierce 660nm Protein Assay Reagent was from ThermoFisher Scientific (Dublin, Ireland). For immunofluorescence microscopy and immunoblotting, primary antibodies were obtained from NovoCastra, Leica Biosystems, Newcastle Upon Tyne, UK (NCL-Dys2 to the carboxy terminus of dystrophin isoform Dp427-M) and Sigma Chemical Company, Dorset, UK (mAb T11, T9030 to titin). Chemicon International (Temecula, CA, USA) provided peroxidase-conjugated secondary antibodies. Normal goat serum and goat anti-mouse IgG RRX (Rhodamine Red-X) were purchased from Molecular Probes, Life Technologies (Darmstadt, Germany) and Jackson ImmunoResearch (West Grove, PA, USA), respectively.

### Urine and muscle specimens from the *mdx-4cv* mouse model of dystrophinopathy

The sampling of urine and harvesting of *post-mortem* muscle tissue samples was carried out according to institutional regulations. All mice were handled in strict adherence to local governmental and institutional animal care regulations and were approved by the Institutional Animal Care and Use Committee (Amt für Umwelt, Verbraucherschutz und Lokale Agenda der Stadt Bonn, North Rhine-Westphalia, Germany). Comparative biofluid proteomics was carried out by standardized procedures, as previously described in detail.<sup>49,66</sup> Fresh urine specimens were collected from 12-month old dystrophic *mdx-4cv* mice and age-matched wild type C57BL/6 mice through the Bioresource Unit of the University of Bonn<sup>46</sup>, where animals were kept under standard conditions according to German legislation on the use of animals in experimental research. Commonly used procedures to sample urine from small rodents, such as abdominal pressure or urinary catheterization<sup>36</sup>, was not applied in this study. Parallel to urine sampling, skeletal muscle specimens were dissected and prepared for immunofluorescence microscopical comparison between wild type and dystrophic mice. The collected urine samples were immediately quick-frozen in liquid nitrogen and then transported

on dry ice to Maynooth University in accordance with the Department of Agriculture (animal by-product register number 2016/16 to the Department of Biology, National University of Ireland, Maynooth). Samples were stored at -80 °C prior to proteomic analysis.

### **Proteolytic digestion of urine proteins**

The protein concentration of 50µl urine samples was equalized with label-free solubilisation buffer (6M urea, 2M thiourea, 10mM Tris, pH 8.0 in LC-MS grade water). The Pierce 660nm protein assay system was used to determine protein concentration.<sup>67</sup> This assay has previously been used to determine the concentration of urine protein.<sup>68</sup> Suspensions were then buffer exchanged using the filter-aided sample preparation (FASP) method in a buffer containing 8M urea/50 mM NH<sub>4</sub>HCO<sub>3</sub>/0.1% ProteaseMax, as described in detail by Wiśniewski.<sup>69</sup> After reduction with dithiothreitol and iodoacetic acid-mediated alkylation, a double digestion was performed using Lys-C (for 4 hours at 37°C) and trypsin (overnight at 37°C) on 5µg of urinary protein. Digested samples were desalted prior to analysis using C18 spin columns (Thermo Scientific, UK), dried through vacuum centrifugation and re-suspended in mass spectrometry loading buffer (2% acetonitrile (CAN), 0.05% trifluoroacetic acid (TFA) in LC-MS grade water).<sup>46</sup> Peptides were vortexed, sonicated and briefly centrifuged at 14,000xg and the supernatant transferred to mass spectrometry vials for label-free liquid chromatography mass spectrometry (LC-MS/MS)<sup>53</sup>, a robust and reliable method for the comparative analysis of protein expression patterns.<sup>70-72</sup> Both, label-free and label-based strategies exhibit comparable levels of reproducibility in relation to protein quantification. Label-free mass spectrometry was shown to provide excellent peptide sequence coverage and the detection of a large number of differentially expressed protein species.<sup>73,74</sup>

### **Label-free liquid chromatography mass spectrometry**

For the comparative proteomic survey of urine samples from *mdx-4cv* (n=7 biological repeats; n=2 technical repeats) versus wild type (n=7 biological repeats; n=2 technical repeats) mice, 500ng of each digested sample was loaded onto a Q-Exactive high-resolution accurate mass spectrometer connected to a Dionex Ultimate 3000 (RSLCnano) chromatography system (ThermoFisher Scientific, Hemel Hempstead, UK). Sample loading was carried out by an auto-sampler onto a C18 trap column (C18 PepMap, 300 µm id × 5 mm, 5 µm particle size, 100 Å pore size; Thermo Fisher Scientific). The trap column was switched on-line with an analytical Biobasic C18 Picofrit column (C18 PepMap, 75 µm id × 50 cm, 2 µm particle size, 100 Å pore size; Dionex). Peptides were eluted over a 65-minute binary gradient [solvent A: (2% (v/v)

ACN and 0.1% (v/v) formic acid in LC-MS grade water and solvent B: 80% (v/v) ACN and 0.1% (v/v) formic acid in LC-MS grade water]: 3% solvent B for 5 minutes, 3-10% solvent B for 5 minutes, 10-40% solvent B for 30 minutes, 40-90% solvent B for 5 minutes, 90% solvent B for 5 minutes and 3% solvent B for 10 minutes.<sup>47</sup> The column flow rate was set to 0.3  $\mu$ L/min. Data were acquired with Xcalibur software (Thermo Fisher Scientific). The mass spectrometer was externally calibrated and operated in positive, data-dependent mode. A full survey MS scan was performed in the 300-1700 m/z range with a resolution of 140,000 (m/z 200) and a lock mass of 445.12003. Collision-induced dissociation (CID) fragmentation was carried out with the fifteen most intense ions per scan and at 17,500 resolution. Within 30 seconds a dynamic exclusion window was applied. An isolation window of 2 m/z and one microscan were used to collect suitable tandem mass spectra.

### **Protein identification and quantification**

Data analysis, processing and visualisation for urine protein identification and label-free quantification (LFQ) normalisation of MS/MS data was performed using MaxQuant v1.5.2.8 (<http://www.maxquant.org>) and Perseus v.1.5.6.0 ([www.maxquant.org/](http://www.maxquant.org/)) software. Differential protein expression patterns in the *mdx-4cv* versus wild type urinary proteomes were initially identified using Proteome Discoverer 1.4 against Sequest HT (SEQUENT HT algorithm, licence Thermo Scientific, registered trademark University of Washington, USA) using the UniProtKB/Swiss-Prot database for *Mus musculus*. The following search parameters were used for protein identification: (i) peptide mass tolerance set to 10 ppm, (ii) MS/MS mass tolerance set to 0.02 Da, (iii) an allowance of up to two missed cleavages, (iv) carbamidomethylation set as a fixed modification and (v) methionine oxidation set as a variable modification. Peptides were filtered using a minimum XCorr score of 1.5 for 1, 2.0 for 2, 2.25 for 3 and 2.5 for 4 charge states, with peptide probability set to high confidence. XCorr is a search-dependent score employed by the SEQUEST HT search engine in Proteome Discoverer, and reflects the number of fragment ions that are common to two different peptides with the same precursor mass. Since the XCorr value is dependent upon the number of identified fragment ions, its value is usually higher for larger peptides. XCorr scores are filtered based on charge state, whereby larger XCorr thresholds are used for higher charge states. For quantitative analysis, samples were evaluated with MaxQuant software and the Andromeda search engine used to explore the detected features against the UniProtKB/SwissProt database for *Mus musculus*. The following search parameters were used: i) first search peptide tolerance of 20ppm, ii) main search peptide tolerance of 4.5ppm, iii) cysteine carbamidomethylation set as a fixed

modification, iv) methionine oxidation set as a variable modification, v) a maximum of two missed cleavage sites and vi) a minimum peptide length of seven amino acids. The false discovery rate (FDR) was set to 1% for both peptides and proteins using a target-decoy approach. Relative quantification was performed using the MaxLFQ algorithm. The “proteinGroups.txt” file produced by MaxQuant was further analysed in Perseus. Proteins that matched to the reverse database or a contaminants database or that were only identified by site were removed. The LFQ intensities were log<sub>2</sub> transformed, and only proteins found in all eight replicates in at least one group were used for further analysis. Data imputation was performed to replace missing values with values that simulate signals from peptides with low abundance chosen from a normal distribution specified by a downshift of 1.8 times the mean standard deviation of all measured values and a width of 0.3 times this standard deviation. A two-sample *t*-test was performed using  $p < 0.05$  on the post imputed data to identify statistically significant differentially abundant proteins. The freely available software packages PANTHER<sup>75</sup> (<http://pantherdb.org/>) and STRING<sup>76</sup> (<https://string-db.org/>) were used to identify protein classes and characterise potential protein interactions, respectively.

### **Immunofluorescence microscopy and immunoblot analysis**

Microscopical procedures were carried out as previously described in detail.<sup>45</sup> Transverse diaphragm muscle sections of 10 μm thickness from wild type and dystrophic *mdx-4cv* mice were incubated overnight at 4°C with an appropriately diluted primary antibody to dystrophin isoform Dp427-M. Following washing with phosphate-buffered saline and incubation with fluorescently-labelled secondary antibodies, as well as counter-staining of nuclei, muscle tissue sections were examined under a Zeiss Axioskop 2 epifluorescence microscope equipped with a digital Zeiss AxioCam HRc camera (Carl Zeiss Jena GmbH, Jena, Germany). Comparative immunoblotting was used as an orthogonal method for the independent verification of changes in urine-associated titin in the *mdx-4cv* mouse and carried out by an optimized method.<sup>46</sup>

### **References**

1. É. Csósz, G. Kalló, B. Márkus, E. Deák, A. Csutak, J. Tózsér, Quantitative body fluid proteomics in medicine - A focus on minimal invasiveness, *J. Proteomics*, 2017, **153**, 30-43.

2. N.A. Brunzel, *Fundamentals of Urine and Body Fluid Analysis*, 4th edition, Elsevier/Saunders, St. Louis, MO, 2016.
3. L. Zou, W. Sun, Human urine proteome: a powerful source for clinical research, *Adv. Exp. Med. Biol.*, 2015, **845**, 31-42.
4. A. Beasley-Green, Urine Proteomics in the Era of Mass Spectrometry, *Int. Neurourol. J.* 2016, **20**, S70-S75.
5. M. Zhao, M. Li, Y. Yang, Z. Guo, Y. Sun, C. Shao, M. Li, W. Sun, Y. Gao, A comprehensive analysis and annotation of human normal urinary proteome, *Sci. Rep.*, 2017, **7**, 3024.
6. S. Thomas, L. Hao, W.A. Ricke, L. Li, Biomarker discovery in mass spectrometry-based urinary proteomics, *Proteomics Clin. Appl.*, 2016, **10**, 358-370.
7. K. Fischer, Urinary marker-old wine in new bottles?, *Urologe*, 2018, **57**, 1040-1047.
8. E. Rodríguez-Suárez, J. Siwy, P. Zürgbig, M. Mischak, Urine as a source for clinical proteome analysis: from discovery to clinical application, *Biochim. Biophys. Acta*, 2014, **1844**, 884-898.
9. A. Marimuthu, R.N. O'Meally, R. Chaerkady, Y. Subbannayya, V. Nanjappa, P. Kumar, D.S. Kelkar, S.M. Pinto, R. Sharma, S. Renuse, R. Goel, R. Christopher, B. Delanghe, R.N. Cole, H.C. Harsha, A. Pandey, A comprehensive map of the human urinary proteome, *J. Proteome Res.*, 2011, **10**, 2734-2743.
10. L. Santucci, G. Candiano, A. Petretto, M. Bruschi, C. Lavarello, E. Inglese, P.G. Righetti, G.M. Ghiggeri, From hundreds to thousands: Widening the normal human Urinome (1), *J. Proteomics*, 2015, **112**, 53-62.
11. L. Santucci, M. Bruschi, G. Candiano, F. Lugani, A. Petretto, A. Bonanni, G.M. Ghiggeri, Urine Proteome Biomarkers in Kidney Diseases. I. Limits, Perspectives, and First Focus on Normal Urine, *Biomark. Insights*, 2016, **11**, 41-48.
12. S. Filip, J. Zoidakis, A. Vlahou, H. Mischak, Advances in urinary proteome analysis and applications in systems biology, *Bioanalysis*, 2014, **6**, 2549-2569.
13. N. Nagaraj, M. Mann, Quantitative analysis of the intra- and inter-individual variability of the normal urinary proteome. *J. Proteome Res*, 2011, **10**, 637-645.
14. N. Khristenko, B. Domon, Quantification of proteins in urine samples using targeted mass spectrometry methods, *Methods Mol. Biol.*, 2015, **1243**, 207-220.
15. M. Harpole, J. Davis, V. Espina, Current state of the art for enhancing urine biomarker discovery. *Expert Rev. Proteomics*, 2016, **13**, 609-626.

16. C. Shao, M. Zhao, X. Chen, H. Sun, Y. Yang, X. Xiao, Z. Guo, X. Liu, Y. Lv, X. Chen, W. Sun, D. Wu, Y. Gao, Comprehensive Analysis of Individual Variation in the Urinary Proteome Revealed Significant Gender Differences, *Mol. Cell. Proteomics*, 2019, **18**, 1110-1122.
17. J. Wu, Y. Gao, Physiological conditions can be reflected in human urine proteome and metabolome, *Expert Rev. Proteomics*, 2015, **12**, 623-636.
18. E. Mercuri, C.G. Bönnemann, F. Muntoni, Muscular dystrophies, *Lancet*, 2019, **394**, 2025-2038.
19. Y. Hathout, H. Seol, M.H. Han, A. Zhang, K.J. Brown, E.P. Hoffman, Clinical utility of serum biomarkers in Duchenne muscular dystrophy. *Clin. Proteomics*, 2016, **13**, 9.
20. S. Murphy, M. Zweyer, R.R. Mundegar, D. Swandulla, K. Ohlendieck, Proteomic serum biomarkers for neuromuscular diseases. *Expert Rev. Proteomics*, 2018, **15**, 277-291.
21. P. Dowling, S. Murphy, M. Zweyer, M. Raucamp, D. Swandulla, K. Ohlendieck, Emerging proteomic biomarkers of X-linked muscular dystrophy, *Expert Rev. Mol. Diagn.*, 2019, **19**, 739-755.
22. J.K. Mah, L. Korngut, K.M. Fiest, J. Dykeman, L.J. Day, T. Pringsheim, N. Jette, A Systematic Review and Meta-analysis on the Epidemiology of the Muscular Dystrophies, *Can. J. Neurol. Sci.*, 2016, **43**, 163-177.
23. J. Shin, M.M. Tajrishi, Y. Ogura, A. Kumar, Wasting mechanisms in muscular dystrophy, *Int. J. Biochem. Cell Biol.*, 2013, **45**, 2266-2279.
24. A. Holland, S. Murphy, P. Dowling, K. Ohlendieck, Pathoproteomic profiling of the skeletal muscle matrisome in dystrophinopathy associated myofibrosis. *Proteomics*, 2016, **16**, 345-366.
25. J.G. Tidball, S.S. Welc, M. Wehling-Henricks, Immunobiology of Inherited Muscular Dystrophies, *Compr. Physiol.*, 2018, **8**, 1313-1356.
26. J.D. Hsu, R. Quinlivan, Scoliosis in Duchenne muscular dystrophy (DMD), *Neuromuscul. Disord.*, 2013, **23**, 611-617.
27. V. Ricotti, W.P. Mandy, M. Scoto, M. Pane, N. Deconinck, S. Messina, E. Mercuri, D.H. Skuse, F. Muntoni, Neurodevelopmental, emotional, and behavioural problems in Duchenne muscular dystrophy in relation to underlying dystrophin gene mutations, *Dev. Med. Child Neurol.*, 2016, **58**, 77-84.
28. D.J. Birnkrant, K. Bushby, C.M. Bann, B.A. Alman, S.D. Apkon, A. Blackwell, L.E. Case, L. Cripe, S. Hadjiyannakis, A.K. Olson, D.W. Sheehan, J. Bolen, D.R. Weber,

- L.M. Ward, DMD Care Considerations Working Group, Diagnosis and management of Duchenne muscular dystrophy, part 2: respiratory, cardiac, bone health, and orthopaedic management, *Lancet Neurol.* 2018, **17**, 347-361.
29. S. Guiraud, A. Aartsma-Rus, N.M. Vieira, K.E. Davies, G.J. van Ommen, L.M. Kunkel, The Pathogenesis and Therapy of Muscular Dystrophies, *Annu. Rev. Genomics Hum. Genet.*, 2015, **16**, 281-308.
  30. S. Murphy, K. Ohlendieck, The biochemical and mass spectrometric profiling of the dystrophin complexome from skeletal muscle, *Comput. Struct. Biotechnol. J.*, 2015, **14**, 20-27.
  31. J.M. Ervasti, K.J. Sonnemann, Biology of the striated muscle dystrophin-glycoprotein complex, *Int. Rev. Cytol.*, 2008, **265**, 191-225.
  32. K. Ohlendieck, Towards an understanding of the dystrophin-glycoprotein complex: linkage between the extracellular matrix and the membrane cytoskeleton in muscle fibers, *Eur. J. Cell Biol.*, 1996, **69**, 1-10.
  33. J.M. Ervasti, K. Ohlendieck, S.D. Kahl, M.G. Gaver, K.P. Campbell, Deficiency of a glycoprotein component of the dystrophin complex in dystrophic muscle, *Nature*, 1990, **345**, 315-319.
  34. K. Ohlendieck, K. Matsumura, V.V. Ionasescu, J.A. Towbin, E.P. Bosch, S.L. Weinstein, S.W. Sernett, K.P. Campbell, Duchenne muscular dystrophy: deficiency of dystrophin-associated proteins in the sarcolemma, *Neurology*, 1993, **43**, 795-800.
  35. Holland A, Carberry S, Ohlendieck K. Proteomics of the dystrophin-glycoprotein complex and dystrophinopathy. *Curr Protein Pept Sci.* 2013 Dec;14(8):680-97.
  36. J. Rouillon, A. Zocevic, T. Leger, C. Garcia, J.M. Camadro, B. Udd, B. Wong, L. Servais, T. Voit, F. Svinartchouk, Proteomics profiling of urine reveals specific titin fragments as biomarkers of Duchenne muscular dystrophy, *Neuromuscul. Disord.*, 2014, **24**, 563-573.
  37. N. Maruyama, T. Asai, C. Abe, A. Inada, T. Kawauchi, K. Miyashita, M. Maeda, M. Matsuo, Y.I. Nabeshima, Establishment of a highly sensitive sandwich ELISA for the N-terminal fragment of titin in urine, *Sci. Rep.*, 2016, **6**, 39375.
  38. A.S. Robertson, M.J. Majchrzak, C.M. Smith, R.C. Gagnon, N. Devidze, G.B. Banks, S.C. Little, F. Nabbie, D.I. Bounous, J. DiPiero, L.K. Jacobsen, L.J. Bristow, M.K. Ahljanian, S.A. Stimpson, Dramatic elevation in urinary amino terminal titin fragment excretion quantified by immunoassay in Duchenne muscular dystrophy patients and in dystrophin deficient rodents, *Neuromuscul. Disord.*, 2017, **27**, 635-645.

39. H. Awano, M. Matsumoto, M. Nagai, T. Shirakawa, N. Maruyama, K. Iijima, Y.I. Nabeshima, M. Matsuo, Diagnostic and clinical significance of the titin fragment in urine of Duchenne muscular dystrophy patients, *Clin. Chim. Acta*, 2018, **476**, 111-116.
40. M. Matsuo, T. Shirakawa, H. Awano, H. Nishio, Receiver operating curve analyses of urinary titin of healthy 3-y-old children may be a noninvasive screening method for Duchenne muscular dystrophy, *Clin. Chim. Acta*, 2018, **486**, 110-114.
41. M. Matsuo, H. Awano, N. Maruyama, H. Nishio, Titin fragment in urine: A noninvasive biomarker of muscle degradation, *Adv. Clin. Chem.*, 2019, **90**, 1-23.
42. W.B. Im, S.F. Phelps, E.H. Copen, E.G. Adams, J.L. Slightom, J.S. Chamberlain, Differential expression of dystrophin isoforms in strains of mdx mice with different mutations, *Hum. Mol. Genet.*, 1996, **5**, 1149-1153.
43. E.D. Tichy, F. Mourkioti, A new method of genotyping MDX4CV mice by PCR-RFLP analysis, *Muscle Nerve*, 2017, **56**, 522-524.
44. N.E. Bengtsson, J.K. Hall, G.L. Odom, M.P. Phelps, C.R. Andrus, R.D. Hawkins, S.D. Hauschka, J.R. Chamberlain, J.S. Chamberlain, Muscle-specific CRISPR/Cas9 dystrophin gene editing ameliorates pathophysiology in a mouse model for Duchenne muscular dystrophy, *Nat. Commun.*, 2017, **8**, 14454.
45. S. Murphy, P. Dowling, M. Zweyer, R.R. Mundegar, M. Henry, P. Meleady, D. Swandulla, K. Ohlendieck, Proteomic analysis of dystrophin deficiency and associated changes in the aged mdx-4cv heart model of dystrophinopathy-related cardiomyopathy, *J. Proteomics*, 2016, **145**, 24-36.
46. S. Murphy, M. Zweyer, M. Henry, P. Meleady, R.R. Mundegar, D. Swandulla, K. Ohlendieck, Proteomic analysis of the sarcolemma-enriched fraction from dystrophic mdx-4cv skeletal muscle, *J. Proteomics*, 2019, **191**, 212-227.
47. P. Dowling, M. Zweyer, M. Raucamp, M. Henry, P. Meleady, D. Swandulla, K. Ohlendieck, Proteomic and cell biological profiling of the renal phenotype of the *mdx-4cv* mouse model of Duchenne muscular dystrophy, *Eur. J. Cell Biol.*, 2020, **99**, 151059.
48. S. Murphy, P. Dowling, M. Zweyer, D. Swandulla, K. Ohlendieck, Proteomic profiling of giant skeletal muscle protein, *Expert Rev. Proteomics*, 2019, **16**, 241-256.
49. S. Murphy, P. Dowling, M. Zweyer, M. Henry, P. Meleady, R.R. Mundegar, D. Swandulla, K. Ohlendieck, Proteomic profiling of mdx-4cv serum reveals highly elevated levels of the inflammation-induced plasma marker haptoglobin in muscular dystrophy, *Int. J. Mol. Med.*, 2017, **39**, 1357-1370.

50. S. Carberry, H. Brinkmeier, Y. Zhang, C.K. Winkler, K. Ohlendieck, Comparative proteomic profiling of soleus, extensor digitorum longus, flexor digitorum brevis and interosseus muscles from the mdx mouse model of Duchenne muscular dystrophy, *Int. J. Mol. Med.*, 2013, **32**, 544-556.
51. S. Rayavarapu, W. Coley, E. Cakir, V. Jahnke, S. Takeda, Y. Aoki, H. Grodish-Dressman, J.K. Jaiswal, E.P. Hoffman, K.J. Brown, Y. Hathout, K. Nagaraju, Identification of disease specific pathways using in vivo SILAC proteomics in dystrophin deficient mdx mouse, *Mol. Cell. Proteomics*, 2013, **12**, 1061-1073.
52. A. Holland, P. Dowling, P. Meleady, M. Henry, M. Zweyer, R.R. Mundegar, D. Swandulla, K. Ohlendieck, Label-free mass spectrometric analysis of the mdx-4cv diaphragm identifies the matricellular protein periostin as a potential factor involved in dystrophinopathy-related fibrosis, *Proteomic*, 2015, **15**, 2318-2331.
53. S. Murphy, M. Zweyer, M. Raucamp, M. Henry, P. Meleady, D. Swandulla, K. Ohlendieck, Proteomic profiling of the mouse diaphragm and refined mass spectrometric analysis of the dystrophic phenotype, *J. Muscle Res. Cell. Motil.*, 2019, **40**, 9-28.
54. Y. Hathout, R.L. Marathi, S. Rayavarapu, A. Zhang, K.J. Brown, H. Seol, H. Gordish-Dressman, S. Cirak, L. Bello, K. Nagaraju, T. Partridge, E.P. Hoffman, S. Takeda, J.K. Mah, E. Henricson, C. McDonald, Discovery of serum protein biomarkers in the mdx mouse model and cross-species comparison to Duchenne muscular dystrophy patients, *Hum. Mol. Genet.*, 2014, **23**, 6458-6469.
55. S. Guiraud, B. Edwards, S.E. Squire, A. Babbs, N. Shah, A. Berg, H. Chen, K.E. Davies, Identification of serum protein biomarkers for utrophin based DMD therapy, *Sci. Rep.*, 2017, **7**, 43697.
56. A. Holland, P. Dowling, M. Zweyer, D. Swandulla, M. Henry, M. Clynes, K. Ohlendieck, Proteomic profiling of cardiomyopathic tissue from the aged mdx model of Duchenne muscular dystrophy reveals a drastic decrease in laminin, nidogen and annexin, *Proteomics*, 2013, **13**, 2312-2323.
57. S. Murphy, H. Brinkmeier, M. Krautwald, M. Henry, P. Meleady, K. Ohlendieck, Proteomic profiling of the dystrophin complex and membrane fraction from dystrophic mdx muscle reveals decreases in the cytolinker desmoglein and increases in the extracellular matrix stabilizers biglycan and fibronectin. *J. Muscle Res. Cell Motil.*, 2017, **38**, 251-268.

58. F. Cynthia Martin, M. Hiller, P. Spitali, S. Oonk, H. Dalebout, M. Palmblad, A. Chaouch, M. Guglieri, V. Straub, H. Lochmüller, E.H. Niks, J.J. Verschuuren, A. Aartsma-Rus, A.M. Deelder, Y.E. van der Burgt, P.A. 't Hoen, Fibronectin is a serum biomarker for Duchenne muscular dystrophy *Proteomics Clin. Appl.*, 2014, **8**, 269-728.
59. L.O. Chavez, M. Leon, S. Einav, J. Varon, Beyond muscle destruction: a systematic review of rhabdomyolysis for clinical practice. *Crit. Care*, 2016, **20**, 135.
60. K. Rodríguez-Capote, C.M. Balion, S.A. Hill, R. Cleve, L. Yang, A. El Sharif, Utility of urine myoglobin for the prediction of acute renal failure in patients with suspected rhabdomyolysis: a systematic review, *Clin. Chem.*, 2009, **55**, 2190-2197.
61. D.R. Scoles, S.M. Pulst, Antisense therapies for movement disorders, *Mov. Disord.*, 2019, **34**, 1112-1119.
62. C.S. Young, A.D. Pyle, M.J. Spencer, CRISPR for Neuromuscular Disorders: Gene Editing and Beyond, *Physiology (Bethesda)*, 2019, **34**, 341-353.
63. C. Sun, C. Serra, G. Lee, K.R. Wagner, Stem cell-based therapies for Duchenne muscular dystrophy, *Exp. Neurol.*, 2020, **323**, 113086.
64. M.A. Waldrop, K.M. Flanigan, Update in Duchenne and Becker muscular dystrophy, *Curr. Opin. Neurol.*, 2019, **32**, 722-727.
65. M. Thangarajh, A. Zhang, K. Gill, H.W. Resson, Z. Li, R.S. Varghese, E.P. Hoffman, K. Nagaraju, Y. Hathout, S.M. Boca, Discovery of potential urine-accessible metabolite biomarkers associated with muscle disease and corticosteroid response in the mdx mouse model for Duchenne, *PLoS One*, 2019, **14**, e0219507.
66. S. Murphy, M. Zweyer, R.R. Mundegar, D. Swandulla, K. Ohlendieck, Proteomic identification of elevated saliva kallikrein levels in the mdx-4cv mouse model of Duchenne muscular dystrophy, *Biochem. Biophys. Rep.*, 2018, **18**, 100541.
67. B.S. Antharavally, K.A. Mallia, P. Rangaraj, P. Haney, P.A. Bell, Quantitation of proteins using a dye-metal-based colorimetric protein assay, *Anal. Biochem.*, 2009, **385**, 342-345.
68. V. Urquidi, M. Chang, Y. Dai, J. Kim, E.D. Wolfson, S. Goodison, C.J. Rosser, IL-8 as a urinary biomarker for the detection of bladder cancer. *BMC Urol.*, 2012, **12**, 12.
69. J.R. Wiśniewski, Filter-Aided Sample Preparation: The Versatile and Efficient Method for Proteomic Analysis, *Methods Enzymol.*, 2017, **585**, 15-27.
70. R. Aebersold, M. Mann, Mass-spectrometric exploration of proteome structure and function, *Nature*, 2016, **537**, 347-355.

71. S. Anand, M. Samuel, C.S. Ang, S. Keerthikumar, S. Mathivanan, Label-Based and Label-Free Strategies for Protein Quantitation. *Methods Mol. Biol.*, 2017, **1549**, 31-43.
72. J.A. Ankney, A. Muneer, X. Chen, Relative and Absolute Quantitation in Mass Spectrometry-Based Proteomics. *Annu. Rev. Anal. Chem. (Palo Alto Calif)*, 2018, **11**, 49-77.
73. D.A. Megger, L.L. Pott, M. Ahrens, J. Padden, T. Bracht, K. Kuhlmann, M. Eisenacher, H.E. Meyer, B. Sitek, Comparison of label-free and label-based strategies for proteome analysis of hepatoma cell lines. *Biochim. Biophys. Acta*, 2014, **1844**, 967-976.
74. A. Latosinska, K. Vougas, M. Makridakis, J. Klein, W. Mullen, M. Abbas, K. Stravodimos, I. Katafigiotis, A.S. Merseburger, J. Zoidakis, H. Mischak, A. Vlahou, V. Jankowski, Comparative Analysis of Label-Free and 8-Plex iTRAQ Approach for Quantitative Tissue Proteomic Analysis. *PLoS One*, 2015, **10**, e0137048.
75. H. Mi, A. Muruganujan, D. Ebert, X. Huang, P.D. Thomas, PANTHER version 14: more genomes, a new PANTHER GO-slim and improvements in enrichment analysis tools. *Nucleic Acids Res.*, 2019, **47(D1)**, D419-D426.
76. D. Szklarczyk, A.L. Gable, D. Lyon, A. Junge, S. Wyder, J. Huerta-Cepas, M. Simonovic, N.T. Doncheva, J.H. Morris, P. Bork, L.J. Jensen, C.V. Mering, STRING v11: protein-protein association networks with increased coverage, supporting functional discovery in genome-wide experimental datasets. *Nucleic Acids Res.*, 2019, **47(D1)**, D607-D613.

Chapter 7

**General discussion**

## Discussion

This thesis has focused on the description of mass spectrometry-based proteomics with special reference to dystrophic skeletal muscle. The proteomic characterization was mostly concerned with the genetic *mdx-4cv* mouse model of Duchenne muscular dystrophy. Studies have included (i) the detailed description of sample preparation for proteomics and mass spectrometry for bottom-up proteomics, (ii) sample preparation and protein determination for top-down proteomics, (iii) the proteomic identification of markers of membrane repair, regeneration and fibrosis in the aged and dystrophic *mdx-4cv* mouse diaphragm, (iv) the mass spectrometric profiling of extraocular muscle and proteomic adaptations in the *mdx-4cv* mouse, and (v) the identification of biofluid marker proteins of muscular dystrophy in the urine proteome from the *mdx-4cv* mouse. Major biochemical findings, as described in detail in Chapters 2-6, are summarized in below table:

Summary of the published work that was carried out for the mass spectrometry-based proteomic analysis of muscle specimens, and the listing of major findings on the proteomic characterization of the *mdx-4cv* mouse model of Duchenne muscular dystrophy, as presented in this thesis.

Focus of published studies	Experimental approach	Bioanalytical findings
Sample preparation for proteomics and mass spectrometry for bottom-up proteomics	Detailed protocol that outlines sample preparation for proteomics and mass spectrometry from clinical muscle tissue specimens	The article describes in detail sample preparation from muscle biopsy material for proteomic surveys, including tissue harvesting, homogenization, determination of protein concentration, removal of potentially interfering chemicals, controlled digestion of proteins to produce representative peptide populations to be analysed by mass spectrometry
Sample preparation and protein	Detailed description of the individual steps	This methods paper describes the optimal application of sample

determination for top-down proteomics	involved in sample handling, homogenization, subcellular fractionation and the determination of protein concentration for gel-based proteomics	preparation and protein determination. The chapter outlines sample homogenization and a standardized protein assay for the preparation of homogenates with a known protein concentration for subsequent gel electrophoretic separation and proteomic analysis.
Proteomic identification of markers of membrane repair, regeneration and fibrosis in the aged and dystrophic <i>mdx-4cv</i> mouse diaphragm	Comparative proteomic analysis of young versus aged diaphragm muscles from wild type versus the dystrophic <i>mdx-4cv</i> mouse model of dystrophinopathy	The proteomic survey confirmed the drastic reduction of the dystrophin-glycoprotein complex in the <i>mdx-4cv</i> diaphragm muscle and concomitant age-dependent changes in key markers of muscular dystrophy, including proteins involved in cytoskeletal organization, metabolite transportation, the cellular stress response and excitation-contraction coupling. Importantly, proteomic markers of the regulation of membrane repair, tissue regeneration and reactive myofibrosis were detected by mass spectrometry and changes in key proteins were confirmed by immunoblotting.
Mass spectrometric profiling of extraocular muscle and proteomic adaptations in the <i>mdx-4cv</i> mouse	Proteomic survey of wild type mice versus the dystrophic <i>mdx-4cv</i> model was carried out to determine the broad spectrum of sarcomere-associated proteoforms, including components of the thick filament,	The mass spectrometric analysis of extraocular muscles revealed unusual expression levels of contractile proteins, especially isoforms of myosin heavy chain (MyHCs 13-15). The analysis of the mildly affected <i>mdx-4cv</i> extraocular muscles identified elevated levels of glycolytic enzymes and molecular

	thin filament, M-band and Z-disk, as well as a variety of muscle-specific markers in extraocular muscle and muscular dystrophy	chaperones, as well as decreases in mitochondrial enzymes.
Identification of biofluid marker proteins of muscular dystrophy in the urine proteome from the <i>mdx-4cv</i> mouse	This study focused on the urine proteome in the <i>mdx-4cv</i> mouse model. In order to avoid potential artefacts due to the manipulation of the biofluid proteome prior to mass spectrometry, crude urine specimens were analysed without the prior usage of centrifugation steps or concentration procedures	Comparative proteomics revealed 21 increased and 8 decreased proteins out of 870 identified urinary proteoforms using 50 µl of biofluid per investigated sample, i.e. 14 wild type versus 14 <i>mdx-4cv</i> specimens. Promising marker proteins that were almost exclusively found in <i>mdx-4cv</i> urine included nidogen, parvalbumin and titin. Interestingly, the mass spectrometric identification of urine-associated titin revealed a wide spread of peptides over the sequence of this giant muscle protein.

## 7.1 Analysis of altered proteome in aged dystrophic diaphragm

### 7.1.1 Extracellular matrix proteins

There are considerable similarities between the muscle weakness associated with muscular dystrophies, and that of sarcopenia of old age. It was of interest to perform a comparative mass spectrometric analysis, and to examine how the aging process can compound with the effects of muscular dystrophy seen in the *mdx-4cv* mouse. Fibrosis is a hallmark feature of both dystrophic and sarcopenic muscle. The regeneration process following muscular injury ensures that some proteins of the extracellular matrix are deposited into muscle fibres, forming scar tissue. Over many cycles of degeneration and regeneration, an excess amount of ECM components infiltrate the muscle. This fibrosis reduces the contractile force of muscle (Serrano and Muñoz-Cánoves., 2017). The first event in tissue repair following injury is generally the

activation of the innate immune system. Resident macrophages located in the perimysium and epimysium secrete monocyte chemoattractant protein 1, which recruits neighbouring resident macrophages along with monocytes from the circulatory system (Chazaud et al., 2009). Depletion of macrophages and monocytes can impair or even prevent the muscle regeneration process (Arnold et al., 2007).

M1 macrophages secrete and attract high levels of pro-inflammatory cytokines, such as TGF- $\beta$  and interleukin. Transforming growth factor type beta 1, TGF- $\beta$ 1, is a growth factor and cytokine with a central role in muscle pathologies featuring development of fibrosis and atrophy of skeletal muscle (Abrigo et al., 2018). TGF- $\beta$ 1 lies dormant in the ECM, being sealed by a propeptide homodimer known as latency associated peptide until it is made bio-available through binding with its chaperone protein (Todorovic and Rifkin., 2012). Activated TGF- $\beta$  binds to a cell membrane located complex, where it promotes fibroblasts to start producing ECM proteins, such as collagen and fibronectin (Serrano and Muñoz-Cánoves, 2017). Fibroblasts derived from DMD muscle have a significantly higher expression of TGF- $\beta$  than those from healthy muscle (Vidal et al., 2008).

The collagen superfamily of proteins represents 30% of all protein mass for humans, and for most mammals. A defining feature of this family is its triple helical structure. These three chains of protein wrap around each other to form massive supramolecules of mass that supports the load of the extracellular matrix. Individual isoforms of collagen also perform unique and various roles. Collagen IV for example, is required for maintaining stability of the synaptic clefts, from which all action potentials must pass through to kickstart the mechanism of muscle contraction. While some forms of collagen are simple triple helical structure, The sequence of some isoforms contains domains shared with non-collagen matrix molecules, like fibronectin and thrombospondin (Shaw and Olsen., 1991). Collagen is considered to be a key marker of reactive myofibrosis, as well as a marker for tissue regeneration. Fifteen isoforms of collagen were found to be significantly increased in the diaphragm muscle of aged dystrophic mice. Immunoblotting has clearly demonstrated a significant increase in collagen-vi in the aged diaphragm.

Proteoglycans are a form of protein containing at least one attached glycosaminoglycan chain (Yanagishita., 1997). Small leucine-rich proteoglycans, SLRP, are a subfamily defined by the structural presence of multiple Leucine-Rich Repeats. SLRP are known to regularly occupy the ECM. Increased expression of various members of this group, including decorin, asporin, biglycan, mimecan/osteoglycin, and lumican, were found in diaphragm muscle. SLRPs regulate the organisation and structure of the ECM. Decorin has been shown to inhibit

fibrillogenesis by binding to collagen types i and ii, and by acting as a bridge between these isoforms and other regulatory collagens (Bidanset et al., 1992). SLRPs can also interact with growth factors, including TGF- $\beta$ , to regulate cell activities (Corsi et al., 2002). Biglycan can alter the signalling involved in the TGF- $\beta$  /smad2 pathway (Melchior-Becker et al., 2011). Lumican interacts with the TGF- $\beta$  receptor-1, ALK5 to form a stable complex which promotes wound healing by preventing further TGF- $\beta$  signalling (Yamanaka et al., 2013). The matricellular protein, periostin, was also increased. This is not an ECM structural protein, instead it has a range of important roles. Different areas of the protein structure are adapted for these roles. Periostin is classed as a member of the elastin microfibrillar interface protein, EMILIN, family, due to the presence of an EMI domain located at the N-terminal. Interactions between collagens and periostin promote the development of new collagen fibrils, and periostin knockout mice displayed reduced diameter of collagen fibrils compared to WT mice (Norris et al., 2007). Following the EMI domain, there exists four fasciclin like domains, which can bind with integrins to activate various signalling pathways in cells, including the FAK, PI3K, and AKT signaling pathways (González-González and Alonso., 2018). Fasciclin was originally discovered in drosophilla, where it functions as a neural cell adhesion molecule (Clout et al., 2003). this fasciclin like region of periostin is also capable of binding with the protein tenascin-c, along with bone morphogenic factor, and cellular communication network factor 3. This suggests that the function of the fas-1 region is to act as an anchor point, to allow the EMI region to interact with other ECM components (Zhu et al., 2021). The c-terminal domain of periostin contains an arginine rich domain that interacts with heparin. Heparin is a polysaccharide that attaches to proteins to form what is known as heparin sulphated proteoglycans (Kii and Ito., 2017). In addition to binding glycosaminoglycans, the c-terminal domain of periostin also bind with other ECM proteins. Alternative splicing of the this c-terminal domain results in various protein isoforms (Hoersch and Andrade-Navarro., 2010). Removal of this C-terminal region results in the paralogous protein TGF $\beta$ i. Periostin expression is induced by TGF $\beta$ , and as its name suggests, so too is TGF $\beta$ i. These two proteins can interact to form dimers. Mutations to TGF $\beta$ i can prevent this dimer from forming and are strongly implicated in corneal dystrophy (Kim et al., 2009). While periostin is ubiquitously expressed during embryogenesis, postnatally, it is only temporarily expressed during myoblast differentiation and muscle regeneration (Ozdemir et al., 2014). It is constantly and drastically elevated in cases of chronic injury and repair, thus making it an appropriate marker for fibrosis (Holland et al., 2015). Deletion of periostin from a sarcoglycan null mouse model of muscular dystrophy results in enhanced myofiber regeneration (Lorts et al., 2012).

### 7.1.2 Excitation-contraction coupling proteins

Impaired expression of proteins involved in EC coupling and calcium homeostasis is observed in many pathologies and is a major contributor to the severe pathology of DMD. The instability caused by the absence of Dp427-M results in a greater leakage of calcium ions from the sarcoplasmic reticulum (Takagi et al., 1992). This is reflected by the comparative proteomics study results showing a drastic decrease in expression of various key proteins of the excitation-contraction coupling process. Located in the membrane of T-tubules, L-type  $\text{Ca}^{2+}$  channels are the primary route of entry for calcium ions into skeletal, cardiac, and smooth muscle (Bean., 1989). While  $\text{Ca}^{2+}$  entry through these channels is not required to initiate contraction in vertebrate skeletal muscle, it likely replenishes internal calcium stores in the sarcoplasmic reticulum. Invertebrate skeletal muscle, on the other hand, is highly dependent on an influx of extracellular calcium ions to contract (Fatt and Ginsborg., 1958). The L in L-type refers to the long-lasting duration of this activation type. These high threshold currents act as a voltage sensor for EC coupling in skeletal muscle. In response to the initial depolarization step of EC coupling, a conformational change occurs in the  $\alpha 1$  subunit. This change is transmitted to the linked ryanodine receptor protein, which functions as the  $\text{Ca}^{2+}$  release channel of the SR (Miller., 1992). Structurally, the  $\alpha 1$  subunit is made up of four homologous hydrophobic repeats, each containing membrane spanning helices. These helices contain positively charged amino acids that constitute the voltage-sensing region of the protein (Neely and Hidalgo., 2014). While isolation studies have demonstrated that the  $\alpha 1$  subunit is capable of forming  $\text{Ca}^{2+}$  channel by itself (Lacerda et al., 1991), the other subunits aid in the process by acting as regulatory proteins. The  $\alpha 2/\delta$ -subunit can be divided into two segments, the N-terminal  $\alpha 2$  sequence, and its corresponding disulfide linked C-terminal  $\delta$  sequence. Both proteins are products of a single gene, and are highly glycosylated (Catterall., 1988). The  $\alpha 2/\delta$ -subunit has been shown to enhance the rate of  $\text{Ca}^{2+}$  influx through L-channels (Gutierrez et al., 1991). The ryanodine receptors are huge tetrameric  $\text{Ca}^{2+}$  release channel proteins, responsible for releasing  $\text{Ca}^{2+}$  from the sarcoplasmic reticulum. This is a crucial step in the muscle contraction process, as this released  $\text{Ca}^{2+}$  then binds with troponin C, to free up actin filaments from their tropomyosin shackles. Three members of the RyR family are known to exist, encoded by three separate genes. The skeletal muscle isoform RyR1 was considerably decreased in aged dystrophic muscle, indicating a dysfunctional release of  $\text{Ca}^{2+}$  in these tissues. RyR2 is predominantly expressed in cardiac muscle, while RyR3 is expressed in numerous tissues, albeit at small amounts (Sorrentino., 1995). The homotetrameric structure of RYRs contains

four spheres which cross the cytoplasm to span the gap between the SR and T-tubules. These four spheres together are known as “feet”, which are physically linked to the DHPR (Ferguson et al., 1984). The molecular bond between RyR and DHPR is quite strong, and even after forced dissociation, these vesicles are capable of reassociating with each other (Flucher and Franzini-Armstrong., 1996).

The energy of the action potential is much the same in *mdx* mice as in *wt* mice (Woods et al., 2004). Despite this, multiple studies have determined that less  $ca^{2+}$  is released as a result of the action potentials (Head., 2010, Hollingworth et al., 2008). This is due, not only to the reduced amount of RyR, but also their increased leakiness due to s-nitrosylation (Bellinger et al., 2009). Exon skipping is a potential therapy for DMD. Skipping of exons 45-55 has been suggested as a potential strategy, as this is where most DMD mutations occur. The resulting dystrophin would be missing part of the key neuronal nitric oxide synthase, nNOS $\mu$ , binding sites located on exon 42-45, leading to a greater cytosolic nNOS $\mu$  concentration. In BMD patients with a natural deletion of exons 45-55, a more severe phenotype is associated with cytosolic mislocalisation of nNOS $\mu$ , which leads to a greater nitrosylation of the RyRs (Gentil et al., 2012). This conjugation of nitric oxide to cysteine residues of the RyR, can reduce the affinity for which it binds with calmodulin, a calcium binding protein that regulates the release channel (Sun et al., 2001). S-nitrosylation also interferes with the RyR-calstabin complex. Calstabin-1 is a crucial stabiliser of the RyR channel, which helps to maintain its closed state for resting myocytes, preventing leakage of  $ca^{2+}$  ions (Brillantes et al., 1994). A decrease in levels of fast calsequestrin, CASQ1, in aged dystrophic muscle confirms findings of Previous studies that have shown an impaired calcium binding and buffering system in dystrophic muscle, along with an associated decrease in calsequestrin-like proteins (Dowling et al., 2004, Culligan et al., 2002). CASQ1 is the main calcium binding protein of the SR. It has a high capacity and low affinity for  $ca^{2+}$ , and is essential for storing and buffering these ions (Wang and Michalak., 2020). Crystal studies have shown that CASQ1 isoforms are made up of three domains, each displaying sequence similarity to the redox protein, thioredoxin (Wang et al., 1998). At the C-terminal end, CASQ1 has a flexible tail domain that is rich in aspartic acid. This tail region is the major  $ca^{2+}$  binding site on calsequestrin (Beard and Dulhunty., 2015). Binding with  $ca^{2+}$  causes a conformational change in the CASQ1 protein, making it more compact. An increasing  $ca^{2+}$  concentration triggers the reversible polymerisation of calsequestrin molecules. The C-tail is thought to be involved in this polymerisation process, as proteins with this domain deleted will not form polymers (Park et al., 2003). CASQ1 is located in the terminal cisternae, but can be localised to RyR through a quaternary complex connection, with the proteins triadin

and junction (Murray and Ohlendieck., 1998). When luminal  $ca^{2+}$  levels are low, CASQ1 protects the stores from further  $ca^{2+}$  depletion by reducing the RyR activity (Wei et al., 2006). A decrease in calsequestrin levels would result in less  $ca^{2+}$  being bound and available for release, and this decreased amount would leave the SR with greater ease due to the dysregulated RyR channels.

Named for its localisation to excitable cell junctions, the junctophilin, JP, family of proteins help to maintain the close contact between the SR and T-tubules, ensuring efficient ER coupling (Hirata et al., 2006). JP1 and JP2 are both expressed in the triad junction of skeletal muscle, while JP2 is the primary isoform found in cardiac junctions (Takeshima et al., 2000). All JP isoforms attach to the plasma membrane through their N-terminal located membrane occupation and recognition nexus domain. After this is an alpha-helical structure bridge, which crosses the junction. The sequence of JP is highly conserved between species. Any differences are due to additional amino acids in the following “divergent” region. The final domain on this protein is a hydrophobic tail, that anchors junctophilin into the sarcoplasmic reticulum (Lehnart and Wehrens., 2022).

JP1 knockout mice die within one day of birth. They struggle to open their mouths, and thus, cannot feed. No skeletal muscle abnormalities were found directly after birth, but after 15-20 hours the orientation of SR networks was found to irregular, and the terminal regions of the SR were swollen. Contractile force of the hindlimb muscles from the mutant mice were half of that from the wild type controls (Ito et al., 2001). Mice with JP2 knocked out did not survive embryogenesis due to cardiac myocyte dysfunction, and reduced heart pump function (Takeshima et al., 2000).

An increased concentration of  $ca^{2+}$  in the SR can activate the calpains proteases, which cleave junctophilin 1 & 2 (Murphy et al., 2013). Increased cytosolic  $ca^{2+}$  levels can also activate proteases, and induce calcium signalling pathways, therefore it is essential for the cell to be able to regulate internal calcium levels. The Sarco(endo)plasmic Reticulum Calcium ATPase, SERCA, is responsible for pumping calcium ions back into the SR following muscle contraction. The ability to recycle  $ca^{2+}$  ions make this protein a key regulator of calcium homeostasis (Xu and Van Remmen., 2021). Primary abnormalities to the SERCA gene result in the Brody’s disease, a rare muscular dystrophy associated with exercise induced impairment of muscle relaxation, along with severe cramping (Odermatt et al., 1996). SERCA molecules will preferentially oligomerise with themselves in the process of self-aggregation (Schreiber & Ohlendieck., 2007). In addition to self-linkage, SERCA1 has been shown to associate closely with various regulatory proteins, such as sarcolipin (Shaikh et al., 2016). This small 31 amino

acid protein competes with  $Ca^{2+}$  for SERCA binding. This reduces the serca- $Ca^{2+}$  coupling but does not prevent ATP hydrolysis. The release of a phosphate group without the  $Ca^{2+}$  pumping results in thermogenesis and is important in muscle temperature homeostasis (Pant et al., 2016). An increased temperature can also inhibit SERCA activity. HSP70 can bind with SERCA1 and protect its function against thermal inactivation (Tupling et al., 2004). An increase of intramuscular HSP72 levels in dystrophic mice preserves muscle strength and improves dystrophin pathology (Gehrig et al., 2012). SERCA levels are often found to be decreased in sarcopenic muscle, likely due to the increased oxidative stress associated with aging. Multiple cysteine residues on SERCA are susceptible to oxidative modification, and oxidation inhibits the effectiveness of this calcium ion pump protein (Dremina et al., 2007). Previous studies have shown SERCA to be decreased in dystrophic muscle (Murphy et al., 2017b, Murphy et al., 2017a). An overexpression of SERCA1 in muscle can protect from the dystrophic phenotype (Goonasekera et al., 2011).

### **7.1.3 Membrane repair and calcium sensing**

Membrane disturbance is a common feature of cellular injury. The most affected cells are myocytes, due to the regular contractile force applied to them, and this is exacerbated in the chronically unstable dystrophic myocytes (Petrof et al., 1993). Dystrophic muscle from mdx mice accrues six times greater wounding than WT, but both groups are able to repair the wounds, leading to cell survival (Clarke et al., 1993). The annexin family of proteins is implicated in the process of membrane repair. These calcium dependent proteins are responsible for sealing pores in damaged membranes. Of the twelve annexin isoforms found in vertebrates, a common characteristic is the presence of a highly conserved C-terminal core domain with 4 amino acid repeats, each containing a  $Ca^{2+}$  binding site. The N-terminal domain of annexin proteins is not conserved, and the differences here allow various annexins to bind with their unique cytoplasmic partners. Annexin genes have been seen to fuse with other genes to create hybrids. Annexin A6 gene is thought to be a fusion of *ANXA5* and *ANXA10*. In *Drosophilla*, a recent gene has evolved from the fusion of *annX* and *Cdic*, which encodes the intermediate polypeptide chain of the cytoplasmic dynein (Ranz et al., 2003). The effectiveness of glucocorticoid in treating DMD may be due to annexin modulation, as dexamethasone causes annexins to be expressed and translocated from the cytosol to the plasma membrane, in certain cells (Solito et al., 1991). Six members of the annexin family are increased in this proteomic study, and the increase in annexin A2 has been confirmed through western blotting. Annexin A1 and A2 co-localise with dysferlin during muscle repair (Lennon et al., 2003).

Dysferlin is another protein increased in the dystrophic diaphragm, especially the aged diaphragm. This is a member of the Ferlin family of proteins, whose characteristic cytosolic c2 domains mediate lipid and protein binding (Lek et al., 2012). Mutations to the dysferlin gene, *dysf*, are responsible for myoshi myopathy, limb girdle muscular dystrophy 2b, and distal anterior compartment myopathy (Liu et al., 1998, Illa et al., 2001). The plasma membrane located dysferlin acts as a hook to allow other proteins to form a patch at the wound site. In addition to the annexins, dysferlin interacts with caveolin 3 at the membrane. Mutations to caveolin 3 result in Limb girdle muscular dystrophy1C (Minetti et al., 1998). Cav-3 is highly enriched in T-tubules (Parton et al., 1997), and directly interacts with the L-type  $Ca^{2+}$  channels, a depletion of cav-3 results in a reduced conductance of these channels (Couchoux et al., 2011). Caveolins are named for the cave-like hollows that they form in the membrane, called caveolae. Both ends of caveolin molecules extend into the cytoplasm, while the hydrophobic middle section loops into the lipid bilayer of the membrane (Schlegel and Lisanti., 2000). The hydrophobic loop binds with cholesterol, which can then accumulate proteins, including annexin A2 and dysferlin (Bittel et al., 2020). Caveolins appear to be a multifunctional protein, and may be involved in PI3K-AKT-mTOR pathway through signalling AKT (Shack et al., 2003). The caveolae located on sarcolemma may break open when the muscle is elongated as a result of stretching, thus acting as mechanosensors (Dulhunty and Franzini-Armstrong., 1975).

The integrins are a large family of cell adhesion proteins capable of transmitting signals from the cell membrane into both the cytoplasm and the cell membrane (Hynes., 2002). The cytosolic anchor domain of integrins is quite small, usually 75 amino acids long, but is still capable of binding various cytoskeletal, and signalling proteins, acting as an intermediate link between these, and whichever ECM protein that it binds at the far end. Integrins are heterodimeric proteins, consisting of an A and B subunit. B1 is the most common  $\beta$  subunit found in these heterodimers, as this protein can pair with multiple forms of  $\alpha$  chains to form 12 integrins (Fu et al., 2012). Integrin A7 is an isoform responsible for linking laminin to the cytoskeleton, giving it some shared function with the DGC. Promoting upregulation of A7B1 in dystrophic mice muscle doubled the pool of satellite cells available. This consequently expanded their lifespan up to threefold and alleviated pathogenic symptoms (Burkin et al., 2005). Another member of this family involved in plasma membrane stability is integrin beta-1.

## **7.2 Extraocular proteome analysis**

The extraocular muscles, EOM, that surround and control the eye represent a unique form of skeletal muscle. This specialised muscle group has a range of distinctive characteristics. Perhaps the most interesting feature of the EOM is the resistance to the degeneration usually associated with dystrophin deficiency. The ability of these muscles to remain relatively unaffected during the course of DMD disease progression, makes them of special interest to those studying this disease. To gain a better understanding of the proteomic changes that distinguish EOM from general skeletal muscle, a comparison was made between the sarcomeric proteins of the EOM and those of the diaphragm. To further ascertain how the EOM proteome adapts to this disease, a comparative proteomic analysis was performed between *wt* and *mdx-4cv* extraocular muscles.

Embryonic development of EOM is mediated by the paired-like homeodomain transcription factor 2, PITX2, protein. Overexpression of this potent transcription factor in dystrophic satellite cells enhances their regenerative ability (Vallejo et al., 2018). EOM morphogenesis is directly correlated to the dose of *pitx2* received, with each allele providing 50% of protein expression. *Pitx2*<sup>+/+</sup> mice embryos develop well-formed EOM condensations, compared to *pitx2* double knockout mice, who lack EOM altogether. Furthermore, some EOMs are more sensitive to *pitx2* than others. With one functional *pitx2* allele, the superior oblique muscle being absent in all mice studied, while the inferior oblique muscle was present in some but not all mice (Diehl et al., 2006). This differential sensitivity to PITX2 is reflective of the development of the pituitary gland, where individual cell lineages vary in their responsiveness to this transcription factor (Suh et al., 2002). PITX2 may also play a role in successful innervation of the EOMs, by guiding motor neuron axons to their targets. Three somatomotor neurons perform this innervation. The oculomotor nerve innervates the superior rectus, inferior rectus, medial rectus, and inferior oblique, The trochlear nerve innervates the superior oblique muscle, and The abducens nerve innervates the lateral rectus muscle (Chandrasekhar., 2004). EOMs are not classified according to the typical fibre type model. Instead, they can be classified into six distinct fibre types based on their location i.e. distributed in orbital or global layer, if they are innervated by a single or multiple nerves, and layer, if they are innervated by a single or multiple nerves, and mitochondrial/oxidative enzyme content. This scheme allows classification into orbital singly, orbital multiply, global red singly, global intermediate singly, global pale singly, and global multiply innervated fibre types (Porter and Baker., 1996). A highly specialised form of EOM is found in Istiophoriformes, a group of saltwater fish, commonly known as billfish. These fish have modified superior rectus muscles that function as a heat generating organ to provide warming to the brain. This muscle inserts normally into

the eye, but as it moves towards the brain, it transitions from normal muscle, to heat generating. These specialised muscle cells have increased mitochondria and sarcoplasmic reticulum, but no contractile filaments. It is thought that the  $ca^{2+}$  cycling of the SR that normally results in muscle contraction, is instead here used to generate heat (Block and Franzini-Armstrong., 1988).

A distinctive feature of the EOM proteome is the lifelong expression of protein isoforms that are typically considered to be developmental. Examples of these isoforms include the fetal acetyl-choline receptor, and polysialated neural cell adhesion molecule (Andrade et al., 2000). At the neuromuscular junction, nicotinic acetylcholine receptor, nAChR, binding with acetylcholine triggers the opening of a central pore within the nAChR, permitting the influx of cations. This influx leads to the depolarization of the muscle membrane, and Subsequently, to the activation of voltage-gated sodium channels, initiating the propagation of an action potential along the muscle. Ultimately, this cascade of events culminates in muscle contraction (Simon-Keller et al., 2013). Adult nAChRs are much more conducive than their fetal counterparts (Mishina et al., 1986). Both isoforms are expressed in adult EOMs (Horton et al., 1993). The decreased conductance of the fetal nAChR isoform may contribute to the efficient calcium handling ability of the EOM. Other factors may include the expression of ryanodine receptor 3, along with cardiac calsequestrin and the  $\alpha 1$  subunit of the cardiac dihydropyridine receptor, which were identified in a study characterising human EOM (Sekulic-Jablanovic et al., 2015).

Cell adhesion molecules are a large family of proteins that work to form and maintain tissue structure (Edelman and Crossin., 1991). Neural Cell adhesion molecule, N-CAM, is a major member of this family, which mediates adhesion between neurons and other neurons, and between neurons and muscle (Cunningham et al., 1987). Alternative gene splicing results in various forms of N-CAM, and further differentiation occurs due to post-translational modifications, such as the attachment of polysialic acid, PSA, to the cell surface of N-CAM (Yang et al., 1992). The amount of this carbohydrate polymer present, correlates negatively with the adhesivity of the protein. This reduced adhesivity makes PSA-N-CAM better for permitting cellular changes. PSA-N-CAM has often been called embryonic N-CAM, due to its predominant expression in embryonic and post-natal stages of development (Bonfanti and Theodosis., 1994). The continuous expression of PSA-N-CAM in adult EOM is likely to be a factor in the increased structural remodelling and plasticity of this muscle. It has been hypothesised that the extraocular muscles remain in their immature state, including their expression of developmental proteins due to an activated population of satellite cells, that may

result in myonuclear addition to uninjured EOMs (McLoon and Wirtschafter., 2002). The presence of these activated satellite cells appears to be life long, as they were found in the eyes of donors aged 74, and 82 respectively (McLoon and Wirtschafter., 2003). This likely also explains EOMs resistance to age related sarcopenia (McMullen et al., 2009).

### **7.2.1 Sarcomeric proteins found in the EOM**

The proteomic analysis of WT EOM outlined in chapter 5, established the presence of 15 distinct myosin heavy chains. When compared to the previously established proteome of WT diaphragm muscle (Murphy et al., 2019), An increased expression of multiple myosin isoforms was observed in the EOM, including MYH2, MYH13, MYH14, MYH15, and myosin light polypeptide 6, MYL6. In addition to these isoforms of myosin, slow cardiac alpha-actin-1, ACTC1, was also increased. MYH2a is one of the predominant forms of MHC in adult skeletal muscle, and it is typically associated with the fast myofiber type 2a (Pette and Staron., 2000). These fast twitching and relatively fatigue resistant fibres are likely upregulated to help the EOM with its rapid movements, and to sustain those movements for extended periods. Global red singly innervated fibres express only type 2a myosin (Spencer and Porter., 2006). Even extremely fast twitching EOM displays considerable resistance to fatigue, and the oxidative capacity of EOM has been found to be nine times that of fast twitching adductor magnus muscle and two times higher than in the slow-twitch soleus muscle (Asmussen et al., 2008).

In 1985, an MHC protein specific to the extraocular muscle was identified (Wieczorek et al., 1985). This was later termed “extraocular myosin/MYH13”. This specialised form of myosin was subsequently found to be present in laryngeal muscles, which contract rapidly, and have low twitch tensions, similar to EOM (Briggs and Schachat., 2000). In the clawed frog, *Xenopus Laevis*, a homologous isoform, named laryngeal myosin is only present in larynx of the males. This extremely fast twitching isoform is needed to facilitate the mating song. Administration of the androgen dihydrotestosterone to female and juvenile males facilitates the fibre type transition to fast twitch, while castration of juvenile males will block this transition from naturally occurring. This reflects the ability of androgens to influence myofibres (Catz et al., 1992).

While the coding gene for myh13, *myh13* is a member of the fast/developmental myosin gene cluster, it is quite distinct from other members. This gene spans 64kb, which is nearly twice the length of any other member. In addition to this, the exon organisation of *myh13* does not reflect the patterns seen in most members (Schachat and Briggs., 2002). The *myh13* loci is associated with formal thought disorder AKA disorganised speech, which is a key indicator of

schizophrenia (Wang et al., 2012). This association is possibly due to the laryngeal expression of *myh13*. The *myh13* gene has also been investigated as a potential candidate gene for association with dementia (Cacabelos et al., 2012). Fish skeletal muscle is composed of different fibre layers. These are fast white, and slow red. A recent study characterising the *myh* genes of Chinese perch fish found that they expressed three forms of *myh13*, namely, *myh13.1*, *myh13.2*, and *myh13.3*. This study identified *myh13.2* as the predominant form of *myh* expressed in the fast white muscle, making up >90% of the *myh* expression, with *myh13.3* also being highly expressed here (Chen et al., 2023). Another study investigating Atlantic Cod, found a substantial downregulation of *myh13* during the spawning period of this fish. In this period, a significant decrease in muscle mass can be observed, as large amounts of energy are being used in the process of gonad maturation (Nagasawa et al., 2016).

Saccades are quick shifts in gaze orientation. The extremely fast MYH13 is thought to drive these rapid changes of direction. Myh13 expression in EOM is localised to the innervation zone, it is likely that transcription of this protein is regulated by motor nerves. In these fibres, MYH13 is never uniquely expressed. Instead it usually colocalises with MYH2b, the fastest of the limb and trunk myosins, indicating a functional overlap of these two isoforms in powering rapid saccades (Briggs and Schachat., 2002). The dependence of these myosins, in particular, *myh13* on neural activity was established in a study where a rat was paralysed with botulinum toxin. One month after paralysis, the MYH2b isoform had been massively decreased, while MYH13 had nearly disappeared altogether. Eight months following paralysis, MYH2b levels had increased, while MYH13 levels remained below detection levels (Kranjc et al., 2001). The Myosin heavy chain 14, MYH14, gene is also known as *MYH7b*. The product of this gene is termed “slow tonic myosin” it was discovered relatively recently, along with MyHC15 and MyHC16. These myosins, classed as “ancient/ancestral myosins” exist outside of the regular myosin gene clusters on chromosome’s 14 and 17. Instead, these genes are each mapped to their own chromosomes, these being 20, 3, and 7 respectively (Desjardins et al., 2002). Intron 19 of the MYH14 gene encodes the microRNA, miR-499, which belongs to a family of myosin located microRNAs called MyomiRs. The seed region of this microRNA shares 6 bases with miR-208, implying possible shared functions, such as facilitating the switch in myosin types (van Rooij et al., 2008). Increased levels of miR-499 in circulation have recently been identified as a potential biomarker for acute myocardial infarction (Xin et al., 2016). Studies into the expression of the *myh14* gene found that while it is expressed at a transcriptional level in cardiac and in slow skeletal muscles like the soleus, the protein product is only found to be present in slow-tonic fibres of the EOM, and in bag fibres of spindles. No transcripts of *myh15*

were found outside of the EOM, and the associated protein is present in the majority of fibres located in the orbital layer of the EOM, and in the extracapsular region of spindle bag fibres (Rossi et al., 2010). The muscle spindle acts as the primary stretch receptor of the muscle, they convey information about the length of a Muscle to the central nervous system (Hunt., 1990). Spindles found in the EOM differ from those found in most skeletal muscle (Bruenech and Ruskell., 2001).

A myosin hexamer contains four light chains, two being regulatory, and two being essential. Both forms of MLC belong to the EF-hand calcium binding protein superfamily, which also includes the likes of troponin C, calmodulin, and parvalbumin (Strynadka and James., 1989). Essential light chains have lost the ability to bind with  $Ca^{2+}$ , apart from the myosin ELC of molluscs, whose muscle contraction is regulated by direct binding of  $Ca^{2+}$  to myosin, instead of the tropomyosin–troponin system used in vertebrate muscle (Houdusse and Cohen., 1996). Essential light chains contribute to structural stability of the myosin structure (Timson et al., 1999). They also have an important role in muscle shortening speeds, and removal results in a sixfold decrease in actin sliding velocity. Removal of both classes of MLC resulted in a 10 fold decrease (Lowey et al., 1993). A different study demonstrated that while the removal of RLC has little impact on isometric force production, removing ELC resulted in at least a 50% reduction (VanBuren et al., 1994).

The only myosin light chain protein found to have an increased expression in EOM over diaphragm muscle is the myosin light chain MLC-3, encoded by the *myl6* gene. This protein is believed to be confined to smooth muscle (Heissler and Sellers., 2014). It plays an important role in contraction of smooth muscle, and irregular splicing events can impair this contractile ability (Koi et al., 2007). MLC-3 mediates the movement and morphological changes of cells, through its interaction with actin (Yoshinari et al., 2022). The increased expression this isoform suggests that the EOM display some features characteristic of smooth muscle, which is a topic that has been investigated previously (Ko et al., 2014).

The only non-myosin protein found to be increased in EOM compared to diaphragm muscle, is slow cardiac alpha-actin-1, ACTC1. This is one of six known actin isomers, and one of the four “muscle isomers”, with the other two being cytoplasmic (Vandekerckhove and Weber., 1978). Cardiac actin and skeletal actin, known as  $\alpha$ -cardiac and  $\alpha$ -skeletal, respectively, are highly homologous, with only four amino acid residue difference between them. These two actins are co-expressed in both cardiac and skeletal muscle, with cardiac being the primary isoform expressed in embryonic and developing muscle, before skeletal becomes the predominant version expressed in adult muscle (Vandekerckhove et al., 1986). Mutations in the skeletal muscle  $\alpha$ -actin gene

can result in various myopathies, including actin myopathy and nemaline myopathy (Nowak et al., 2013). The EOM remain functionally unaffected in these diseases, as they do in DMD (Ryan et al., 2001). Ravenscroft *et al* have suggested that this sparing is due to greater expression levels of  $\alpha$ -cardiac than  $\alpha$ -skeletal in the EOM, and have shown that up to 73% of the total striated actin present in the EOM belongs to the cardiac isoform (Ravenscroft et al., 2008). Actc1 can also protect cells against oxidative stress (Angelini et al., 2020), which could further serve to protect the EOMs.

### **7.2.2 EOM proteomic changes in dystrophinopathy**

The comparative proteomic analysis of wild type and dystrophic mice EOM found various proteins to be increased and decreased respectively in the EOM. In general, an increase in glycolytic enzymes and molecular chaperones was observed, while mitochondrial enzymes were decreased.

The protein that displayed the greatest increase was glyceraldehyde-3-phosphate dehydrogenase, GAPDH. This tetrameric glycolytic enzyme had an 18.45-fold increase in the dystrophic EOM. During the process of glycolysis, GAPDH catalyses the oxidation and phosphorylation of D-glyceraldehyde 3-phosphate to yield 1,3-bisphosphoglycerate and NADH (Canellas and Cleland., 1991). GAPDH is also involved in glucose transport, through binding of the major glucose carrier in muscle, glucose transporter 4 ,GLUT4, and regulates its activity (Zaid et al., 2009). While GAPDH has long been considered a classical component in energy production through the glycolytic pathway, it also has many functions outside of glycolysis. Microtubules are a vital component of the cytoskeletal in all eukaryote cells. They act as tracks for motor proteins such as kinesin and dynein to move along (Sweeney and Holzbaur, 2018). GAPDH has been shown to bind to the protein tubulin, and aid in the polymerisation of tubulin into bundles, generating the microtubules (Huitorel and Pantaloni., 1985). The multifunctional GAPDH is implicated in DNA repair also. The enzyme, uracil DNA glycosylase, UDG, functions to remove uracil residues from DNA by cleaving the base-sugar glycosyl bond. This results in the formation of an apyrimidinic site in the DNA, needed for DNA repair. GAPDH has been shown to exhibit UDG activity, to remove uracil from DNA (Baxi and Vishwanatha., 1995). GAPDH is also involved in apoptosis. Although the relevant homo-tetramer of GAPDH is too large to enter the cell nucleus, s-nitrosylation of GAPDH allows it to bind to the E3 ubiquitin ligase Siah1, which then translocates into the nucleus. GAPDH mediated stabilisation of Siah1, allowing to break down nuclear targets and cause cell death (Hara et al., 2005). A complete list of GAPDH's diverse functions has been previously

reviewed (Sirover., 1999, Nicholls et al., 2012). The increase of GAPDH in dystrophic EOM suggests a shift from oxidative to a more glycolytic energy pathway, but it could be the case that this increased expression also contributes to the sparing of the eye muscles from disease due to the secondary functions. There is evidence of channels forming between dehydrogenase molecules. One dehydrogenase that GAPDH has been shown to interact with is lactate dehydrogenase, LDH, (Svedruzić and Spivey., 2006). This glycolytic enzyme was also increased in dystrophic EOM. Lactate dehydrogenase catalyses the reversible transformation between the end products of glycolysis, pyruvate and lactate. LDH is a tetramer formed by four polypeptide chains. These chains are coded for by separate genes, H or M, with different combinations resulting in different LDH isoenzymes (Koukourakis et al., 2003). An abnormal LDH isoenzyme pattern is often observed in DMD muscle (Pearson et al., 1965).

Enolase is another glycolytic enzyme seen to be increased in *mdx-4cv* EOM. In glycolysis, this enzyme is responsible for the formation of Phosphoenolpyruvate from 2-phosphoglycerate. Alpha-enolase was the specific isoform that displayed a greater expression. Enolase is a homo or hetero dimer, made up of  $\alpha$ ,  $\beta$ , or  $\gamma$  subunits. The embryonic form,  $\alpha\alpha$ , remains expressed in most adult tissues, whereas  $\gamma$ -enolase is only found in neuron and neuroendocrine tissues, while  $\beta$ -enolase is predominantly expressed in muscle (Keller et al., 2000). Like GAPDH,  $\alpha$ -enolase is described as a “moonlighting protein”, one that has multiple functions (Jeffery., 1999). The plasminogen activation/plasmin system is a key component of ECM remodelling through its ability to degrade ECM proteins like fibronectin. It can also indirectly degrade collagens through the activation of matrix metalloproteinases. Latent forms of growth factors can also be activated by plasmin (Irigoyen et al., 1999).  $\alpha$ -enolase acts as a cell-surface receptor for plasminogen (Redlitz et al., 1995). After interaction with  $\alpha$ -enolase, plasminogen is better able to be converted into its activated form, plasmin. In addition to this activation, plasmin receives protection from its primary inhibitor,  $\alpha$ 2-antiplasmin (Díaz-Ramos et al., 2012). In addition enolases role in the glycolytic process, it is also involved in muscle development, and is an early marker of myogenesis (Fougerousse et al., 2001).

Following on from GAPDH, the two proteins that show the largest increase in dystrophic EOM are both heat shock proteins, namely heat shock protein 1 $\beta$ , and heat shock cognate 71 kDa protein. The heat shock proteins are a ubiquitous family of highly conserved molecular chaperones. Originally discovered and named for their activation following temperature shock, further studies soon implicated them in responses to many forms of cellular stress (Ritossa., 1964). These stressors can cause proteins to misassemble, forming nonfunctional structures.

Molecular chaperone proteins are generally involved in regulating correct protein folding (Ellis., 2007).

Heat shock protein 1 $\beta$ , also known as hsp27, is a multifunctional protein. It is often associated with apoptosis and autophagy (Shan et al., 2021). In DMD and other hereditary myopathies, Hsp27 translocates and binds to titin in the sarcomeric I-band. This association protects the structural integrity and function of the giant spring like protein, titin (Unger et al., 2017). HSP27 also functions as an antioxidant, lowering the levels of reactive oxygen species (Vidyasagar et al., 2012). The upregulation of this protective protein in the EOM muscle is in stark contrast to a previous proteomic study of aged dystrophic tibialis anterior muscle, which showed a decreased abundance of Hsp27 (Carberry et al., 2012). This drastic difference in protein expression highlights the role Hsp27 plays in protection from dystrophin associated muscle degeneration. Hsp70 is an important factor in cell homeostasis and survival (Silva et al., 2021). Mice with transgenically overexpressed Hsp70 display a natural resistance to age associated muscle weakness (McArdle et al., 2004). Using Hsp70 agonists has been suggested as a potential therapeutic intervention for DMD (Cosemans et al., 2022).

### **7.3. Analysing the dystrophic urine proteome**

Body fluids can be used in proteomic biomarker identification studies. Biofluids that are readily available and can be collected non-invasively are particularly useful (Csósz et al., 2017). Urine fits into these parameters and the protein constituents of this excretion can reflect disease associated bodily alterations. The kidneys produce urine through the process of ultrafiltration. The human kidney can be divided into two sections, the glomerulus, which filters the plasma to create the “primitive” urine, and the renal tubule, which reabsorbs most of this urine. Over 99% is reabsorbed, and the remaining urine travels to the bladder through the ureter (Decramer, et al., 2018). Urinary proteins are a mixture of plasma and kidney proteins, with approximately 30% coming from the plasma, and 70% from the kidney (Thongboonkerd and Malasit., 2005). In the absence of a urological disease, an increase in abundance of certain proteins found in the urine, could make them prime candidates for proteomic biomarkers of systemic degeneration. It is hoped that in the future, improved urine based biopsy techniques will bring urinary studies to the forefront of proteomic biomarker investigations, thus eliminating the need for invasive and potentially harmful biopsies. The protein concentration of the giant muscle protein, titin, was present in *mdx-4cv* urine. This discovery is in agreement with previous studies screening urine from DMD boys (Rouillon et al., 2014). A novel finding of this current study, however, was the identification of titin peptides originating from across

the entire protein sequence. Previously the observed fragments were only from the extreme ends of titin. Titin is a half sarcomere spanning protein that functions as a molecular spring. The I-band of titin connects the end of the thick filament to the z-disk wall. Alternative splicing to this I-band results in various isoforms of titin. In general, the faster a muscle is, the shorter its titin isoform will be. The structure of titin consists of 244 protein repeat domains. Most of these are fibronectin or immunoglobulin like domains. The list of 21 proteins with an increased concentration in *mdx-4cv* urine also includes fibronectin, and different immunoglobulin chains. Both isoforms of nidogen, 1 and 2, were found exclusively in the *mdx-4cv* mice urine. These glycoproteins are integral components of the basement membrane, BM. The BM is a specialised thin layer of the ECM that underlies all epithelial cells and surrounds fat cells, muscle, and peripheral nerves (Kleinman et al., 1987). Nidogens are known to bind with numerous proteins including various other basement membrane components. These being laminin, collagen IV, perlecan, and fibulin (Kramer., 2005). Nidogens are considered adaptor proteins of the BM because of their range of binding partners (Ho et al., 2008). The two nidogen isoforms have a similar structure, comprised of three globular domains, connected by rod like regions. The main difference between these proteins is their length, with nidogen-1 being 150kda, and nidogen-2 200kda (Kohfeldt et al., 1998). Knocking out either *nid1* or *nid2* does not affect BM development, simultaneous deletion of both genes results in death during embryogenesis, due to heart and lung defects (Bader et al., 2005). Nidogen-1 has a role in formation of skeletal myotubes (Funanage et al., 1992, Grefte et al., 2016). Nidogen-2 is concentrated in synapses of adult muscle, where it associates with the basal lamina. This isoform is responsible for maintenance and maturation of the synapse (Fox et al., 2008). Nidogen-1 has previously been shown to be significantly decreased in the heart of aged dystrophic mice (Holland et al., 2013). The STRING analysis for this study showed that the two nidogen isoforms are connected to Fibronectin on one side, and on the other end of this cluster is vascular cell adhesion protein 1, VCAM1. VCAM1 belongs to the immunoglobulin superfamily of proteins, and is generally expressed on the side of endothelial cells under inflammatory conditions, where it mediates the rolling of lymphocytes (Ley et al., 2007). A study using pluripotent stem cell derived cardiomyocytes from DMD patients found that VCAM was reduced compared to a control group, and that inducing expression of this protein improves cardiac contractility, mitochondrial respiration, and sarcomere structure, and reduces ROS levels (Li et al., 2021). Interestingly, this study used traditional Chinese medicine herbs to induce VCAM1 expression. Gavina et al, in 2006 showed that following exercise, the expression of VCAM1 is increased in dystrophic muscle, and that this higher expression level

greatly increased the adherence of implanted stem cells.

Myc box-dependent-interacting protein 1, also known as bridging integrator-1, BIN1, is another protein that was found only in the urine of mdx mice. This membrane remodeling protein is encoded for by the *bin1* gene. Mutations to this gene result in centronuclear myopathies which are characterised by small myofibres with centrally placed nuclei (Pierson et al., 2005). Mutations are also associated with myotonic dystrophy (Fugier et al., 2011). The N-terminal located BAR domain of this protein induces and recognises membrane curvature (Peter et al., 2004). Bin-1 is localised at T-tubules and is important for their development. Mutations to the orthologues drosophila gene *Amphiphysin* result in a severely disrupted T-tubule/sarcoplasmic reticulum system (Razzaq et al., 2001). While various isoforms of BIN-1 exist, the phosphoinositide-binding domain is found almost exclusively in skeletal muscle isoforms (Toussaint et al., 2011). Overexpression of this domain leads to a greater formation of t-tubules, indicating that this domain promotes membrane remodelling (Lee et al., 2002). The unstable membrane, and impaired calcium handling seen in dystrophin deficient muscle likely results in a breakdown of this protein, which is then excreted through the urine. The resulting deficiency of BIN-1 in myofibres could possibly contribute to the central nucleation often seen in dystrophic fibres, as this protein is also crucial to proper positioning of the nucleus by linking the nuclear envelope protein, nesprin, to the actin and microtubule cytoskeleton (D'Alessandro et al., 2015). Parvalbumin alpha is another protein that was detected exclusively in the mdx mice urine. This is a small cytosolic protein of approximately 12kda. It belongs to the EF-hand family of calcium binding proteins. This family of proteins is characterised by two helices linked together by a loop. The EF hand motif is responsible for binding to  $ca^{2+}$  ions (Permyakov and Uversky., 2022). Parvalbumins are linked to various cell processes, one of which is to end muscle contraction. This is performed by transferring  $ca^{2+}$  ions from its family member, troponin-c, to the SERCA pump where they will be redistributed back into the SR following muscle contraction (Arif., 2009). In addition to troponin-c, parvalbumin also shares a high sequence homology with myosin alkali light chains (Weeds and McLachlan., 1974). In mdx mice also deficient in parvalbumin, a slightly more severe phenotype was observed than mdx alone. The most prominent change being a greater development of fibrosis (Raymackers et al., 2003) Parvalbumin- $\alpha$  in the urine has previously been identified as a marker of skeletal muscle toxicity (Dare et al., 2002). The finding that Angiopoietin-related protein 2, ANGPTL2, was excreted solely in the *mdx-4cv* urine is possibly related to the cardiac trouble associated with dystrophinopathy. Levels of this protein in circulation Increase in Humans and Mice Exhibiting Cardiac Dysfunction (Tian et al., 2018). It is also possible that this pro-angiogenic

protein was upregulated in the fibrotic tissue of the *mdx-4cv* mice, where vascular remodelling is critical to fibrogenesis (Wynn., 2007). ANGPTL2 expression is suppressed by angiotensin II (Wang et al., 2020), Angiotensin-converting enzyme, which converts angiotensin I to angiotensin II, was decreased in the *mdx-4cv* urine in this study. It is possible that the altered expression of these two proteins is related.

Ubiquitin-60S ribosomal protein L40, UBL40, was increased 4.4 fold in the *mdx-4cv* mice urine. This efficient fusion protein is comprised of ubiquitin at the N-terminus, and the 60S ribosomal protein L40 at the c-terminus. Ubl40 is a member of the ubiquitin proteasome system, which is responsible for degradation of a large number of cellular proteins. One of the many cellular processes that it is involved in, is the cellular response to stress (Schwartz and Ciechanover., 2009). While the ubiquitin segment of this protein is involved in protein degradation, the RPL40 subunit likely contributes to protein synthesis, through recruitment of the translation elongation factor eEF2 (Fernández-Pevida et al., 2012). UBL40 has been shown to be downregulated in a rat model of parkinsons disease, where it is needed to ubiquilate HSP90 (Tiwari et al., 2022), It was also found to be absent on the striatum of a rat model of neurodegeneration, compared to a wt control group (Vincenzetti et al., 2016). mRNA levels of UBA52 were significantly reduced in the ipsilateral hippocampus of a rat seven days following traumatic brain injury (Yao et al., 2007). It could be the case that this protein was found to be expressed higher in the dystrophic mice urine due to some DMD associated kidney damage, as it was previously identified as urinary marker for nephrotic syndrome (Wang et al., 2017). Cadherin-13 was increased just over twofold in the *mdx-4cv* urine. This coincides with our proteomic analysis of aged and dystrophic diaphragm muscle, where this protein was also increased.

## Chapter 8

### **Conclusion and future research**

DMD is a complex and severe disease. Through the use of biochemical extraction and separation methodology, controlled protein digestion and mass spectrometry, it is possible to gain a better understanding of the complex proteomic alterations associated with the pathology of DMD. Gel electrophoresis, immunoblotting and immunofluorescence microscopy can be conveniently used for verification experiments. The end goal of these research endeavours is the identification of novel protein biomarkers. Hopefully, the results presented in this thesis will contribute to the pool of knowledge about DMD proteomics. Future research would involve further comparative studies, along with characterisation studies of novel muscles. One such project is currently underway in our lab, attempting to characterise the naturally protected muscles of the *mdx-4cv* tongue.

## Chapter 9

### Bibliography

- ABMAYR, S., GREGOREVIC, P., ALLEN, J. M. & CHAMBERLAIN, J. S. 2005. Phenotypic improvement of dystrophic muscles by rAAV/microdystrophin vectors is augmented by Igf1 codelivery. *Mol Ther*, 12, 441-50.
- ABRIGO, J., SIMON, F., CABRERA, D., CORDOVA, G., TROLLET, C. & CABELLO-VERRUGIO, C. 2018. Central Role of Transforming Growth Factor Type Beta 1 in Skeletal Muscle Dysfunctions: An Update on Therapeutic Strategies. *Curr Protein Pept Sci*, 19, 1189-1200.
- ACCILI, D., NAKAE, J., KIM, J. J., PARK, B. C. & ROTHER, K. I. 1999. Targeted gene mutations define the roles of insulin and IGF-I receptors in mouse embryonic development. *J Pediatr Endocrinol Metab*, 12, 475-85.
- ADAM, M. P., FELDMAN, J., MIRZAA, G. M., PAGON, R. A., WALLACE, S. E., BEAN, L. J. H., GRIPP, K. W. & AMEMIYA, A. 1993. GeneReviews.
- ADAMS, G. R. & BAMMAN, M. M. 2012. Characterization and regulation of mechanical loading-induced compensatory muscle hypertrophy. *Compr Physiol*, 2, 2829-70.
- ANDERSON, J. L., HEAD, S. I., RAE, C. & MORLEY, J. W. 2002. Brain function in Duchenne muscular dystrophy. *Brain*, 125, 4-13.
- ANDRADE, F. H., PORTER, J. D. & KAMINSKI, H. J. 2000. Eye muscle sparing by the muscular dystrophies: lessons to be learned? *Microsc Res Tech*, 48, 192-203.
- ANGELINI, A., GOREY, M. A., DUMONT, F., MOUGENOT, N., CHATZIFRANGKESKOU, M., MUCHIR, A., LI, Z., MERICKSKAY, M. & DECAUX, J. F. 2020. Cardioprotective effects of  $\alpha$ -cardiac actin on oxidative stress in a dilated cardiomyopathy mouse model. *FASEB J*, 34, 2987-3005.
- ARIF, S. H. 2009. A Ca(2+)-binding protein with numerous roles and uses: parvalbumin in molecular biology and physiology. *Bioessays*, 31, 410-21.
- ARNOLD, L., HENRY, A., PORON, F., BABA-AMER, Y., VAN ROOIJEN, N., PLONQUET, A., GHERARDI, R. K. & CHAZAUD, B. 2007. Inflammatory monocytes recruited after skeletal muscle injury switch into antiinflammatory macrophages to support myogenesis. *J Exp Med*, 204, 1057-69.
- ARNOLD, S. J. & ROBERTSON, E. J. 2009. Making a commitment: cell lineage allocation and axis patterning in the early mouse embryo. *Nat Rev Mol Cell Biol*, 10, 91-103.

- ASMUSSEN, G., PUNKT, K., BARTSCH, B. & SOUKUP, T. 2008. Specific metabolic properties of rat oculorotatory extraocular muscles can be linked to their low force requirements. *Invest Ophthalmol Vis Sci*, 49, 4865-71.
- AYALON, G., DAVIS, J. Q., SCOTLAND, P. B. & BENNETT, V. 2008. An ankyrin-based mechanism for functional organization of dystrophin and dystroglycan. *Cell*, 135, 1189-200.
- BADER, B. L., SMYTH, N., NEDBAL, S., MIOSGE, N., BARANOWSKY, A., MOKKAPATI, S., MURSHED, M. & NISCHT, R. 2005. Compound genetic ablation of nidogen 1 and 2 causes basement membrane defects and perinatal lethality in mice. *Mol Cell Biol*, 25, 6846-56.
- BALACHANDER, N., MASTHAN, K. M., BABU, N. A. & ANBAZHAGAN, V. 2015. Myoepithelial cells in pathology. *J Pharm Bioallied Sci*, 7, S190-3.
- BANDI, S., SINGH, S. M. & MALLELA, K. M. 2015. Interdomain Linker Determines Primarily the Structural Stability of Dystrophin and Utrophin Tandem Calponin-Homology Domains Rather than Their Actin-Binding Affinity. *Biochemistry*, 54, 5480-8.
- BARRESI, R. & CAMPBELL, K. P. 2006. Dystroglycan: from biosynthesis to pathogenesis of human disease. *J Cell Sci*, 119, 199-207.
- BARTON, E. R., MORRIS, L., MUSARO, A., ROSENTHAL, N. & SWEENEY, H. L. 2002. Muscle-specific expression of insulin-like growth factor I counters muscle decline in mdx mice. *J Cell Biol*, 157, 137-48.
- BAXI, M. D. & VISHWANATHA, J. K. 1995. Uracil DNA-glycosylase/glyceraldehyde-3-phosphate dehydrogenase is an Ap4A binding protein. *Biochemistry*, 34, 9700-7.
- BEAN, B. P. 1989. Classes of calcium channels in vertebrate cells. *Annu Rev Physiol*, 51, 367-84.
- BEARD, N. A. & DULHUNTY, A. F. 2015. C-terminal residues of skeletal muscle calsequestrin are essential for calcium binding and for skeletal ryanodine receptor inhibition. *Skelet Muscle*, 5, 6.
- BELANTO, J. J., MADER, T. L., ECKHOFF, M. D., STRANDJORD, D. M., BANKS, G. B., GARDNER, M. K., LOWE, D. A. & ERVASTI, J. M. 2014. Microtubule binding distinguishes dystrophin from utrophin. *Proc Natl Acad Sci U S A*, 111, 5723-8.
- BELLINGER, A. M., REIKEN, S., CARLSON, C., MONGILLO, M., LIU, X., ROTHMAN, L., MATECKI, S., LACAMPAGNE, A. & MARKS, A. R. 2009. Hypernitrosylated

- ryanodine receptor calcium release channels are leaky in dystrophic muscle. *Nat Med*, 15, 325-30.
- BERGER J., SZTAL T., CURRIE P. D. (2012). Quantification of birefringence readily measures the level of muscle damage in zebrafish. *Biochem. Biophys. Res. Commun.* 423, 785–788
- BHAT, S. S., ALI, R. & KHANDAY, F. A. 2019. Syntrophins entangled in cytoskeletal meshwork: Helping to hold it all together. *Cell Prolif*, 52, e12562.
- BIDANSET, D. J., GUIDRY, C., ROSENBERG, L. C., CHOI, H. U., TIMPL, R. & HOOK, M. 1992. Binding of the proteoglycan decorin to collagen type VI. *J Biol Chem*, 267, 5250-6.
- BISCHOFF, R. & SCHLÜTER, H. 2012. Amino acids: chemistry, functionality and selected non-enzymatic post-translational modifications. *J Proteomics*, 75, 2275-96.
- BITTEL, D. C., CHANDRA, G., TIRUNAGRI, L. M. S., DEORA, A. B., MEDIKAYALA, S., SCHEFFER, L., DEFOUR, A. & JAISWAL, J. K. 2020. Annexin A2 Mediates Dysferlin Accumulation and Muscle Cell Membrane Repair. *Cells*, 9.
- BLOCK, B. A. & FRANZINI-ARMSTRONG, C. 1988. The structure of the membrane systems in a novel muscle cell modified for heat production. *J Cell Biol*, 107, 1099-112.
- BOLAÑOS, P. & CALDERÓN, J. C. 2022. Excitation-contraction coupling in mammalian skeletal muscle: Blending old and last-decade research. *Front Physiol*, 13, 989796.
- BONFANTI, L. & THEODOSIS, D. T. 1994. Expression of polysialylated neural cell adhesion molecule by proliferating cells in the subependymal layer of the adult rat, in its rostral extension and in the olfactory bulb. *Neuroscience*, 62, 291-305.
- BONIFATI, M. D., RUZZA, G., BONOMETTO, P., BERARDINELLI, A., GORNI, K., ORCESI, S., LANZI, G. & ANGELINI, C. 2000. A multicenter, double-blind, randomized trial of deflazacort versus prednisone in Duchenne muscular dystrophy. *Muscle Nerve*, 23, 1344-7.
- BRIGGS, M. M. & SCHACHAT, F. 2000. Early specialization of the superfast myosin in extraocular and laryngeal muscles. *J Exp Biol*, 203, 2485-94.
- BRIGGS, M. M. & SCHACHAT, F. 2002. The superfast extraocular myosin (MYH13) is localized to the innervation zone in both the global and orbital layers of rabbit extraocular muscle. *J Exp Biol*, 205, 3133-42.

- BRILLANTES, A. B., ONDRIAS, K., SCOTT, A., KOBRINSKY, E., ONDRIASOVÁ, E., MOSCHELLA, M. C., JAYARAMAN, T., LANDERS, M., EHRLICH, B. E. & MARKS, A. R. 1994. Stabilization of calcium release channel (ryanodine receptor) function by FK506-binding protein. *Cell*, 77, 513-23.
- BRODERICK, M. J. & WINDER, S. J. 2005. Spectrin, alpha-actinin, and dystrophin. *Adv Protein Chem*, 70, 203-46.
- BRUENECH, J. R. & RUSKELL, G. L. 2001. Muscle spindles in extraocular muscles of human infants. *Cells Tissues Organs*, 169, 388-94.
- BUCHWALD, P. & BODOR, N. 2004. Soft glucocorticoid design: structural elements and physicochemical parameters determining receptor-binding affinity. *Pharmazie*, 59, 396-404.
- BULFIELD, G., SILLER, W. G., WIGHT, P. A. & MOORE, K. J. 1984. X chromosome-linked muscular dystrophy (mdx) in the mouse. *Proc Natl Acad Sci U S A*, 81, 1189-92.
- BURKIN, D. J., WALLACE, G. Q., MILNER, D. J., CHANEY, E. J., MULLIGAN, J. A. & KAUFMAN, S. J. 2005. Transgenic expression of  $\alpha 7\beta 1$  integrin maintains muscle integrity, increases regenerative capacity, promotes hypertrophy, and reduces cardiomyopathy in dystrophic mice. *Am J Pathol*, 166, 253-63.
- BURNS, D. P., DRUMMOND, S. E., BOLGER, D., COISCAUD, A., MURPHY, K. H., EDGE, D. & O'HALLORAN, K. D. 2019. N-acetylcysteine Decreases Fibrosis and Increases Force-Generating Capacity of. *Antioxidants (Basel)*, 8.
- BUTLER-BROWNE, G. S., ERIKSSON, P. O., LAURENT, C. & THORNELL, L. E. 1988. Adult human masseter muscle fibers express myosin isozymes characteristic of development. *Muscle Nerve*, 11, 610-20.
- CACABELOS, R., MARTÍNEZ, R., FERNÁNDEZ-NOVOA, L., CARRIL, J. C., LOMBARDI, V., CARRERA, I., CORZO, L., TELLADO, I., LESZEK, J., MCKAY, A. & TAKEDA, M. 2012. Genomics of Dementia: APOE- and CYP2D6-Related Pharmacogenetics. *Int J Alzheimers Dis*, 2012, 518901.
- CANELLAS, P. F. & CLELAND, W. W. 1991. Carbon-13 and deuterium isotope effects on the reaction catalyzed by glyceraldehyde-3-phosphate dehydrogenase. *Biochemistry*, 30, 8871-6.
- CARBERRY, S., ZWEYER, M., SWANDULLA, D. & OHLENDIECK, K. 2012. Profiling of age-related changes in the tibialis anterior muscle proteome of the mdx mouse model of dystrophinopathy. *J Biomed Biotechnol*, 2012, 691641.

- CATTERALL, W. A. 1988. Structure and function of voltage-sensitive ion channels. *Science*, 242, 50-61.
- CATZ, D. S., FISCHER, L. M., MOSCHELLA, M. C., TOBIAS, M. L. & KELLEY, D. B. 1992. Sexually dimorphic expression of a laryngeal-specific, androgen-regulated myosin heavy chain gene during *Xenopus laevis* development. *Dev Biol*, 154, 366-76.
- CHANDRASEKHAR, A. 2004. Turning heads: development of vertebrate branchiomotor neurons. *Dev Dyn*, 229, 143-61.
- CHANG, N. C., CHEVALIER, F. P. & RUDNICKI, M. A. 2016. Satellite Cells in Muscular Dystrophy - Lost in Polarity. *Trends Mol Med*, 22, 479-496.
- CHAPMAN, V. M., MILLER, D. R., ARMSTRONG, D. & CASKEY, C. T. 1989. Recovery of induced mutations for X chromosome-linked muscular dystrophy in mice. *Proc Natl Acad Sci U S A*, 86, 1292-6.
- CHAZAUD, B., BRIGITTE, M., YACOUB-YOUSSEF, H., ARNOLD, L., GHERARDI, R., SONNET, C., LAFUSTE, P. & CHRETIEN, F. 2009. Dual and beneficial roles of macrophages during skeletal muscle regeneration. *Exerc Sport Sci Rev*, 37, 18-22.
- CHEN, L., PAN, Y., CHENG, J., ZHU, X., CHU, W., MENG, Y. Y., BIN, S. & ZHANG, J. 2023. Characterization of myosin heavy chain (MYH) genes and their differential expression in white and red muscles of Chinese perch, *Siniperca chuatsi*. *Int J Biol Macromol*, 250, 125907.
- CHEN, W., YOU, W., VALENACK, T., SHAN, T. (2024). Bidirectional roles of skeletal muscle fibro-adipogenic progenitors in homeostasis and disease. *Ageing research reviews*. 80, 101682
- CLAMP, M., FRY, B., KAMAL, M., XIE, X., CUFF, J., LIN, M. F., KELLIS, M., LINDBLAD-TOH, K. & LANDER, E. S. 2007. Distinguishing protein-coding and noncoding genes in the human genome. *Proc Natl Acad Sci U S A*, 104, 19428-33.
- CLARKE, M. S., KHAKEE, R. & MCNEIL, P. L. 1993. Loss of cytoplasmic basic fibroblast growth factor from physiologically wounded myofibers of normal and dystrophic muscle. *J Cell Sci*, 106 ( Pt 1), 121-33.
- CLOUT, N. J., TISI, D. & HOHENESTER, E. 2003. Novel fold revealed by the structure of a FAS1 domain pair from the insect cell adhesion molecule fasciclin I. *Structure*, 11, 197-203.
- CONSTANTIN, B. 2014. Dystrophin complex functions as a scaffold for signalling proteins. *Biochim Biophys Acta*, 1838, 635-42.

- CORDOVA, G., NEGRONI, E., CABELLO-VERRUGIO, C., MOULY, V. & TROLLET, C. 2018. Combined Therapies for Duchenne Muscular Dystrophy to Optimize Treatment Efficacy. *Front Genet*, 9, 114.
- CORSI, A., XU, T., CHEN, X. D., BOYDE, A., LIANG, J., MANKANI, M., SOMMER, B., IOZZO, R. V., EICHSTETTER, I., ROBEY, P. G., BIANCO, P. & YOUNG, M. F. 2002. Phenotypic effects of biglycan deficiency are linked to collagen fibril abnormalities, are synergized by decorin deficiency, and mimic Ehlers-Danlos-like changes in bone and other connective tissues. *J Bone Miner Res*, 17, 1180-9.
- COSEMANS, G., MERCKX, C., DE BLEECKER, J. L. & DE PAEPE, B. 2022. Inducible Heat Shock Protein 70 Levels in Patients and the mdx Mouse Affirm Regulation during Skeletal Muscle Regeneration in Muscular Dystrophy. *Front Biosci (Schol Ed)*, 14, 19.
- COUCHOUX, H., BICHRAOUI, H., CHOUABE, C., ALTAF AJ, X., BONVALLET, R., ALLARD, B., RONJAT, M. & BERTHIER, C. 2011. Caveolin-3 is a direct molecular partner of the Cav1.1 subunit of the skeletal muscle L-type calcium channel. *Int J Biochem Cell Biol*, 43, 713-20.
- COZZOLI, A., CAPOGROSSO, R. F., SBLENDORIO, V. T., DINARDO, M. M., JAGERSCHMIDT, C., NAMOUR, F., CAMERINO, G. M. & DE LUCA, A. 2013. GLPG0492, a novel selective androgen receptor modulator, improves muscle performance in the exercised-mdx mouse model of muscular dystrophy. *Pharmacol Res*, 72, 9-24.
- CRABTREE, N. J., ADAMS, J. E., PADIDELA, R., SHAW, N. J., HÖGLER, W., ROPER, H., HUGHES, I., DANIEL, A. & MUGHAL, M. Z. 2018. Growth, bone health & ambulatory status of boys with DMD treated with daily vs. intermittent oral glucocorticoid regimen. *Bone*, 116, 181-186.
- CROS, D., HARNDEN, P., PELLISSIER, J. F. & SERRATRICE, G. 1989. Muscle hypertrophy in Duchenne muscular dystrophy. A pathological and morphometric study. *J Neurol*, 236, 43-7.
- CSŐSZ, É., KALLÓ, G., MÁRKUS, B., DEÁK, E., CSUTAK, A. & TŐZSÉR, J. 2017. Quantitative body fluid proteomics in medicine - A focus on minimal invasiveness. *J Proteomics*, 153, 30-43.
- CULLIGAN, K., BANVILLE, N., DOWLING, P. & OHLENDIECK, K. 2002. Drastic reduction of calsequestrin-like proteins and impaired calcium binding in dystrophic mdx muscle. *J Appl Physiol (1985)*, 92, 435-45.

- CULLIGAN, K. & OHLENDIECK, K. 2002. Diversity of the Brain Dystrophin-Glycoprotein Complex. *J Biomed Biotechnol*, 2, 31-36.
- CUNNINGHAM, B. A., HEMPERLY, J. J., MURRAY, B. A., PREDIGER, E. A., BRACKENBURY, R. & EDELMAN, G. M. 1987. Neural cell adhesion molecule: structure, immunoglobulin-like domains, cell surface modulation, and alternative RNA splicing. *Science*, 236, 799-806.
- D'ALESSANDRO, M., HNIA, K., GACHE, V., KOCH, C., GAVRIILIDIS, C., RODRIGUEZ, D., NICOT, A. S., ROMERO, N. B., SCHWAB, Y., GOMES, E., LABOUESSE, M. & LAPORTE, J. 2015. Amphiphysin 2 Orchestrates Nucleus Positioning and Shape by Linking the Nuclear Envelope to the Actin and Microtubule Cytoskeleton. *Dev Cell*, 35, 186-98.
- DANGAIN, J. & VRBOVA, G. 1984. Muscle development in mdx mutant mice. *Muscle Nerve*, 7, 700-4.
- DANKO, I., CHAPMAN, V. & WOLFF, J. A. 1992. The frequency of revertants in mdx mouse genetic models for Duchenne muscular dystrophy. *Pediatr Res*, 32, 128-31.
- DARE, T. O., DAVIES, H. A., TURTON, J. A., LOMAS, L., WILLIAMS, T. C. & YORK, M. J. 2002. Application of surface-enhanced laser desorption/ionization technology to the detection and identification of urinary parvalbumin-alpha: a biomarker of compound-induced skeletal muscle toxicity in the rat. *Electrophoresis*, 23, 3241-51.
- DAVIES, K. E. & GUIRAUD, S. 2019. Micro-dystrophin Genes Bring Hope of an Effective Therapy for Duchenne Muscular Dystrophy. *Mol Ther*, 27, 486-488.
- DE LATEUR, B. J. & GIACONI, R. M. 1979. Effect on maximal strength of submaximal exercise in Duchenne muscular dystrophy. *Am J Phys Med*, 58, 26-36.
- DECRAMER, S., GONZALEZ DE PEREDO, A., BREUIL, B., MISCHAK, H., MONSARRAT, B., BASCANDS, J. L. & SCHANSTRA, J. P. 2008. Urine in clinical proteomics. *Mol Cell Proteomics*, 7, 1850-62.
- DESGUERRE, I., MAYER, M., LETURCQ, F., BARBET, J. P., GHERARDI, R. K. & CHRISTOV, C. 2009. Endomysial fibrosis in Duchenne muscular dystrophy: a marker of poor outcome associated with macrophage alternative activation. *J Neuropathol Exp Neurol*, 68, 762-73.
- DESJARDINS, P. R., BURKMAN, J. M., SHRAGER, J. B., ALLMOND, L. A. & STEDMAN, H. H. 2002. Evolutionary implications of three novel members of the human sarcomeric myosin heavy chain gene family. *Mol Biol Evol*, 19, 375-93.

- DHARGAVE, P., NALINI, A., NAGARATHNA, R., SENDHILKUMAR, R., JAMES, T. T., RAJU, T. R. & SATHYAPRABHA, T. N. 2021. Effect of Yoga and Physiotherapy on Pulmonary Functions in Children with Duchenne Muscular Dystrophy - A Comparative Study. *Int J Yoga*, 14, 133-140.
- DIEHL, A. G., ZAREPARSI, S., QIAN, M., KHANNA, R., ANGELES, R. & GAGE, P. J. 2006. Extraocular muscle morphogenesis and gene expression are regulated by Pitx2 gene dose. *Invest Ophthalmol Vis Sci*, 47, 1785-93.
- DOGRA, C., CHANGOTRA, H., WERGEDAL, J. E. & KUMAR, A. 2006. Regulation of phosphatidylinositol 3-kinase (PI3K)/Akt and nuclear factor-kappa B signaling pathways in dystrophin-deficient skeletal muscle in response to mechanical stretch. *J Cell Physiol*, 208, 575-85.
- DONADON, M. & SANTORO, M. M. 2021. The origin and mechanisms of smooth muscle cell development in vertebrates. *Development*, 148.
- DOWBEN, R. M. 1959. Prolonged survival of dystrophic mice treated with 17 alpha-ethyl-19-nortestosterone. *Nature*, 184(Suppl 25), 1966-7.
- DOWBEN, R. M. & PERLSTEIN, M. A. 1961. Muscular dystrophy treated with norethandrolone. *Arch Intern Med*, 107, 245-51.
- Dowling, P., Trollet, C., Muraine, L., Negroni, E., Swandulla, D., & Ohlendieck, K. (2024). The potential of proteomics for in-depth bioanalytical investigations of satellite cell function in applied myology. *Expert review of proteomics*, 21(5-6), 229–235
- DOWLING, P., DORAN, P. & OHLENDIECK, K. 2004. Drastic reduction of sarcalumenin in Dp427 (dystrophin of 427 kDa)-deficient fibres indicates that abnormal calcium handling plays a key role in muscular dystrophy. *Biochem J*, 379, 479-88.
- DOWLING, P., GARGAN, S., ZWEYER, M., HENRY, M., MELEADY, P., SWANDULLA, D. & OHLENDIECK, K. 2020. Proteome-wide Changes in the. *iScience*, 23, 101500.
- DOWLING, P., GARGAN, S., ZWEYER, M., SWANDULLA, D. & OHLENDIECK, K. 2023. Extracellular Matrix Proteomics: The. *Biomolecules*, 13.
- DREMINA, E. S., SHAROV, V. S., DAVIES, M. J. & SCHÖNEICH, C. 2007. Oxidation and inactivation of SERCA by selective reaction of cysteine residues with amino acid peroxides. *Chem Res Toxicol*, 20, 1462-9.
- DULHUNTY, A. F. & FRANZINI-ARMSTRONG, C. 1975. The relative contributions of the folds and caveolae to the surface membrane of frog skeletal muscle fibres at different sarcomere lengths. *J Physiol*, 250, 513-39.

- DÍAZ-RAMOS, A., ROIG-BORRELLAS, A., GARCÍA-MELERO, A. & LÓPEZ-ALEMANY, R. 2012.  $\alpha$ -Enolase, a multifunctional protein: its role on pathophysiological situations. *J Biomed Biotechnol*, 2012, 156795.
- EDELMAN, G. M. & CROSSIN, K. L. 1991. Cell adhesion molecules: implications for a molecular histology. *Annu Rev Biochem*, 60, 155-90.
- ELLIS, R. J. 2007. Protein misassembly: macromolecular crowding and molecular chaperones. *Adv Exp Med Biol*, 594, 1-13.
- ERVASTI, J. M. & SONNEMANN, K. J. 2008. Biology of the striated muscle dystrophin-glycoprotein complex. *Int Rev Cytol*, 265, 191-225.
- ESER, G. & TOPALOĞLU, H. 2022. Current Outline of Exon Skipping Trials in Duchenne Muscular Dystrophy. *Genes (Basel)*, 13.
- FANG, X. B., SONG, Z. B., XIE, M. S., LIU, Y. M. & ZHANG, W. X. 2020. Synergistic effect of glucocorticoids and IGF-1 on myogenic differentiation through the Akt/GSK-3 $\beta$  pathway in C2C12 myoblasts. *Int J Neurosci*, 130, 1125-1135.
- FATT, P. & GINSBORG, B. L. 1958. The ionic requirements for the production of action potentials in crustacean muscle fibres. *J Physiol*, 142, 516-43.
- FENICHEL, G. M., GRIGGS, R. C., KISSEL, J., KRAMER, T. I., MENDELL, J. R., MOXLEY, R. T., PESTRONK, A., SHENG, K., FLORENCE, J., KING, W. M., PANDYA, S., ROBISON, V. D. & WANG, H. 2001. A randomized efficacy and safety trial of oxandrolone in the treatment of Duchenne dystrophy. *Neurology*, 56, 1075-9.
- FERGUSON, D. G., SCHWARTZ, H. W. & FRANZINI-ARMSTRONG, C. 1984. Subunit structure of junctional feet in triads of skeletal muscle: a freeze-drying, rotary-shadowing study. *J Cell Biol*, 99, 1735-42.
- FERNÁNDEZ-PEVIDA, A., RODRÍGUEZ-GALÁN, O., DÍAZ-QUINTANA, A., KRESSLER, D. & DE LA CRUZ, J. 2012. Yeast ribosomal protein L40 assembles late into precursor 60 S ribosomes and is required for their cytoplasmic maturation. *J Biol Chem*, 287, 38390-407.
- FLITNEY, F. W. & HIRST, D. G. 1978. Cross-bridge detachment and sarcomere 'give' during stretch of active frog's muscle. *J Physiol*, 276, 449-65.
- FLUCHER, B. E. & FRANZINI-ARMSTRONG, C. 1996. Formation of junctions involved in excitation-contraction coupling in skeletal and cardiac muscle. *Proc Natl Acad Sci U S A*, 93, 8101-6.

- FOUGEROUSSE, F., EDOM-VOVARD, F., MERKULOVA, T., OTT, M. O., DURAND, M., BUTLER-BROWNE, G. & KELLER, A. 2001. The muscle-specific enolase is an early marker of human myogenesis. *J Muscle Res Cell Motil*, 22, 535-44.
- FOX, M. A., HO, M. S., SMYTH, N. & SANES, J. R. 2008. A synaptic nidogen: developmental regulation and role of nidogen-2 at the neuromuscular junction. *Neural Dev*, 3, 24.
- FU, G., WANG, W. & LUO, B. H. 2012. Overview: structural biology of integrins. *Methods Mol Biol*, 757, 81-99.
- FUGIER, C., KLEIN, A. F., HAMMER, C., VASSILOPOULOS, S., IVARSSON, Y., TOUSSAINT, A., TOSCH, V., VIGNAUD, A., FERRY, A., MESSADDEQ, N., KOKUNAI, Y., TSUBURAYA, R., DE LA GRANGE, P., DEMBELE, D., FRANCOIS, V., PRECIGOUT, G., BOULADE-LADAME, C., HUMMEL, M. C., LOPEZ DE MUNAIN, A., SERGEANT, N., LAQUERRIÈRE, A., THIBAUT, C., DERYCKERE, F., AUBOEUF, D., GARCIA, L., ZIMMERMANN, P., UDD, B., SCHOSER, B., TAKAHASHI, M. P., NISHINO, I., BASSEZ, G., LAPORTE, J., FURLING, D. & CHARLET-BERGUERAND, N. 2011. Misregulated alternative splicing of BIN1 is associated with T tubule alterations and muscle weakness in myotonic dystrophy. *Nat Med*, 17, 720-5.
- FUNANAGE, V. L., SMITH, S. M. & MINNICH, M. A. 1992. Entactin promotes adhesion and long-term maintenance of cultured regenerated skeletal myotubes. *J Cell Physiol*, 150, 251-7.
- GAMSTORP, I. 1964. CLINICAL EVALUATION OF AN ORAL ANABOLIC STEROID (METHANDROSTENOLONE, DIANABOL CIBA) IN CHILDREN WITH MUSCULAR WEAKNESS AND WASTING. *Acta Paediatr (Stockh)*, 53, 570-7.
- GARG, K., CORONA, B. T. & WALTERS, T. J. 2014. Losartan administration reduces fibrosis but hinders functional recovery after volumetric muscle loss injury. *J Appl Physiol (1985)*, 117, 1120-31.
- GAVINA, M., BELICCHI, M., ROSSI, B., OTTOBONI, L., COLOMBO, F., MEREGALLI, M., BATTISTELLI, M., FORZENIGO, L., BIONDETTI, P., PISATI, F., PAROLINI, D., FARINI, A., ISSEKUTZ, A. C., BRESOLIN, N., RUSTICHELLI, F., CONSTANTIN, G., & TORRENTE, Y. (2006). VCAM-1 expression on dystrophic muscle vessels has a critical role in the recruitment of human blood-derived CD133+ stem cells after intra-arterial transplantation. *Blood*, 108(8), 2857–2866

- GEHRIG, S. M., VAN DER POEL, C., SAYER, T. A., SCHERTZER, J. D., HENSTRIDGE, D. C., CHURCH, J. E., LAMON, S., RUSSELL, A. P., DAVIES, K. E., FEBBRAIO, M. A. & LYNCH, G. S. 2012. Hsp72 preserves muscle function and slows progression of severe muscular dystrophy. *Nature*, 484, 394-8.
- GENTIL, C., LETURCQ, F., BEN YAOU, R., KAPLAN, J. C., LAFORET, P., PÉNISSON-BESNIER, I., ESPIL-TARIS, C., VOIT, T., GARCIA, L. & PIÉTRI-ROUXEL, F. 2012. Variable phenotype of del45-55 Becker patients correlated with nNOS $\mu$  mislocalization and RYR1 hypernitrosylation. *Hum Mol Genet*, 21, 3449-60.
- GIESELER, K., BESSOU, C. & SÉGALAT, L. 1999. Dystrobrevin- and dystrophin-like mutants display similar phenotypes in the nematode *Caenorhabditis elegans*. *Neurogenetics*, 2, 87-90.
- GIESELER, K., GRISONI, K. & SÉGALAT, L. 2000. Genetic suppression of phenotypes arising from mutations in dystrophin-related genes in *Caenorhabditis elegans*. *Curr Biol*, 10, 1092-7.
- GONZÁLEZ-GONZÁLEZ, L. & ALONSO, J. 2018. Periostin: A Matricellular Protein With Multiple Functions in Cancer Development and Progression. *Front Oncol*, 8, 225.
- GOONASEKERA, S. A., LAM, C. K., MILLAY, D. P., SARGENT, M. A., HAJJAR, R. J., KRANIAS, E. G. & MOLKENTIN, J. D. 2011. Mitigation of muscular dystrophy in mice by SERCA overexpression in skeletal muscle. *J Clin Invest*, 121, 1044-52.
- GOZAL, D. & THIRIET, P. 1999. Respiratory muscle training in neuromuscular disease: long-term effects on strength and load perception. *Med Sci Sports Exerc*, 31, 1522-7.
- GRABAREK, Z. 2011. Insights into modulation of calcium signaling by magnesium in calmodulin, troponin C and related EF-hand proteins. *Biochim Biophys Acta*, 1813, 913-21.
- GREFTE, S., ADJOBHO-HERMANS, M. J. W., VERSTEEG, E. M. M., KOOPMAN, W. J. H. & DAAMEN, W. F. 2016. Impaired primary mouse myotube formation on crosslinked type I collagen films is enhanced by laminin and entactin. *Acta Biomater*, 30, 265-276.
- GREGOREVIC, P., PLANT, D. R., LEEDING, K. S., BACH, L. A. & LYNCH, G. S. 2002. Improved contractile function of the mdx dystrophic mouse diaphragm muscle after insulin-like growth factor-I administration. *Am J Pathol*, 161, 2263-72.
- GUIRAUD, S., AARTSMA-RUS, A., VIEIRA, N. M., DAVIES, K. E., VAN OMMEN, G. J. & KUNKEL, L. M. 2015. The Pathogenesis and Therapy of Muscular Dystrophies. *Annu Rev Genomics Hum Genet*, 16, 281-308.

- GUTIERREZ, L. M., BRAWLEY, R. M. & HOSEY, M. M. 1991. Dihydropyridine-sensitive calcium channels from skeletal muscle. I. Roles of subunits in channel activity. *J Biol Chem*, 266, 16387-94.
- HAFEZI-MOGHADAM, A., SIMONCINI, T., YANG, Z., LIMBOURG, F. P., PLUMIER, J. C., REBSAMEN, M. C., HSIEH, C. M., CHUI, D. S., THOMAS, K. L., PROROCK, A. J., LAUBACH, V. E., MOSKOWITZ, M. A., FRENCH, B. A., LEY, K. & LIAO, J. K. 2002. Acute cardiovascular protective effects of corticosteroids are mediated by non-transcriptional activation of endothelial nitric oxide synthase. *Nat Med*, 8, 473-9.
- HARA, M. R., AGRAWAL, N., KIM, S. F., CASCIO, M. B., FUJIMURO, M., OZEKI, Y., TAKAHASHI, M., CHEAH, J. H., TANKOU, S. K., HESTER, L. D., FERRIS, C. D., HAYWARD, S. D., SNYDER, S. H. & SAWA, A. 2005. S-nitrosylated GAPDH initiates apoptotic cell death by nuclear translocation following Siah1 binding. *Nat Cell Biol*, 7, 665-74.
- HARISH, P., FORREST, L., HERATH, S., DICKSON, G., MALERBA, A. & POPPLEWELL, L. 2020. Inhibition of Myostatin Reduces Collagen Deposition in a Mouse Model of Oculopharyngeal Muscular Dystrophy (OPMD) With Established Disease. *Front Physiol*, 11, 184.
- HARISH, P., MALERBA, A., LU-NGUYEN, N., FORREST, L., CAPPELLARI, O., ROTH, F., TROLLET, C., POPPLEWELL, L. & DICKSON, G. 2019. Inhibition of myostatin improves muscle atrophy in oculopharyngeal muscular dystrophy (OPMD). *J Cachexia Sarcopenia Muscle*, 10, 1016-1026.
- HEAD, S. I. 2010. Branched fibres in old dystrophic mdx muscle are associated with mechanical weakening of the sarcolemma, abnormal Ca<sup>2+</sup> transients and a breakdown of Ca<sup>2+</sup> homeostasis during fatigue. *Exp Physiol*, 95, 641-56.
- HESSLER, S. M. & SELLERS, J. R. 2014. Myosin light chains: Teaching old dogs new tricks. *Bioarchitecture*, 4, 169-88.
- HENDERSON, D. M., LEE, A. & ERVASTI, J. M. 2010. Disease-causing missense mutations in actin binding domain 1 of dystrophin induce thermodynamic instability and protein aggregation. *Proc Natl Acad Sci U S A*, 107, 9632-7.
- HENDRIKSEN, R. G. F., VLES, J. S. H., AALBERS, M. W., CHIN, R. F. M. & HENDRIKSEN, J. G. M. 2018. Brain-related comorbidities in boys and men with Duchenne Muscular Dystrophy: A descriptive study. *Eur J Paediatr Neurol*, 22, 488-497.

- HENRY, M. & MELEADY, P. 2023. Clinical Proteomics: Liquid Chromatography-Mass Spectrometry (LC-MS) Purification Systems. *Methods Mol Biol*, 2699, 255-269.
- HIND, D., PARKIN, J., WHITWORTH, V., REX, S., YOUNG, T., HAMPSON, L., SHEEHAN, J., MAGUIRE, C., CANTRILL, H., SCOTT, E., EPPS, H., MAIN, M., GEARY, M., MCMURCHIE, H., PALLANT, L., WOODS, D., FREEMAN, J., LEE, E., EAGLE, M., WILLIS, T., MUNTONI, F. & BAXTER, P. 2017. Aquatic therapy for boys with Duchenne muscular dystrophy (DMD): an external pilot randomised controlled trial. *Pilot Feasibility Stud*, 3, 16.
- HIRATA, Y., BROTTTO, M., WEISLEDER, N., CHU, Y., LIN, P., ZHAO, X., THORNTON, A., KOMAZAKI, S., TAKESHIMA, H., MA, J. & PAN, Z. 2006. Uncoupling store-operated Ca<sup>2+</sup> entry and altered Ca<sup>2+</sup> release from sarcoplasmic reticulum through silencing of junctophilin genes. *Biophys J*, 90, 4418-27.
- HO, M. S., BÖSE, K., MOKKAPATI, S., NISCHT, R. & SMYTH, N. 2008. Nidogens-Extracellular matrix linker molecules. *Microsc Res Tech*, 71, 387-95.
- HOERSCH, S. & ANDRADE-NAVARRO, M. A. 2010. Periostin shows increased evolutionary plasticity in its alternatively spliced region. *BMC Evol Biol*, 10, 30.
- HOLLAND, A., DOWLING, P., MELEADY, P., HENRY, M., ZWEYER, M., MUNDEGAR, R. R., SWANDULLA, D. & OHLENDIECK, K. 2015. Label-free mass spectrometric analysis of the mdx-4cv diaphragm identifies the matricellular protein periostin as a potential factor involved in dystrophinopathy-related fibrosis. *Proteomics*, 15, 2318-31.
- HOLLAND, A., DOWLING, P., ZWEYER, M., SWANDULLA, D., HENRY, M., CLYNES, M. & OHLENDIECK, K. 2013. Proteomic profiling of cardiomyopathic tissue from the aged mdx model of Duchenne muscular dystrophy reveals a drastic decrease in laminin, nidogen and annexin. *Proteomics*, 13, 2312-23.
- HOLLINGWORTH, S., ZEIGER, U. & BAYLOR, S. M. 2008. Comparison of the myoplasmic calcium transient elicited by an action potential in intact fibres of mdx and normal mice. *J Physiol*, 586, 5063-75.
- HOLZ, M. K., BALLIF, B. A., GYGI, S. P. & BLENIS, J. 2021. mTOR and S6K1 mediate assembly of the translation preinitiation complex through dynamic protein interchange and ordered phosphorylation events. *Cell*, 184, 2255.
- HORTON, R. M., MANFREDI, A. A. & CONTI-TRONCONI, B. M. 1993. The 'embryonic' gamma subunit of the nicotinic acetylcholine receptor is expressed in adult extraocular muscle. *Neurology*, 43, 983-6.

- HOUDUSSE, A. & COHEN, C. 1996. Structure of the regulatory domain of scallop myosin at 2 Å resolution: implications for regulation. *Structure*, 4, 21-32.
- HUITOREL, P. & PANTALONI, D. 1985. Bundling of microtubules by glyceraldehyde-3-phosphate dehydrogenase and its modulation by ATP. *Eur J Biochem*, 150, 265-9.
- HUNT, C. C. 1990. Mammalian muscle spindle: peripheral mechanisms. *Physiol Rev*, 70, 643-63.
- HUXLEY, A. F. 1957. Muscle structure and theories of contraction. *Prog Biophys Biophys Chem*, 7, 255-318.
- HYNES, R. O. 2002. Integrins: bidirectional, allosteric signaling machines. *Cell*, 110, 673-87.
- ILLA, I., SERRANO-MUNUERA, C., GALLARDO, E., LASA, A., ROJAS-GARCÍA, R., PALMER, J., GALLANO, P., BAIGET, M., MATSUDA, C. & BROWN, R. H. 2001. Distal anterior compartment myopathy: a dysferlin mutation causing a new muscular dystrophy phenotype. *Ann Neurol*, 49, 130-4.
- IM, W. B., PHELPS, S. F., COPEN, E. H., ADAMS, E. G., SLIGHTOM, J. L. & CHAMBERLAIN, J. S. 1996. Differential expression of dystrophin isoforms in strains of mdx mice with different mutations. *Hum Mol Genet*, 5, 1149-53.
- INNES, J. R. 1951. Myopathies in animals; a record of some cases including progressive muscular dystrophy (pseudo-hypertrophic) (dog), "weisses Fleisch" (lamb), neuropathic muscular atrophy (sheep) and lymphocytic/histiocytic myositis, neuritis, radiculitis (dog). *Br Vet J*, 107, 131-43.
- IRIGOYEN, J. P., MUÑOZ-CÁNOVES, P., MONTERO, L., KOZICZAK, M. & NAGAMINE, Y. 1999. The plasminogen activator system: biology and regulation. *Cell Mol Life Sci*, 56, 104-32.
- ITO, K., KOMAZAKI, S., SASAMOTO, K., YOSHIDA, M., NISHI, M., KITAMURA, K. & TAKESHIMA, H. 2001. Deficiency of triad junction and contraction in mutant skeletal muscle lacking junctophilin type 1. *J Cell Biol*, 154, 1059-67.
- JANSEN, M., VAN ALFEN, N., GEURTS, A. C. & DE GROOT, I. J. 2013. Assisted bicycle training delays functional deterioration in boys with Duchenne muscular dystrophy: the randomized controlled trial "no use is disuse". *Neurorehabil Neural Repair*, 27, 816-27.
- JEFFERY, C. J. 1999. Moonlighting proteins. *Trends Biochem Sci*, 24, 8-11.
- KAWAHARA, G., KARPFF, J. A., MYERS, J. A., ALEXANDER, M. S., GUYON, J. R. & KUNKEL, L. M. 2011. Drug screening in a zebrafish model of Duchenne muscular dystrophy. *Proc Natl Acad Sci U S A*, 108, 5331-6.

- KELLER, A., DEMEURIE, J., MERKULOVA, T., GÉRAUD, G., CYWINER-GOLENZER, C., LUCAS, M. & CHÂTELET, F. P. 2000. Fibre-type distribution and subcellular localisation of alpha and beta enolase in mouse striated muscle. *Biol Cell*, 92, 527-35.
- KII, I. & ITO, H. 2017. Periostin and its interacting proteins in the construction of extracellular architectures. *Cell Mol Life Sci*, 74, 4269-4277.
- KIM, B. Y., OLZMANN, J. A., CHOI, S. I., AHN, S. Y., KIM, T. I., CHO, H. S., SUH, H. & KIM, E. K. 2009. Corneal dystrophy-associated R124H mutation disrupts TGFBI interaction with Periostin and causes mislocalization to the lysosome. *J Biol Chem*, 284, 19580-91.
- KINYAMU, H. K. & ARCHER, T. K. 2004. Modifying chromatin to permit steroid hormone receptor-dependent transcription. *Biochim Biophys Acta*, 1677, 30-45.
- KLEINMAN, H. K., GRAF, J., IWAMOTO, Y., KITTEN, G. T., OGLE, R. C., SASAKI, M., YAMADA, Y., MARTIN, G. R. & LUCKENBILL-EDDS, L. 1987. Role of basement membranes in cell differentiation. *Ann N Y Acad Sci*, 513, 134-45.
- KO, M. K., CHU, E. R. & TAN, J. C. H. 2014. Smooth muscle features of mouse extraocular muscle. *Clin Exp Ophthalmol*, 42, 295-6.
- KOENIG, M., MONACO, A. P. & KUNKEL, L. M. 1988. The complete sequence of dystrophin predicts a rod-shaped cytoskeletal protein. *Cell*, 53, 219-28.
- KOHFELDT, E., SASAKI, T., GÖHRING, W. & TIMPL, R. 1998. Nidogen-2: a new basement membrane protein with diverse binding properties. *J Mol Biol*, 282, 99-109.
- KOI, P. T., MILHOUA, P. M., MONROSE, V., MELMAN, A. & DISANTO, M. E. 2007. Expression of myosin isoforms in the smooth muscle of human corpus cavernosum. *Int J Impot Res*, 19, 62-8.
- KORNEGAY, J. N., BOGAN, J. R., BOGAN, D. J., CHILDERS, M. K., LI, J., NGHIEM, P., DETWILER, D. A., LARSEN, C. A., GRANGE, R. W., BHAVARAJU-SANKA, R. K., TOU, S., KEENE, B. P., HOWARD, J. F., WANG, J., FAN, Z., SCHATZBERG, S. J., STYNER, M. A., FLANIGAN, K. M., XIAO, X. & HOFFMAN, E. P. 2012. Canine models of Duchenne muscular dystrophy and their use in therapeutic strategies. *Mamm Genome*, 23, 85-108.
- KOUKOURAKIS, M. I., GIATROMANOLAKI, A., SIVRIDIS, E. & GROUP, T. A. A. R. 2003. Lactate dehydrogenase isoenzymes 1 and 5: differential expression by neoplastic and stromal cells in non-small cell lung cancer and other epithelial malignant tumors. *Tumour Biol*, 24, 199-202.
- KRAMER, J. M. 2005. Basement membranes. *WormBook*, 1-15.

- KRANJC, B. S., SKETELJ, J., D'ALBIS, A. & ERZEN, I. 2001. Long-term changes in myosin heavy chain composition after botulinum toxin a injection into rat medial rectus muscle. *Invest Ophthalmol Vis Sci*, 42, 3158-64.
- KUO, I. Y. & EHRLICH, B. E. 2015. Signaling in muscle contraction. *Cold Spring Harb Perspect Biol*, 7, a006023.
- LACERDA, A. E., KIM, H. S., RUTH, P., PEREZ-REYES, E., FLOCKERZI, V., HOFMANN, F., BIRNBAUMER, L. & BROWN, A. M. 1991. Normalization of current kinetics by interaction between the alpha 1 and beta subunits of the skeletal muscle dihydropyridine-sensitive Ca<sup>2+</sup> channel. *Nature*, 352, 527-30.
- LARCHER, T., LAFOUX, A., TESSON, L., REMY, S., THEPENIER, V., FRANÇOIS, V., LE GUINER, C., GOUBIN, H., DUTILLEUL, M., GUIGAND, L., TOUMANIANTZ, G., DE CIAN, A., BOIX, C., RENAUD, J. B., CHEREL, Y., GIOVANNANGELI, C., CONCORDET, J. P., ANEGON, I., & HUCHET, C. (2014). Characterization of dystrophin deficient rats: a new model for Duchenne muscular dystrophy. *PLoS one*, 9(10), e110371.
- LEE, E., MARCUCCI, M., DANIELL, L., PYPART, M., WEISZ, O. A., OCHOA, G. C., FARSAF, K., WENK, M. R. & DE CAMILLI, P. 2002. Amphiphysin 2 (Bin1) and T-tubule biogenesis in muscle. *Science*, 297, 1193-6.
- LEE, T., TAKESHIMA, Y., KUSUNOKI, N., AWANO, H., YAGI, M., MATSUO, M. & IJIMA, K. 2014. Differences in carrier frequency between mothers of Duchenne and Becker muscular dystrophy patients. *J Hum Genet*, 59, 46-50.
- LEFTER, S., HARDIMAN, O. & RYAN, A. M. 2017. A population-based epidemiologic study of adult neuromuscular disease in the Republic of Ireland. *Neurology*, 88, 304-313.
- LEHNART, S. E. & WEHRENS, X. H. T. 2022. The role of junctophilin proteins in cellular function. *Physiol Rev*, 102, 1211-1261.
- LEK, A., EVELSON, F. J., SUTTON, R. B., NORTH, K. N. & COOPER, S. T. 2012. Ferlins: regulators of vesicle fusion for auditory neurotransmission, receptor trafficking and membrane repair. *Traffic*, 13, 185-94.
- LENNON, N. J., KHO, A., BACSKAI, B. J., PERLMUTTER, S. L., HYMAN, B. T. & BROWN, R. H. 2003. Dysferlin interacts with annexins A1 and A2 and mediates sarcolemmal wound-healing. *J Biol Chem*, 278, 50466-73.
- LEPPER, C. & FAN, C. M. 2010. Inducible lineage tracing of Pax7-descendant cells reveals embryonic origin of adult satellite cells. *Genesis*, 48, 424-36.

- LEVINE, H., GOLDFARB, I., KATZ, J., CARMELI, M., SHOCHAT, T., MUSSAFFI, H., AHARONI, S., PRAIS, D. & NEVO, Y. 2023. Pulmonary function tests for evaluating the severity of Duchenne muscular dystrophy disease. *Acta Paediatr.*
- LEY, K., LAUDANNA, C., CYBULSKY, M. I. & NOURSHARGH, S. 2007. Getting to the site of inflammation: the leukocyte adhesion cascade updated. *Nat Rev Immunol*, 7, 678-89.
- LI, B., XIONG, W., LIANG, W. M., CHIOU, J. S., LIN, Y. J. & CHANG, A. C. Y. 2021. Targeting of CAT and VCAM1 as Novel Therapeutic Targets for DMD Cardiomyopathy. *Front Cell Dev Biol*, 9, 659177.
- LINDSAY, A., LARSON, A. A., VERMA, M., ERVASTI, J. M. & LOWE, D. A. 2019. Isometric resistance training increases strength and alters histopathology of dystrophin-deficient mouse skeletal muscle. *J Appl Physiol (1985)*, 126, 363-375.
- LIU, J., AOKI, M., ILLA, I., WU, C., FARDEAU, M., ANGELINI, C., SERRANO, C., URTIZBEREA, J. A., HENTATI, F., HAMIDA, M. B., BOHLEGA, S., CULPER, E. J., AMATO, A. A., BOSSIE, K., OELTJEN, J., BEJAOUI, K., MCKENNA-YASEK, D., HOSLER, B. A., SCHURR, E., ARAHATA, K., DE JONG, P. J. & BROWN, R. H. 1998. Dysferlin, a novel skeletal muscle gene, is mutated in Miyoshi myopathy and limb girdle muscular dystrophy. *Nat Genet*, 20, 31-6.
- LORTS, A., SCHWANEKAMP, J. A., BAUDINO, T. A., MCNALLY, E. M. & MOLKENTIN, J. D. 2012. Deletion of periostin reduces muscular dystrophy and fibrosis in mice by modulating the transforming growth factor- $\beta$  pathway. *Proc Natl Acad Sci U S A*, 109, 10978-83.
- LOTT, D. J., TAIVASSALO, T., COOKE, K. D., PARK, H., MOSLEMI, Z., BATRA, A., FORBES, S. C., BYRNE, B. J., WALTER, G. A. & VANDENBORNE, K. 2021. Safety, feasibility, and efficacy of strengthening exercise in Duchenne muscular dystrophy. *Muscle Nerve*, 63, 320-326.
- LOWEY, S., WALLER, G. S. & TRYBUS, K. M. 1993. Skeletal muscle myosin light chains are essential for physiological speeds of shortening. *Nature*, 365, 454-6.
- MAH, J. K., KORNGUT, L., FIEST, K. M., DYKEMAN, J., DAY, L. J., PRINGSHEIM, T. & JETTE, N. 2016. A Systematic Review and Meta-analysis on the Epidemiology of the Muscular Dystrophies. *Can J Neurol Sci*, 43, 163-77.
- MAHDY, M. A. A. 2019. Skeletal muscle fibrosis: an overview. *Cell Tissue Res*, 375, 575-588.

- MARKAKI, M. & TAVERNARAKIS, N. 2020. *Caenorhabditis elegans* as a model system for human diseases. *Curr Opin Biotechnol*, 63, 118-125.
- MATTHEWS, E., BRASSINGTON, R., KUNTZER, T., JICHI, F. & MANZUR, A. Y. 2016. Corticosteroids for the treatment of Duchenne muscular dystrophy. *Cochrane Database Syst Rev*, 2016, CD003725.
- MAUREL, D. B., JÄHN, K. & LARA-CASTILLO, N. 2017. Muscle-Bone Crosstalk: Emerging Opportunities for Novel Therapeutic Approaches to Treat Musculoskeletal Pathologies. *Biomedicines*, 5.
- MCARDLE, A., DILLMANN, W. H., MESTRIL, R., FAULKNER, J. A. & JACKSON, M. J. 2004. Overexpression of HSP70 in mouse skeletal muscle protects against muscle damage and age-related muscle dysfunction. *FASEB J*, 18, 355-7.
- MCKAY, L. I. & CIDLOWSKI, J. A. 1999. Molecular control of immune/inflammatory responses: interactions between nuclear factor-kappa B and steroid receptor-signaling pathways. *Endocr Rev*, 20, 435-59.
- MCLOON, L. K. & WIRTSCHAFTER, J. 2003. Activated satellite cells in extraocular muscles of normal adult monkeys and humans. *Invest Ophthalmol Vis Sci*, 44, 1927-32.
- MCLOON, L. K. & WIRTSCHAFTER, J. D. 2002. Continuous myonuclear addition to single extraocular myofibers in uninjured adult rabbits. *Muscle Nerve*, 25, 348-58.
- MCMULLEN, C. A., FERRY, A. L., GAMBOA, J. L., ANDRADE, F. H. & DUPONT-VERSTEEGDEN, E. E. 2009. Age-related changes of cell death pathways in rat extraocular muscle. *Exp Gerontol*, 44, 420-5.
- MELCHIOR-BECKER, A., DAI, G., DING, Z., SCHÄFER, L., SCHRADER, J., YOUNG, M. F. & FISCHER, J. W. 2011. Deficiency of biglycan causes cardiac fibroblasts to differentiate into a myofibroblast phenotype. *J Biol Chem*, 286, 17365-75.
- MENDELL, J. R., MOXLEY, R. T., GRIGGS, R. C., BROOKE, M. H., FENICHEL, G. M., MILLER, J. P., KING, W., SIGNORE, L., PANDYA, S. & FLORENCE, J. 1989. Randomized, double-blind six-month trial of prednisone in Duchenne's muscular dystrophy. *N Engl J Med*, 320, 1592-7.
- METZINGER, L., PASSAQUIN, A. C., LEIJENDEKKER, W. J., POINDRON, P. & RÜEGG, U. T. 1995. Modulation by prednisolone of calcium handling in skeletal muscle cells. *Br J Pharmacol*, 116, 2811-6.
- MILLER, R. J. 1992. Voltage-sensitive Ca<sup>2+</sup> channels. *J Biol Chem*, 267, 1403-6.
- MINETTI, C., SOTGIA, F., BRUNO, C., SCARTEZZINI, P., BRODA, P., BADO, M., MASETTI, E., MAZZOCCO, M., EGEO, A., DONATI, M. A., VOLONTE, D.,

- GALBIATI, F., CORDONE, G., BRICARELLI, F. D., LISANTI, M. P. & ZARA, F. 1998. Mutations in the caveolin-3 gene cause autosomal dominant limb-girdle muscular dystrophy. *Nat Genet*, 18, 365-8.
- MISHINA, M., TAKAI, T., IMOTO, K., NODA, M., TAKAHASHI, T., NUMA, S., METHFESSEL, C. & SAKMANN, B. 1986. Molecular distinction between fetal and adult forms of muscle acetylcholine receptor. *Nature*, 321, 406-11.
- MOENS, P., BAATSEN, P. H. & MARÉCHAL, G. 1993. Increased susceptibility of EDL muscles from mdx mice to damage induced by contractions with stretch. *J Muscle Res Cell Motil*, 14, 446-51.
- MONCEAU, A., MOUTACHI, D., LEMAITRE, M., GARCIA, L., TROLLET, C., FURLING, D., KLEIN, A. & FERRY, A. 2022. Dystrophin Restoration after Adeno-Associated Virus U7-Mediated Dmd Exon Skipping Is Modulated by Muscular Exercise in the Severe D2-Mdx Duchenne Muscular Dystrophy Murine Model. *Am J Pathol*, 192, 1604-1618.
- MUKUND, K. & SUBRAMANIAM, S. 2020. Skeletal muscle: A review of molecular structure and function, in health and disease. *Wiley Interdiscip Rev Syst Biol Med*, 12, e1462.
- MURAINÉ, L., BENSALAH, M., BUTLER-BROWNE, G., BIGOT, A., TROLLET, C., MOULY, V. & NEGRONI, E. 2023. Update on anti-fibrotic pharmacotherapies in skeletal muscle disease. *Curr Opin Pharmacol*, 68, 102332.
- MURAINÉ, L., BENSALAH, M., DHIAB, J., CORDOVA, G., ARANDEL, L., MARHIC, A., CHAPART, M., VASSEUR, S., BENKHALIFA-ZIYYAT, S., BIGOT, A., BUTLER-BROWN, G., MOULY, V., NEGRONI, E., & TROLLET, C. (2020). Transduction Efficiency of Adeno-Associated Virus Serotypes After Local Injection in Mouse and Human Skeletal Muscle. *Human gene therapy*, 31(3-4), 233–240.
- MURPHY, A. C. & YOUNG, P. W. 2015. The actinin family of actin cross-linking proteins - a genetic perspective. *Cell Biosci*, 5, 49.
- MURPHY, R. M., DUTKA, T. L., HORVATH, D., BELL, J. R., DELBRIDGE, L. M. & LAMB, G. D. 2013. Ca<sup>2+</sup>-dependent proteolysis of junctophilin-1 and junctophilin-2 in skeletal and cardiac muscle. *J Physiol*, 591, 719-29.
- MURPHY, S., BRINKMEIER, H., KRAUTWALD, M., HENRY, M., MELEADY, P. & OHLENDIECK, K. 2017a. Proteomic profiling of the dystrophin complex and membrane fraction from dystrophic mdx muscle reveals decreases in the cytolinker

- desmoglein and increases in the extracellular matrix stabilizers biglycan and fibronectin. *J Muscle Res Cell Motil*, 38, 251-268.
- MURPHY, S., DOWLING, P., ZWEYER, M., HENRY, M., MELEADY, P., MUNDEGAR, R. R., SWANDULLA, D. & OHLENDIECK, K. 2017b. Proteomic profiling of mdx-4cv serum reveals highly elevated levels of the inflammation-induced plasma marker haptoglobin in muscular dystrophy. *Int J Mol Med*, 39, 1357-1370.
- MURPHY, S., ZWEYER, M., RAUCAMP, M., HENRY, M., MELEADY, P., SWANDULLA, D. & OHLENDIECK, K. 2019. Proteomic profiling of the mouse diaphragm and refined mass spectrometric analysis of the dystrophic phenotype. *J Muscle Res Cell Motil*, 40, 9-28.
- MURRAY, B. E. & OHLENDIECK, K. 1998. Complex formation between calsequestrin and the ryanodine receptor in fast- and slow-twitch rabbit skeletal muscle. *FEBS Lett*, 429, 317-22.
- NAGASAWA, K., SARROPOULOU, E., EDVARDBSEN, V. & FERNANDES, J. M. 2016. Substantial Downregulation of Myogenic Transcripts in Skeletal Muscle of Atlantic Cod during the Spawning Period. *PLoS One*, 11, e0148374.
- NEELY, A. & HIDALGO, P. 2014. Structure-function of proteins interacting with the  $\alpha 1$  pore-forming subunit of high-voltage-activated calcium channels. *Front Physiol*, 5, 209.
- NGUYEN, B. Y., RUIZ-VELASCO, A., BUI, T., COLLINS, L., WANG, X. & LIU, W. 2019. Mitochondrial function in the heart: the insight into mechanisms and therapeutic potentials. *Br J Pharmacol*, 176, 4302-4318.
- NICHOLLS, C., LI, H. & LIU, J. P. 2012. GAPDH: a common enzyme with uncommon functions. *Clin Exp Pharmacol Physiol*, 39, 674-9.
- NORRIS, R. A., DAMON, B., MIRONOV, V., KASYANOV, V., RAMAMURTHI, A., MORENO-RODRIGUEZ, R., TRUSK, T., POTTS, J. D., GOODWIN, R. L., DAVIS, J., HOFFMAN, S., WEN, X., SUGI, Y., KERN, C. B., MJAATVEDT, C. H., TURNER, D. K., OKA, T., CONWAY, S. J., MOLKENTIN, J. D., FORGACS, G. & MARKWALD, R. R. 2007. Periostin regulates collagen fibrillogenesis and the biomechanical properties of connective tissues. *J Cell Biochem*, 101, 695-711.
- NOWAK, K. J., RAVENSCROFT, G. & LAING, N. G. 2013. Skeletal muscle  $\alpha$ -actin diseases (actinopathies): pathology and mechanisms. *Acta Neuropathol*, 125, 19-32.
- ODERMATT, A., TASCHNER, P. E., KHANNA, V. K., BUSCH, H. F., KARPATI, G., JABLECKI, C. K., BREUNING, M. H. & MACLENNAN, D. H. 1996. Mutations in

- the gene-encoding SERCA1, the fast-twitch skeletal muscle sarcoplasmic reticulum Ca<sup>2+</sup> ATPase, are associated with Brody disease. *Nat Genet*, 14, 191-4.
- OH, K. H. & KIM, H. 2013. Reduced IGF signaling prevents muscle cell death in a *Caenorhabditis elegans* model of muscular dystrophy. *Proc Natl Acad Sci U S A*, 110, 19024-9.
- OZDEMIR, C., AKPULAT, U., SHARAFI, P., YILDIZ, Y., ONBAŞILAR, I. & KOCAEFE, C. 2014. Periostin is temporally expressed as an extracellular matrix component in skeletal muscle regeneration and differentiation. *Gene*, 553, 130-9.
- PANT, M., BAL, N. C. & PERIASAMY, M. 2016. Sarcolipin: A Key Thermogenic and Metabolic Regulator in Skeletal Muscle. *Trends Endocrinol Metab*, 27, 881-892.
- PARK, H., WU, S., DUNKER, A. K. & KANG, C. 2003. Polymerization of calsequestrin. Implications for Ca<sup>2+</sup> regulation. *J Biol Chem*, 278, 16176-82.
- PARTON, R. G., WAY, M., ZORZI, N. & STANG, E. 1997. Caveolin-3 associates with developing T-tubules during muscle differentiation. *J Cell Biol*, 136, 137-54.
- PASQUINI, F., GUERIN, C., BLAKE, D., DAVIES, K., KARPATI, G. & HOLLAND, P. 1995. The effect of glucocorticoids on the accumulation of utrophin by cultured normal and dystrophic human skeletal muscle satellite cells. *Neuromuscul Disord*, 5, 105-14.
- PATTERSON, G., CONNER, H., GRONEMAN, M., BLAVO, C., & PARMAR, M. S. (2023). Duchenne muscular dystrophy: Current treatment and emerging exon skipping and gene therapy approach. *European journal of pharmacology*, 947, 175675
- PEARSON, C. M., KAR, N. C., PETER, J. B. & MUNSAT, T. L. 1965. MUSCLE LACTATE DEHYDROGENASE PATTERNS IN TWO TYPES OF X-LINKED MUSCULAR DYSTROPHY. *Am J Med*, 39, 91-7.
- PERMYAKOV, E. A. & UVERSKY, V. N. 2022. What Is Parvalbumin for? *Biomolecules*, 12.
- PETER, A. K., CHENG, H., ROSS, R. S., KNOWLTON, K. U. & CHEN, J. 2011. The costamere bridges sarcomeres to the sarcolemma in striated muscle. *Prog Pediatr Cardiol*, 31, 83-88.
- PETER, B. J., KENT, H. M., MILLS, I. G., VALLIS, Y., BUTLER, P. J., EVANS, P. R. & MCMAHON, H. T. 2004. BAR domains as sensors of membrane curvature: the amphiphysin BAR structure. *Science*, 303, 495-9.
- PETROF, B. J., SHRAGER, J. B., STEDMAN, H. H., KELLY, A. M. & SWEENEY, H. L. 1993. Dystrophin protects the sarcolemma from stresses developed during muscle contraction. *Proc Natl Acad Sci U S A*, 90, 3710-4.

- PETTE, D. & STARON, R. S. 2000. Myosin isoforms, muscle fiber types, and transitions. *Microsc Res Tech*, 50, 500-9.
- PIERSON, C. R., TOMCZAK, K., AGRAWAL, P., MOGHADASZADEH, B. & BEGGS, A. H. 2005. X-linked myotubular and centronuclear myopathies. *J Neuropathol Exp Neurol*, 64, 555-64.
- PORTER, J. D. & BAKER, R. S. 1996. Muscles of a different 'color': the unusual properties of the extraocular muscles may predispose or protect them in neurogenic and myogenic disease. *Neurology*, 46, 30-7.
- POWELL-BRAXTON, L., HOLLINGSHEAD, P., WARBURTON, C., DOWD, M., PITTS-MEEK, S., DALTON, D., GILLETT, N. & STEWART, T. A. 1993. IGF-I is required for normal embryonic growth in mice. *Genes Dev*, 7, 2609-17.
- POWNALL, M. E., GUSTAFSSON, M. K. & EMERSON, C. P. 2002. Myogenic regulatory factors and the specification of muscle progenitors in vertebrate embryos. *Annu Rev Cell Dev Biol*, 18, 747-83.
- PRADNYA, D., NALINI, A., NAGARATHNA, R., RAJU, T. R., SENDHILKUMAR, R., MEGHANA, A. & SATHYAPRABHA, T. N. 2019. Effect of Yoga as an Add-on Therapy in the Modulation of Heart Rate Variability in Children with Duchenne Muscular Dystrophy. *Int J Yoga*, 12, 55-61.
- QUATTROCELLI, M., BAREFIELD, D. Y., WARNER, J. L., VO, A. H., HADHAZY, M., EARLEY, J. U., DEMONBREUN, A. R. & MCNALLY, E. M. 2017. Intermittent glucocorticoid steroid dosing enhances muscle repair without eliciting muscle atrophy. *J Clin Invest*, 127, 2418-2432.
- RAGHAVAN, M., FEE, D. & BARKHAUS, P. E. 2019. Generation and propagation of the action potential. *Handb Clin Neurol*, 160, 3-22.
- RAMAMOORTHY, S. & CIDLOWSKI, J. A. 2016. Corticosteroids: Mechanisms of Action in Health and Disease. *Rheum Dis Clin North Am*, 42, 15-31, vii.
- RANZ, J. M., PONCE, A. R., HARTL, D. L. & NURMINSKY, D. 2003. Origin and evolution of a new gene expressed in the Drosophila sperm axoneme. *Genetica*, 118, 233-44.
- RAVENSCROFT, G., COLLEY, S. M., WALKER, K. R., CLEMENT, S., BRINGANS, S., LIPSCOMBE, R., FABIAN, V. A., LAING, N. G. & NOWAK, K. J. 2008. Expression of cardiac alpha-actin spares extraocular muscles in skeletal muscle alpha-actin diseases--quantification of striated alpha-actins by MRM-mass spectrometry. *Neuromuscul Disord*, 18, 953-8.

- RAYMACKERS, J. M., DEBAIX, H., COLSON-VAN SCHOOR, M., DE BACKER, F., TAJEDDINE, N., SCHWALLER, B., GAILLY, P. & GILLIS, J. M. 2003. Consequence of parvalbumin deficiency in the mdx mouse: histological, biochemical and mechanical phenotype of a new double mutant. *Neuromuscul Disord*, 13, 376-87.
- RAZZAQ, A., ROBINSON, I. M., MCMAHON, H. T., SKEPPER, J. N., SU, Y., ZELHOF, A. C., JACKSON, A. P., GAY, N. J. & O'KANE, C. J. 2001. Amphiphysin is necessary for organization of the excitation-contraction coupling machinery of muscles, but not for synaptic vesicle endocytosis in *Drosophila*. *Genes Dev*, 15, 2967-79.
- REDLITZ, A., FOWLER, B. J., PLOW, E. F. & MILES, L. A. 1995. The role of an enolase-related molecule in plasminogen binding to cells. *Eur J Biochem*, 227, 407-15.
- RENNIE, M. J., EDWARDS, R. H., HALLIDAY, D., MATTHEWS, D. E., WOLMAN, S. L. & MILLWARD, D. J. 1982. Muscle protein synthesis measured by stable isotope techniques in man: the effects of feeding and fasting. *Clin Sci (Lond)*, 63, 519-23.
- RIFAI, Z., WELLE, S., MOXLEY, R. T., LORENSON, M. & GRIGGS, R. C. 1995. Effect of prednisone on protein metabolism in Duchenne dystrophy. *Am J Physiol*, 268, E67-74.
- RITOSSA, F. M. 1964. EXPERIMENTAL ACTIVATION OF SPECIFIC LOCI IN POLYTENE CHROMOSOMES OF DROSOPHILA. *Exp Cell Res*, 35, 601-7.
- ROBERTSON, P. L. & ROLOFF, D. W. 1994. Chronic respiratory failure in limb-girdle muscular dystrophy: successful long-term therapy with nasal bilevel positive airway pressure. *Pediatr Neurol*, 10, 328-31.
- RODRIGUES, M. R., CARVALHO, C. R., SANTAELLA, D. F., LORENZI-FILHO, G. & MARIE, S. K. 2014. Effects of yoga breathing exercises on pulmonary function in patients with Duchenne muscular dystrophy: an exploratory analysis. *J Bras Pneumol*, 40, 128-33.
- ROSSI, A. C., MAMMUCARI, C., ARGENTINI, C., REGGIANI, C. & SCHIAFFINO, S. 2010. Two novel/ancient myosins in mammalian skeletal muscles: MYH14/7b and MYH15 are expressed in extraocular muscles and muscle spindles. *J Physiol*, 588, 353-64.
- ROUILLON, J., ZOCEVIC, A., LEGER, T., GARCIA, C., CAMADRO, J. M., UDD, B., WONG, B., SERVAIS, L., VOIT, T. & SVINARTCHOUK, F. 2014. Proteomics profiling of urine reveals specific titin fragments as biomarkers of Duchenne muscular dystrophy. *Neuromuscul Disord*, 24, 563-73.
- RUTTER, M. M., WONG, B. L., COLLINS, J. J., SAWNANI, H., TAYLOR, M. D., HORN, P. S. & BACKELJAUW, P. F. 2020. Recombinant human insulin-like growth factor-1

- therapy for 6 months improves growth but not motor function in boys with Duchenne muscular dystrophy. *Muscle Nerve*, 61, 623-631.
- RYAN, M. M., SCHNELL, C., STRICKLAND, C. D., SHIELD, L. K., MORGAN, G., IANNACCONE, S. T., LAING, N. G., BEGGS, A. H. & NORTH, K. N. 2001. Nemaline myopathy: a clinical study of 143 cases. *Ann Neurol*, 50, 312-20.
- RYBAKOVA, I. N. & ERVASTI, J. M. 1997. Dystrophin-glycoprotein complex is monomeric and stabilizes actin filaments in vitro through a lateral association. *J Biol Chem*, 272, 28771-8.
- SADOULET-PUCCIO, H. M., RAJALA, M. & KUNKEL, L. M. 1997. Dystrobrevin and dystrophin: an interaction through coiled-coil motifs. *Proc Natl Acad Sci U S A*, 94, 12413-8.
- SANDONÀ, D. & BETTO, R. 2009. Sarcoglycanopathies: molecular pathogenesis and therapeutic prospects. *Expert Rev Mol Med*, 11, e28.
- SCHACHAT, F. & BRIGGS, M. M. 2002. Phylogenetic implications of the superfast myosin in extraocular muscles. *J Exp Biol*, 205, 2189-201.
- SCHERTZER, J. D., VAN DER POEL, C., SHAVLAKADZE, T., GROUNDS, M. D. & LYNCH, G. S. 2008. Muscle-specific overexpression of IGF-I improves E-C coupling in skeletal muscle fibers from dystrophic mdx mice. *Am J Physiol Cell Physiol*, 294, C161-8.
- SCHLEGEL, A. & LISANTI, M. P. 2000. A molecular dissection of caveolin-1 membrane attachment and oligomerization. Two separate regions of the caveolin-1 C-terminal domain mediate membrane binding and oligomer/oligomer interactions in vivo. *J Biol Chem*, 275, 21605-17.
- SCHREIBER, D. & OHLENDIECK, K. 2007. Oligomerisation of sarcoplasmic reticulum Ca<sup>2+</sup>-ATPase monomers from skeletal muscle. *Protein Pept Lett*, 14, 219-26.
- SCHWARTZ, A. L. & CIECHANOVER, A. 2009. Targeting proteins for destruction by the ubiquitin system: implications for human pathobiology. *Annu Rev Pharmacol Toxicol*, 49, 73-96.
- SCHÄCKE, H., DÖCKE, W. D. & ASADULLAH, K. 2002. Mechanisms involved in the side effects of glucocorticoids. *Pharmacol Ther*, 96, 23-43.
- SEIDEL, T., FIEGLE, D. J., BAUR, T. J., RITZER, A., NAY, S., HEIM, C., WEYAND, M., MILTING, H., OAKLEY, R. H., CIDLOWSKI, J. A. & VOLK, T. 2019. Glucocorticoids preserve the t-tubular system in ventricular cardiomyocytes by upregulation of autophagic flux. *Basic Res Cardiol*, 114, 47.

- SEKULIC-JABLANOVIC, M., PALMOWSKI-WOLFE, A., ZORZATO, F. & TREVES, S. 2015. Characterization of excitation-contraction coupling components in human extraocular muscles. *Biochem J*, 466, 29-36.
- SERRANO, A. L. & MUÑOZ-CÁNOVES, P. 2017. Fibrosis development in early-onset muscular dystrophies: Mechanisms and translational implications. *Semin Cell Dev Biol*, 64, 181-190.
- SHACK, S., WANG, X. T., KOKKONEN, G. C., GOROSPE, M., LONGO, D. L. & HOLBROOK, N. J. 2003. Caveolin-induced activation of the phosphatidylinositol 3-kinase/Akt pathway increases arsenite cytotoxicity. *Mol Cell Biol*, 23, 2407-14.
- SHAIKH, S. A., SAHOO, S. K. & PERIASAMY, M. 2016. Phospholamban and sarcolipin: Are they functionally redundant or distinct regulators of the Sarco(Endo)Plasmic Reticulum Calcium ATPase? *J Mol Cell Cardiol*, 91, 81-91.
- SHAN, R., LIU, N., YAN, Y. & LIU, B. 2021. Apoptosis, autophagy and atherosclerosis: Relationships and the role of Hsp27. *Pharmacol Res*, 166, 105169.
- SHARP, N. J., KORNEGAY, J. N., VAN CAMP, S. D., HERBSTREITH, M. H., SECORE, S. L., KETTLE, S., HUNG, W. Y., CONSTANTINOU, C. D., DYKSTRA, M. J. & ROSES, A. D. 1992. An error in dystrophin mRNA processing in golden retriever muscular dystrophy, an animal homologue of Duchenne muscular dystrophy. *Genomics*, 13, 115-21.
- SHAW, L. M. & OLSEN, B. R. 1991. FACIT collagens: diverse molecular bridges in extracellular matrices. *Trends Biochem Sci*, 16, 191-4.
- SILVA, N. S. M., RODRIGUES, L. F. C., DORES-SILVA, P. R., MONTANARI, C. A., RAMOS, C. H. I., BARBOSA, L. R. S. & BORGES, J. C. 2021. Structural, thermodynamic and functional studies of human 71 kDa heat shock cognate protein (HSPA8/hHsc70). *Biochim Biophys Acta Proteins Proteom*, 1869, 140719.
- SIMON-KELLER, K., BARTH, S., VINCENT, A. & MARX, A. 2013. Targeting the fetal acetylcholine receptor in rhabdomyosarcoma. *Expert Opin Ther Targets*, 17, 127-38.
- SIROVER, M. A. 1999. New insights into an old protein: the functional diversity of mammalian glyceraldehyde-3-phosphate dehydrogenase. *Biochim Biophys Acta*, 1432, 159-84.
- SOLITO, E., RAUGEI, G., MELLI, M. & PARENTE, L. 1991. Dexamethasone induces the expression of the mRNA of lipocortin 1 and 2 and the release of lipocortin 1 and 5 in differentiated, but not undifferentiated U-937 cells. *FEBS Lett*, 291, 238-44.

- SORRENTINO, V. 1995. The ryanodine receptor family of intracellular calcium release channels. *Adv Pharmacol*, 33, 67-90.
- SPENCER, R. F. & PORTER, J. D. 2006. Biological organization of the extraocular muscles. *Prog Brain Res*, 151, 43-80.
- SQUIRE, J. M. & MORRIS, E. P. 1998. A new look at thin filament regulation in vertebrate skeletal muscle. *FASEB J*, 12, 761-71.
- STRIMBU, K. & TAVEL, J. A. 2010. What are biomarkers? *Curr Opin HIV AIDS*, 5, 463-6.
- STRYNADKA, N. C. & JAMES, M. N. 1989. Crystal structures of the helix-loop-helix calcium-binding proteins. *Annu Rev Biochem*, 58, 951-98.
- SUH, H., GAGE, P. J., DROUIN, J. & CAMPER, S. A. 2002. Pitx2 is required at multiple stages of pituitary organogenesis: pituitary primordium formation and cell specification. *Development*, 129, 329-37.
- SUN, J., XIN, C., EU, J. P., STAMLER, J. S. & MEISSNER, G. 2001. Cysteine-3635 is responsible for skeletal muscle ryanodine receptor modulation by NO. *Proc Natl Acad Sci U S A*, 98, 11158-62.
- SUSLOV, V. M., LIEBERMAN, L. N., CARLIER, P. G., PONOMARENKO, G. N., IVANOV, D. O., RUDENKO, D. I., SUSLOVA, G. A. & ADULAS, E. I. 2023. Efficacy and safety of hydrokinesitherapy in patients with dystrophinopathy. *Front Neurol*, 14, 1230770.
- SVEDRUŽIĆ, Z. M. & SPIVEY, H. O. 2006. Interaction between mammalian glyceraldehyde-3-phosphate dehydrogenase and L-lactate dehydrogenase from heart and muscle. *Proteins*, 63, 501-11.
- SWEENEY, H. L. & HOLZBAUR, E. L. F. 2018. Motor Proteins. *Cold Spring Harb Perspect Biol*, 10.
- TAKAGI, A., KOJIMA, S., IDA, M. & ARAKI, M. 1992. Increased leakage of calcium ion from the sarcoplasmic reticulum of the mdx mouse. *J Neurol Sci*, 110, 160-4.
- TAKESHIMA, H., KOMAZAKI, S., NISHI, M., IINO, M. & KANGAWA, K. 2000. Junctophilins: a novel family of junctional membrane complex proteins. *Mol Cell*, 6, 11-22.
- TARAKCI, H. & BERGER, J. 2016. The sarcoglycan complex in skeletal muscle. *Front Biosci (Landmark Ed)*, 21, 744-56.
- TENNYSON, C. N., KLAMUT, H. J. & WORTON, R. G. 1995. The human dystrophin gene requires 16 hours to be transcribed and is cotranscriptionally spliced. *Nat Genet*, 9, 184-90.

- THONGBOONKERD, V. & MALASIT, P. 2005. Renal and urinary proteomics: current applications and challenges. *Proteomics*, 5, 1033-42.
- TIAN, Z., MIYATA, K., MORINAGA, J., HORIGUCHI, H., KADOMATSU, T., ENDO, M., ZHAO, J., ZHU, S., SUGIZAKI, T., SATO, M., TERADA, K., OKUMURA, T., MUROHARA, T. & OIKE, Y. 2018. Circulating ANGPTL2 Levels Increase in Humans and Mice Exhibiting Cardiac Dysfunction. *Circ J*, 82, 437-447.
- TIMSON, D. J., TRAYER, H. R., SMITH, K. J. & TRAYER, I. P. 1999. Size and charge requirements for kinetic modulation and actin binding by alkali 1-type myosin essential light chains. *J Biol Chem*, 274, 18271-7.
- TIWARI, S., SINGH, A., GUPTA, P. & SINGH, S. 2022. UBA52 Is Crucial in HSP90 Ubiquitylation and Neurodegenerative Signaling during Early Phase of Parkinson's Disease. *Cells*, 11.
- TODOROVIC, V. & RIFKIN, D. B. 2012. LTBP<sub>s</sub>, more than just an escort service. *J Cell Biochem*, 113, 410-8.
- TOPIN, N., MATECKI, S., LE BRIS, S., RIVIER, F., ECHENNE, B., PREFAUT, C. & RAMONATXO, M. 2002. Dose-dependent effect of individualized respiratory muscle training in children with Duchenne muscular dystrophy. *Neuromuscul Disord*, 12, 576-83.
- TOUSSAINT, A., COWLING, B. S., HNIA, K., MOHR, M., OLDFORS, A., SCHWAB, Y., YIS, U., MAISONOBE, T., STOJKOVIC, T., WALLGREN-PETTERSSON, C., LAUGEL, V., ECHANIZ-LAGUNA, A., MANDEL, J. L., NISHINO, I. & LAPORTE, J. 2011. Defects in amphiphysin 2 (BIN1) and triads in several forms of centronuclear myopathies. *Acta Neuropathol*, 121, 253-66.
- TULANGEKAR, A. & SZTAL, T. E. 2021. Inflammation in Duchenne Muscular Dystrophy- Exploring the Role of Neutrophils in Muscle Damage and Regeneration. *Biomedicines*, 9.
- TUPLING, A. R., GRAMOLINI, A. O., DUHAMEL, T. A., KONDO, H., ASAHI, M., TSUCHIYA, S. C., BORRELLI, M. J., LEPOCK, J. R., OTSU, K., HORI, M., MACLENNAN, D. H. & GREEN, H. J. 2004. HSP70 binds to the fast-twitch skeletal muscle sarco(endo)plasmic reticulum Ca<sup>2+</sup>-ATPase (SERCA1a) and prevents thermal inactivation. *J Biol Chem*, 279, 52382-9.
- UNGER, A., BECKENDORF, L., BÖHME, P., KLEY, R., VON FRIELING-SALEWSKY, M., LOCHMÜLLER, H., SCHRÖDER, R., FÜRST, D. O., VORGERD, M. & LINKE, W. A. 2017. Translocation of molecular chaperones to the titin springs is common in

- skeletal myopathy patients and affects sarcomere function. *Acta Neuropathol Commun*, 5, 72.
- UPADHYAY, V., BANDI, S., PANJA, S., SABA, L. & MALLELA, K. M. G. 2020. Tissue-Specificity of Dystrophin-Actin Interactions: Isoform-Specific Thermodynamic Stability and Actin-Binding Function of Tandem Calponin-Homology Domains. *ACS Omega*, 5, 2159-2168.
- VALLEJO, D., HERNÁNDEZ-TORRES, F., LOZANO-VELASCO, E., RODRIGUEZ-OUTEIRIÑO, L., CARVAJAL, A., CREUS, C., FRANCO, D. & ARÁNEGA, A. E. 2018. PITX2 Enhances the Regenerative Potential of Dystrophic Skeletal Muscle Stem Cells. *Stem Cell Reports*, 10, 1398-1411.
- VAN ROOIJ, E., LIU, N. & OLSON, E. N. 2008. MicroRNAs flex their muscles. *Trends Genet*, 24, 159-66.
- VANBUREN, P., WALLER, G. S., HARRIS, D. E., TRYBUS, K. M., WARSHAW, D. M. & LOWEY, S. 1994. The essential light chain is required for full force production by skeletal muscle myosin. *Proc Natl Acad Sci U S A*, 91, 12403-7.
- VANDEKERCKHOVE, J., BUGAISKY, G. & BUCKINGHAM, M. 1986. Simultaneous expression of skeletal muscle and heart actin proteins in various striated muscle tissues and cells. A quantitative determination of the two actin isoforms. *J Biol Chem*, 261, 1838-43.
- VANDEKERCKHOVE, J. & WEBER, K. 1978. Mammalian cytoplasmic actins are the products of at least two genes and differ in primary structure in at least 25 identified positions from skeletal muscle actins. *Proc Natl Acad Sci U S A*, 75, 1106-10.
- VIAL, C., GUTIÉRREZ, J., SANTANDER, C., CABRERA, D. & BRANDAN, E. 2011. Decorin interacts with connective tissue growth factor (CTGF)/CCN2 by LRR12 inhibiting its biological activity. *J Biol Chem*, 286, 24242-52.
- VIDAL, B., SERRANO, A. L., TJWA, M., SUELVE, M., ARDITE, E., DE MORI, R., BAEZA-RAJA, B., MARTÍNEZ DE LAGRÁN, M., LAFUSTE, P., RUIZ-BONILLA, V., JARDÍ, M., GHERARDI, R., CHRISTOV, C., DIERSSEN, M., CARMELIET, P., DEGEN, J. L., DEWERCHIN, M. & MUÑOZ-CÁNOVES, P. 2008. Fibrinogen drives dystrophic muscle fibrosis via a TGFbeta/alternative macrophage activation pathway. *Genes Dev*, 22, 1747-52.
- VIDYASAGAR, A., WILSON, N. A. & DJAMALI, A. 2012. Heat shock protein 27 (HSP27): biomarker of disease and therapeutic target. *Fibrogenesis Tissue Repair*, 5, 7.

- VINCENZETTI, S., NASUTI, C., FEDELI, D., RICCIUTELLI, M., PUCCIARELLI, S. & GABBIANELLI, R. 2016. Proteomic analysis for early neurodegenerative biomarker detection in an animal model. *Biochimie*, 121, 79-86.
- WANG, K. S., ZHANG, Q., LIU, X., WU, L. & ZENG, M. 2012. PKNOX2 is associated with formal thought disorder in schizophrenia: a meta-analysis of two genome-wide association studies. *J Mol Neurosci*, 48, 265-72.
- WANG, Q. & MICHALAK, M. 2020. Calsequestrin. Structure, function, and evolution. *Cell Calcium*, 90, 102242.
- WANG, S., LI, Y., MIAO, W., ZHAO, H., ZHANG, F., LIU, N., SU, G. & CAI, X. 2020. [Corrigendum] Angiotensin-like protein 2 expression is suppressed by angiotensin II via the angiotensin II type 1 receptor in rat cardiomyocytes. *Mol Med Rep*, 21, 1408.
- WANG, S., TRUMBLE, W. R., LIAO, H., WESSON, C. R., DUNKER, A. K. & KANG, C. H. 1998. Crystal structure of calsequestrin from rabbit skeletal muscle sarcoplasmic reticulum. *Nat Struct Biol*, 5, 476-83.
- WANG, Y., ZHENG, C., WANG, X., ZUO, K. & LIU, Z. 2017. Proteomic profile-based screening of potential protein biomarkers in the urine of patients with nephrotic syndrome. *Mol Med Rep*, 16, 6276-6284.
- WEBB, R. C. 2003. Smooth muscle contraction and relaxation. *Adv Physiol Educ*, 27, 201-6.
- WEEDS, A. G. & MCLACHLAN, A. D. 1974. Structural homology of myosin alkali light chains, troponin C and carp calcium binding protein. *Nature*, 252, 646-9.
- WEI, L., VARSÁNYI, M., DULHUNTY, A. F. & BEARD, N. A. 2006. The conformation of calsequestrin determines its ability to regulate skeletal ryanodine receptors. *Biophys J*, 91, 1288-301.
- WIECZOREK, D. F., PERIASAMY, M., BUTLER-BROWNE, G. S., WHALEN, R. G. & NADAL-GINARD, B. 1985. Co-expression of multiple myosin heavy chain genes, in addition to a tissue-specific one, in extraocular musculature. *J Cell Biol*, 101, 618-29.
- WILKINS, M. R., SANCHEZ, J. C., GOOLEY, A. A., APPEL, R. D., HUMPHERY-SMITH, I., HOCHSTRASSER, D. F. & WILLIAMS, K. L. 1996. Progress with proteome projects: why all proteins expressed by a genome should be identified and how to do it. *Biotechnol Genet Eng Rev*, 13, 19-50.
- WOOD, C. L., VAN 'T HOF, R., DILLON, S., STRAUB, V., WONG, S. C., AHMED, S. F. & FARQUHARSON, C. 2022. Combined growth hormone and insulin-like growth factor-1 rescues growth retardation in glucocorticoid-treated mdx mice but does not prevent osteopenia. *J Endocrinol*, 253, 63-74.

- WOODS, C. E., NOVO, D., DIFRANCO, M. & VERGARA, J. L. 2004. The action potential-evoked sarcoplasmic reticulum calcium release is impaired in mdx mouse muscle fibres. *J Physiol*, 557, 59-75.
- WYNN, T. A. 2007. Common and unique mechanisms regulate fibrosis in various fibroproliferative diseases. *J Clin Invest*, 117, 524-9.
- XIE, B., LAOUAR, A. & HUBERMAN, E. 1998. Fibronectin-mediated cell adhesion is required for induction of 92-kDa type IV collagenase/gelatinase (MMP-9) gene expression during macrophage differentiation. The signaling role of protein kinase C-beta. *J Biol Chem*, 273, 11576-82.
- XIN, Y., YANG, C. & HAN, Z. 2016. Circulating miR-499 as a potential biomarker for acute myocardial infarction. *Ann Transl Med*, 4, 135.
- XU, H. & VAN REMMEN, H. 2021. The SarcoEndoplasmic Reticulum Calcium ATPase (SERCA) pump: a potential target for intervention in aging and skeletal muscle pathologies. *Skelet Muscle*, 11, 25.
- YAMAGUCHI, Y., MANN, D. M. & RUOSLAHTI, E. 1990. Negative regulation of transforming growth factor-beta by the proteoglycan decorin. *Nature*, 346, 281-4.
- YAMANAKA, O., YUAN, Y., COULSON-THOMAS, V. J., GESTEIRA, T. F., CALL, M. K., ZHANG, Y., ZHANG, J., CHANG, S. H., XIE, C., LIU, C. Y., SAIKA, S., JESTER, J. V. & KAO, W. W. 2013. Lumican binds ALK5 to promote epithelium wound healing. *PLoS One*, 8, e82730.
- YANAGISHITA, M. 1997. [Function of proteoglycans in the extracellular matrix]. *Kokubyo Gakkai Zasshi*, 64, 193-204.
- YANG, P., YIN, X. & RUTISHAUSER, U. 1992. Intercellular space is affected by the polysialic acid content of NCAM. *J Cell Biol*, 116, 1487-96.
- YAO, X., LIU, J. & MCCABE, J. T. 2007. Ubiquitin and ubiquitin-conjugated protein expression in the rat cerebral cortex and hippocampus following traumatic brain injury (TBI). *Brain Res*, 1182, 116-22.
- YIN, H., PRICE, F. & RUDNICKI, M. A. 2013. Satellite cells and the muscle stem cell niche. *Physiol Rev*, 93, 23-67.
- YOSHINARI, M., NISHIBATA, Y., MASUDA, S., NAKAZAWA, D., TOMARU, U., ARIMURA, Y., AMANO, K., YUZAWA, Y., SADA, K. E., ATSUMI, T., DOBASHI, H., HASEGAWA, H., HARIGAI, M., MATSUO, S., MAKINO, H. & ISHIZU, A. 2022. Low disease activity of microscopic polyangiitis in patients with anti-myosin

light chain 6 antibody that disrupts actin rearrangement necessary for neutrophil extracellular trap formation. *Arthritis Res Ther*, 24, 274.

ZAID, H., TALIOR-VOLODARSKY, I., ANTONESCU, C., LIU, Z. & KLIP, A. 2009. GAPDH binds GLUT4 reciprocally to hexokinase-II and regulates glucose transport activity. *Biochem J*, 419, 475-84.

ZHU, D., ZHOU, W., WANG, Z., WANG, Y., LIU, M., ZHANG, G., GUO, X. & KANG, X. 2021. Periostin: An Emerging Molecule With a Potential Role in Spinal Degenerative Diseases. *Front Med (Lausanne)*, 8, 694800.